GEOLOGICA ULTRAIECTINA

Mededelingen van de
Faculteit Aardwetenschappen
Universiteit Utrecht

No. 131

Deformation Mechanisms in Fine Grained Quartzo-Feldspathic Mylonites

An Electron Microscopy Study

Timon F. Fliervoet

GEOLOGICA ULTRAIECTINA

Mededelingen van de
Faculteit Aardwetenschappen
Universiteit Utrecht

No. 131

Deformation Mechanisms in Fine Grained Quartzo-Feldspathic Mylonites

An Electron Microscopy Study

Timon F. Fliervoet

CIP-GEGEVENS KONINKLIJKE BIBLIOTHEEK, DEN HAAG

Fliervoet, Timon F.

Deformation mechanisms in fine grained quartzo-feldspathic mylonites: an electron microscopy study / Timon F. Fliervoet. - Utrecht : Faculteit Aardwetenschappen, Universiteit Utrecht. - (Geologica Ultraiectina, ISSN 0072 - 1026; no. 131)
Proefschrift Universiteit Utrecht. - Met lit. opg. -
Met samenvatting in het Nederlands.
ISBN 90 - 71577 - 85 - 6
Trefw.: mylonieten ; deformatie / electronenmicroscopie
This thesis is also available on CD-rom

Deformation Mechanisms in Fine Grained Quartzo-Feldspathic Mylonites

An Electron Microscopy Study

Deformatiemechanismen in Fijnkorrelige Kwarts-Veldspaat Mylonieten.

Een Electronenmicroscopische Studie

(met een samenvatting in het Nederlands)

Proefschrift

Ter verkrijging van de graad van doctor aan de Universiteit Utrecht,
op gezag van de Rector Magnificus, Prof. Dr. J.A. van Ginkel,
ingevolge het besluit van het College van Dekanen
in het openbaar te verdedigen op woensdag 18 oktober 1995
des namiddags te 2.30 uur

door

TIMOTHEUS FRANCISCUS FLIERVOET

geboren op 18 april 1967 te Nijmegen

Promotor: Prof. Dr. S.H. White

Co-promotor: Dr. M.R. Drury

Verbonden aan de Faculteit Aardwetenschappen
van de Universiteit Utrecht

Foto omslag: Herman Wijler, Maastricht.

Het onderzoek beschreven in dit proefschrift werd verricht aan de Universiteit Utrecht, Faculteit Aardwetenschappen, Vakgroep Geologie, Budapestlaan 4, Postbus 80.021, 3508 TA Utrecht, Nederland. Het onderzoek werd gesubsidieerd door de Nederlandse Organisatie voor Wetenschappelijk Onderzoek (NWO), project number 751-353-021, en de Stichting Aardwetenschappelijk Onderzoek Nederland (AWON).

There is Nothing makes a Man *Suspect* much,
more then to Know little:
And therefore Men should remedy *Suspicion*,
by procuring to know more,
and not to keep their *Suspicions* in Smother.

Francis Bacon - *Of Suspicion*

Hoe **oer** moet **oer** zijn
om **oer** genoemd te worden

voor Ange

Contents

Voorwoord

Hoewel de kaft van dit proefschrift slechts één auteur vermeld, zijn er vele mensen die direct of indirect een bijdrage hebben geleverd aan mijn promotieonderzoek en aan de voltooiing van dit proefschrift. Voor hun hulp wil ik hen allen graag bedanken.

Ten eerste wil ik mijn promotor Stan White bedanken. Hij was altijd bereid om tijd vrij te maken om ideëen te bespreken en met zijn scherp inzicht de grote lijn van mijn proefschrift duidelijk te maken. Zijn opbouwende kritiek, onze gesprekken en zijn kennis van de electronenmicroscopie hebben een wezenlijke bijdrage geleverd aan mijn proefschrift.

Evenzoveel dank gaat uit naar mijn co-promotor Martyn Drury. Hij stond altijd open voor nieuwe ideëen en onze vele discussies over microstructuren en electronenmicroscopie hebben veel bijgedragen aan de uiteindelijke vorm en inhoud van mijn proefschrift.

Verder wil ik al mijn collega's van de faculteit aardwetenschappen bedanken voor hun hulp. Speciale dank gaat uit naar mijn twee paranimfen Coen ten Brink en Gill Drury-Pennock voor hun nimmer aflatende steun. Coen was er altijd op de momenten dat het even wat tegenzat, momenten die zich altijd voordoen tijdens een promotieonderzoek. Hij was bereid te luisteren en mij van daaruit verder te helpen. Gill heeft vanuit haar achtergrond als materiaalkundige, geholpen mijn proefschrift begrijpbaar te maken voor materiaalwetenschappers. Ook heeft zij zich grote moeite getroost om mijn proefschrift op het Engels na te kijken en te corrigeren. Hugo de Boorder, Mirjam van Daalen, Bernard de Jong, Rene de Kloe, Rob McDonnell, Siese de Meer, Herman van Roermund, Patrick Speck, Rian Visser, Reinoud Vissers en Dirk van der Wal wil ik bedanken voor hun hulp. Zij waren altijd geïnteresseerd in de voortgang van mijn onderzoek en waren bereid nieuwe inzichten kritisch te beschouwen in boeiende gesprekken. Verder lazen ze de tekst en hadden goede suggesties voor verbeteringen. Magda Mathot-Martens wil ik bedanken voor haar hulp bij het regelen van allerlei practische zaken in en rond mijn promotieonderzoek.

Joop Pieters, Brad Smith en Herman van Roermund brachten mij de beginselen van de electronenmicroscopie bij en wekten op die manier mijn interesse in deze specialistische techniek. Pim van Maurik stond altijd klaar om samen met mij practische problemen op te lossen die zich voordeden met de electronenmicroscoop. Zijn hulp en advies waren onmisbaar.

Het veldwerk in centraal Australië was niet mogelijk zonder de hulp van Russell Shaw, Bill Collins en de mensen van de Northern Territory Geological Survey, Alice Springs Office. David Young en Tania Madigan wil ik hartelijk bedanken voor hun gastvrijheid tijdens het veldwerk. Hun woning werd een thuisbasis van waaruit ik het veld inging. De audiovisuele dienst maakten tekeningen, foto's, dia's en posters voor mij. Paul van Oudenallen wil ik bedanken voor de opmaak van het proefschrift. Martin de Bouter gaf me veel hulp en advies bij de lithografie.

Mijn dank gaat uit naar de Nederlandse Organisatie voor Wetenschappelijk Onderzoek (NWO) en de stichting Aardwetenschappelijk Onderzoek Nederland (AWON) voor de

financiële ondersteuning van mijn onderzoek en voor reisbeurzen. Verder dank ik de Stichting tot Bevordering van de Electronenmicroscopie in Nederland (SEN) en Philips Nederland B.V. Analytical voor hun bijdrage in de drukkosten van dit proefschrift.

Gesprekken met vrienden die leek zijn op het gebied van de geologie zijn relativerend en motiverend geweest. Hierdoor is mij duidelijk geworden dat het moeilijk, maar belangrijk is de strekking van academisch onderzoek in het algemeen en mijn promotieonderzoek in het bijzonder aan geïnteresseerde leken duidelijk te maken. Met name wil ik Kees Dijkman bedanken voor het leesbaar maken van de Nederlandse samenvatting voor een niet-geologisch publiek. Ook wil ik mijn bridge-maatjes Remco van der Heijden, Dennis Kruis en Bron Vos bedanken voor het begrip dat zij hebben opgebracht wanneer ik weer eens zo met mijn onderzoek bezig was, dat ik geen kaart meer recht kon leggen. De prachtige foto op de voorpagina is het werk van fotografisch kunstenaar Herman Wijler. Mijn ouders wil ik bedanken dat ze mij de mogelijkheid hebben gegeven om te studeren en mijn onderzoekende geest hebben gestimuleerd.
Ange, jou wil ik graag bedanken voor al je steun, hulp en liefde. Jij bent van onschatbare waarde!

Timon Fliervoet

Augustus 1995

Samenvatting[1]

Inleiding

Zoals een auto sterk van vorm verandert wanneer deze wordt aangereden door een zware vrachtauto, zo zal ook een gesteente sterk van vorm veranderen wanneer er een kracht op wordt uitgeoefend. Dit is vervorming of deformatie van gesteenten. Echter, deformatie in de aardkorst en mantel is niet op alle plaatsen even groot. Sommige delen zijn meer vervormd dan andere delen. De deformatie is in bepaalde delen van de aardkorst en mantel gelocaliseerd, de zogenoemde deformatiezones. Zelfs binnen één deformatiezone zijn er kleinere zones van meer en minder sterke vervorming aan te wijzen. De allergrootste deformatiezones ontstaan bij het opbreken van de continenten en de vorming van oceanen en gebergtes. Zulke deformatiezones doorsnijden de gehele aardkorst en zijn daarom transcrustaal. Het bovenste deel van zulke zones, tot een diepte van circa 10 km, is koud en vervormt bros. Hierdoor ontstaan aardbevingen. Het onderste deel van de aardkorst is echter veel warmer, namelijk meer dan 250° à 300°C, en vervormt plastisch. Hier vinden geen bevingen plaats.

De sterkte van een deformatiezone wordt bepaald door de mechanische eigenschappen van de gesteenten erin. In het plastische deel van de aardkorst worden gesteenten in deformatiezones mylonieten genoemd. Bij zeer sterke deformatie ontstaan vaak ultramylonieten. Stenen zijn opgebouwd uit mineraalkorrels. Mylonieten hebben kleinere korrels dan het omliggende gesteente. Hoe dichter bij het centrum van de deformatiezone, hoe fijnkorreliger het mylonitisch gesteente. De mate van deformatie is in het centrum van de deformatiezone het grootst. Ultramylonieten zijn meestal uiterst fijnkorrelig.

De sterkte van deformatiezones wordt dus vooral bepaald door de meest fijnkorrelige, meest gedeformeerde gesteenten in die zones. Studies naar de sterkte van deformatiezones dienen zich dus op deze gesteenten te concentreren.

In de bovenste 25 km van de aardkorst zijn naast het hoofdmineraal kwarts ook nog andere mineralen zoals plagioklaas, kali-veldspaat, mica en amfibool aanwezig. Zulke gesteenten heten kwarts-veldspaat gesteenten. Tot nu toe heeft het onderzoek naar de sterkte van deformatiezones zich vooral gericht op het mineraal kwarts. De reden hiervoor is dat kwarts veel voorkomt en een eenvoudige kristalstructuur heeft. Onderzoek in de afgelopen jaren, waaronder dit promotieonderzoek, toont echter aan dat in de meest fijnkorrelige en meest vervormde delen van een deformatiezone dit onderzoek aan alleen kwarts tekort schiet. In de meest fijnkorrelige delen blijkt namelijk dat niet het mineraal kwarts alléén de sterkte van de deformatiezone bepaalt, maar dat de sterkte wordt bepaald door een mengsel dat behalve uit kwarts ook uit de bovengenoemde mineralen bestaat. Deze mengsels worden kwarts-veldspaat mengsels genoemd.

[1] Deze samenvatting is geschreven voor hen die niet geologisch onderlegd zijn. Het is derhalve geen directe vertaling van de Engelse samenvatting.

Het doel van mijn promotieonderzoek is te achterhalen hoe zulke kwarts-veldspaat mengsels vervormen, en bovendien in hoeverre hun mechanisch gedrag verschilt van dat van pure kwarts.

Deformatiemechanismen

Gesteenten kunnen op verschillende manieren plastisch deformeren. De belangrijkste mechanismen zijn dislocatiekruip, korrelgrensschuif en diffusiekruip.

Een dislocatie is een onregelmatigheid, een defect in de kristallografische ordening van de atomen binnen in een mineraalkorrel. Onder invloed van een kracht kunnen deze dislocaties zich verplaatsen en zo de mineraalkorrels van vorm veranderen. Deformatie door dit mechanisme heet dislocatiekruip. Bij korrelgrensschuif schuiven de mineraalkorrels langs elkaar heen, zonder zelf van vorm of samenstelling te veranderen. Echter, omdat het gaat om een proces van plastische vervorming, wordt de cohesie van het gesteente niet aangetast. Die cohesie wordt meestal bewaard door een derde mechanisme, diffusiekruip. Korrelgrensschuif en diffusiekruip komen dus meestal samen voor. Bij diffusie wordt materiaal van de ene kant van een mineraalkorrel naar een andere kant getransporteerd. Dit proces kan optreden door een korrel heen of langs de korrelgrenzen.

Of een gesteente deformeert door dislocatiekruip of door korrelgrensschuif hangt af van de grootte van de mineraalkorrels. Een gesteente dat bestaat uit grote mineraalkorrels deformeert door dislocatiekruip. Beneden een kritische korrelgrootte deformeert gesteente door korrelgrensschuif.

Als een gesteente deformeert door dislocatiekruip is de deformatiesnelheid niet afhankelijk van de korrelgrootte. Bij korrelgrensschuif in combinatie met diffusiekruip is de vervormingssnelheid wel afhankelijk van de korrelgrootte.

Gesteenten deformeren sneller als dat gebeurt door korrelgrensschuif en diffusiekruip, dan wanneer er dislocatiekruip plaatsvindt. Tenminste, als de temperatuur en de kracht in beide situaties gelijk zijn. Daardoor is gesteente dat deformeert door dislocatiekruip sterker dan gesteente dat deformeert door middel van korrelgrensschuif met diffusiekruip.

Als een gesteente deformeert, ontwikkelt er zich in dat gesteente een karakteristieke microstructuur[2] en textuur[3] afhankelijk van het deformatiemechanisme. Dus, de microstructuur en textuur van een gesteente geeft informatie over het mechanisme waardoor het gesteente gedeformeerd is. De microstructuur en textuur kun je bestuderen in het veld en met behulp van lichtmicroscopie en transmissie en scanning electronenmicroscopie.

Veldgegevens

De Redbank Deformed Zone in centraal Australië is tussen de 1500 en 400 miljoen jaar geleden actief geweest. Deze zone is 400 km lang en 20 km breed. De gesteenten in deze zone zijn plastische gedeformeerd op grote diepte in de aardkorst. Inmiddels liggen de gedeformeerde ge steenten aan het aardoppervlak en kunnen ze ter plekke in het veld bestudeerd worden.

[2] De microstructuur van een materiaal wordt onder meer bepaald door de grootte en de vorm van de korrels, hoe deze korrels door het materiaal verspreid zijn, de interne structuur van de korrels zoals roosterfouten (dislocaties) en de aard en het type van de korrelgrenzen.

[3] De term textuur beschrijft of de korrels in het materiaal al of niet een (kristallografische) voorkeursrichting hebben. Als een materiaal een sterke textuur heeft zijn de korrels volgens een voorkeursrichting georienteerd.

Het eerste deel van mijn onderzoek omvatte studies van deze gesteenten in het veld. Daar is duidelijk waar te nemen dat het gebied niet homogeen gedeformeerd is, maar zones bevat die meer en minder intens vervormd zijn (Fig. 2.3). Enkele van zulke kleinere, sterk gedeformeerde zones heb ik in detail bestudeerd. Het minder sterk gedeformeerde gesteente, waar de deformatiezones in zijn ontstaan, is een lichtgrijze granitische gneis met grote veldspaat kristallen, ook wel ogen genoemd (Fig. 2.5a). Deze ogen kunnen zo groot zijn als een voetbal. Naar het centrum van de deformatiezone neemt de mate van vervorming toe. Ook nemen de hoeveelheid en de grootte van de ogen af en wordt het gesteente fijnkorreliger. In het centrum van de zone is het gesteente het meest gedeformeerd. Het heeft hier een donkergrijze tot zwarte kleur en zijn er nog maar enkele, kleinere veldspaat ogen over (Fig. 2.5b en c). Van deze gesteenten heb ik monsters genomen, die telkens een grotere deformatie laten zien. Die monsters heb ik naar Utrecht verscheept voor verder onderzoek met behulp van licht- en electronenmicroscopie.

Licht- en electronenmicroscopie

Na geringe deformatie van de granitische gneis ontstond een myloniet. Dit gesteente bestaat uit banden van pure kwarts, afgewisseld met fijnkorrelige kwarts-veldspaat banden (Fig. 2.7a en 2.8a). In het centrum van de zone, bij de hoogste deformatie, is deze gebandheid afwezig. Hier bestaat de ultramyloniet uit een zeer fijnkorrelig, homogeen mengsel van kwarts-veldspaat (Fig. 2.7b en 2.8c).

Om het mechanisch gedrag van deformatiezones te kunnen bepalen, is het essentieel om te weten hoe het gesteente gedeformeerd is in het centrum van de zone en hoe het gesteente aan weerszijden daarvan is gedeformeerd. Met behulp van de lichtmicroscoop en de electronenmicroscoop heb ik de microstructuur en textuur van deze beide gesteenten geanalyseerd. Deze studies tonen aan dat dislocatiekruip het belangrijkste deformatiemechanisme is in de pure kwarts banden (Fig. 2.11, 3.3 en 3.4), terwijl de fijnkorrelige kwarts-veldspaat mengsels in het centrum van de deformatiezone voornamelijk deformeren door korrelgrensschuif met diffusiekruip (Fig. 4.9, 4.10 en 4.13).

Deformatie van fijnkorrelige mengsels

Om meer inzicht te krijgen de vervorming van de aardkorst, is het dus nodig om te weten wat de mechanische eigenschappen zijn van fijnkorrelige kwarts-veldspaat mengels. Helaas zijn deze gegevens tot op heden niet beschikbaar. Om nu toch een beeld te krijgen van de mechanische eigenschappen van fijnkorrelige kwarts-veldspaat mengsels ten opzichte van die van grofkorreliger pure kwarts, heb ik in mijn onderzoek een lood-tin legering bestudeerd. Van zo'n lood-tin legering worden ondermeer soldeerdraden gemaakt.

In deze studie heb ik de relatie bepaald tussen de microstructuur en de mechanische eigenschappen van lood-tin legeringen. Ik ben er van uitgegaan, dat de resultaten op een vergelijkbare manier van toepassing zouden kunnen zijn op het verband tussen de microstructuur en de mechanische eigenschappen van fijnkorrelige kwarts-veldspaat mengsels. De microstructuur van deze mengsels kende ik immers al, uit het voorgaande microscopische onderzoek. Via deze omweg valt er dus wel degelijk iets te zeggen over de mechanische eigenschappen van deze kwarts-veldspaat mengsels!

Fijnkorrelig lood-tin kan, net als gesteente, op verschillende manieren vervormen. De legering is echter vele malen zwakker dan kwarts-veldspaat mengsels en het deformeert al plastisch bij kamertemperatuur. Er zijn vele studies verricht aan de mechanische eigenschappen van fijnkorrelige lood-tin legeringen. Die studies tonen aan dat als een lood-tin legering deformeert door korrelgrensschuif met diffusiekruip, ze zwakker is dan wanneer ze door dislocatiekruip deformeert. Bovendien blijkt een mengsel bestaande uit 50% lood en 50% tin het zwakste te zijn als het vervormt door korrelgrensschuif met diffusiekruip. Zo'n mengsel is zelfs zwakker dan puur lood of puur tin. Experimentele studies van lood-tin legeringen tonen verder aan dat met toenemende deformatie de lood-tin legering zwakker wordt.

Het blijkt dat als lood-tin legeringen bestaan uit een mengsel van 50% lood en 50% tin, er meer korrels lood naast korrels tin liggen, dan bijvoorbeeld in een 70% lood en 30% tin legering. Het aantal korrelcontacten tussen deze twee elementen is in een 50/50 mengsel dus het grootst.

In mijn promotieonderzoek heb ik vervolgens de aantallen lood-tin contacten gemeten in een niet gedeformeerde en in een sterk gedeformeerde legering. Uit deze analyse blijkt, dat het aantal lood-tin korrelcontacten in gedeformeerde lood-tin legeringen groter is dan in niet gedeformeerde lood-tin legeringen.

Ook blijkt dat diffusie door een lood-tin contact sneller verloopt dan door een lood-lood of tin-tin kontact. Kortom, hoe meer lood-tin contacten er in de legering aanwezig zijn, hoe sneller de totale diffusie verloopt. Als de legering deformeert door korrelgrensschuif met diffusiekruip, dan verloopt de deformatie sneller naarmate er meer lood-tin korrelcontacten aanwezig zijn. Dit maakt de legering dus zwakker.

In het algemeen blijken de mechanische eigenschappen van fijnkorrelig mengsels dus niet alleen bepaald te worden door het deformatiemechanisme, maar ook door de microstructuur. Dit geldt voor elk fijnkorrelig mengsel. Voor fijnkorrelige kwarts-veldspaat mengsels evengoed als voor lood-tin legeringen.

Modellen van de sterkte van de aardkorst

Tot op heden hebben onderzoekers modellen gemaakt van de sterkte van de aardkorst door gebruik te maken van de mechanische eigenschappen van kwarts, zoals dat deformeert door dislocatiekruip. Hoewel dit als een eerste benadering goed heeft gewerkt, tonen de gegevens in mijn proefschrift aan, dat deze benadering te kort schiet. De vervorming in deformatiezones is namelijk geconcentreerd in de ultramyolieten. Dat zijn fijnkorrelige kwarts-veldspaat mengsels, en die deformeren niet door dislocatiekruip, maar voornamelijk door korrelgrensschuif met diffusiekruip. Dus de mechanische eigenschappen van deze fijnkorrelige kwarts-veldspaat mengsels, en niet die van de pure kwarts banden zijn bepalend voor de sterkte van de Redbank Deformed Zone en daarmee voor de middenkorst.

De oude modellen geven dus een te hoge sterkte voor deformatiezones. Uit mijn onderzoek blijkt dat deze pure kwarts aanname de sterkte van deformatiezones tenminste 100 tot 1000 keer overschat. Dat wil zeggen, de aardkorst is in deformatiezones vele malen zwakker dan tot nu toe altijd werd aangenomen.

Synopsis

Previous work on the deformation mechanisms in quartzo-feldspathic rocks from the upper- and middle-crust has predominantly concentrated on single phase quartz bands within these rocks. This has served well as a first approach, but several shortcomings have become evident concerning the highest strained and most fined grained parts of shear zones. It will be shown in this thesis, that under some circumstances the single phase approach is appropriate, but in many cases it is inadequate and can lead to erroneous interpretations of lithospheric rheologies.

This thesis concentrates on the investigation of the intra- and intercrystalline deformation mechanisms in fine grained quartzo-feldspathic rocks from the Redbank Deformed Zone, a major transcrustal shear zone in Central Australia. In this research, advanced transmission electron microscopical (TEM) techniques, together with field work, light microscopy (LM) and scanning electron microscopy (SEM) have been used to study the microstructures and microtextures of these rocks. Concepts developed within the metals and materials sciences have been utilised to quantify and understand the deformation of the quartzo-feldspathic rocks.

These studies have shown that, during deformation, the quartzo-feldspathic rocks of the Redbank Deformed Zone are transformed by mechanical breakdown processes accompanied by mineral chemical reactions and subsequently followed by mechanical mixing. At first a mylonite, having a banded microstructure consisting of quartz and polyphase bands is produced. Eventually at high strains a homogeneous, fine grained polyphase ultramylonite is developed. Shear zone geometry and microscale structures indicate that these polyphase ultramylonites were weaker than the encapsulating mylonites. Consequently, the deformation and rheology of these quartzo-feldspathic rocks (and by implication the rheology of the Redbank Deformed Zone) was controlled by the fine grained polyphase ultramylonites.

Microstructural studies have often been used to investigate the deformation mechanisms operative in naturally deformed rocks. There are, however, problems in identifying which of the deformation mechanisms has been dominant. In this thesis, microtextural analyses using TEM has been applied for the first time to naturally deformed rocks. A key criteria for the identification of grain boundary sliding deformation is the analysis of crystal rotations between adjacent grains. Application of this method to the Redbank Deformed Zone mylonites indicates that dislocation creep was the dominant deformation mechanism in quartz bands, while grain boundary sliding deformation was dominant in the fine grained polyphase bands and the high strain ultramylonites.

In view of the lack of pertinent rheological data on the deformation of polyphase geological materials, the deformation mechanisms and microstructures in some simple analogue materials have been investigated. Previously published studies on experimentally deformed fine grained Pb-Sn alloys have shown that the 2-phase alloy was weaker than its constituent phases when undergoing deformation by diffusion accommodated grain boundary sliding processes. These studies also showed a progressive weakening of such 2-phase alloys with strain. Current models of diffusional creep predict that two-phase materials will be weaker than the single phase end-members. These models, however, fail to explain the microstructural evolution and strain softening behaviour found in superplastic alloys.

In view of these shortcomings, a new quantitative model for the deformation of 2-phase materials has been developed. The model predicts that the strain rate of a polyphase material deforming by diffusion accommodated grain boundary sliding depends on the interface population. During deformation grain neighbour switching produced by grain boundary sliding and grain growth processes will result in the development of a "minimum interfacial energy microstructure (MIEM)" where the proportion of low energy interfaces is maximised. The development of a MIEM will result in an enhancement of creep kinetics if higher boundary diffusivities are associated with low energy interfaces, as is the case for many polyphase materials. This new model explains for the first time the variation of creep rate and microstructural evolution during deformation of these systems. The new model for enhanced creep associated with MIEM, together with the previous models for enhanced diffusion creep in 2-phase materials, can explain why many polymineralic rocks are weaker than the individual end members.

This work has important implications for the rheology of the lithosphere. In most models of upper- to middle-crustal deformation it is assumed that, irrespective of the rock composition or metamorphic conditions, the rheology is controlled by quartz deforming by dislocation creep processes. Whereas such an assumption might be a good approximation for "low strain" mylonites, these models are inappropriate for "high strain" polyphase ultramylonites. In the latter, the rheology will depend on the composition of the ultramylonite, which in turn will depend on the type of metamorphic reactions occurring during deformation. Two distinct regimes can be identified in quartzo-feldspathic mylonites: at low temperatures in hydrous environments (generally lower to middle-greenschist facies conditions), the reactions lead to mica-rich mylonites in which phyllosilicates determine the rheology. Whereas at higher temperatures and dry conditions (generally upper greenschist facies and higher), the production of phyllosilicates is limited and the flow is controlled by the grain-size-sensitive deformation of fine grained polyphase rocks.

In summary, at low strains, upper- and middle-crustal rheology, will be controlled by quartz. At high strains, however, depending on metamorphic conditions, the rheology will be controlled either by mica-rich mylonites or by fine grained polyphase ultramylonites.

Chapter 1

Introduction

1.1 General background

Transcrustal shear zones play a fundamental role in the deformation and dynamics of the earth's continental lithosphere. They characteristically exhibit multiple reactivations since their initiation and have been foci for continental tectonism. Reflection seismic studies (e.g. McGeary & Warner 1985; Choukroune *et al.* 1989; Goleby *et al.* 1989) across shear zones exhibiting the greatest extent of reactivation and the greatest influence on tectonic evolution show that they traverse the entire continental crust, extend into the upper mantle and significantly displace the Moho. Such shear zones commonly exhibit zones of very fine grained mylonites encapsulated within coarser grained mylonites and contain mylonite zones of different metamorphic grade, which are thought to represent different crustal levels. Examples of such major transcrustal shear zones are: the San Andreas Fault, California (Scholz 1990), the Alpine Fault Zone, New Zealand (Sibson *et al.* 1979), the North Pyrenean Fault Zone, France (Choukroune *et al.* 1989), the Outer Hebrides Thrust Zone, Scotland (Sibson 1977; Buttler & Coward 1984), the Indus Suture or Main Mantle Thrust, Himalayas (Coward *et al.* 1986), the Darling Mobile Zone, Western Australia (White *et al.* 1986) and the Redbank Deformed Zone, Central Australia (Obee 1985; Obee & White 1985; 1986; Goleby *et al.* 1989; Shaw & Black 1991; Shaw *et al.* 1992). The Redbank Deformed Zone has been taken as a sampling area for the mylonites described in this thesis.

The reason that transcrustal shear zones are fundamental planes of weakness in the crust and upper mantle lies in the rheology of the rocks (mylonites) that develop within them, i.e. deformation (strain) becomes progressively concentrated into the finest grained parts of these zones (e.g. Watterson 1975; Hobbs *et al.* 1976; White 1976; 1979b; 1979c; Sibson 1977; Watts & Williams 1979; White *et al.* 1980; Passchier 1982). Consequently the rheology of, and deformation within transcrustal shear zones, more particular their finest grained parts, are of major significance in controlling both reactivation and the role that these major shears have in lithosphere dynamics.

A large portion of the basement of the middle- to upper-continental crust consists of rocks with a quartzo-feldspathic bulk composition, such as granites, granodiorites and many ortho- and para-gneisses; such rocks are hereafter called quartzo-feldspathic rocks or granitoids. The mineralogical composition of such granitoids can be approximated by the following five minerals: quartz, K-feldspar, plagioclase, mica and amphibole. The mica and amphibole content can be as high as 25%, but usually ranges between 2% and 12% (Yardley 1989; Philpotts 1990; Fitz Gerald & Stünitz 1993). Although a high mica/amphibole content might influence the deformational properties of such rocks (Knipe & Wintsch 1985; Vernon & Flood 1988; Schmid & Handy 1991) most studies on granitoid deformation do not take the mica and amphibole content into account but treat

granitoids as of a mixture of quartz ± K-feldspar ± plagioclase (Allison *et al.* 1979; Behrmann & Mainprice 1987; Gillotti 1992; Fitz Gerald & Stünitz 1993; Stünitz & Fitz Gerald 1993).

In many quartzo-feldspathic rocks deformed under middle- to upper-crustal conditions, quartz forms a framework that supports the stress (Vernon & Flood 1988; Handy 1990; Schmid & Handy 1991). Under these conditions, shear deformation leads to a familiar mesoscopic augen-gneiss structure consisting of elongate quartz bands anastomosing around slightly or undeformed feldspar augen (Behrmann & Mainprice 1987). Within these quartz bands, intracrystalline plasticity has been inferred to be the dominant deformation mechanism (e.g. White 1973b; 1976; 1977; Watts & Williams 1979; Lloyd & Knipe 1992). Dislocation creep processes are therefore generally assumed to be the main factor controlling the deformation of granitoid shear zones, so that the plastic flow strength of the crust under these conditions is controlled by wet quartzite deforming by dislocation creep processes (e.g. White & Bretan 1985; Hobbs *et al.* 1986; White *et al.* 1986; Carter & Tsenn 1987; Ord & Hobbs 1989; Rutter & Brodie 1991).

Many studies on shear zone development in granitoids, however, report that the highest strains are recorded within ultramylonites which are composed of a fine grained polyphase mixture made up of quartz ± K-feldspar ± plagioclase ± mica ± epidote (Ramsay & Graham 1970; Ramsay & Allison 1979; Handy & Zingg 1991; Gillotti 1992; Stünitz & Fitz Gerald 1993). The actual mineralogy of this mixture depends on the metamorphic conditions during deformation. Establishing the deformation mechanisms within such polyphase ultramylonites is essential to the understanding of the rheological behaviour of shear zones. A number of studies on such polyphase, highly strained ultramylonites indicate that the flow of such polyphase rocks is not controlled by wet quartzite deforming by dislocation creep processes, but by a grain-size-sensitive creep mechanism with major grain boundary sliding creep processes (e.g. Behrmann & Mainprice 1987; Stünitz & Fitz Gerald 1993).

1.2 Problem definition, aims and scope of the present work

The above section points to the problem concerning the use of experimentally determined rock flow laws for single phase materials to model and predict the rheology of shear zones. As noted by Stünitz & Fitz Gerald (1993): "care should be taken before applying extrapolations based purely on single mineral intracrystalline deformation mechanisms without first establishing that these do indeed control the bulk rock rheology". Similar statements have been made previously by numerous authors (e.g. Poirier 1987; Knipe 1991; Rutter & Brodie 1991; Wenk & Christie 1991).

The present study aims to determine the changes in deformation mechanisms that accompany systematic grain size reduction. These changes in deformation mechanism might lead to the observed strain softening in major shear zones. To achieve this aim, samples were systematically taken across two, progressively deformed mylonites from the Redbank Deformed Zone, a major shear zone in Central Australia. Light optical and electron microscopy techniques have been used to study the microstructures and (micro)textures of these single- and polyphase rocks.

The microstructure of a material includes the sizes and shapes of the grains, their distribution through the material, the internal substructures within the grains such as dislocations and subgrain boundaries, the interfacial characters and interfacial type between two grains (*cf.* Hobbs et al. 1976). In this thesis an interface between two grains of a similar phase are referred to as grain boundaries, whereas a boundary between two dissimilar phases is called an interphase boundary. The term grain boundary sliding denotes, unless specifically stated otherwise, sliding along both grain and interphase boundaries.

The texture of a material is the bulk crystallographic preferred orientation (CPO) of all grains within the material, without any reference to a particular grain (*cf.* Randle 1992). The term microtexture has been adopted to refer to a CPO on a scale which is consistent with a single unit of orientation, i.e. a grain or a subgrain. The measurement of the microtexture enables the determination of the misorientation relationships between two adjacent grains or subgrains (*cf.* Randle 1992).

Light microscopy (LM) and Scanning Electron Microscopy (SEM) were used for grain size, grain shape and interfacial character analyses, phase distribution and interface population determination, and texture measurements. A microprobe was used for mineral chemical analyses. Image analyses was used to quantify the microstructures and microstructural changes.

The description of the interfacial and intercrystalline deformation microstructures have been made using various standard and advanced Transmission Electron Microscopy (TEM) techniques. These include standard bright-field (BF), conical dark-field (ConDF), selected area and microdiffraction modes. Since many samples studied were fine grained (< 10 μm) and polyphase, a universal stage (U-stage) attached to an optical microscope or X-ray goniometry could not be used for texture measurements. TEM has been used to measure the texture and microtexture of quartz in these samples. TEM can provide unique information on the correlation between the defect structure induced by deformation (i.e. the microstructure) and the preferred orientation of a certain grain (i.e. the microtexture). Furthermore, when using TEM to measure the CPO, information about all the crystallographic directions can be obtained, this in contrast to the U-stage method. This allows the relationship between two adjacent grains or subgrains to be determined by means of an axis and angle of misorientation (*cf.* Randle & Ralph 1986; Randle 1992).

As many of the rocks studied in this work contained more than one phase, one would like to investigate the deformation mechanisms and microstructural development in experimentally deformed polyphase rocks. Since the experimental data on polyphase rock deformation is limited, an analogue material, namely a 2-phase fine grained lead-tin (Pb-Sn) alloy which showed similar deformation mechanisms as the polyphase ultramylonites, has been studied. The reason for the choice of the Pb-Sn system is two fold. Firstly, the Pb-Sn system has a relative simple binary phase diagram, similar to that of albite-quartz, anorthite-orthoclase and albite-orthoclase (*cf.* Ehlers 1972). Secondly, the Pb-Sn system is a classical superplastic alloy, its deformational behaviour is well characterised and extensive data is available for comparative studies.

The present study aims to provide much needed data on the deformation mechanisms in major shear zones. It is hoped that the data presented in this thesis will find applications and provoke further studies in future modelling of the rheological behaviour and microstructural development within ductile shear zones.

1.3 Organisation of this thesis

The thesis has been written in view of future publications, apart from the introduction (Chapter 1) and the summary and final conclusions (Chapter 7). Each chapter is planned to be submitted as one or more separate scientific papers. Chapter 3 has already been published in the Journal of Structural Geology. Because of this some repetition occurs particularly in the sections dealing with the experimental techniques. The relevant literature is summarised and reviewed in each chapter. The linkage between each chapter is as follows.

A first step in the determination of the dominant deformation mechanisms operative within mylonites of the Redbank Deformed Zone is the analyses of the microstructures and textures across two different mylonite zones. One greenschist facies and one amphibolite facies shear zone have been sampled and have been studied by LM and SEM. The observations, together with the geological setting of the Redbank Deformed Zone are described in Chapter 2.

Chapter 3 presents the microstructure and microtexture of very fine grained pure quartz bands within the greenschist facies mylonite using TEM. The results are discussed in terms of the dominant deformation mechanisms within these quartz bands.

The microstructures, textures and microtextures of the highest strained parts of the mylonites, *viz.* the fine grained polyphase ultramylonites, are the subject of Chapter 4. The most probable dominant deformation mechanisms within these high strain polyphase mixtures were deduced from SEM and TEM observations.

Chapter 5 presents a study of the microstructural changes of a 2-phase Pb-Sn alloy during deformation, in terms of phase distribution and interface populations. The observed changes are discussed in relation to the mechanical properties of the alloy and are compared to the microstructures of naturally deformed polyphase quartzo-feldspathic ultramylonites.

In Chapter 6, the observations of the Redbank Deformed Zone mylonites are compared with data from other studies on quartz and granitoid deformation; some strain rate estimates are given. Finally, Chapter 7 lists a summary and final conclusions of this study together with suggestions for further work.

Chapter 2

Microstructural changes across quartzo-feldspathic shear zones

2.1 Introduction

Studies of the progressive development of shear zones commonly indicate that the microstructure of the rocks change with increasing strain from protomylonitic (0 - 50% matrix) to mylonitic (50 - 90% matrix) and eventually to ultramylonitic (90 - 100% matrix) (e.g. Sibson 1977; Wakefield 1977; Berthé *et al.* 1979; Kerrich *et al.* 1980; White *et al.* 1982; Williams & Dixon 1982; Dixon & Williams 1983; Vernon *et al.* 1983; Watts & Williams 1983; Knipe & Wintsch 1985; Vauchez 1987; Gilotti 1992). In quartzo-feldspathic rocks, the shear deformation often results in a well defined compositional banding of alternating quartzose and feldspathic ± phyllosilicate rich layers which define the mylonitic foliation. These layers anastomose around less deformed feldspar augen (Wakefield 1977; Behrmann & Mainprice 1987). Within ultramylonites, this compositional layering generally vanishes and becomes replaced by a fairly homogeneous, fine grained matrix in which micas define the foliation (Wakefield 1977; Knipe & Wintsch 1985; Gilotti 1992; Mitra 1992). At low temperatures and hydrous conditions, typically lower to middle-greenschist facies conditions (Philpotts 1990), phyllonitic rocks are formed resulting from the break-down of the feldspar minerals to phyllosilicates (White & Knipe 1978; Kerrich *et al.* 1980; Wilson 1980; Williams & Dixon 1982; Dixon & Williams 1983; Knipe & Wintsch 1985; Obee 1985; Obee & White 1985; 1986; Janecke & Evans 1988).

Aims and approach

As a first step in this study of the mechanical properties of quartzo-feldspathic mylonites, this chapter aims to analyse the progressive mylonitization of granitic gneisses of the Redbank Deformed Zone, Central Australia. A microstructural[1] and textural[1] study, using both light optical and scanning electron microscopical techniques, is presented of samples taken systematically across two shear zones; one deformed at amphibolite facies and the other deformed at upper greenschist facies conditions. The results are subsequently discussed in terms of strain(rate) variations across both shear zones and in terms of ultramylonite formation. Detailed microstructural and microtextural studies aiming to assess the dominant deformation mechanisms operative within the various microstructural elements, i.e. the quartzose and feldspathic ± phyllosilicate rich layers, are presented in Chapters 3 and 4.

[1] Terms as defined in Chapter 1

2.2 Geological setting

The Arunta Block is a large Proterozoic Inlier in Australia, with a size roughly equivalent to that of Great Britain (≈ 200,000 km²). Within the Arunta Block, three tectonic provinces occur showing different lithological, metamorphic and deformational histories. These provinces are separated by major thrust zones (Fig. 2.1) (Shaw & Wells 1983; Offe & Shaw 1983; Shaw *et al.* 1984; Glikson 1987; 1989; Shaw & Black 1991; Black & Shaw 1992).

The major thrust boundary (> 400 km long) separating the Central and Southern Arunta Provinces is the Redbank Deformed Zone (RBDZ). Seismic reflection profiles show that the Zone dissects the entire continental crust and extends into the upper mantle (Goleby *et al.* 1989). To the north of the main thrust zone (Fig. 2.3), there are large granulite massifs of variable felsic, mafic and 'mafic-intermediate' compositions, as well as minor bodies of mafic granulite and pyroxene-bearing granitoid, all belonging to the Central Arunta Province (Shaw & Black 1991). The rocks of the Southern Arunta province are predominantly quartzo-feldspathic and migmatitic gneisses, and potassic anatectic granitoids (Obee & White 1985; Shaw & Black 1991). The Northern Arunta Province consists of metamorphosed sedimentary and volcanic rocks (Black & Shaw 1992). Several deformational, metamorphic and magmatic events have been recognised in the Central and Southern Arunta Provinces, and a summary of these events is presented in Table 2.1 and Fig. 2.2.

The Redbank Deformed Zone is a complicated zone, up to 20 km across, of intense deformation and exhibits zones of very fine grained ultramylonites (typically a few centimetres

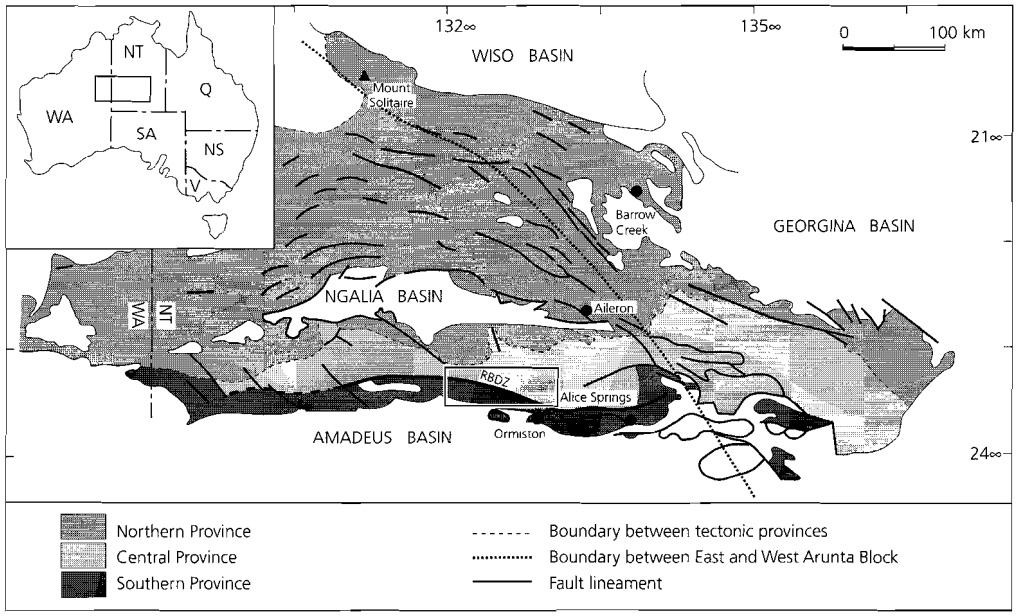

Fig. 2.1 Schematic map of the Arunta Inlier showing the tectonic provinces and the principle structural features (after Shaw *et al.* 1984; Shaw & Black 1991; Black & Shaw 1992). RBDZ: Redbank Deformed Zone.

Table 2.1 Summary of deformational, metamorphic and magmatic events in the Central and Southern Arunta provinces (after Shaw & Black 1991)

	Central Arunta Province		Southern Arunta Province	Regional Event (orogeny)	Inferred Age (Ma) (approximately)
D_1/D_2	Deformation, granulite facies metamorphism			Stangeways	1800 - 1750
		D_1/D_2	Deformation, amphibolite facies metamorphism	Chewings	1600
D_3	Amphibolite facies (type 1) mylonites		Amphibolite facies (type 1) mylonites	Anmathira	1500 - 1400
D_4	Open folding, migmatisation	D_3	Migmatisation, open folding	Ormiston (South of RBDZ)	1050 - 900
D_5	Greenschist facies (type 2) mylonites	D_4	Greenschist facies (type 2) mylonites	Alice Springs	400 - 300

to a few tens of metres wide) amidst coarser grained mylonites (Fig. 2.3 & 2.4). The mylonites show N-dipping foliations and a strong down-dip stretching lineation (Obee 1985; Obee & White 1985; Shaw & Black 1991). Two types of mylonite zones have been recognised in the Redbank Deformed Zone (Shaw & Black 1991): type 1 mylonites contain amphibolite facies mineral assemblages (550 - 650 °C; Shaw & Black 1991), whereas the type 2 mylonites contain greenschist facies mineral assemblages (350 - 450 °C; Shaw & Black 1991). The type 1 mylonites occur mainly in the granulite massifs north of the main thrust (Fig 2.3), whilst the type 2 mylonites are

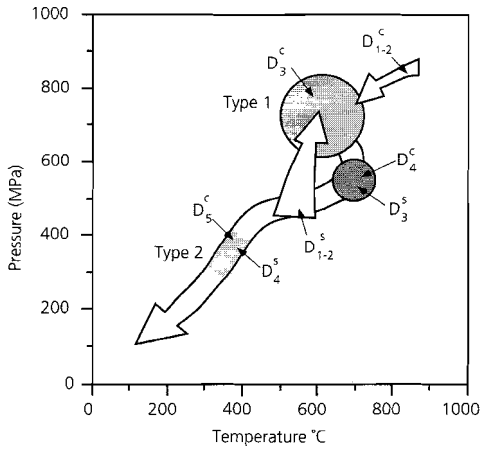

Fig. 2.2 Schematic P-T-t evolution for the Central and Southern Arunta Provinces (after Shaw & Black 1991). D = deformation; superscripts 'c' and 's' denote the Central and Southern Provinces respectively; subscripts 1-5 denote deformation events, are numbered independently for each province and are outlined in Table 2.1.

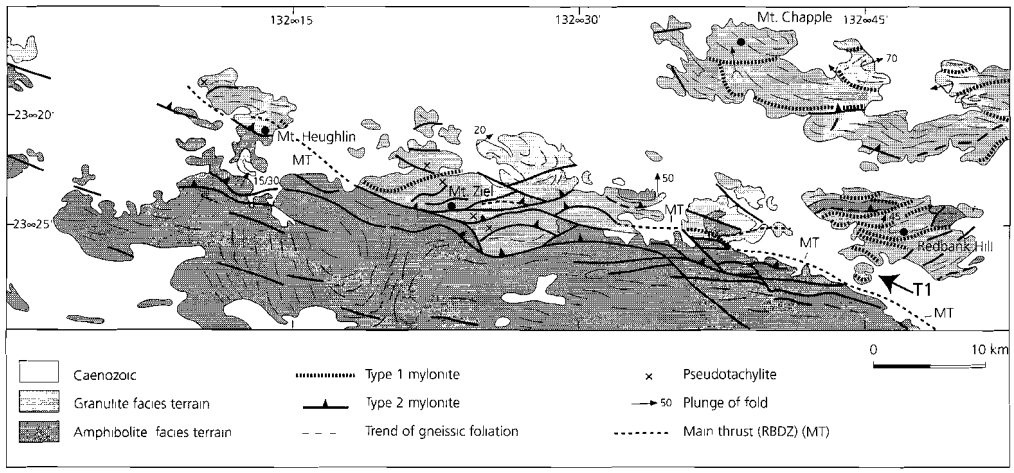

Fig. 2.3 Schematic map showing the distribution of type 1 and type 2 ultramylonitic zone centres in the Redbank Deformed Zone (after Shaw & Black 1991). The T1 indicates the type 1 shear zone sampling locality.

developed predominantly along the main thrust zone but also within the granulite massifs (Fig. 2.3).

Type 1 mylonites have been dated by Shaw & Black (1991), and yield Rb-Sr whole rock and Rb-Sr mineral ages between 1400 - 1500 Ma. Using the same methods, unfoliated pegmatite and narrow aplitic veins cross-cutting these type 1 mylonites have been dated by Shaw & Black (1991) at 1140 ± 56 Ma. In contrast, Shaw & Black (1991), using Rb-Sr whole rock and Rb-Sr mineral, and Shaw *et al.* (1992), using ^{40}Ar-^{39}Ar and K-Ar on K-feldspar, muscovite and hornblende, report ages between 300 - 400 Ma for the type 2 mylonites.

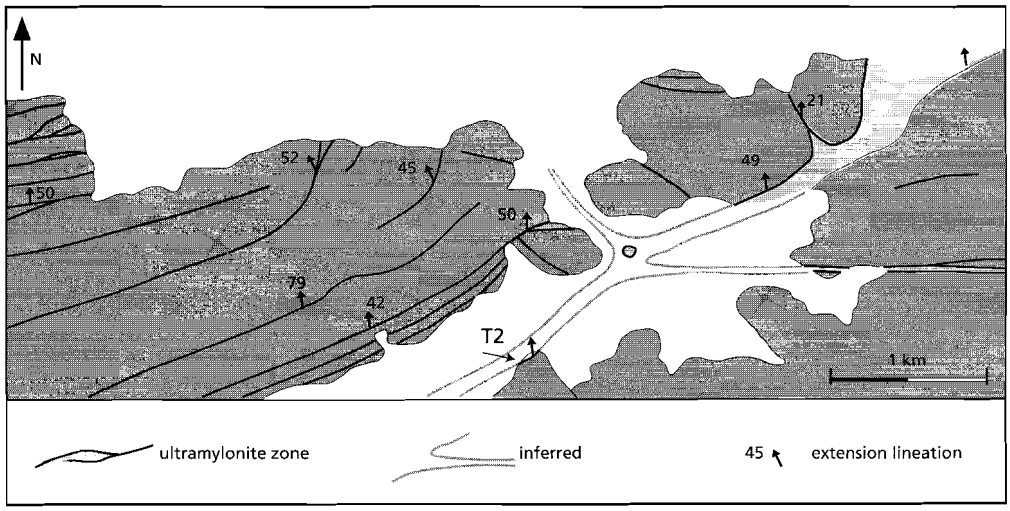

Fig. 2.4 Schematic map showing the main type 2 ultramylonitic shear zone centres within the New Well area (after Obee 1985; Obee & White 1985). The T2 indicates the type 2 shear zone sampling locality.

From both types of mylonite zones, oriented specimens were taken for detailed light optical and electron optical studies. The type 1 mylonite studied is from a 250 m wide shear zone containing a 40 - 50 m wide dark ultramylonite in its centre; it is located south of Redbank Hill (grid reference: 7207800 N and 359500 E; Fig. 2.3) in an area previously studied by Marjoribanks (Marjoribanks & Black 1974) and R. Shaw (personal comm.). The type 2 mylonite is from a 2 m wide shear zone located in the south eastern part of the New Well area (grid reference: 7389500 N and 356600 E; Fig. 2.4) previously studied by Obee and White (Obee 1985; Obee & White 1985; 1986).

2.3 Field descriptions

Both the type 1 and type 2 mylonite zones are marked by a moderately to steeply north dipping mylonitic foliation (40° - 70°) and a down-dip stretching lineation defined by elongate K-feldspar, plagioclase and quartz grains. Asymmetric porphyroclast systems, asymmetric folds and shear bands have been used as shear sense indicators (*cf.* White *et al.* 1986) and these consistently show a reverse movement sense. The country rock surrounding the two studied mylonites is similar and consists in both cases of a slightly foliated granitic gneiss with large feldspar augen (Fig. 2.5a).

In both types of mylonites, the matrix grain size decreases towards the shear zone centre, whilst the feldspar clasts decrease in size, and form augen which commonly develop tails defining the mineral stretching lineation. This decrease in grain size is thought to reflect an increase in deformation intensity. The ultramylonites are the finest grained parts of these shear zones and define the shear zone centre. In the ultramylonites, only a few small feldspar augen occur in a fine grained matrix. These rocks have a black or very dark grey colour in hand specimen (type 1: Fig. 2.5b; type 2: Fig. 2.5c). Both type 1 and type 2 mylonites studied show a gradational change from (proto)mylonite to ultramylonite. This change in microstructure is accompanied by a decrease in the dip of the foliation: from 60° - 70° N in the protomylonites, via 50° - 55° N in the mylonites, to dips of 40° - 45° N in the ultramylonitic shear zone centre (type 1: Fig. 2.9a; type 2: Fig. 2.14a). The progressive change of the microstructure and the allied changes in orientation of the rock-fabric strongly suggest an increasing intensity of the deformation.

2.4 Experimental and analytical techniques

Oriented hand specimens were taken systematically across the two mylonite zones. Both optical and electron optical studies were undertaken for microstructural observations. Scanning electron microscopy (SEM) analyses were carried out on a CamScan (operating at 15 - 25 kV) using atomic number contrast imaging (for a review see Lloyd & Hall 1981; Hall & Lloyd 1981; White *et al.* 1984). The higher the back-scatter coefficient the brighter the mineral appears in a back-scattered electron image.

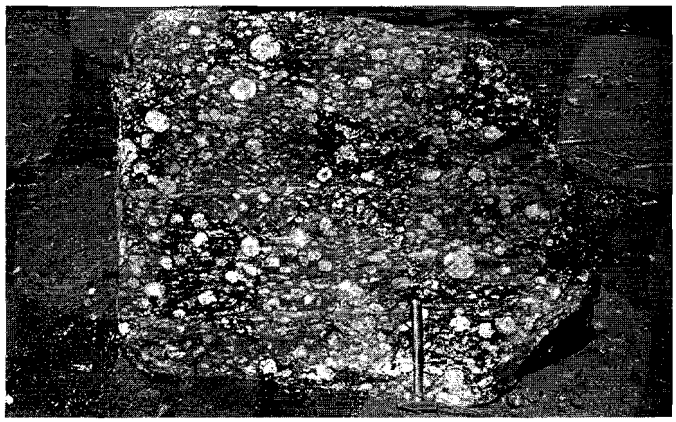

(a) Coarse grained country rock (slightly foliated granitic gneiss) in which the studied shear zones are developed. Feldspar clasts may be up to 30 cm in diameter.

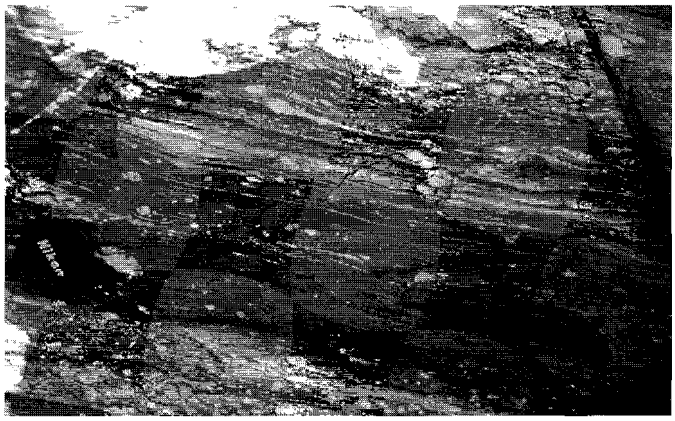

(b) Fine grained type 1 quartzo-feldspathic ultramylonite south of Redbank Hill.

(c) Fine grained type 2 ultramylonitic band (arrowed) at New Well; the diameter of the coin is approximately 2 cm. Note that feldspar clasts characteristic of the mylonites tend to be absent in the ultramylonites (b, c).

Fig. 2.5 Field aspects of typical quartzo-feldspathic rocks of the Redbank Deformed Zone.

The back-scatter coefficients (η) of the minerals encountered in this research are calculated using (White *et al.* 1984):

$$\eta_{mineral} = -0.0254 + 0.0162\,\overline{Z} - 0.000186\,\overline{Z}^2 \qquad (2.1)$$

where

$$\overline{Z} = \sum Z_i C_i \qquad (2.2)$$

and Z is the average atomic number of the mineral and C_i is the weight fraction of a chemical component in the mineral with atomic number Z_i; the summation is over all chemical components in the mineral. The back-scatter coefficients are listed in Tables 2.3 and 2.5.

Mineral chemical analyses have been performed by combined wavelength- (WDS) and energy-dispersive spectrometry (EDS) using a Jeol JXA 8600 Superprobe. The instrument operated at an acceleration voltage of 15 kV, a beam current of 10 nA and a probe size of 1 μm. For each analysis the counting time was 60 seconds. Corrections were made for atomic number (Z), absorption (A) and fluorescence (F) using a Tracor Northern PROZA ZAF correction program. Weight percentages were converted to molar percentages by assuming a fixed number of oxygen per unit formula; no corrections for ferric iron have been made. The results are summarised in Tables 2.3 and 2.5.

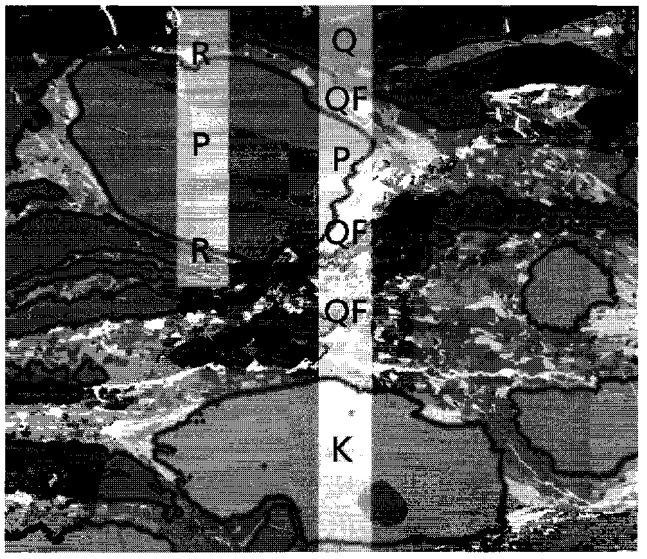

Q: pure quartz band
P: plagioclase
K: K-feldspar clast
QF: quartz-feldspar band

The two vertical lines represent the measurement lines.

Fig 2.6 Photosketch illustrating how the various microstructural elements within the mylonites are measured.

Grain and subgrain sizes have been measured from line drawings made from a number of photographs taken at 4 different flat stage orientations with respect to the polarisation directions of the light microscope. The average of the long and short axis of each grain were measured and were subsequently corrected for sectioning effects using a factor of 1.2 (*cf.* Underwood 1970). Because the grain size and subgrain size, in general, both show lognormal distributions (Ranalli 1984; Clark & Hosking 1986; Davis 1986), the median (Md) of the distribution was taken as a measure of the grain size and subgrain size; half the inter-quartile range is taken as a measure of variability; the skewness (Sk) and kurtosis (Km) are given to characterise the spread of data around the median.

The microstructural variations associated with mylonitization and ultramylonite development of the shear zone were quantified using 10 to 30 SEM photographs per sample. A measurement grid was superimposed on the drawing with grid lines perpendicular to the foliation. The line percentage of the different microstructural elements were calculated along these lines as outlined in Fig. 2.6. As shown by Underwood (1970, Chapter 2), the resultant lineal fraction is equivalent to the volume fraction of the microstructural element. Where grain sizes permitted, *c*-axis orientations were measured using conventional U-stage techniques (Turner & Weiss 1963).

2.5 Type 1 shear zone

Microstructure and microstructural variations

PROTOMYLONITE AND MYLONITE — The country rock in which the studied type 1 shear zone has developed is a foliated granitic gneiss with large feldspar augen and is referred to as protomylonite. A summary of the microstructures is provided in Table 2.2 and the mineral compositions in Table 2.3.

Table 2.2 Summary of microstructures within type 1 shear zone

	1	2	3	4	5	6	7	8
% QF	43.2 ± 10.2	31.5 ± 5.4		53.8 ± 8.4	96.4 ± 2.6	90.1 ± 4.4	92.0 ± 5.3	26.1 ± 6.2
% KF	14.8 ± 6.4	15.1 ± 3.3		9.6 ± 5.4	0.7 ± 0.8	3.4 ± 3.1	3.0 ± 4.6	26.4 ± 10.4
% PL	16.3 ± 7.5	21.3 ± 3.6		11.5 ± 7.3	2.9 ± 2.8	4.8 ± 4.0	3.8 ± 3.4	11.4 ± 8.2
% C	31.0 ± 7.9	36.3 ± 4.0		21.1 ± 6.3	3.6 ± 2.6	8.3 ± 4.2	6.9 ± 3.8	37.8 ± 7.9
% Q	25.8 ± 5.0	32.2 ± 6.0		25.1 ± 4.9		1.6 ± 1.1	1.2 ± 1.8	36.1 ± 5.1
% rim	14.3 ± 6.7	10.0 ± 6.1		25.0 ± 8.8	96.4 ± 2.6	92.3 ± 3.4	92.4 ± 3.5	9.4 ± 5.7
Dqtz	60 ± 24	56 ± 17	65 ± 26	56 ± 21		60 ± 19	53 ± 15	65 ± 29
Sk	1.6	1.7	2.0	1.5		2.1	1.7	1.4
Km	3.7	4.1	6.1	2.8		6.2	4.1	3.9
D_{QF}					11 ± 4	11 ± 4	11 ± 4	
Sk					0.4	0.4	0.4	
Km					-0.5	-0.5	-0.5	

key: % QF: vol. % quartz-feldspar band, % KF: vol. % K-feldspar, PL: vol. % plagioclase, % C: vol. % porphyroclasts, % Q: vol. % pure quartz bands, % rim: vol. % rim around porphyroclast, Dqtz: grain size of pure quartz ribbons, D_{QF}: quartz grain size in quartz-feldspar bands.

(a) (Proto)mylonite: porphyroclasts of plagioclase and K-feldspar are embedded in a matrix of finer grained bands of K-feldspar, plagioclase, quartz and biotite, alternating with pure quartz bands (plane polarised light, PPL). Scale bar: 300 μm.

(b) Ultramylonite: porphyroclasts of K-feldspar, plagioclase and garnet embedded in a fine grained homogeneous matrix (PPL). Scale bar: 300 μm

Fig. 2.7 Optical micrographs of microstructures in the type 1 shear zone studied.

Both the protomylonitic and mylonitic rocks consist of porphyroclasts (20% - 40% of the rock volume) of K-feldspar (Or 92.6), of plagioclase (An 38.3) and occasionally of garnet embedded in a fine grained foliated matrix (Fig. 2.7a). The feldspar porphyroclasts commonly show weak undulatory extinction and subgrain formation and usually have tails aligned parallel to the foliation. The clasts have a homogeneous mineral composition and show no exsolution. Within these rocks, most of the quartz occurs in discrete zones, 50 - 1000 μm thick, defining the foliation (Fig. 2.8a & 2.11). These pure quartz bands (60 μm grain size) alternate with continuous bands of finer grained (5 - 11 μm) K-feldspar (Or 94.2), plagioclase (An 33.5), quartz and biotite, hereafter called quartz-feldspar bands (Fig. 2.8a). All of the K-feldspar and plagioclase porphyroclasts are embedded within and mantled by these quartz-feldspar bands (Fig. 2.8b).

Table 2.3 Mineral chemistry of type 1 mylonites.

	protomylonite and mylonite						ultramylonite				
	biotite	garnet	K-feldspar clast	K-feldspar matrix	plagioclase clast	plagioclase matrix	biotite	epidote	garnet	K-feldspar matrix	plagioclase matrix
SiO_2	37.9 ± 5.2	37.8 ± 3.3	64.2 ± 0.5	64.3 ± 0.4	58.8 ± 1.0	60.3 ± 1.6	35.4 ± 1.8	38.0 ± 0.3	37.6 ± 0.3	64.3 ± 0.6	59.0 ± 0.5
TiO_2	3.1 ± 0.5	n.d	n.d	n.d	n.d	n.d	3.4 ± 0.2	n.d	n.d	n.d	n.d
Al_2O_3	16.4 ± 0.7	20.5 ± 0.8	18.3 ± 0.2	18.2 ± 0.3	25.8 ± 0.8	24.9 ± 1.2	16.3 ± 0.7	25.4 ± 0.4	21.1 ± 1.5	18.2 ± 0.3	25.7 ± 0.2
CaO	n.d	7.9 ± 1.6	n.d	n.d	7.7 ± 0.9	6.7 ± 0.8	n.d	23.4 ± 0.3	10.9 ± 4.6	n.d	7.6 ± 0.2
MgO	5.0 ± 1.0	0.9 ± 0.6	n.d	n.d	n.d	n.d	6.5 ± 0.3	n.d	1.0 ± 0.4	n.d	n.d
FeO	23.0 ± 3.5	26.8 ± 3.6	n.d	n.d	n.d	n.d	23.3 ± 0.8	9.4 ± 0.3	22.3 ± 4.9	n.d	n.d
MnO	n.d	5.0 ± 1.8	n.d	n.d	n.d	n.d	n.d	n.d	6.5 ± 2.5	n.d	n.d
K_2O	10.5 ± 0.7	n.d	16.2 ± 0.4	16.4 ± 0.3	n.d	n.d	10.0 ± 0.4	n.d	n.d	16.4 ± 0.3	n.d
Na_2O	n.d	n.d	0.9 ± 0.1	0.7 ± 0.1	6.8 ± 0.4	7.3 ± 0.5	n.d	n.d	n.d	0.7 ± 0.2	7.1 ± 0.1
F	0.7 ± 0.2	n.d	n.d	n.d	n.d	n.d	0.4 ± 0.1	n.d	n.d	n.d	n.d
Total	96.9	98.1	99.6	99.6	99.2	99.4	94.7	96.5	99.4	99.6	99.4
Si	5.77 ± 0.52	3.04 ± 0.18	2.99 ± 0.01	2.99 ± 0.02	2.64 ± 0.04	2.69 ± 0.06	5.49 ± 0.23	6.18 ± 0.04	3.01 ± 0.02	2.99 ± 0.02	2.65 ± 0.01
Ti	0.36 ± 0.06						0.39 ± 0.03				
Al	2.95 ± 0.16	1.95 ± 0.07	1.00 ± 0.01	1.00 ± 0.02	1.36 ± 0.04	1.31 ± 0.06	2.98 ± 0.13	4.86 ± 0.06	1.95 ± 0.03	1.00 ± 0.02	1.36 ± 0.01
Ca		0.70 ± 0.11			0.37 ± 0.04	0.32 ± 0.04		4.02 ± 0.06	0.80 ± 0.06		0.36 ± 0.01
Mg	1.14 ± 0.25	0.10 ± 0.03					1.50 ± 0.08		0.14 ± 0.03		
Fe	2.97 ± 0.51	1.81 ± 0.25					3.02 ± 0.13	1.27 ± 0.05	1.60 ± 0.09		
Mn		0.35 ± 0.12							0.50 ± 0.05		
K	1.96 ± 0.15		0.96 ± 0.03	0.98 ± 0.03	0.04 ± 0.02	0.04 ± 0.04	1.98 ± 0.11			0.97 ± 0.03	0.04 ± 0.04
Na			0.08 ± 0.02	0.06 ± 0.00	0.59 ± 0.04	0.64 ± 0.05				0.06 ± 0.01	0.60 ± 0.02
F	0.37 ± 0.09						0.17 ± 0.06				
O	22	12	8	8	8	8	22	25	12	8	8
An			0	0	38.3 ± 4.2	33.5 ± 4.2				0	37.7 ± 1.2
Ab			7.4 ± 1.0	5.8 ± 1.0	61.7 ± 4.2	66.3 ± 4.2				6.0 ± 0.9	62.3 ± 1.2
Or			92.6 ± 1.0	94.2 ± 1.0	0	0				94.0 ± 1.0	0
N	49	48	49	34	24	32	31	26	15	14	14
η	0.1653	0.1736	0.1398	0.1401	0.1329	0.1322	0.1656	0.1552	0.1730	0.1400	0.1328

Key: n.d: below 1 wt. %; N: number of analyses; errors are given as 1 standard deviation of the mean; An = anorthite content; Or = orthoclase content; Ab = albite content; η = back-scatter electron coefficient, note h of quartz = 0.1279.

ULTRAMYLONITE — Towards the shear zone centre the rock type progressively changes to a 40 - 50 m wide ultramylonite (Fig. 2.9b) At the microscale, this change results from a progressive increase in vol.% of quartz-feldspar bands together with a decrease in the vol.% of both the pure quartz bands and the K-feldspar and plagioclase porphyroclasts (compare Fig. 2.7a with 2.7b and Fig. 2.8a with 2.8c). Sparse epidote may also occur within the ultramylonite. Although the modal mineral content of the thin (< 200 μm) quartz-feldspar bands of the protomylonitic and mylonitic rocks is quite variable (Fig. 2.8b), the ultramylonite has a fairly constant modal mineral content of 40% quartz, 25% K-feldspar (Or 94.0), 25% plagioclase (An 37.7) and 10% biotite (Fig. 2.8c). A more detailed description of the microstructures of the fine grained (5 - 11 μm) polyphase ultramylonite is given in Chapter 4.

Quartz-feldspar band formation

As mentioned, above the vol.% of quartz-feldspar bands increases towards the shear zone centre, allied with a decrease in vol.% of porphyroclasts and of pure quartz bands. The formation of the quartz-feldspar bands, with a modal mineral content of 40% quartz, 25% K-feldspar, 25% plagioclase and 10% biotite (mineral chemical compositions listed in Table 2.3) may be either due to mechanical breakdown (recrystallisation) of the porphyroclasts and/or to chemical reactions. In the case of purely mechanical breakdown, no chemical differences are expected between the porphyroclasts and the newly formed grains.

Figure 2.8(b) shows K-feldspar and plagioclase porphyroclasts embedded within and mantled by the quartz-feldspar bands. The modal mineral composition of these bands is variable in that K-feldspar porphyroclasts may have tails composed of K-feldspar + biotite + quartz (KBQ in Fig. 2.8b), or of plagioclase + quartz + biotite (PQB in Fig. 2.8b). Similar observations are made on tails extending from plagioclase clasts.

Using the modal mineral content of the quartz-feldspar bands and their mineral chemistry (Table 2.3), the formation of the quartz-feldspar bands can be described by:

$$\begin{aligned} &0.28\ KF^{clast} + 0.22\ PL^{clast} + 0.40\ Q^{band} + 0.07\ K^{bt} = \\ &0.25\ KF^{matrix} + 0.25\ PL^{matrix} + 0.40\ Q^{matrix} + 0.10\ K^{bt} \end{aligned} \qquad (2.3)$$

where KF: composition K-Feldspar, PL: composition plagioclase, Q: quartz and K^{bt}: K content in biotite, and where clast denotes the porphyroclasts, band refers to the pure quartz bands, and matrix to the minerals in the quartz-feldspar bands.

The variation between the different microstructural elements, associated with progressive mylonitization and ultramylonite development of the type 1 shear zone, are closely correlated. The decrease in vol.% of porphyroclasts and of pure quartz bands is allied with an increase in vol.% of quartz-feldspar bands (Fig. 2.9b & 2.10).

(a) (Proto)mylonite: porphyroclasts of plagioclase (P) and K-feldspar (K) are embedded in a matrix of finer grained bands of K-feldspar, plagioclase, quartz (Q) and biotite (B), alternating with pure quartz bands. Scale bar: 300 μm.

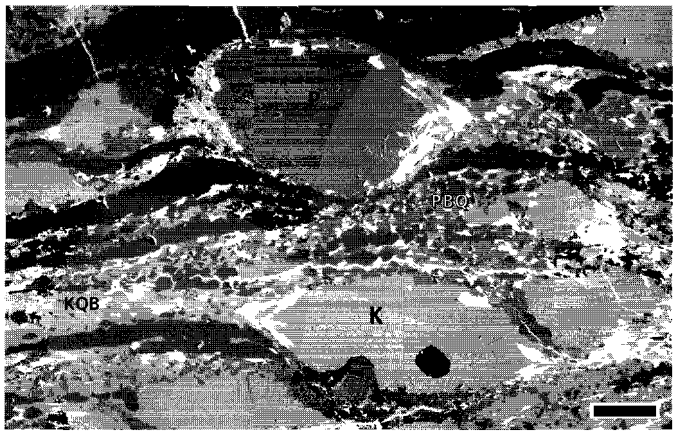

(b) (Proto)mylonite: K-feldspar might be rimmed by very fine grained (5 - 11 μm) K-feldspar, biotite and quartz (marked as KBQ) or by plagioclase, quartz and biotite (marked as PBQ). Scale bar: 100 μm.

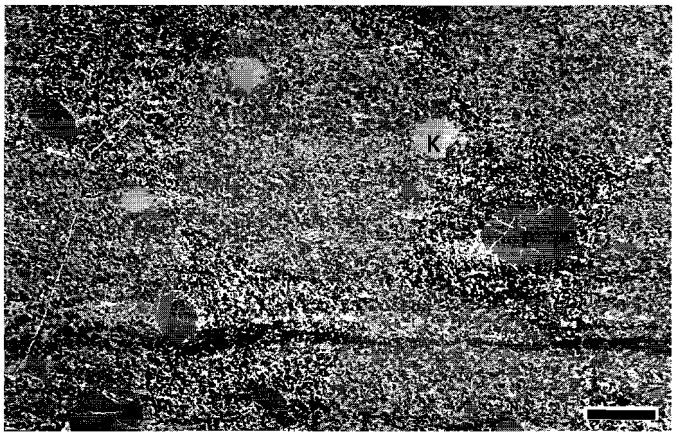

(c) Ultramylonite: porphyroclasts of K-feldspar, plagioclase and garnet embedded in a fine grained (5 - 11 μm) homogeneous polyphase matrix. Note the decrease in size and in number of both the K-feldspar (K) and plagioclase (P) clasts, and the increase in quartz-feldspar band content in the ultramylonite.
Scale bar: 300 μm.

Fig. 2.8 Back-scattered electron images of typical microstructures in the type 1 shear zone; back-scatter coefficients are given in Table 2.3.

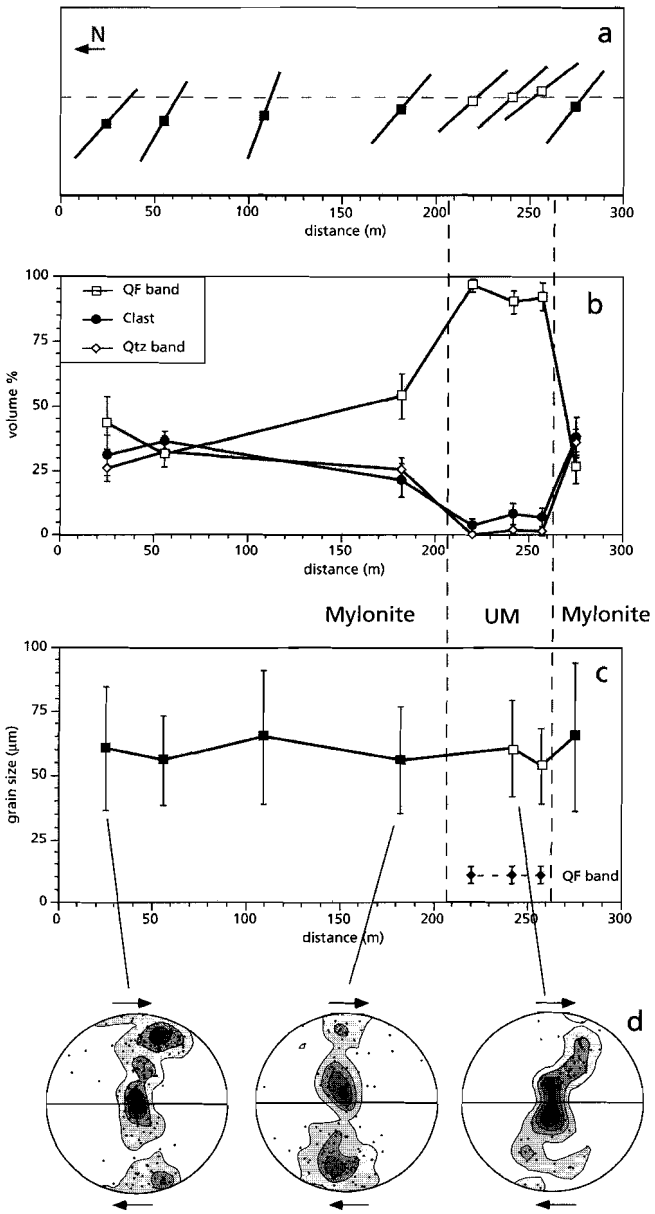

Fig. 2.9 Variations of microstructural features within the type 1 shear zone studied. (a) Profile showing orientation of mylonitic foliation. Open symbols denote ultramylonitic rocks, closed symbols denote encapsulating (proto)mylonitic rocks. (b) Variation of quartz-feldspar band (QF), pure quartz band (Q) and K-feldspar and plagioclase clast (C) content. (c) Variation of the median grain size of pure quartz bands, error bars represent half the inter-quartile range; the grain size of the QF bands are also indicated. (d) Variation of quartz c-axis textures; N = 203, N = 150 and N = 100 respectively. The foliation is horizontal, whereas the lineation is at the edge of the pole figure. Contours at 1, 3, 5 .. times a uniform distribution.

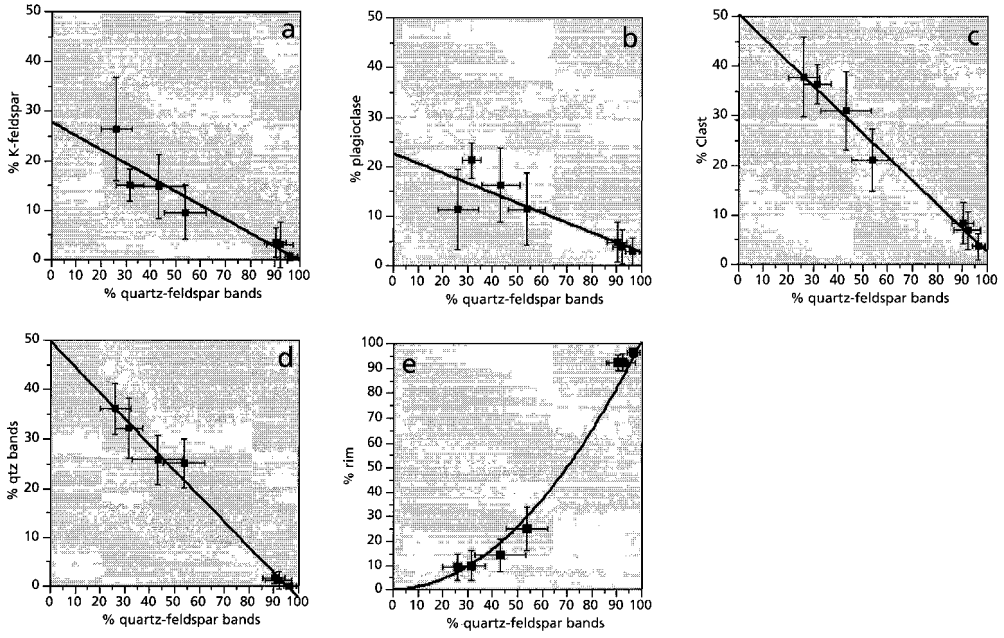

Fig. 2.10 Variations of K-feldspar clasts (a), plagioclase clasts (b), total clasts (c), pure quartz bands (d) and rim% (e) with quartz-feldspar band for the type 1 shear zone. See text for discussion. The relations are given in Eq. 2.4; the data are presented in Table 2.2.

The equations describing these relations, obtained using least-squares regression analysis, are :

$$\begin{aligned} KF^{clast} &= -0.28 \pm 0.12\ QF^{matrix} + 27.6 & R^2 &= 0.85 \\ PL^{clast} &= -0.20 \pm 0.13\ QF^{matrix} + 22.7 & R^2 &= 0.72 \\ KF^{clast} + PL^{clast} &= -0.48 \pm 0.06\ QF^{matrix} + 50.3 & R^2 &= 0.98 \\ Q^{band} &= -0.52 \pm 0.06\ QF^{matrix} + 49.7 & R^2 &= 0.99 \end{aligned} \qquad (2.4)$$

where KF^{clast}: vol.% K-Feldspar porphyroclast, PL^{clast}: vol.% plagioclase porphyroclast, Q^{band}: vol.% pure quartz bands, and QF^{matrix}: vol.% of quartz-feldspar bands; errors are given at 95% confidence interval, and R^2 is the correlation coefficient (Davis 1986).

Temperature estimates

Temperature and pressure estimates in quartzo-feldspathic rocks are limited by the fact that the pertinent minerals can be stable over a wide range of conditions. The mineral paragenesis of the type 1 mylonite suggests that deformation occurred at lower amphibolite facies conditions (Yardley 1989). The use of the Fe - Mg exchange garnet - biotite thermometer of Ferry & Spear (1978) is invalidated by the high Mn and Ca content of the garnet. In addition, the Ferry &

Spear (1978) thermometer assumes ideal mixing between garnet and biotite and does not take the Ti and Al^{VI} contents of biotite into account. The garnet-biotite thermometer of Kleemann & Reinhardt (1994), however, compensates for these effects of non-ideal mixing and the effects of Ca, Mn, Ti and Al^{VI}, and has been used in this study (Eq. 2.5; see inset), resulting in analytical temperatures around 600 ± 75 °C.

The occurrence of epidote and garnet in the shear zone centre indicates slightly lower temperatures for the ultramylonite as compared to the (proto)mylonitic rocks (Chatterjee *et al.* 1984). Plagioclase with an anorthite content of 38% stable with epidote in the ultramylonite indicates temperatures around 550 °C (*cf.* Fig 11 of Goldsmith 1982b). These temperature estimates are comparable to those reported by Shaw & Black (1991), who, on the basis of the Ferry & Spear (1978) garnet - biotite thermometer, inferred that deformation conditions were at middle-amphibolite facies (550 - 650 °C) in similar type 1 shear zones of the Redbank Deformed Zone.

Kleeman & Reinhardt (1994) garnet-biotite thermometer:

$$T[K] = \frac{\Delta H^\circ - \Delta W^{Bt}_{H,MgFeAl} X^{Bt}_{Al} - \Delta W^{Bt}_{H,MgFeTi} X^{Bt}_{Ti} + P\Delta V^\circ}{\Delta S^\circ - R \ln K_D - R \ln \gamma^{*Grt} - \Delta W^{Bt}_{S,MgFeAl} X^{Bt}_{Al} - \Delta W^{Bt}_{S,MgFeTi} X^{Bt}_{Ti}} \quad (2.5)$$

where:

$$X^{Bt}_{Al} = \frac{Al^{VI}}{Al^{VI} + Ti + Mg + Fe + Mn} \quad (2.5a)$$

$$X^{Bt}_{Ti} = \frac{Ti}{Al^{VI} + Ti + Mg + Fe + Mn} \quad (2.5b)$$

$$K_D = \frac{Mg^{grt}}{Fe^{grt}} \frac{Fe^{Bt}}{Mg^{Bt}} \quad (2.5c)$$

and where DW are the Margules parameters describing the non-ideal mixing behaviour of biotite with $\Delta W^{*}_{H,MgFeAl}$ = 77785 J mol^{-1}, $\Delta W^{*}_{H,MgFeTi}$ = -18138 J mol^{-1}, $\Delta W^{*}_{S,MgFeAl}$ = -94.1 J $mol^{-1}K^{-1}$, and $\Delta W^{*}_{S,MgFeTi}$ = 11.7 J $mol^{-1}K^{-1}$; and where $R\ln\gamma^{*grt}$ are the activity coefficients describing the non-ideal mixing behaviour of garnet and are taken from Berman (1990); and where the standard molar volume change ΔV° = 0.1 cm^3mol^{-1}, the average standard enthalpy difference ΔH° = 20253 J mol^{-1}, the average entropy difference ΔS° = 10.66 J $mol^{-1}K^{-1}$, and P the pressure and R the universal gas constant; grt = garnet and Bt = biotite .

Pure quartz band textures and microstructures

Within the pure quartz bands, quartz occurs as slightly elongated polygonal grains. The quartz grains show abundant undulatory extinction, subgrain formation (20 ± 5 μm) and serrated grain boundaries (Fig. 2.11). The grain sizes of the quartz remain constant across the mylonite zone at around 60 μm (ranging from 53 to 65 μm) (Fig. 2.9c). Note, however, that in the pure quartz bands in the centre of the shear zones, the average grain size is about half the width of the quartz bands in question, which will limit the size of the constituent grains. The measured grain size would thus be a lower estimate of the grain size of the pure quartz bands.

Small scale folds of pure quartz bands occur primarily within the ultramylonitic shear zone centre (Fig. 2.12a), whereas folding is limited within the (proto)mylonitic rocks. Many of these folds within the ultramylonite are asymmetric with cusps in the fold hinges (Fig. 2.12a). The lengths of these folded pure quartz bands are approximately half of them measured when unfolded.

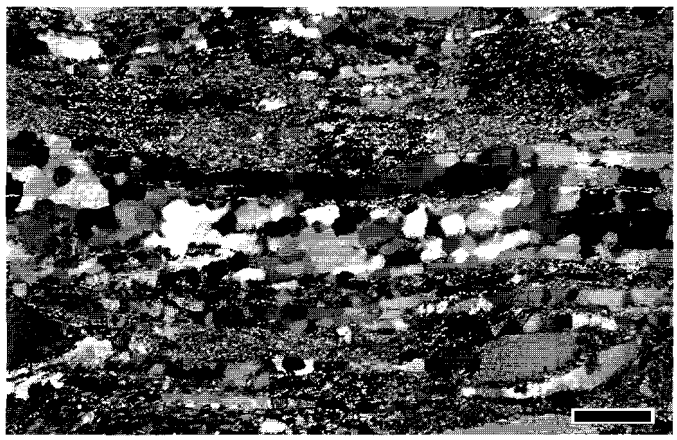

(a) Mylonite: alternation of pure quartz bands with quartz-feldspar bands. The pure quartz bands are made up of a coarse grained (60 μm) recrystallized mosaic (crossed nicols, CN).
Scale bar: 100 μm.

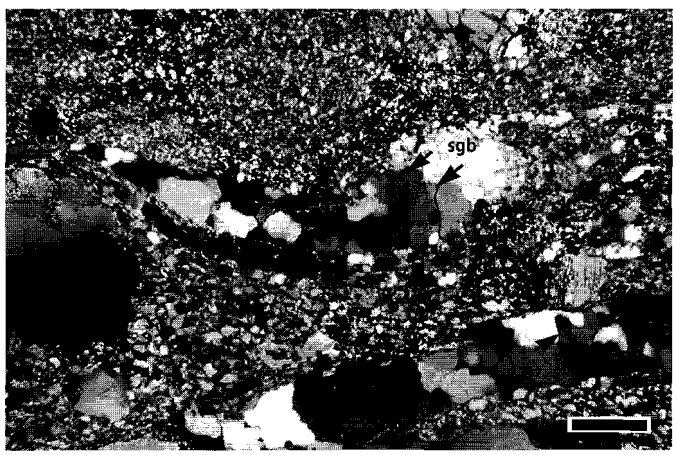

(b) Mylonite: detail of the quartzes within a pure quartz band. The grains show undulatory extinction and subgrain formation (sgb); some of the grain boundaries are serrated (arrowed) (CN).
Scale bar: 100 μm.

Fig. 2.11 Optical micrographs of pure quartz band microstructures in the type 1 shear zone studied.

These pure quartz bands although long (up to several cm) are not continuous and appear to laterally thin (Fig. 2.12b). The interface between the pure quartz bands and the adjacent quartz-feldspar bands is not straight, but show necks and boudinaged microstructures.

Figure 2.9(d) shows the variation of *c*-axis textures of the pure quartz bands across the mylonite zone. All *c*-axis textures are type 1 girdles (Lister 1977), with some marked differences between them. The texture measured in the mylonitic rocks are more symmetrically arranged to the foliation, while the texture measured in the shear zone centre shows a marked asymmetry consistent with a reverse movement along the shear zone. The pole figures are similar to quartz *c*-axis textures previously measured in similar rocktypes along the Redbank Deformed Zone (Obee 1985; Obee & White 1986). The microstructures and textures suggest that deformation in these pure quartz bands involved a major contribution of dislocation creep mechanisms.

(a) Small scale folding of pure quartz bands (PPL). Scale bar: 300 μm.

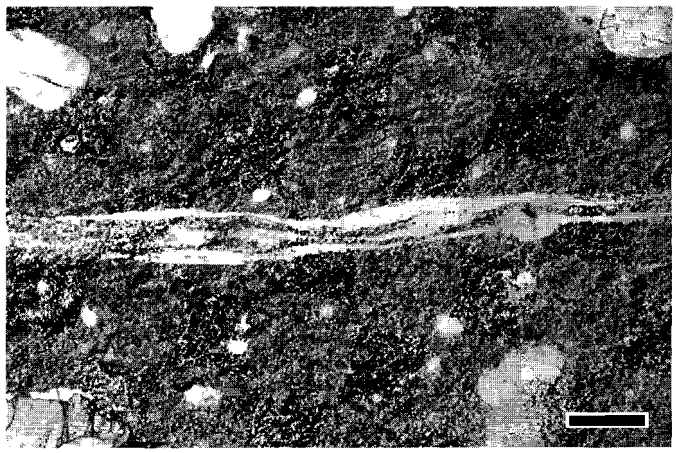

(b) Boudin type microstructures of pure quartz bands (PPL). Scale bar: 300 μm.

Fig. 2.12 Optical micrographs of type 1 ultramylonitic shear zone centre studied.

2.6 Type 2 shear zone

Microstructure and microstructural variations

PROTOMYLONITE AND MYLONITE — The rock enclosing the type 2 shear zone studied is similar to that of the type 1 mylonite: a foliated granitic gneiss with large feldspar augen. The mineral compositions are listed in Table 2.5, and a summary of the microstructures is presented in Table 2.4.

Similar to the type 1 shear zone, the protomylonitic and mylonitic rocks of the type 2 shear zone (Fig. 2.13) consist of porphyroclasts (20% - 30% of the rock volume) of K-feldspar (Or 92.5), plagioclase (An 27.5) and epidote, embedded in a fine-grained foliated matrix (Fig. 2.13a). The porphyroclasts commonly show weak undulatory extinction, limited fracturing and limited subgrain formation, and commonly have tails aligned parallel to the foliation. The clasts have a homogeneous mineral composition and the K-feldspar clasts show limited exsolution to sodic-plagioclase. Within these rocks, most of the quartz occurs in discrete zones, 10 - 200 μm thick, defining the foliation (Fig. 2.13a). These pure quartz bands (grain size: 31 ± 9 μm; Sk = 1.2; Km = 1.8) alternate with continuous bands of finer grained (0.5 ± 0.2 μm; Sk = 2.5; Km = 7.8) K-feldspar (Or 92.6), plagioclase (An 21.2), quartz and biotite, hereafter called quartz-feldspar bands (Fig. 2.13a). All of the K-feldspar and plagioclase porphyroclasts are embedded within and rimmed by these quartz-feldspar bands (Fig. 2.13a).

ULTRAMYLONITE — Towards the shear zone centre the rock type progressively changes to a 5 - 10 cm wide ultramylonite (Fig. 2.13b & 2.14). At the microscale, this change is allied with a progressive increase in vol.% of quartz-feldspar bands, and a decrease in the vol.% of both the pure quartz bands and of the K-feldspar and plagioclase porphyroclasts (compare Fig. 2.13a with 2.13b). Concurrent with this increase in vol.% quartz-feldspar band, is a decrease in grain size of

Table 2.4 Summary of microstructures within type 2 shear zone

	1	2	3
% QF	33.6 ± 8.7	48.9 ± 11.3	71.5 ± 10.6
% KF	18.7 ± 6.6	13.2 ± 3.2	4.6 ± 4.2
% PL	16.3 ± 4.9	15.3 ± 3.3	10.6 ± 5.3
% C	35.0 ± 3.5	28.5 ± 8.1	15.2 ± 7.7
% Q	31.4 ± 5.2	22.6 ± 5.2	13.3 ± 4.2
% rim	13.1 ± 10.3	21.2 ± 10.6	82.5 ± 4.6
Dqtz	31 ± 9	2.3 ± 0.8	
Sk	1.2	1.7	
Km	1.8	2.6	
D_{QF}			0.5 ± 0.2
Sk			2.5
Km			7.8

key: % QF: vol. % quartz-feldspar band, % KF: vol. % K-feldspar, PL: vol. % plagioclase, % C: vol. % porphyroclasts, % Q: vol. % pure quartz bands, % rim: vol. % rim around porphyroclast, Dqtz: grain size of pure quartz ribbons, D_{QF}: quartz grain size in quartz-feldspar bands.

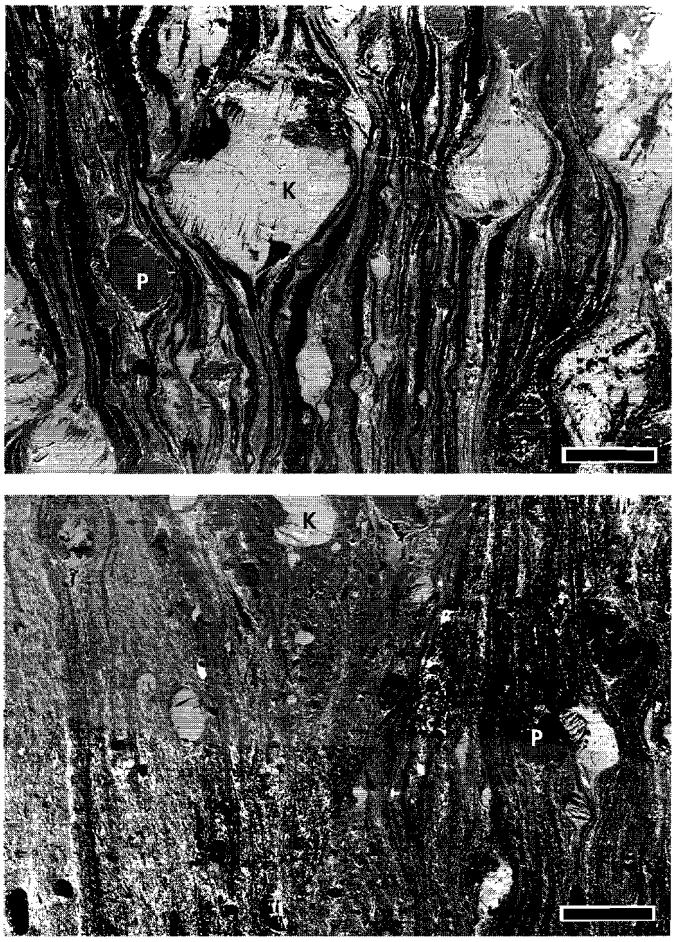

(a) (Proto)mylonite: porphyroclasts of plagioclase, K-feldspar and epidote are embedded in a matrix of finer grained bands of K-feldspar, plagioclase, quartz and biotite, alternating with pure quartz bands. Scale bar 300 μm.

(b) Ultramylonite: porphyroclasts of K-feldspar, plagioclase and garnet embedded in a fine grained (0.5 μm) homogeneous polyphase matrix. Note the decrease in number of both the K-feldspar (K) and plagioclase (P) clasts, and the increase in quartz-feldspar band content in the ultramylonite.
Scale bar 300 μm.

Fig. 2.13 Back-scattered electron images of microstructures in the type 2 shear zone studied; back scatter coefficients are given in Table 2.5.

the pure quartz bands from 31 ± 9 μm (Sk = 1.2; Km = 1.8) in the (proto)mylonitic rocks down to 2.3 ± 0.8 μm (Sk = 1.7; Km = 2.6) in the ultramylonitic shear zone centre (Fig. 2.13c). An electron microscopical study of the microstructures and microtextures in these very fine grained (2.3 μm) pure quartz bands is presented in Chapter 3.

The ultramylonite has a fairly constant modal mineral content of 35% quartz, 25% K-feldspar (Or 92.6), 40% plagioclase (An 21.2) and various amounts of biotite (up to 20%). A more detailed description of the microstructures of the fine grained (0.5 μm) polyphase ultramylonitic shear zone centre is given in Chapter 4.

Table 2.5 Mineral chemistry of type 2 mylonites.

	biotite	epidote	K-feldspar clast	K-feldspar matrix	plagioclase clast	plagioclase matrix
SiO_2	40.3 ± 6.1	38.2 ± 0.6	64.8 ± 0.4	62.9 ± 1.2	62.1 ± 0.9	64.9 ± 2.4
TiO_2	1.2 ± 0.9	n.d	n.d	n.d	n.d	n.d
Al_2O_3	17.0 ± 1.4	24.2 ± 0.8	18.4 ± 0.3	18.3 ± 0.7	24.7 ± 0.4	22.6 ± 1.6
CaO	n.d	23.1 ± 0.4	n.d	n.d	5.5 ± 0.1	4.3 ± 1.0
MgO	10.0 ± 2.2	n.d	n.d	n.d	n.d	n.d
FeO	16.8 ± 4.7	10.9 ± 0.8	n.d	n.d	n.d	n.d
MnO	n.d	n.d	n.d	n.d	n.d	n.d
K_2O	9.4 ± 1.4	n.d	16.1 ± 0.8	16.2 ± 0.8	n.d	n.d
Na_2O	n.d	n.d	1.0 ± 0.5	0.8 ± 0.3	8.2 ± 0.2	8.3 ± 0.5
F	1.1 ± 0.6	n.d	n.d	n.d	n.d	n.d
Total	95.8	96.9	100.3	98.2	100.5	100.1
Si	5.84 ± 0.66	6.24 ± 0.07	3.00 ± 0.01	2.99 ± 0.04	2.74 ± 0.02	2.83 ± 0.08
Ti	0.14 ± 0.10					
Al	2.91 ± 0.25	4.64 ± 0.13	1.00 ± 0.01	1.00 ± 0.04	1.26 ± 0.02	1.17 ± 0.09
Ca		4.06 ± 0.08		0.02 ± 0.03	0.26 ± 0.01	0.20 ± 0.05
Mg	2.17 ± 0.50					
Fe	2.06 ± 0.64	1.48 ± 0.13				
Mn						
K	1.75 ± 0.31		0.94 ± 0.05	0.96 ± 0.06		0.02 ± 0.03
Na			0.08 ± 0.05	0.08 ± 0.03	0.70 ± 0.02	0.72 ± 0.04
F	0.52 ± 0.31					
O	22	25	8	8	8	8
An			0	0.7 ± 1.3	27.5 ± 0.7	21.2 ± 4.6
Ab			7.5 ± 3.7	7.4 ± 2.6	72.5 ± 0.7	76.5 ± 4.3
Or			92.5 ± 4.1	91.9 ± 3.6	0	2.3 ± 2.9
N	16	11	10	8	8	7
η	0.1553	0.1571	0.1396	0.1398	0.1307	0.1301

Key: n.d: below 1 wt. %; N: number of analyses; errors are given as 1 standard deviation of the mean; An = anorthite content; Or = orthoclase content; Ab = albite content; η = back-scatter electron coefficient, note η of quartz = 0.1279.

Quartz-feldspar band formation

As mentioned above, the vol.% of quartz-feldspar bands increases towards the type 2 shear zone centre, together with a decrease in vol.% porphyroclasts and pure quartz bands. Using the modal mineral content of the quartz-feldspar bands (see above) and the mineral chemistry listed in Table 2.5, the formation of the type 2 quartz-feldspar bands can be described by:

$$\begin{aligned} 0.25\ KF^{clast} + 0.35\ PL^{clast} + 0.40\ Q^{band} &= \\ 0.18\ KF^{matrix} + 0.44\ PL^{matrix} + 0.33\ Q^{matrix} + 0.05\ K^{bt} & \end{aligned} \quad (2.5)$$

where KF: composition K-Feldspar, PL: composition plagioclase, Q: quartz and K^{bt}: K content in biotite; and where clast denotes the porphyroclasts, band refers to the pure quartz bands and matrix to the minerals in the quartz-feldspar bands.

Like the type 1 shear zones, the variation between the different microstructural elements associated with progressive mylonitization and ultramylonite development of the type 2 shear

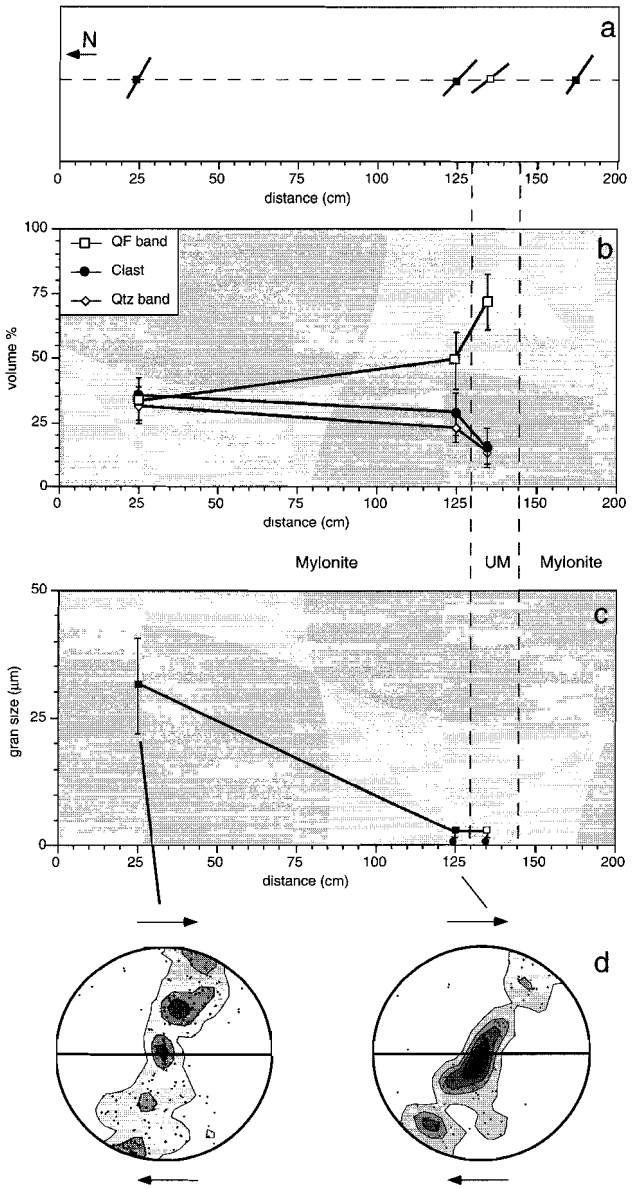

Fig. 2.14 Variations of microstructural features within the type 2 shear zone studied. (a) Profile showing orientation of mylonitic foliation. Open symbols denote ultramylonitic rocks, whereas closed symbols denote encapsulating (proto)mylonitic rocks. (b) Variation of quartz-feldspar band (QF), pure quartz band (Q) and K-feldspar and plagioclase clast (C) content. (c) Variation of the median grain size of the pure quartz bands, error bars represent half the interquartile range; the grain size of the QF bands are also indicated. UM denotes the ultramylonitic shear zone centre. (d) Variation of quartz *c*-axis textures; N = 190 and N = 144; contours are 1, 3, 5.. times a uniform distribution. The foliation is horizontal, whereas the lineation is at the edge of the pole figure.

zone are closely correlated. The decrease in vol.% of porphyroclasts and of pure quartz bands is allied with an increase in vol.% of quartz-feldspar bands (Fig. 2.14b), and can be described by:

$$\begin{array}{lll} KF^{clast} & = -0.27 \pm 0.11\ QF^{matrix} + 25.6 & R^2 = 0.67 \\ PL^{clast} & = -0.36 \pm 0.15\ QF^{matrix} + 34.7 & R^2 = 0.68 \\ KF^{clast} + PL^{clast} & = -0.63 \pm 0.07\ QF^{matrix} + 59.7 & R^2 = 0.91 \\ Q^{band} & = -0.37 \pm 0.07\ QF^{matrix} + 40.3 & R^2 = 0.78 \end{array} \quad (2.6)$$

where KF^{clast}: vol.% K-Feldspar porphyroclast, PL^{clast}: vol.% plagioclase porphyroclast, Q^{band}: vol.% pure quartz bands and QF^{matrix}: vol.% of quartz-feldspar bands; errors are given at 95% confidence interval.

Temperature estimates

The mineral paragenesis of the type 2 mylonite suggests that deformation occurred at upper greenschist facies conditions well above the biotite isograd and close to the boundary with the amphibolite facies (Yardley 1989). Plagioclase with an anorthite content of 21% is stable with epidote in the ultramylonite, indicating temperatures around 375 - 450 °C (*cf.* Fig. 11 of Goldsmith 1982b). These temperature estimates are comparable to those reported by Shaw & Black (1991). These authors inferred greenschist facies (350 - 500 °C) deformation conditions in similar type 2 shear zones of the Redbank Deformed Zone.

2.7 Discussion

Strain variations

Several methods can be used to determine strain variations in shear zones. These include foliation variations (Ramsay & Graham 1970; Sibson 1977; Ramsay & Allison 1979; Ramsay 1982; White *et al.* 1986), finite strain measurements (Ramsay & Graham 1970; Hobbs *et al.* 1976; Ramsay & Allison 1979), and competence contrast analyses (White *et al.* 1980; Ramsay 1982; Treagus 1988).

As pointed out Ramsay & Graham (1970) and Ramsay (1982), the intensity and orientation of the mylonitic foliation in a shear zone depends upon the magnitude of the accumulated finite strain. The foliation develops perpendicular to the direction of maximum finite shortening (Ramsay & Graham 1970). Towards the centre of a simple shear zone, the foliation is generally more strongly developed and makes decreasing angles with the walls of the zone (Ramsay & Graham 1970). As shown by a.o. Ramsay & Graham (1970), Sibson (1977), Ramsay & Allison (1979) and Ramsay (1982), there is a direct correlation between the decrease of this angle, the increase in intensity of the foliation and the finite strain:

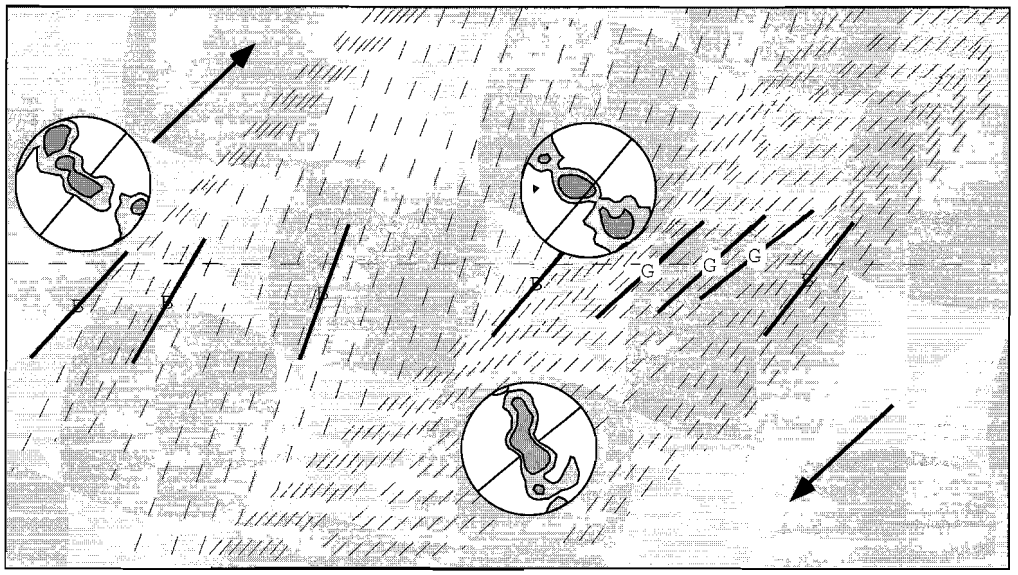

Fig. 2.15 Schematic profile across the type 1 shear zone (*cf.* Fig. 2.9) showing the changing orientation of the mylonitic foliation. Contoured c-axis diagrams (Fig. 2.9d) are added for reference. See text for discussion.

$$\tan 2\Theta' = \frac{2}{\gamma} \qquad (2.7)$$

where Θ' is the angle of the mylonitic foliation with the walls of the shear zone and γ is the finite shear strain. The systematic curvature of the foliation from the margin to the centre of the shear zone thus reflects an increase in accumulated finite strain. For very high shear strains, the foliation becomes virtually subparallel to the direction of shear. For both types of shear zones studied, marked variations in the orientation of the foliation occur (type 1: Fig. 2.9a; type 2: Fig. 2.14a). In general, the foliation within the ultramylonites dip more shallowly than those within the surrounding (proto)mylonites. A schematic profile of the type 1 shear zone studied (Fig. 2.15, *cf.* Fig. 2.9a), clearly illustrates the decreasing dip angle of the foliation within the ultramylonites (open symbols) as compared to that in the mylonites (closed symbols). The orientation of the foliations measured within the type 2 shear zone show a similar trend. From such observations it is concluded that the strain in the ultramylonitic centres of both the type 1 and type 2 shear zones must be higher than in the surrounding mylonites. In assuming that the shear zone walls are subparallel to the foliation of the ultramylonites the accumulated shear strains of the protomylonites and mylonites can be estimated using Eq. 2.7. The angular difference of 20 - 25° between the foliations encountered within the protomylonites and ultramylonites, results in shear strains of at least 2 in the protomylonites. The same methods results in shear strains of

at least 5 in the mylonites. Consequently, shear strains accumulated within the ultramylonites must be higher.

Further evidence for higher finite strains within the ultramylonitic shear zone centres comes from the observation of boudinaged and folded microstructures. Small-scale folds of pure quartz bands occur primarily within the ultramylonitic shear zone centres (Fig. 2.12a), whilst in the adjacent (proto)mylonitic rocks folds are limited. Concomitantly, pure quartz bands within the ultramylonites show necks and boudinaged microstructures, whereas in the (proto)mylonitic rocks pure quartz and quartz-feldspar bands anastomose around the feldspar augen. The presence of such intensively 'strained' structures within the ultramylonites and the virtual absence of these structures within the (proto)mylonites, also suggests that strains were highest in the ultramylonitic shear zone centres. Similar observations are reported by Handy & Zingg (1991) and Stünitz & Fitz Gerald (1993). The lengths measured along the folded pure quartz bands within the ultramylonites are approximately twice of the length measured parallel to the foliation. This result, when combined with the virtual absence of folds in the (proto)mylonitic rocks, indicate that strains in the ultramylonites were at least twice as high in the ultramylonites compared to the surrounding (proto)mylonitic rocks.

Additional evidence for strain partitioning between the ultramylonites and the surrounding (proto)mylonites may come from the differences between *c*-axis textures in the pure quartz bands of the (proto)mylonitic and ultramylonitic rocks. Treagus (1988) suggests that *c*-axis textures in simple shear may be more asymmetric with increasing strain. The *c*-axis textures in the ultramylonite show a marked asymmetry, whereas *c*-axis textures in the (proto)mylonite are more symmetrical with respect to the foliation (type 1: Fig. 2.9d; type 2: Fig. 2.14d). As pointed out by Treagus (1988) in simple shear the higher the strain the more asymmetrical the *c*-axis textures.

In assuming progressive deformation from (proto)mylonite to ultramylonite, the higher strains recorded in the polyphase ultramylonitic shear zone centre can be regarded as reflecting viscosity differences between ultramylonite and (proto)mylonite (Watts & Williams 1979; Handy 1990; Handy & Zingg 1991; Fitz Gerald & Stünitz 1993). The ultramylonites have a lower viscosity than the surrounding (proto)mylonitic rocks, i.e. higher strain rates at the same stress level. It follows that the mechanical properties of the fine grained polyphase ultramylonites must have controlled the rheology of these high strain shear zones. The microstructures and deformation mechanisms within these polyphase ultramylonites will be described and discussed in Chapters 4 & 5.

Progressive mylonitization

The progressive mylonitization seen in the two shear zones studied clearly involved a reduction in size and in number of K-feldspar and plagioclase porphyroclasts, and a decrease in volume of pure quartz bands at the expense of a fine grained polyphase mixture made up of K-feldspar, plagioclase, quartz and biotite. During this progressive mylonitization, the microstructure of the rock changes from (proto)mylonitic to ultramylonitic. The ultramylonitic centre of the studied type 1 shear zone is 40 - 50 m wide, whereas that of the studied type 2 shear zone is 5 - 10 cm wide. Concurrently, the overall grain size of the type 1 shear zone reduces to 5 - 11 μm, whereas the overall grain size of the type 2 shear zone grain size reduced to 0.5 μm.

The breakdown of the clasts and the formation of the polyphase quartz-feldspar bands in the studied type 1 and type 2 shear zones, can be described by the mineral chemical reactions given in Eqns. 2.3 & 2.6, respectively. In the case of the studied type 1 mylonite, Eq. 2.3 describes that 28% of K-feldspar clast, 22% of plagioclase clast and 40% of pure quartz band is consumed in the formation of the quartz-feldspar band. Errors are estimated around 5% (*cf.* Table 2.3). These bands are, in the ultramylonitic shear zone centre, composed of 25% K-feldspar, 25% plagioclase and 40% quartz; the mineral chemistries of the K-feldspar and plagioclase porphyroclasts are about equal to the composition of the K-feldspar and plagioclase in the quartz-feldspar bands. While pure quartz bands occur within the mylonites, they are absent in the ultramylonitic shear zone centre. However, in the mineral reaction (Eq. 2.3) no quartz is consumed nor produced, which indicates that mechanical mixing of quartz with plagioclase and K-feldspar had taken place. Furthermore, in the mylonites K-feldspar and plagioclase porphyroclasts are embedded within quartz-feldspar bands of variable modal mineral composition; the breakdown products of the porphyroclasts are variable. The ultramylonitic shear zone centre, on the other hand is a homogeneous mixture of all phases.

Furthermore, for the type 1 shear zone, the observed relationships between K-feldspar and plagioclase porphyroclast volume, the volume of the pure quartz bands and the quartz-feldspar band volume (Fig. 2.10 & Eq. 2.4) indicate that 28 ± 12% of K-feldspar clast, 20 ± 12% plagioclase clast and 52 ± 6% of pure quartz band are needed to form the quartz-feldspar bands. These values are comparable to those obtained from the mineral chemical reaction. Therefore, the formation of the quartz-feldspar bands and the evolution of the rock type from mylonitic to ultramylonitic, involved both mineral chemical reactions, as well as mechanical mixing of the phases. As the chemistry of the K-feldspar and plagioclase porphyroclasts of the type 1 mylonite are about equal to the composition of the K-feldspar and plagioclase in the quartz-feldspar bands, the latter is expected to be more important. A similar conclusion can be drawn for the formation of the quartz-feldspar bands in the studied type 2 shear zone. The commonly observed retrograde reaction of K-feldspar to form muscovite has not been observed in neither type of shear zones (e.g. Williams & Dixon 1982; Dixon & Williams 1983; Knipe & Wintsch 1985). Therefore a process equivalent to recrystallization has lead to grain refinement of the clasts and pure quartz bands. This is subsequently followed by mechanical mixing by grain boundary sliding processes which produced the fine grained homogeneous mixture in the ultramylonitic shear zone centres (see also Chapters 4 & 5).

The main purpose of this thesis was to assess the deformation mechanisms operative within quartzo-feldspathic shear-zones. Whether the shear zone systems were open or closed, i.e. whether chemical components were introduced to or removed from the shear zone is irrelevant to determine the rheology of the shear zones, and therefore mass balance analyses have not been carried out. It is clear that processes similar to recrystallization with chemical reactions and mechanical mixing have contributed to the ultramylonite formation.

2.8 Conclusions

1) Light optical and scanning electron microscopical studies of samples from two shear zones (type 1 and type 2) in the Redbank Deformed Zone of Central Australia, show that progressive mylonitization from protomylonite to ultramylonite involved the reduction (both in size and in number) of K-feldspar and plagioclase porphyroclasts and pure quartz bands at the expense of very fine grained quartz-feldspar bands: a polyphase mixture made-up of K-feldspar, plagioclase, quartz and biotite.
2) In both the type 1 and type 2 shear zones, the breakdown of the clasts and the formation of the polyphase quartz-feldspar bands involved mechanical reworking (recrystallisation) and neo mineralization, subsequently followed by mechanical mixing.
3) The bulk strain(rate) became largely accommodated in the ultramylonitic shear zone centres. Therefore, the mechanical properties of the fine grained polyphase ultramylonites must have controlled the rheology of these shear zones.

Chapter 3

Quartz deformation in a very fine grained quartzo-feldspathic mylonite:

A lack of evidence for dominant grain boundary sliding deformation[1]

3.1 Introduction

The deformation mechanism of quartzose and quartz framework rocks have been studied in detail in both experimental (e.g. Tullis *et al.* 1973; Jaoul *et al.* 1984; Hirth & Tullis 1992) and natural creep (e.g. White 1973b; 1976; Mitra 1976; Law *et al.* 1984; Behrmann 1985; Knipe and Law 1987; Lloyd *et al.* 1992). Intracrystalline plasticity by dislocation processes has been identified as an important deformation mechanism and there is evidence in the literature (White 1973b; 1976; 1977; Bossière & Vauchez 1978; Berthé *et al.* 1979; Watts & Williams 1979; Simpson 1985) that it is one of the main factors controlling the deformation of quartzo-feldspathic granitoid rocks. It has been shown (e.g. White 1976; Etheridge & Wilkie 1979; Behrmann 1985; Lloyd *et al.* 1992) that with a decrease in grain size, the deformation mechanism in some cases changes from grain-size-insensitive to grain-size-sensitive flow with a major contribution of grain boundary sliding, a type of behaviour sometimes tentatively called superplasticity.

Behrmann (1985) inferred that this change occurred, in quartzite, at a grain size of 10 μm at temperatures around 250 - 400°C, from a switch in the relation between dislocation density and grain size from proportional to inverse. Other microstructural criteria often used to infer grain boundary sliding include (i) a diamond or blocky grain shape (White 1977; Drury & Humphreys 1988), (ii) a continuous alignment of grain boundaries over several grain diameters (White 1977; Stünitz & Fitz Gerald 1993), iii) high dislocation densities at triple junctions, (iv) a grain size comparable to or smaller than the equilibrium subgrain size (White 1977; 1979b; Gapais & White 1982), (v) an inverse relation between finite strain and grain size (Evans *et al.* 1980), (vi) grain boundary voids at triple junctions (White 1977; Behrmann 1985) and (vii) a grain size generally less then 10 μm (Boullier & Gueguen 1975; White 1977; Behrmann 1985). In addition, any crystallographic preferred orientation (CPO) generated should be weak (Padmanabhan & Davies 1980, pp 111 - 117; Rutter *et al.* 1994) and there should be no crystallographic relation between adjacent grains due to grain rotations and neighbour switching events which accompany grain

[1] Reprinted from Journal of Structural Geology, 17, 1095 - 1109, Fliervoet, T.F. & White, S.H., Quartz deformation in a very fine grained quartzo-feldspathic mylonite: A lack of evidence for dominant grain boundary sliding deformation,

boundary sliding (Beeré 1978). However, the textural[2] and microtextural[2] evidence is difficult to obtain, especially in multiphase rocks, and there is uncertainty about the role of grain boundary sliding deformation in fine grained rocks.

Aims and approach

The aim of the present chapter is to determine the dominant deformation mechanism operative within the very fine grained (2.3 μm) quartz bands of the type 2 shear zone described in Chapter 2. A microstructural[2] and microtextural[2] study, using both optical and transmission electron microscopical techniques, has been performed. A new microtextural technique using TEM, has been employed to obtain crystal rotation data between adjacent grains in order to assess whether grain boundary sliding has contributed significantly to the deformation.

3.2 Experimental techniques

Detailed light optical studies were first undertaken on thin sections from fine and coarse grained zones within the mylonite and *c*-axis orientations were measured, where grain size permitted, by traditional universal stage techniques. Following these studies, electron-transparent foils (thickness < 1 μm) of selected areas from the thin sections from the fine grained zones were prepared by ion-beam thinning. After thinning, the specimens were coated with a thin carbon layer to eliminate sample charging during observation. Transmission electron microscopy (TEM) analyses were carried out on a Philips CM20 operating at 200 kV. The TEM observations were made in standard bright-field (BF) and diffraction modes (*cf.* McLaren 1991). A double-tilting goniometer stage capable of giving ± 30° of tilt about two orthogonal axes was used in all cases. Wherever possible, imaging was done under dynamical 2-beam diffraction conditions.

The TEM has been used to measure the CPO of quartz in the very fine grained zones, this technique has been used previously by Gapais & White (1982) and Mawer & Fitz Gerald (1993). Despite the drawback that only a small volume can be measured, a fuller description of the CPO can be obtained in contrast to the U-stage method, i.e. both the orientation of the *c*- and the *a*-axes can be determined. However, because no record was made of intensities of in-equivalent reflections (e.g. *r* vs. *z*), the diffraction symmetry of the quartz crystals was effectively treated as hexagonal (Mainprice *et al.* 1993; Mawer & Fitz Gerald 1993). These are drawbacks when compared to SEM based techniques such as channelling patterns and electron back-scatter diffraction (Schwarzer & Weiland 1988; Schwarzer 1990; Forwood & Clarebrough 1991; Lloyd *et al.* 1992; Mainprice *et al.* 1993; Randle 1992; 1993), but these SEM techniques provide only limited data on the intra- and inter-grain defect structures. TEM can provide unique information on the correlation between the defect structure induced by deformation and the CPO.

The grain orientation measurement involved tilting the specimen so that a low index zone axis was parallel to the electron beam; the diffraction pattern and tilt angles were

[2] Terms as defined in Chapter 1

recorded [for more details on the technique the reader is referred to Edington (1974) and McLaren (1991)]. The diffraction patterns were obtained using 'microdiffraction' techniques outlined by McLaren (1991). The orientation of an individual grain is uniquely determined from the zone axes parallel to [*c*], <*a*>, or normal to m, while for other cases at least two zone axes must be measured. Tilting errors were reduced by rotating into the low index zone from the same direction (i.e. always clockwise or counter clockwise). The accuracy of the measurement is estimated at 2 - 3° (Schwarzer & Weiland 1988).

The grain and subgrain diameters were determined by taking the averages of the long and short axes directly from the micrographs and were subsequently corrected for sectioning effects using a factor 1.2 (*cf.* Underwood 1970). Measurements of numbers of free dislocations were carried out by counting dislocation terminations in a constant area ($\approx 0.5\ \mu m^2$) of the micrograph. Up to 100 subareas were counted in each foil studied, revealing large variations between the subareas. To avoid low counts, very thin areas in the foils were neglected. The free dislocation density is defined by the number per unit area of all linear lattice defects which appear not to be bound in subgrain walls or dislocation tangles. In the analyses a random distribution of the dislocation lines has been assumed (*cf.* Underwood 1970).

As all of the grain size, subgrain size and dislocation density reveal lognormal or positively skewed distributions (Ranalli 1984; Clark & Hosking 1986), the median (Md) of the distribution was taken as a measure of the grain size, subgrain size and dislocation density; half the inter-quartile range is taken as a measure of variability, the skewness (Sk) and kurtosis (Km) are given to characterise the spread of data around the median.

Rapid irradiation damage prevented direct characterisation of dislocation Burgers vectors (see Ardell *et al.* 1973; 1974). The $\mathbf{g}.\mathbf{b} = 0$ and the $\mathbf{g}.\mathbf{b} \times \mathbf{u} = 0$ criteria (*cf.* McLaren 1991) could not be used, as irradiated dislocations have a radial displacement or strain field, which has no unique relation to the original Burgers vector.

3.3 Optical microstructures & textures

Detailed studies concentrated on the fine grained zone shown in Fig 2.5(c) (Chapter 2) with comparative studies in the surrounding coarser grained zones. The mylonite consists of porphyroclasts (up to 20% of the rock volume) of K-feldspar, plagioclase and epidote embedded in a very fine grained foliated matrix (Figs. 3.1a - c). The foliation is defined by the alignment of biotite flakelets. Inferred deformation conditions are at upper greenschist facies (*cf.* Obee & White 1985; Shaw & Black 1991; Chapter 2). The porphyroclasts commonly have tails aligned parallel to the foliation.

Within both the fine and the coarse grained parts of the mylonite, most of the quartz occurs in discrete zones 10 - 200 μm thick (sub)parallel to the foliation (Figs. 3.1a - c), which alternate with continuous bands of finer grained K-feldspar, plagioclase, biotite, quartz ± epidote. Most of the K-feldspar and plagioclase clasts are embedded within such bands, suggesting that the latter originated from the porphyroclasts and have been simply rolled out by progressive deformation

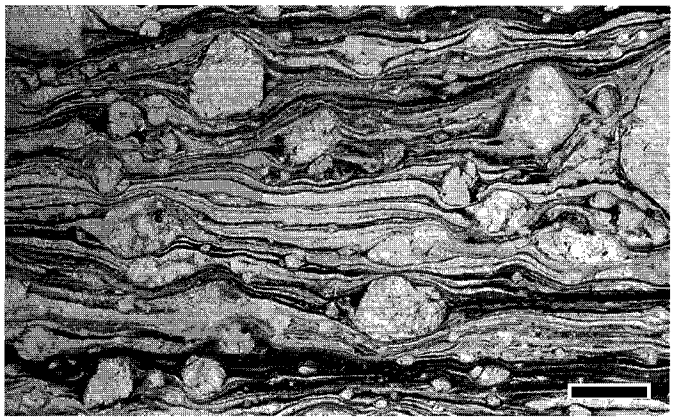

(a) Large porphyroclasts of plagioclase, K-feldspar and epidote embedded in a matrix of finer grained bands of K-feldspar, plagioclase, quartz and biotite ± epidote, alternating with quartz bands in a fine grained mylonite. Scale bar: 300 µm.

(b) Quartz bands with domains of elongated quartzes with similar *c*-axes parallel to the main foliation. Scale bar: 25 µm.

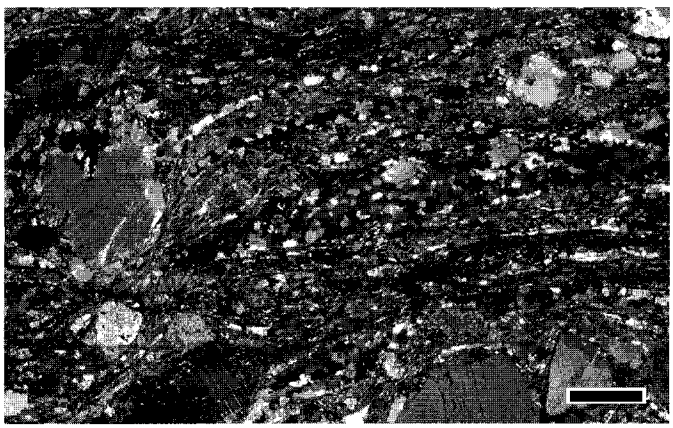

(c) Low strain zone: note that the clast size and the grain size of quartzes are 10 - 20 times larger than in the high strain bands in (a). Scale bar: 100 µm.

Fig. 3.1 Optical photomicrographs of a fine grained part (a and b) and of a hosting mylonite (c) of type 2 shearzone

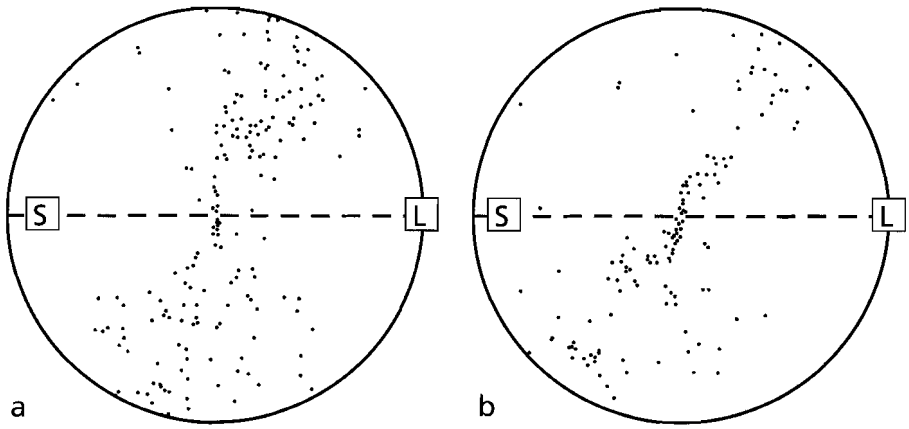

Fig. 3.2 Quartz *c*-axis fabrics, optical measurements. (a) Coarse grained zones (*cf.* Fig. 3.1c); N = 190. (b) Fine grained zones (*cf.* Fig. 3.1b); N= 144. The foliation (S) is horizontal with the extension lineation (L) at the edge of the fabric diagram.

accompanied by chemical reactions. This implies that the fine grained parts are the higher strained equivalents of the coarse grained parts and arose because of strain partitioning (see also Chapter 2). So, the size and number of porphyroclasts decreases with increasing strain and the grain size of quartz reduces from 30 - 50 μm (Fig. 3.1c), to below 10 μm (see next section).

The grains within the quartz ribbons occur in domains oblique to the foliation with similar *c*-axis orientation. Within the fine grained parts of the mylonite these domains have a size between 10 and 30 μm (Fig 3.1b) and show a very fine, patchy undulatory extinction. The individual domains are elongated and may be (sub)parallel (Fig. 3.1b) or oblique (up to 25°) to the main foliation. The quartz domains of the fine grained parts show a *c*-axis pattern similar to, but stronger than, that of the quartz grains from the coarse grained parts (Fig. 3.2). The *c*-axis textures are asymmetric type 1 girdles with respect to the foliations (Lister 1977), with a high density of *c*-axes in the centre of the pole figure. The sense of asymmetry is consistent with a reverse movement in the shear zone. The pole figures are similar to quartz *c*-axis textures previously measured in similar rock types along the Redbank Deformed Zone (Obee & White 1986).

3.4 Electron Microscopy

The deformation microstructures of quartz from the fine grained zones of the mylonite (*cf.* Figs. 3.1a & b) have been studied using TEM. At this scale (Fig. 3.3), the individual grains are elongate with a grain size ranging from 1 - 10 μm (Md: 2.3 ± 0.8 μm; Sk: 1.7; Km: 2.6). This grain size is much less than the thickness of an optical thin section and can account for the patchy undulatory extinction observed with the optical microscope. The free dislocations within the

Fig. 3.3 Composite electron micrograph (BF) showing the microstructure of the quartz in a fine grained part of the mylonite zone. The larger grains are elongated parallel to the foliation and have well formed subgrains and high dislocation densities. The smaller grains consistently have a lower dislocation density and exhibit, if present, a disorganized cell structure. A line drawing of this area is given in Figs. 3.8 and 3.10. Scale bar: 2 μm.

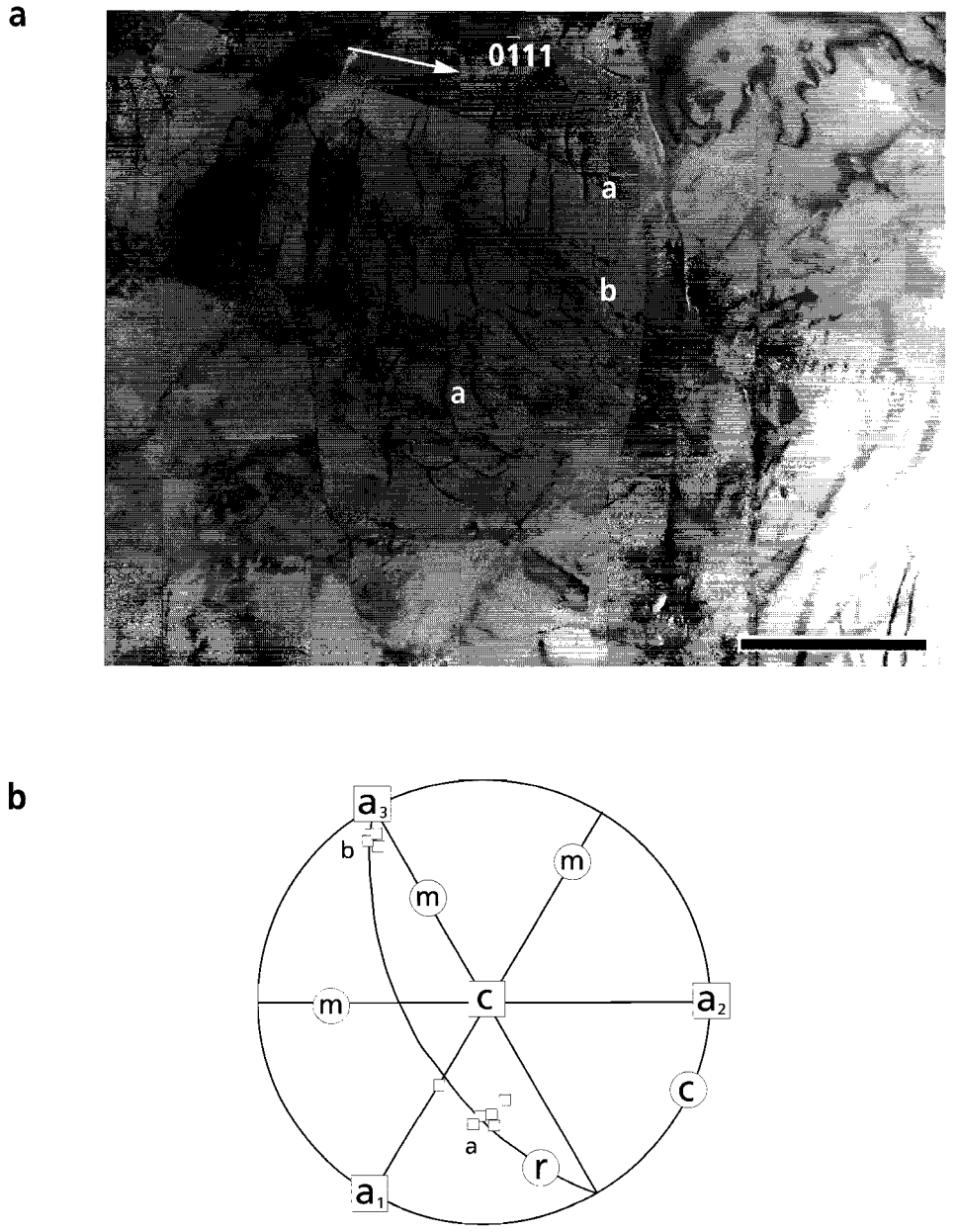

Fig. 3.4 (a) Composite electron micrograph (BF) showing dislocations within a larger grain Scale bar: 1 μm (b) Stereogram showing the orientation of the dislocation lines (labelled a & b) which lie on a rhombohedral plane (marked *r*)

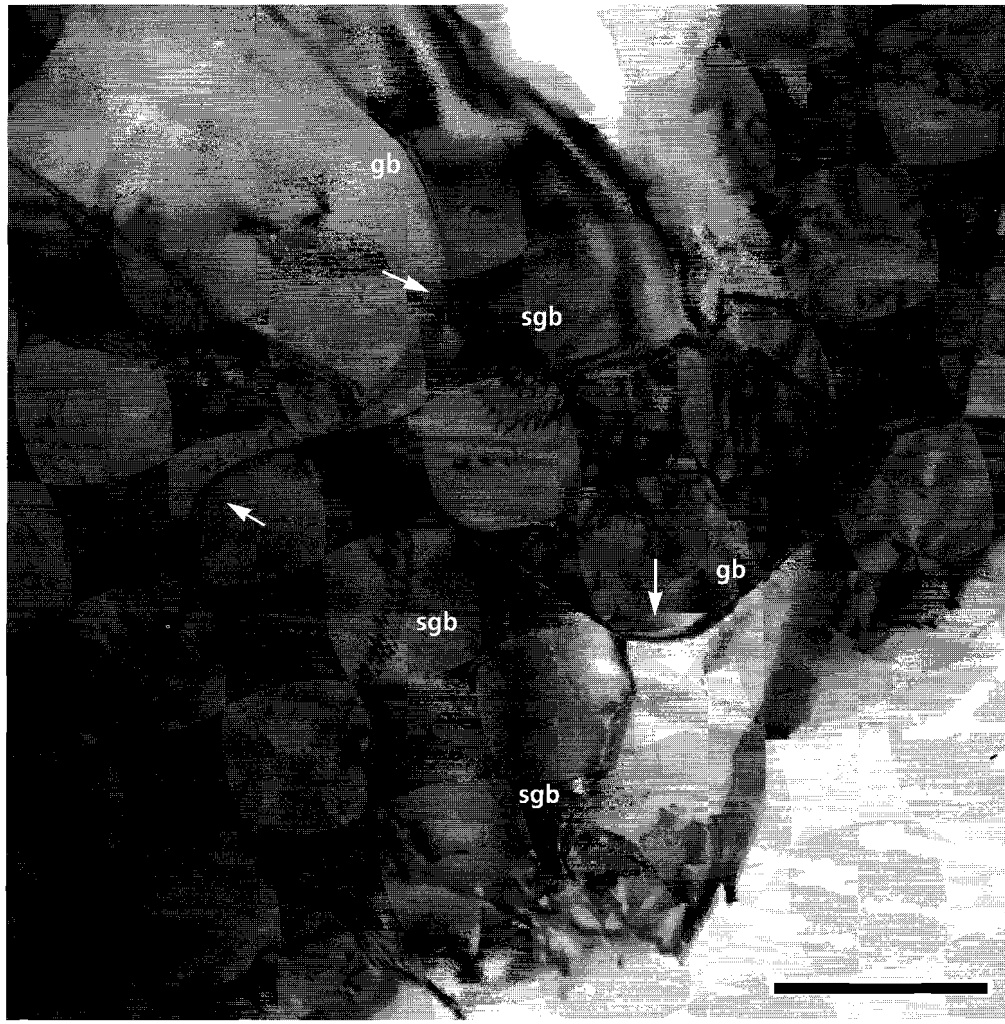

Fig. 3.5 Composite electron micrograph (BF) showing details of typical grain boundaries encountered. Both curved and straight grain boundaries occur. The curved boundaries (arrowed) bow towards regions of high defect densities; the region behind the curvature is virtually defect free. Note the lack of voids (bubbles) along the grain boundaries especially at triple points and at grain boundary - subgrain boundary intersections. **gb**: grain boundary; **sgb**: subgrain boundary. Scale bar: 1 μm.

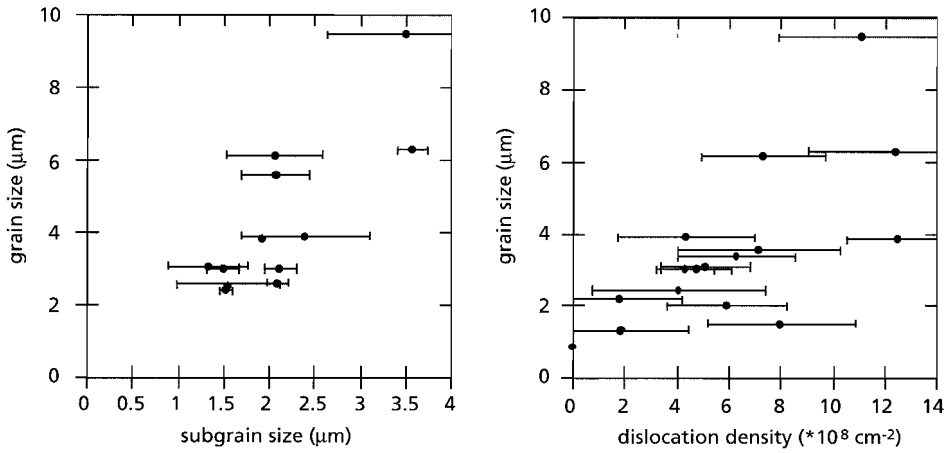

Fig. 3.6 Variations of dislocation density (a) and subgrain size (b) with grain size for the studied quartz band.

larger grains (typically > 2.5 μm) are either curved or straight (Fig. 3.3) and tangles resulting from interacting dislocations are observed. These larger grains commonly have well formed slightly curved and straight low angle subgrain boundaries which are preferentially aligned either parallel or perpendicular to the direction of grain elongation (Fig. 3.3).

The free dislocation densities (Md: 6.5 ± 2.8 x 10^8 cm^{-2}; Sk: 0.3; Km: -0.6) and subgrain sizes (Md: 2.1 ± 0.6 μm; Sk: 0.7; Km: -0.3) vary inhomogeneously throughout the sample (Fig. 3.6) with a general association of higher dislocation densities and larger subgrains with the larger grains and lower densities and smaller or no subgrains with the smaller grains (Fig. 3.6). Trace analyses of curved dislocations and dislocation loops were carried out and revealed that these dislocations commonly lie on rhombohedral crystallographic planes (Fig. 3.4) and, less commonly, on basal planes. The data presented in Fig. 3.4 is typical for all grains studied. Small bubbles are present on many dislocations and dislocation junctions.

Commonly, the high angle grain boundaries are approximately straight and (sub)parallel to the grain elongation. Small bubbles and voids do occur at the grain boundaries but are not common. Curved high angle grain boundaries are observed which bow towards a region of high defect density: i.e. a dislocation network or towards a tangle of dislocations (Fig. 3.5). The region behind the curvature commonly has a lower defect density. This observation suggests that grain boundary migration has occurred (*cf.* Beck & Sperry 1950; White 1976).

3.5 Microtexture analyses

Crystallographic Preferred Orientation (CPO)

The results of the CPO analyses of quartz from a fine grained zones using TEM are shown in Fig. 3.7; three different areas were analysed. The grain elongation in the areas studied is sub-

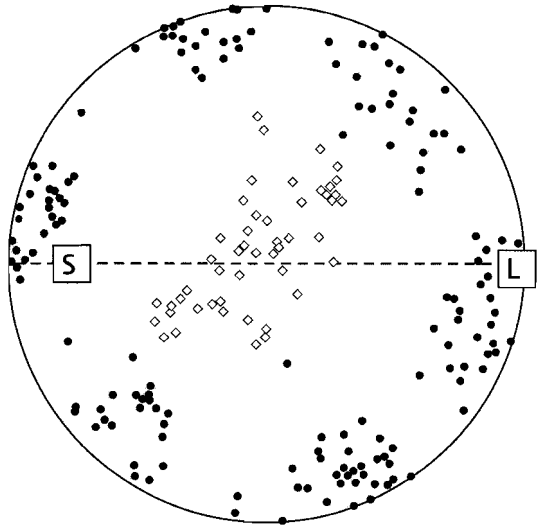

Fig. 3.7 Pole figure showing the crystallographic preferred orientation of *c*- and *a*-axes of quartz from a fine grained band measured using TEM. The foliation is marked S and the stretching lineation is marked L. N = 50; *c*-axes: open symbols; *a*-axes: closed symbols.

parallel to the foliation seen optically. Both the *c*- and *a*-axes reveal a strong preferred orientation. The *c*-axes lie on a great circle girdle asymmetrically arranged to the foliation, the *a*-axes occur in 3 distinct maxima, with one about 20° off the optically determined lineation. The texture measured with the TEM is similar to the one obtained optically from the quartz domains from the fine grained bands (Fig. 3.2b). The main difference is the absence of *c*-axes lying at high angles to the foliation. This is probably due to preferred sampling, in TEM, of grains with a *c*-axis perpendicular to the plane of the section, which is a high density measured optically (Fig 3.2b).

The measured texture shows many similarities with ones measured by Schmid & Casey (1986) in upper greenschist to lower amphibolite facies coarse grained tectonites (*cf.* their specimens CC1 and P248). The latter show a tendency for the high density area of *c*-axes to spread along a great circle girdle, somewhat inclined to the macroscopic fabric axes, i.e. the foliation and lineation. A strong *a*-axis maximum at the margin of the pole figure is situated at an angle of less than 30° to the lineation. The microstructure (White *et al.* 1978) of CC1, a coarse grained (> 30 μm) mylonite is characterised by nearly equant grains with well equilibrated grain boundaries and dislocation substructures indicative of dislocation creep processes being important in the deformation (White *et al.* 1978).

Axes and angles of finite misorientation

When using the TEM to measure the CPO, information about all the crystallographic directions can be obtained. This allows the relationship between two adjacent grains or subgrains to be determined by means of an axis and angle of (finite) misorientation (Randle & Ralph 1986;

Randle 1992); the axis of misorientation is a direction which is common to both the adjacent grains or subgrains and about one must be rotated, by the angle of misorientation, in order to achieve the orientation of the other (Turner & Weiss 1963; Randle & Ralph 1986). This axis of misorientation becomes the axis of external rotation (*cf.* Turner & Weiss 1963, p. 328) if one of the crystals is fixed with respect to an external reference frame.

There are two basic approaches for the determination of axis/angle pairs from diffraction patterns. The first approach relies on standard crystallographic procedures and involves bisecting the angles between corresponding crystallographic planes of adjacent grains or subgrains (for details see Turner & Weiss 1963, p.328; Randle & Ralph 1986). The second method, and the one used in this study, characterises the misorientation by a 3 x 3 orthonormal matrix whose columns represent the direction cosines of the first grain referred to the second grain (for details see Randle 1992; 1993).

Quartz was treated as possessing hexagonal symmetry, and therefore there are 12 crystallographically equivalent ways of indexing each grain, and 144 ways of expressing the misorientation (Grimmer 1980). These misorientations occur in groups of 12, with members of each group having the same angle of misorientation and rotation axes which are symmetrically equivalent. Consequently, a misorientation between two hexagonal grains can be described in 12 different - but equivalent - ways, which in turn give 12 solutions of the axis/angle pair (Grimmer 1980; Forwood & Clarebrough 1991; Randle 1993). Any of these 12 misorientations may be chosen as they are physically indistinguishable. Commonly, the axis/angle pair giving the smallest possible rotation is chosen as the misorientation (see also Randle & Ralph 1986; Randle 1992; 1993; Mainprice *et al.* 1993) and this is the approach adopted in this study.

Because the accuracy in the CPO data is 2° - 3°, the measured axis/angle pair of misorientation may deviate from its true value. This error depends on the angle of misorientation between the two crystals: for large angles (> 10°), the possible error in both the axis and the angle is 5°, but for smaller angles (< 10°) the possible error in the axis is increased to about 10 - 12°, while the error in the angle remains 5°.

A detailed analysis of the axes/angles of finite misorientation for a quartz band area (*cf.* Fig. 3.3) is given in Figs. 3.8 - 3.11. Figure 3.9 shows the angles of finite misorientation between adjacent grains and subgrains measured along three foil traverses as indicated in Fig. 3.8, one parallel (traverse I) and two perpendicular (traverses II and III) to the grain elongation. In the profiles, the angles of finite misorientation are presented with respect to the orientation of the first grain and are cumulative. Looking down the axis of finite misorientation, the angle of finite misorientation is taken negative for a counter clockwise and positive for a clockwise rotation. For example, in traverse II, at the boundary k, grain 7 has an angle of finite misorientation with grain 3 of +44 °; across boundary l grain 8 makes an angle of +8° with grain 7 and 52° with grain 3. At boundary p, grain 4 has an angle of finite misorientation with grain 3 of +11°. The trajectories along which the *c*- and *a*-axes of the grains and subgrains rotate are shown on the stereographic plots in Fig 3.9.

As can be seen in traverse II in Fig. 3.9, the misorientation between adjacent grains is very variable. The angle of finite misorientation changes in sign and magnitude across the profile, so

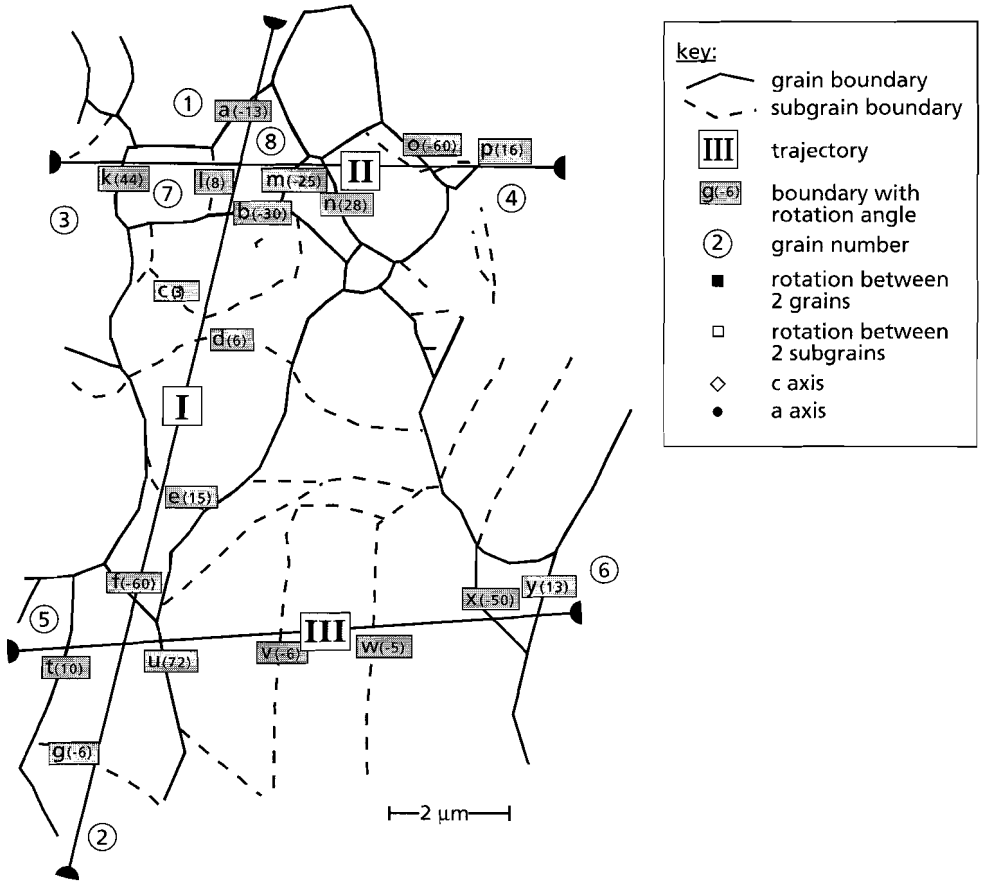

Fig. 3.8 Microtextural analyses of lattice misorientations across grain and subgrain boundaries of a quartz band area. Line drawing is after the composite electron micrograph given in Fig 3.3. Three trajectories (I, II, III), along which the angles of misorientation have been measured are indicated. Individual boundaries are marked a to y, the number accompanying each boundary is the angle of misorientation, positive angles are clockwise when looking down the axis of misorientation and negative if counterclockwise.

that the cumulative angle shows a spiky pattern. Within one grain however, the finite misorientation shows a progressive increase (traverse I between boundaries b and f) or decrease (traverse III between boundaries u and x), with all of the walls having a similar sense of misorientation.

The axial distribution analysis (A.V.A.) of c-axis preferred orientation (Fig. 3.10) shows the presence of domains which are elongated parallel to the foliation and are comparable in size and shape to the domains seen optically (Fig. 3.1b). The traces of the axes of finite misorientation between adjacent grains and subgrains are shown in this A.V.A. as arrows. The length of the arrow in Fig. 3.10(a) corresponds to the plunge of the axis in the stereographic plot (Fig. 3.11), i.e. the larger the arrow the smaller the plunge.

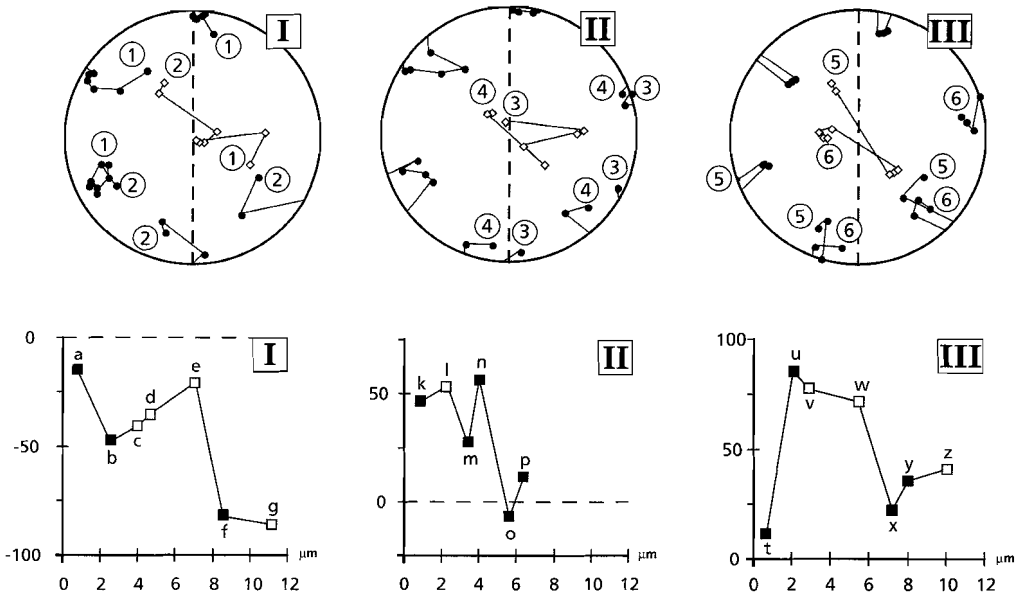

Fig. 3.9 A stereographic plot of the c- and a-axes and a profile along each trajectory marked in Fig. 3.8. The numbers refer to grains shown in Fig. 3.8. The profiles present the angles of finite misorientation with respect to the orientation of the first grain. Key as is Fig. 3.8 (see text for discussion).

The axes of misorientation measured between grains and subgrains within the A.V.A domains (Fig 3.11a) show a preferred orientation within a great circle girdle lying (sub)parallel to the foliation plane with a high density area in the centre of the pole figure. As can be seen in Fig. 3.11(a) the axes between subgrains (open squares) are (sub)parallel to those between grains (filled squares). The axes measured between grains of different A.V.A. domains however (Fig 3.11b), show a strong preferred orientation with a maximum lying at the edge of the pole figure inclined 45° to the foliation.

Slip systems

Due to rapid irradiation damage, the Burgers vectors of the dislocations could not be determined. However, if a crystal is divided into subgrains, the geometry of the subgrain boundary (dislocation lines, boundary orientation, axis/angle pair of misorientation) can elucidate the active slip systems, by using Frank's formula (Amelinckx & Dekeyser 1959; Forwood & Clarebrough 1991). Frank's formula states that the axis of misorientation between two subgrains should be perpendicular to the net Burgers vector of the dislocations required to accommodate the misorientation at a subgrain boundary. Any low angle subgrain boundary can be formed with one, two or three dislocation families (Forwood & Clarebrough 1991). Dislocations with the same Burgers vector and the same line direction belong to the same dislocation family. If a

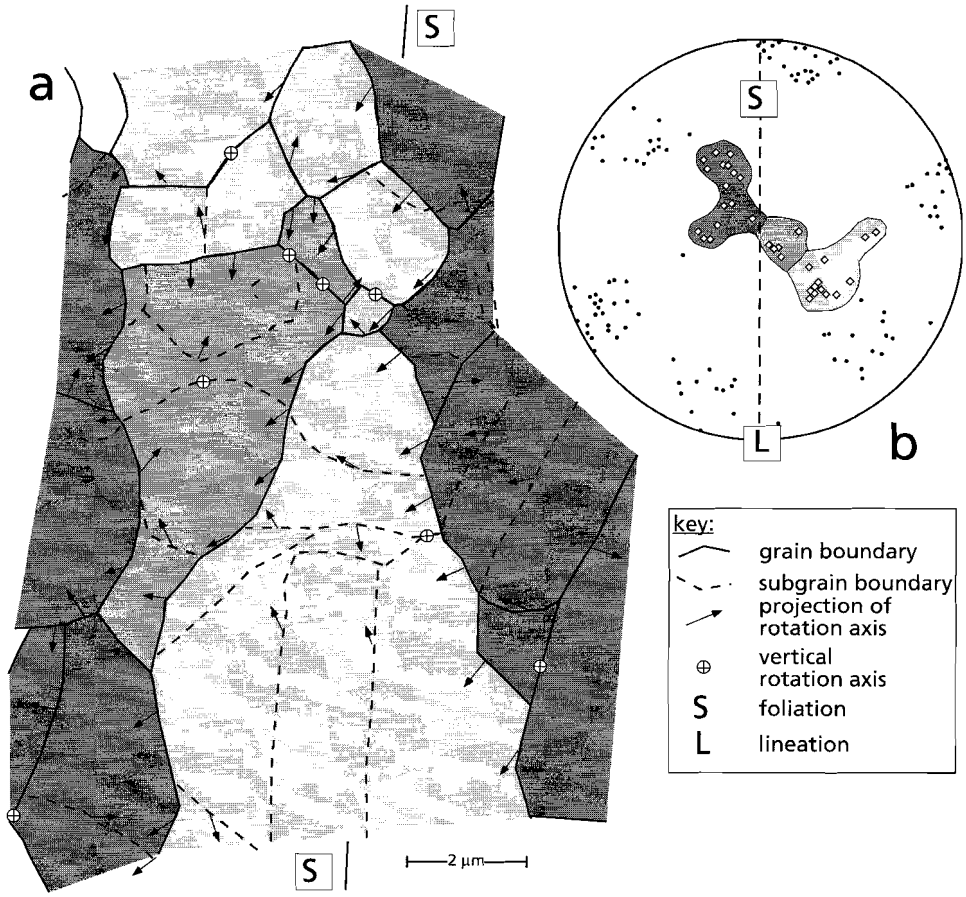

Fig. 3.10 (a) Axial distribution analysis (A.V.A.) diagram of the same area as Figs. 3.3, 3.8 and 3.9, the shading of the different grains and subgrains reflects the grains position in the CPO diagram given in (b). Traces of axes of finite misorientation between adjacent grains and subgrains are shown in the A.V.A. Note the domainal microstructure present in the studied area. (see text for discusion).

subgrain wall is composed either of one or two dislocation families or three dislocation families with coplanar Burgers vectors, the axis of misorientation will be perpendicular to all of the Burgers vectors of the dislocations within the subgrain boundary (Amelinckx & Dekeyser 1959; Trepied *et al.* 1980; Forwood & Clarebrough 1991). If the boundary is composed of three families of dislocations with non-coplanar Burgers vectors, then the axis of misorientation is not perpendicular to all of the Burgers vectors. Trepied *et al.* (1980) have shown that three non-coplanar Burgers vectors cannot produce a subgrain boundary in quartz.

With increasing dislocation content, the subgrain wall eventually becomes a high angle grain boundary. If there are no additional rotations arising from grain boundary sliding processes, the axis of misorientation will still be normal to the Burgers vectors in the (former sub)grain boun-

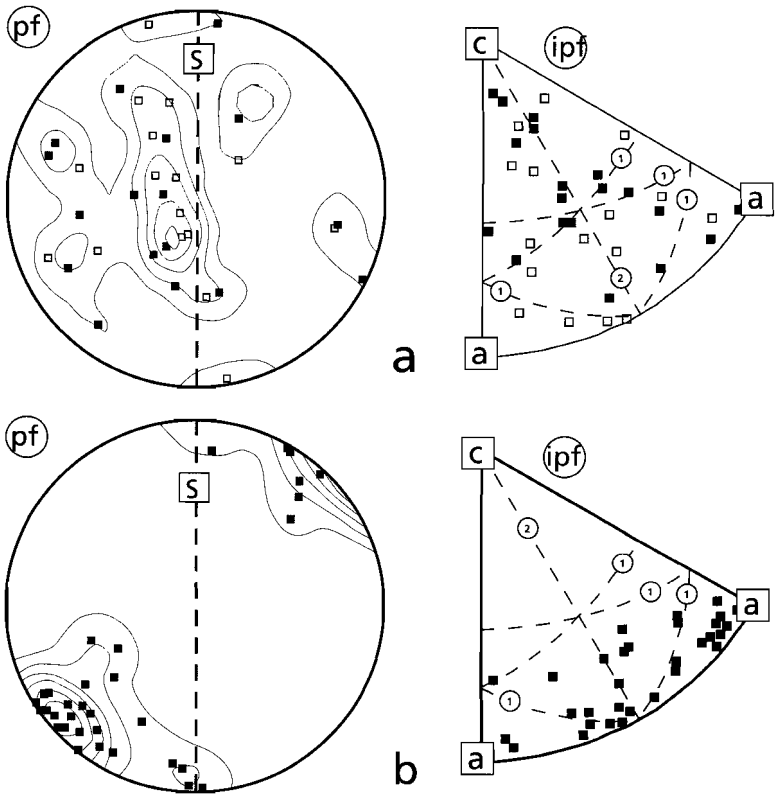

Fig. 3.11 Pole figures (pf) and inverse pole figures (ipf) of the axes of finite misorientation between adjacent grains and subgrains of the same area as Figs. 3.3, 3.8 - 3.10. (a) Axes of misorientation between grains (filled squares) where both belong to the same A.V.A. domain are (sub)parallel to those between subgrains (open squares) and show a preferred orientation in the pf into a girdle parallel to the foliation. Contours are at 1, 2, 3.. times a uniform distribution. In the ipf, the axes show a tendency to lie on great circles prependicular to <*c+a*> (marked 1) or <*a*> (marked 2). (b) The axes between grains from different A.V.A. domains show a strong maxima at the edge of the pole figure inclined at 45° to the foliation. Countours at 1, 3, 5.. times a uniform distribution. Most axes are either (sub)parallel to an *a*-axis or normal to an m plane. (see text for discussion).

dary. For example, if a crystal is misoriented due to <*a*> edge dislocations, the axis of finite misorientation will lie in a plane normal to <*a*>, which is an m plane. To find the Burgers vectors causing the misorientation between two subgrains or two grains involves calculating the angle between the axis of misorientation and any of the known Burgers vectors for quartz, i.e. [*c*], <*a*> and <*c* +*a*> (*cf.* Morrison-Smith *et al.* 1976). This analysis assumes that any purely geometrically necessary dislocation (White 1977) that accommodate the rotations within the subgrain walls are slip dislocations. Frank's formula was successfully applied, in a rigorous form, to slip plane analysis in quartz by Lloyd and Freeman (1991; 1994).

Frank's formula has been applied to the quartz ribbon area presented in Figs. 3.3 and 3.8 - 3.10, and described in the previous sections; the results are shown graphically in inverse pole figures (Fig. 3.11). The axes of misorientation between grains (filled squares) and subgrains (open squares) within the same A.V.A. domain (Fig. 3.11a) both show a tendency to lie on great circles perpendicular to either <*c*+*a*> (marked 1 in Fig. 3.11a) or <*a*> (marked 2 in Fig 3.11a). This suggests that dislocations with <*c*+*a*> and <*a*> Burgers vectors have been operative in accommodating the misorientation between both subgrains and grains within the same A.V.A. domain.

Most of the rotation axes measured between grains of different A.V.A. domains are either (sub)parallel to an *a*-axis or normal to an m plane. Some spread of the axes exists in great circles perpendicular to <*c*+*a*> (marked 1 in Fig. 3.11b) and in a great circle perpendicular to <*a*> (marked 2 in Fig 3.11b). These misorientation relations between grains of different A.V.A. domains were tested against the coincidence site lattice (CSL) theory (see Bollman 1970; Chapter 12) for hexagonal crystals (Bleris *et al.* 1982; McLaren 1986; Grimmer 1989a). The volume ratio of primitive cells for the CSL and crystal lattice is a positive integer Σ, called the multiplicity of the CSL (Grimmer 1989b). The smaller the value of Σ, the larger the coincidence and the better the 'fit' between the grains. In cubic crystals only boundaries with a $\Sigma < 49$ are considered to have a CSL (*cf.* Randle 1993). Brandon's criterion (*cf.* Randle 1993) has been used to calculate the maximum deviation from a CSL orientation. When the misorientation data presented in Fig. 3.11(b) are compared with the CSL relations calculated for quartz (McLaren 1986; his Table 3) it is found that about 80% of the misorientation relations can be described as having a CSL with a Σ value lower than 49. Of these 30% have $\Sigma = 16$ (30° rotation around an *a*-axis), 20% have $\Sigma = 6$ (48.9° rotation around normal to an m plane) and 10% have $\Sigma = 19$ (55.4° rotation around an *a*-axis).

3.6 Discussion

The microstructural and microtextural observations indicate that flow in the fine grained quartz bands of the mylonite studied was due to dislocation creep processes, although the grain size is well below 10 μm (2.3 ± 0.8 μm). The pertinent observations are the presence of dislocations, subgrains and the sharp *c*- and *a*-axis CPO's. The analyses of the axis/angle of finite misorientation between grains indicate that there are no apparent additional rotations, other than those arising from dislocation creep processes. Additional rotations would be expected if grain boundary sliding had contributed significantly to the deformation (Beeré 1978). This view is supported by the results of Lartigue Korinek & Dupau (1994) who measured, using TEM, the axes of finite misorientation between grains in fine grained, superplastically deformed, Mg-doped alumina in which grain boundary sliding had played a prominent role during deformation. They found additional rotations and using their data (their Tables 1 and 2) it is possible to determine that the axes of rotation between grains are not perpendicular to any of the Burgers vectors known for alumina.

The misorientation relations between grains of different A.V.A. domains can be described as CSL relations which are associated with low energy grain boundary structures (*cf.* Gleiter 1982).

It has been shown that CSL relations between grains can have a profound effect on the mechanical and chemical properties of grain boundaries, such as grain boundary migration, grain boundary diffusion, phase transformations and grain growth (*cf.* Gleiter 1982; Forwood & Clarebrough 1991; Peterson 1979; Smith *et al.* 1979; Bishop *et al.* 1979; Randle 1993). Haruna *et al.* (1992) showed that grain boundary sliding is also greatly affected by the presence of CSL boundaries. They compared measured offsets across lead grain boundaries in a superplastically deformed lead-tin alloy with the value of Σ. They observed that grain boundary sliding was difficult at lead grain boundaries with low Σ values, while rather easy at random boundaries with larger Σ values (> 49). It is therefore unlikely that grain boundary sliding has occurred in the very fine grained quartz bands studied here, as 80% of the misorientation relations can be described as having a CSL with a Σ value lower than 49. This fact, plus the rotation data and the presence of characteristic dislocation structures, leads to the conclusion that the dominant deformation mechanism within the fine grained quartz bands was by dislocation creep processes without significant grain boundary sliding. This conclusion is in contrast to that drawn in both the materials science literature (e.g. Padmanabhan & Davies 1980; Gifkins 1982; Langdon 1982; Langdon 1990) and the geological literature (e.g. Boullier & Gueguen 1975; White 1977; Gapais & White 1982; Behrmann 1985), which is, that with grain sizes below 10 μm, the deformation mechanism has a major component of grain boundary sliding with the materials having weak textures.

There is a strong slip component to the dislocation creep involving <*c*+*a*> slip together with <*a*> slip. The role of <*c*+*a*> slip has always been controversial. Although dislocations with a <*c*+*a*> Burgers vector have only rarely been directly confirmed in naturally deformed quartz, they are known to occur experimentally (Baëta and Ashbee 1969a; 1969b; Trepied & Doukhan 1982) in synthetic single crystals of quartz deformed at high temperatures and at differential stresses exceeding 200 MPa. We therefore suggest that <*c*+*a*> slip may take place in high stress environments in nature. Consequently we used microstructural features to get an indication whether the stresses during deformation were abnormally high. There are a number of methods available to determine the paleostress in mylonites deforming by dislocation creep (*cf.* Kohlstedt & Weathers 1980). It has long been known that the size of subgrains and recrystallized grains, and the free dislocation density are related to the magnitude of the differential stress responsible for the deformation of the polycrystal (Twiss 1977; Kohlstedt & Weathers 1980). Dislocation density is highly susceptible to changes in temperature and stress and commonly reflects a later stage stress-free anneal or a late stress pulse (White 1979a). The subgrain size and the recrystallized grain size are better indicators of the paleostress (White 1979a). For grain size, we must also consider the recrystallization mechanism (Twiss 1977; Drury *et al.* 1985). The paleopiezometric relations from Mercier *et al.* (1977) for the recrystallized grain size for quartz with the same recrystallization mechanism as observed in our study, *viz.* a rotation recrystallization mechanism, and from White (1979b) (using the experiments of Ardell *et al.* 1973) for subgrain size have been used to estimate the stress (the equations are given in Chapter 6; Table 6.2). The stresses estimated from the grain size (2.3 ± 0.8 μm) and subgrain size (2.1 ± 0.6 μm) are equal, with 220 ± 40 MPa and 250 ± 65 MPa respectively. That is, the stresses appear to have been of sufficient magnitude to activate <*c*+*a*> slip.

A question arises concerning the softening mechanism that allowed strain partitioning into the very fine grained quartz bands. The usually invoked mechanism of a change to a grain-size-sensitive grain boundary mechanism is not appropriate in this instance (see above). The fine grain size appears to have been maintained by continual recrystallization. The evidence for this comes firstly from the tendency for the larger grains to have higher dislocation densities and well formed subgrains (Fig. 3.6), and secondly, from observations indicative of grain boundary migration (Fig. 3.5). We take these two pieces of evidence to indicate that grain growth occurred via grain boundary migration. As growth continues, the density of the internal dislocations increases and subgrains develop. This increase in internal strain energy and the increasing misorientation of subgrains leads to the preferential recrystallization of the large grains to maintain a quasi steady state grain size. The softening leading to strain partitioning in the very fine grained quartz bands is believed to result from two factors. The first is the continual supply of grains free from dislocations or with low densities of dislocations. The second is due to geometrical softening, because the grains have their lattices reoriented so that their slip planes lie in or near the plane of shear and their slip directions come to lie parallel to the direction of shear (Bouchez 1978; Williams & Dixon 1982; Knipe & Law 1987). The CPO data (Fig. 3.7) indicate that mainly the rhombohedral and prism planes are (sub)parallel to the foliation plane with an *a*-axes maxima close to the lineation. Trace analysis (Fig. 3.4) revealed dominant rhombohedral slip planes, whereas the rotation axes indicated a major contribution of dislocations with <*c*+*a*> and <*a*> Burgers vector to the slip. A strong maximum of <*a*> axes is present near the stretching lineation (Fig. 3.7). Two sets of <*c*+*a*> dislocations on opposite sides of the lineation will result in slip towards the stretching lineation. It is therefore suggested that geometrical softening occurred due to this preferential alignment of rhombohedral planes parallel to the foliation.

The recrystallization mechanism that supplied the new mechanically soft grains and maintained the quasi steady state grain size involved the formation of high angle grain boundaries from low angle subgrain boundaries by a progressive misorientation across subgrain walls (*cf.* Urai *et al.* 1986; Drury & Urai 1990). The coarse grained quartz bands in the lower strain mylonites have c-axis patterns similar to the very fine grained quartz bands from the high strain mylonite studied (Fig. 3.2a & b). The only difference is that the texture is sharper for the latter. The domainal microstructure of the very fine grained (2.3 μm) quartz bands therefore suggests a strong host grain control on the orientation of the newly formed grains. While microstructures indicative of local grain boundary migration have been observed, we have found no evidence for the formation of new strain free nuclei. Similar recrystallization mechanisms in quartz have been reported by White (1973; 1977), Lloyd and Freeman (1991; 1994) and Knipe and Law (1987).

3.7 Conclusions

1) Transmission electron microscopy investigations of the microstructure and microtexture of very fine grained (2.3 ± 0.8 μm) quartz bands in mylonites from the Redbank Deformed Zone of Central Australia, suggest that dislocation creep processes were the dominant deformation mechanism operative with <*c*+*a*> and <*a*> slip being important.
2) Analyses of the axes and angles of finite misorientation between adjacent grains and subgrains indicate that there are no rotations, of the type to be expected if grain boundary sliding had contributed significantly to the deformation.
3) Softening and the maintenance of a quasi-steady state grain size in the fine grained quartz bands was by continual recrystallization. The recrystallization mechanism included local grain boundary migration and the development of high angle grain boundaries from low angle subgrain boundaries by a progressive misorientation across subgrain walls, and resulted in host grain control of the orientation of the recrystallized grains.
4) Stresses operative during the flow of the fine grained mylonite studied have been estimated to be in the range 220 - 250 MPa, which is high. They are however of the magnitude that may be required for the operation of <*c*+*a*> slip.

Chapter 4

Microstructural evidence for dominant grain boundary sliding deformation in polyphase rocks

4.1 Introduction

The result of mylonitization of the granitoids of the Redbank Deformed Zone is the development of an ultramylonitic shear zone centre consisting of a homogeneous mixture of fine grained K-feldspar, plagioclase, quartz and biotite from a (proto)mylonitic precursor (Chapter 2). Strain is observed to be concentrated within the ultramylonite, indicating that these were mechanically softer than the mylonitic country rock they developed in. Strain partitioning within polyphase ultramylonites is commonly found within granitoid shear zones (Watt & Williams 1979; Behrmann & Mainprice 1987; Vauchez 1987; Vernon & Flood 1988; Handy & Zingg 1991; Gilotti 1992; Fitz Gerald & Stünitz 1993; Stünitz & Fitz Gerald 1993). Therefore the mechanical properties of these polyphase ultramylonites will control the rheology of these shear zones.

The inferred softening can be expressed in mechanical terms, as a reduction in stress at a constant strain rate or as an increase in strain rate at a constant stress (*cf.* White *et al.* 1980). Several processes can account for this strain softening, including geometric (or fabric) softening, continual recrystallisation, chemical softening, pore fluid effects, shear heating, reaction softening and a change in deformation mechanism. Details of these processes have been discussed by White *et al.* (1980). Within polyphase granitoid rocks, the main softening processes are thought to be due to metamorphic reactions ("reaction weakening" or "reaction enhanced ductility") (White & Knipe 1978; Rubie 1990; Stünitz & Fitz Gerald 1993) and/or recrystallization processes producing small grains which subsequently deform by grain boundary sliding[1] processes and/or producing new weak (mostly micaeous) phases. Reaction weakening due to the introduction of a mechanically weak phase has been identified in a number of shear zones (e.g. White & Knipe 1978; Brodie 1980; Knipe & Wintsch 1985; Janecke & Evans 1988; Rubie 1990), and is thought to be important under retrograde metamorphic conditions.

The production of a fine grain size from a coarser grained precursor can lead to a change in deformation mechanisms from grain-size-insensitive to grain-size-sensitive flow with a major contribution of grain boundary sliding[1] (White 1976; White & Knipe 1978; Allison *et al.* 1979; Kerrich *et al.* 1980; White *et al.* 1980; Brodie & Rutter 1985; 1986; Behrmann & Mainprice

[1] Terms as defined in Chapter 1

1987; Vauchez 1987; Rutter & Brodie 1988; Rubie 1990; Gilotti, 1992; Stünitz 1993; Stünitz & Fitz Gerald 1993). The microstructural criteria used to infer grain boundary sliding in these polyphase fine grained rocks include: i) a diamond or rectangular grain shape (White 1977; Drury & Humphreys 1988; Stünitz & Fitz Gerald 1993), ii) a continuous alignment of grain and interphase boundaries over several grain diameters (White 1977; Stünitz & Fitz Gerald 1993; Zelin & Mukherjee 1993a; 1993b; 1993d; Zelin *et al.* 1994), iii) open grain and interphase boundaries and voids (Gifkins 1976; Clarke 1987; Perevezentsev *et al.* 1992), and iv) a grain size comparable to or smaller than the equilibrium subgrain size (White 1977; 1979b). In addition, any crystallographic preferred orientation (CPO) generated should be weak (Padmanabhan & Davies 1980, pp 111 - 117; Rutter *et al.* 1994) and there should be no crystallographic relation between adjacent grains due to grain rotations and neighbour switching events which accompany grain boundary sliding (Beeré 1978; Haruna *et al.* 1992).

Aims and approach

The aim of this chapter is to determine the dominant deformation mechanisms operative within the fine grained, polyphase, ultramylonitic shear zone centres of the two shear zones described in Chapter 2. The results of a microstructural and microtextural study, using both scanning and transmission electron microscopy techniques are presented. The main part of this chapter will concentrate on the (coarser grained) type 1 ultramylonites, with comparative studies on the type 2 ultramylonites. The reason for this is that the coarser grained type 1 samples allowed both a SEM and TEM analyses, whereas the grain size of the type 2 samples was too small for SEM work. Furthermore, quartz (micro)texture analyses using TEM were only successful on the type 1 samples (see next section).

4.2 Experimental and analytical techniques

All thin sections of the studied specimens were oriented normal to the foliation and parallel to the lineation and were subsequently prepared for scanning electron microscopy (SEM) and transmission electron microscopy (TEM). For the type 1 ultramylonite, grain size and grain shape analyses were carried out in SEM, while TEM was used for the determination of the interfacial and intercrystalline microstructures. Due to the extremely fine grain size of the type 2 ultramylonite (< 5 μm) SEM could not be performed and TEM has been used to study the microstructure.

Because of the fine grain size and of the polyphase nature of the type 1 ultramylonite, a universal stage attached to an optical microscope could not be used for texture measurements, that is for crystallographic preferred orientations (CPO). Consequently the TEM has been used to measure the CPO of quartz within the polyphase ultramylonite. This has been done previously by Gapais & White (1982), Mawer & Fitz Gerald (1993) (see Chapter 3). Using the TEM to measure the CPO allows the relationship between two adjacent grains and subgrains to be determined by means of an axis and angle of finite misorientation (Randle & Ralph 1986;

Randle 1992). Details of the method are given in Chapter 3. Quartz texture analyses of the type 2 ultramylonite have been attempted, but were not successful because of extremely rapid beam damage. This increase in damage rate is thought to reflect high H_2O contents in the lower metamorphic grade quartz.

Scanning electron microscopy (SEM) analyses were carried out on a CamScan (operating at 15 - 25 kV), using atomic number contrast imaging (for a review see Lloyd & Hall 1981; Hall & Lloyd 1981; White *et al. 1984*). The back-scatter coefficients (η) of the minerals encountered in this research are listed in Table (2.3); they have been calculated using Eq. 2.1 (*cf.* Chapter 2). In the back-scattered SEM images in this chapter, biotite appears as brightest phase, followed by K-feldspar and then plagioclase, the darkest phase is quartz. In order to image the grain and interphase boundaries of the type 1 ultramylonite, polished thin sections were etched at room temperature with HF acid vapour for about 10 - 30 s. In this thesis a boundary between two grains of a similar phase are referred to as grain boundaries (e.g. a quartz-quartz grain boundary), whereas a boundary between two dissimilar phases is called an interphase boundary (e.g. a quartz-plagioclase interphase boundary).

Grain sizes and the orientations of the traces of grain and interphase boundaries have been measured from digitised line drawings of SEM back-scattered images of etched samples; the program NIH Image 1.49 (public domain) has been used for image analysis. The grain diameters were determined by taking the average of the long and short axis of each grain were taken and were subsequently corrected for sectioning effects using a factor of 1.2 (*cf.* Underwood 1970).

Three different measures have been use to specify grain shapes, these are the circularity, elongation and a shape factor, which are defined as follows (see also Davis 1986, pp 342 - 345):

circularity: $$C = \frac{4A\pi}{p^2} \tag{4.1}$$

elongation: $$E = \frac{l}{w} \tag{4.2}$$

shape factor: $$SF = \frac{p_c}{p} \tag{4.3}$$

with A: the area, p: the perimeter, l, w: the long and short axis of the grain, and p_c: the perimeter of a circle having the same area as the grain. Note that a perfect circular grain has C = E = SF = 1.

In order to quantify the average direction of the grain elongation, and the grain and interphase boundary orientation, the vector resultant and the mean resultant length have been calculated (for more details see Davis 1986, pp 314 - 330). The vector resultant quantifies the orientation of the mean elongation or mean grain or interphase boundary orientation; the mean direction (Θ) has been calculated from the vector resultant by standard trigonometry. The mean resultant length ($\bar{R}$) provides information on the dispersion of the measurements. It can range

between 0 (widely dispersed orientations or bimodal distribution) and 1 (orientations are tightly bunched together with a small dispersion). Rayleigh's test of preferred orientation (Davis 1986, pp 321 - 330) has been used to test whether or not the grain and interphase boundaries and the grain elongations show a single preferred orientation. For the number of measurements encountered in this study (> 100), the critical value of R at 5% level of significance is 0.20 (Davis 1986).

Electron transparent foils (thickness < 1 μm) of selected areas from thin sections from the samples of the type 1 and type 2 ultramylonite were prepared by ion-beam thinning. After thinning, the specimens were coated with a thin carbon layer to eliminate sample charging during observation. Transmission electron microscopy (TEM) analyses were carried out on a Philips CM20 operating at 200 kV, with an EDAX DX4 analytical EDS system attached to facilitate mineral identification. The TEM observations were made in standard bright-field (BF), selected area diffraction and microdiffraction modes (*cf.* Hirsch *et al.* 1967; McLaren 1991). A low-background Be double-tilting goniometer stage capable of giving ± 30° of tilt about two orthogonal axes was used in all cases. Wherever possible, imaging was done under dynamical 2-beam diffraction conditions.

Because of the very fine grain size of the type 2 samples, TEM observations were made in conical dark-field (ConDF) imaging mode (*cf.* Harris & King 1994). In ConDf imaging, dark field images are formed by the integration of all electrons that are scattered or diffracted under the same angle but in different directions. The incident beam is tilted by a chosen angle, as for conventional dark-field imaging, and then rotated around the optic axis of the microscope. For grain size determinations, 6 - 8 images were collected at successive rotations around the optic axis. These were superimposed to make line-drawings. Since the material is polyphase, the ConDF technique could not be used to measure the texture of the sample (*cf.* Harris & King 1994).

Measurements of numbers of free dislocations with quartz were carried out by counting dislocation terminations with the foil. The free dislocation density is defined by the number per unit area of all linear lattice defects which appear not to be bound in subgrain walls or dislocation hedges. In the analyses a random orientation distribution of the dislocation lines was assumed (*cf.* Underwood 1970). Rapid irradiation damage prevented direct characterisation of dislocation Burgers vectors (see Ardell *et al.* 1973; 1974). The $\mathbf{g.b} = 0$ and the $\mathbf{g.b} \times \mathbf{u} = 0$ criteria (*cf.* Hirsch *et al.* 1967) could not be used on these samples, as irradiated dislocations have a radial displacement or strain field, which has no unique relation to the original Burgers vector. Grain and subgrain boundary orientations have been measured by tilting the boundary in a vertical position, i.e. parallel to the incident electron beam (*cf.* Forwood & Clarebrough 1991); the image and the tilt angles were recorded. Errors are estimated at 5 - 10° (Forwood & Clarebrough 1991). Standard trace analyses techniques have been used to obtain the orientation of the boundary in crystal coordinates [for more details on the technique the reader is referred to Edington (1974) and Forwood and Clarebrough (1991)].

In TEM the image formed is a 2-D projection of the 3-D objects in the specimen. Consequently the number of bubbles per unit volume can only be determined if the thickness of the TEM sample is known. The thickness was determined by rotating a planar defect, such as a grain boundary, parallel to the electron beam. After rotating the specimen through a mea-

sured angle, the distance between the top and bottom intersections of the planar defect within the foil, and thus the thickness could be determined (Hirsch *et al.* 1967; De Bresser 1991). The average volume around an bubble in which no other bubbles occur is defined as the inverse of the number of bubbles per unit volume; to facilitate calculations, this volume is assumed to be spherical. As a measure of average spacing between objects, twice the radius of such a sphere has been taken, and can be expressed as:

average bubble spacing: $$L = 2 \times \sqrt[3]{\frac{3At}{4\pi B}} \qquad (4.4)$$

with: A: area, t: specimen thickness, B: number of bubbles counted in the volume defined by A.t. Bubbles were imaged using various 2-beam conditions; these images were subsequently superimposed to make line drawings.

As, generally all of the grain size, dislocation density, bubble size and bubble spacing show lognormal distributions (Ranalli 1984; Clark & Hosking 1986; Davis 1986), the median (Md) of the (normal) distribution was taken as a measure of the grain size; half the interquartile range is taken as a measure of variability; the skewness (Sk) and kurtosis (Km) are given to characterise the spread of data around the median.

4.3 SEM microstructures of a type 1 ultramylonite

As shown in Chapter 2, the ultramylonitic centre of the type 1 shear zone consists of (few) porphyroclasts of K-feldspar (Or 92.6), plagioclase (An 38.3), garnet ± epidote embedded in a fine grained homogeneous matrix (Fig. 2.7b & 2.8c). The matrix has a modal mineral content of 40% quartz, 25% K-feldspar (Or 94.0), 25% plagioclase (An 37.7) and 10% biotite, although locally the biotite content might be up to 20%. A summary of the microstructural elements is provided in Table 4.1.

The grain sizes of the minerals are uniformly small. That of the biotite is 5.4 ± 2.4 μm (Sk: 0.60; Km: 0.70) K-feldspar is 6.5 ± 2.5 μm (Sk: 0.72; Km: 1.08) plagioclase is 6.8 ± 3.7 μm (Sk: 1.04; Km: 0.54) and quartz is 10.8 ± 3.6 μm (Sk: 0.39; Km: -0.47). The grains have a rectangular to square grain shape (Figs. 4.1 & 4.2a), and are elongated (sub)parallel to the long axes of the mica laths, which define the foliation (Fig. 4.2b). The is no major difference between the grain shapes of the plagioclase, K-feldspar and the quartz grains as expressed by their circularity, elongation and shape factor (Table 4.1). The elongation of quartz grains (E = 1.51 ± 0.29) is somewhat less compared to the elongation of the plagioclase (E = 1.75 ± 0.44) and K-feldspar (E = 1.85 ± 0.43). Small domains of only plagioclase or K-feldspar or of a two feldspar mixture are occasionally observed within the ultramylonite. These domains have grain sizes (5 - 11 μm) similar to those of the quartz-feldspar bands in the (proto)mylonitic rocks (see Chapter 2) and to those of the 4-phase matrix, suggesting that the feldspar grain sizes are stable. The quartz grain

Table 4.1 Summary of microstructural parameters of a type 1 ultramylonite.

	K-feldspar	plagioclase	quartz	biotite
D	6.5 ± 2.5	6.8 ± 3.7	10.8 ± 3.6	5.4 ± 2.4
Sk	0.72	1.04	0.39	0.60
Km	1.08	0.54	-0.47	0.70
vol.%	25	25	40	10
$\Theta - \Theta_m$	3	16	-14	0
$\bar{R}$	0.44	0.54	0.24	0.72
C	0.78 ± 0.11	0.78 ± 0.09	0.80 ± 0.05	0.65 ± 0.16
E	1.85 ± 0.43	1.75 ± 0.44	1.51 ± 0.29	2.85 ± 1.15
SF	0.88 ± 0.06	0.89 ± 0.05	0.90 ± 0.03	0.81 ± 0.09
N	170	134	158	245

	K-K	P-P	Q-Q	B-B
$\Theta - \Theta_m$	11	11	-16	1
$\bar{R}$	0.09 (*)	0.21	0.11 (*)	0.56
N	97	111	129	157

	K-P	K-Q	K-B	P-Q	P-B	Q-B
$\Theta - \Theta_m$	9	5	2	0	2	-18
$\bar{R}$	0.14 (*)	0.09 (*)	0.42	0.07 (*)	0.22	0.06 (*)
N	117	194	216	180	127	257

key: Q: quartz, K: K-feldspar, P: plagioclase, B: biotite, D: grain size in μm, C: circularity, E: elongation, SF: shape factor, Q - Q_m: angle with respect to mica elongation, $\bar{R}$: mean resultant length, (*) denotes that the mean resultant length is not significant; N: number of measurements

size however, is much smaller than that of the pure quartz bands (60 ± 19 μm, see Chapter 2).

The orientation distributions of the grain and interphase boundaries are shown in pole figures in Fig. 4.3. Both the grain and interphase boundaries show a preferred alignment parallel to the foliation with a second alignment perpendicular to this direction. Due to this bimodal distribution, the mean resultant length ($\bar{R}$) is generally small. Long grain boundaries occur mainly parallel to the foliation (Fig. 4.2a). Many grain and interphase boundaries are interlinked parallel to the foliation and are continuously aligned across several grain diameters (Fig. 4.2a). However, as can be seen in Fig. 4.2(a), not all grain and interphase boundaries link up and the continuous boundaries have a limited extend (up to 100 μm). The average length of these continuous boundaries is 37 ± 18 μm; with an average grain size between 5 - 11 μm, there are 4 - 6 grains adjacent to such a continuous boundary. The average spacing between these continuous grain boundaries is 16 ± 4 μm, which equals 2 - 3 grain diameters.

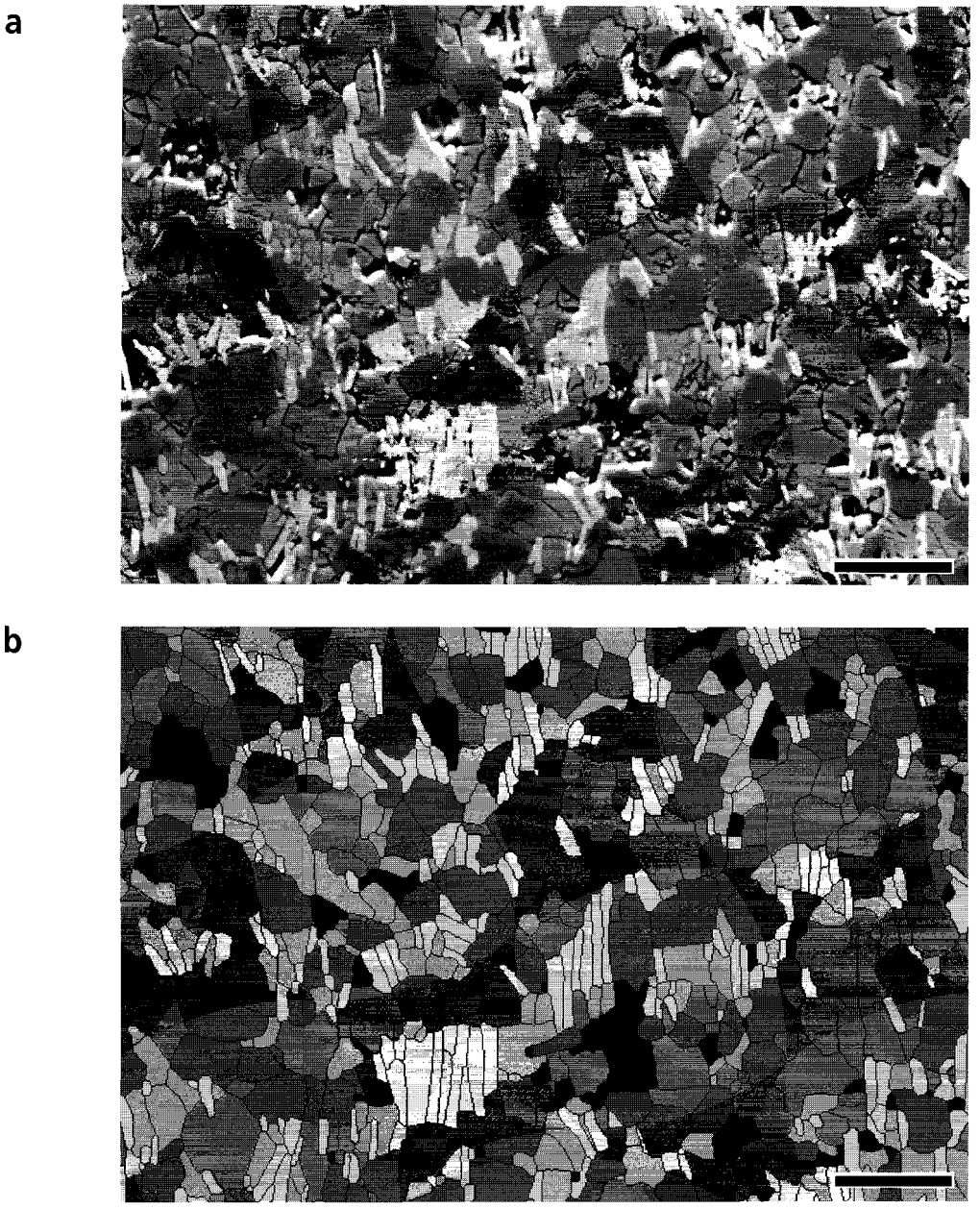

Fig. 4.1 (a) Back-scattered electron micrograph of a polished and etched matrix of a type 1 ultramylonitic shear zone centre. In order of brightness: biotite (brightest), K-feldspar, plagioclase and quartz (darkest). Holes arein the sample are shown in black. Foliation is parallel to the short side of the micrograph. Scale bar: 30 μm. (b) Line drawing after (a).

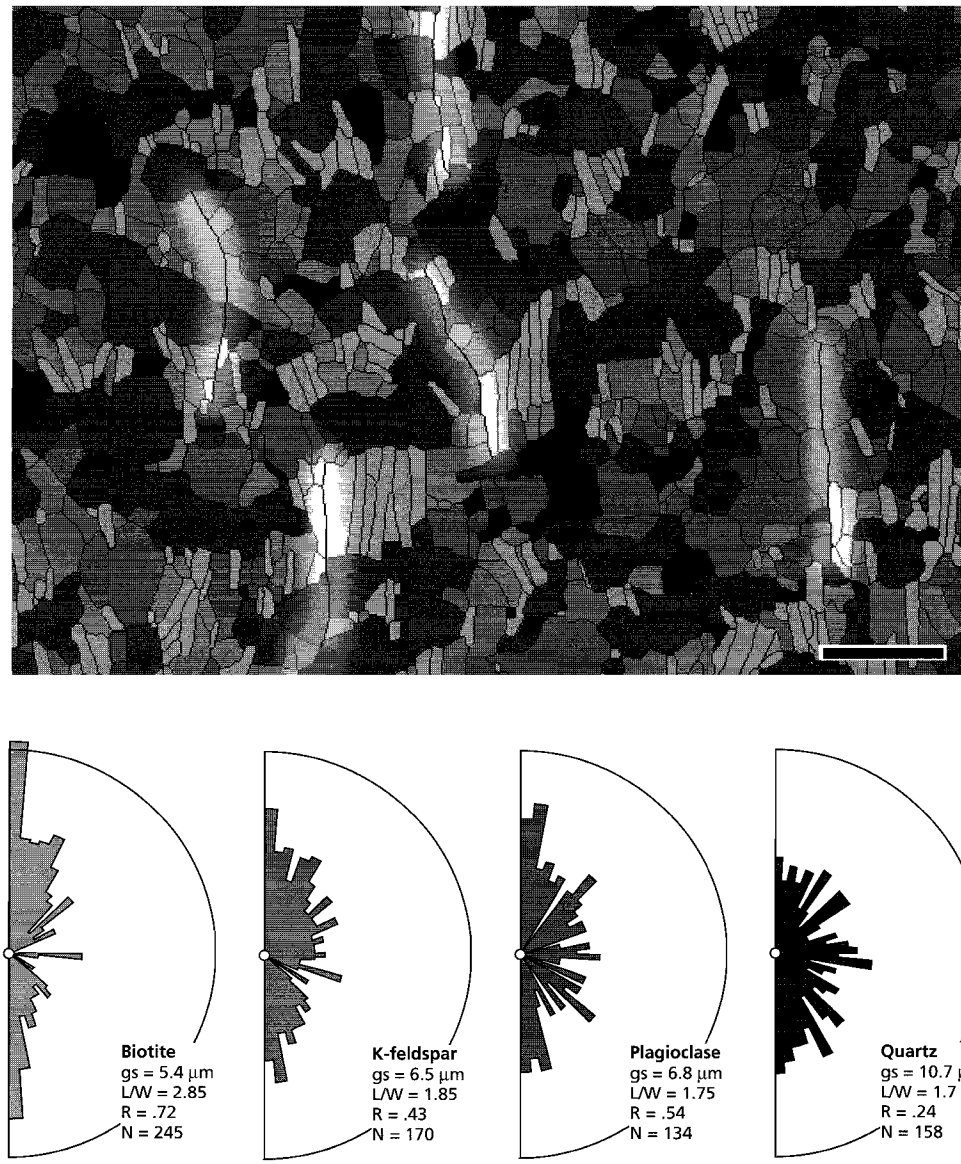

Fig. 4.2 (a) Line drawing after Fig. 4.1 showing the continuous alignment of grain and interphase boundaries across several grain diameters; several of them are highlightened. Scale bar 30 μm. (b) Rose diagram showing the orientation of the gain's long axis with respect to the short side of the photograph.gs: grain size; R: mean resultant length; N: number of observations. Greyscales correspond to those in Figs. 4.1(b) and 4.2(a).

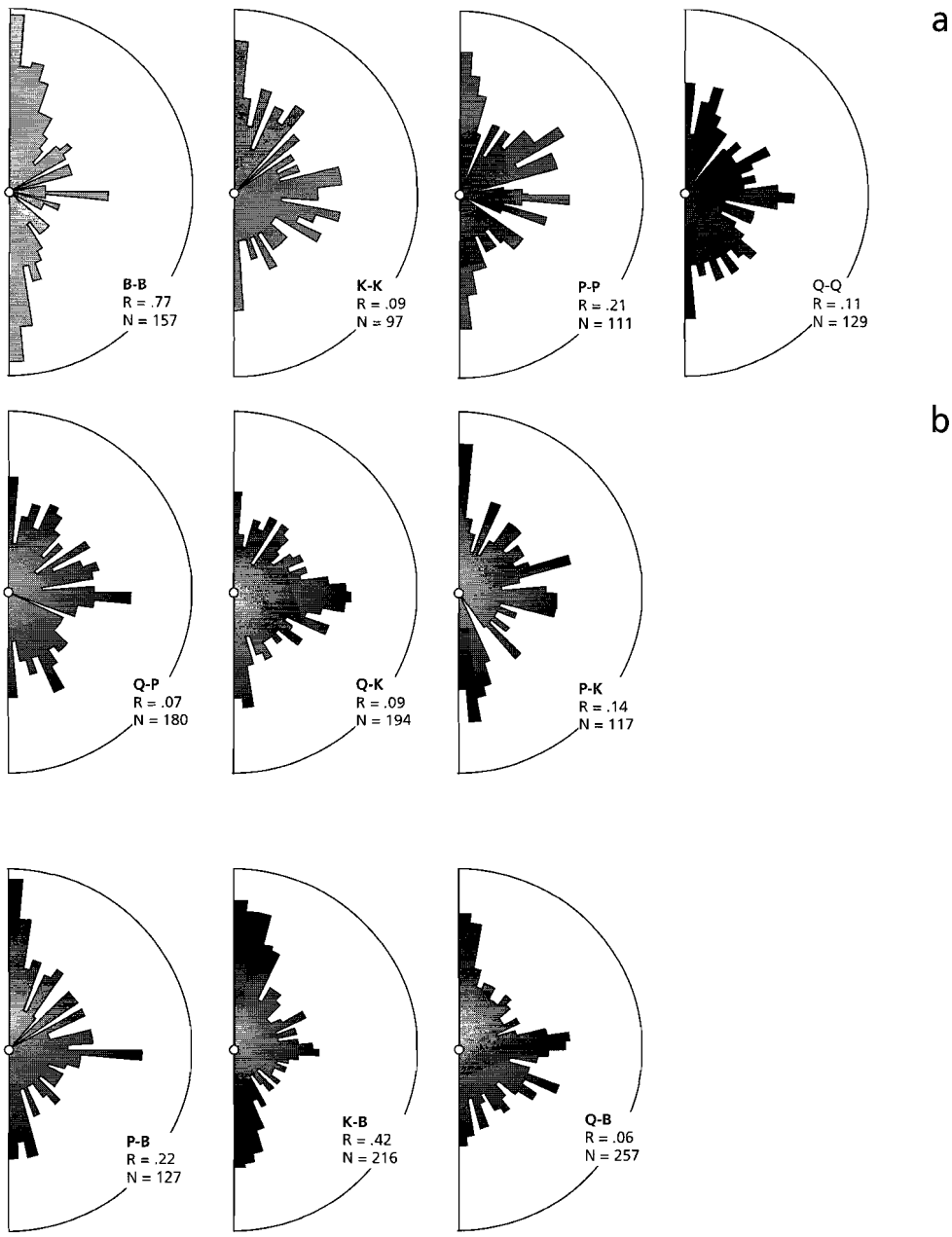

Fig. 4.3 Rose diagrams showing the orientation of the traces of the different types of boundaries. (a) Grain boundaries and (b) interphase boundaries. R: mean resultant length, N: number of observations. B: biotite; K: K-feldspar; P: plagioclase; Q: quartz.

4.4 Transmission Electron Microscopy

Intracrystalline defect structures

The deformation microstructures of quartz, K-feldspar and plagioclase from the fine grained polyphase type 1 ultramylonite have been studied using TEM. At this scale (Fig. 4.4c), the free dislocations within quartz are commonly straight or curved and are decorated with small inclusions (Md: 0.05 ± 0.01 μm; Sk = - 0.26; Km = - 0.53). These inclusions have an ovoid to negative crystal shape and show contrast consistent with that expected from fluid bubbles (Hirsch *et al.* 1976; Edington 1974; McLaren 1991; Drury 1993). Trace analysis on these curved dislocations were carried out and reveal that these dislocations lie mainly on rhombohedral and basal planes

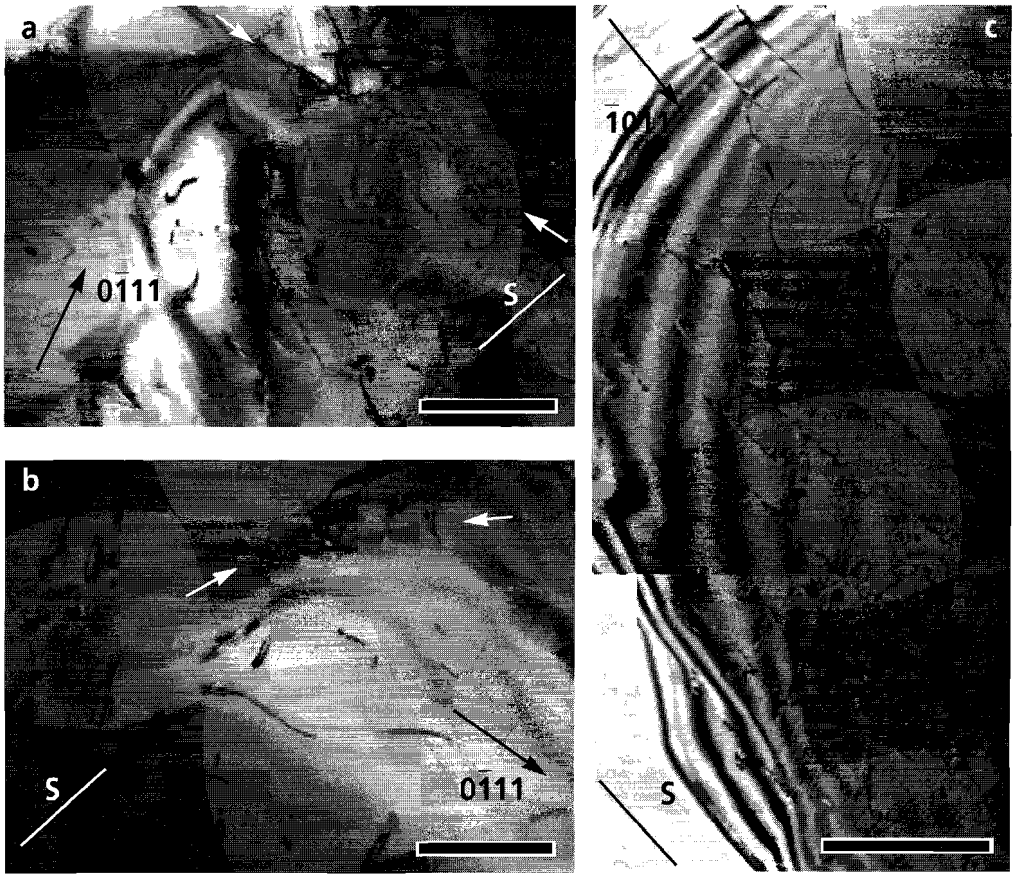

Fig. 4.4 Electron micrographs (BF) showing intracrystalline defect structures of quartz. (a) Medium dislocation density area with subgrain wall (arrowed). (b) Low dislocation density area with low angle dislocation wall. (c) Dislocation substructure of high dislocation density area. Note that the bubble density in (a) & (b) is lower than in (c). The orientation of the foliation is marked (S). All scale bars are 1 μm.

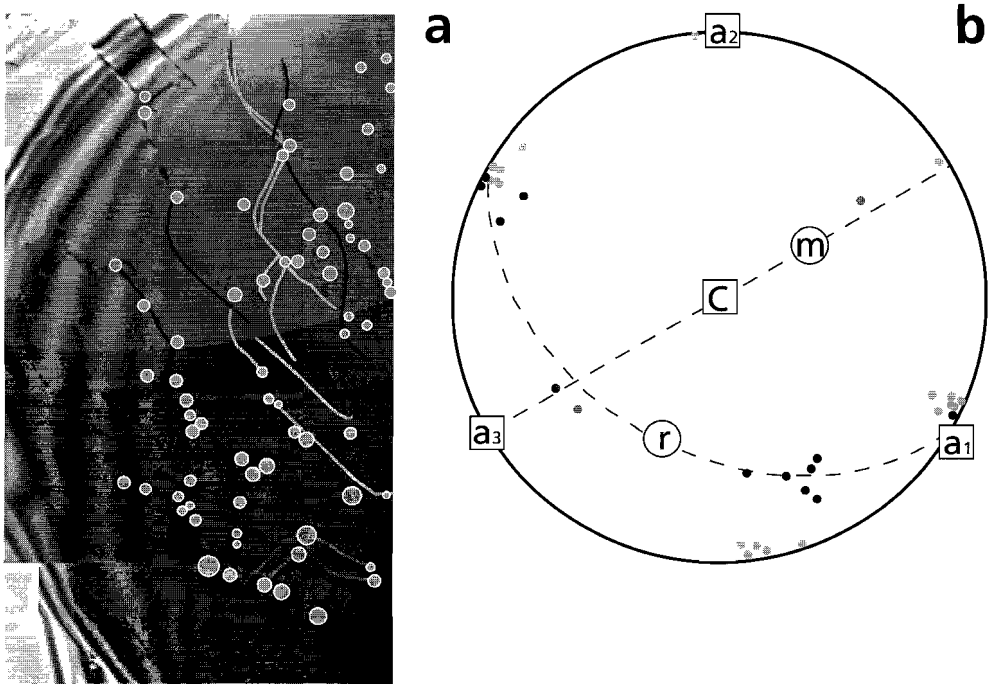

Fig. 4.5 Trace analysis on the bubble-dislocation system of Fig. 4.4(c). (a) Photosketch after Fig. 4.4c showing the dislocations and bubble. Bubbles appear as circles. (b) Stereogram showing the orientation of the dislocation lines. Key: light grey: dislocations defining basal plane; medium grey: dislocations defining m prism (m) plane; dark grey: dislocations defining rhombohedral (r) plane; black: dislocations not analysed.

and, less commonly, on prism planes (Fig. 4.5b). Bubbles occur mostly where the dislocations are curved (Fig. 4.5a). The free dislocation density (Md: 5.9 ± 2.7 x 10^8 cm^{-2}; Sk: 0.02; Km: -1.06) and bubble spacing (Md: 0.65 ± 0.21 μm; Sk: 2.18; Km: 2.78) vary inhomogeneously through the sample (Fig. 4.7) with a general association of high dislocation densities with small bubble spacings.

Within the larger grains (typically > 15 μm) some subgrain boundaries (Fig. 4.4a) and dislocation walls (Fig. 4.4b) have been observed which are preferentially aligned either parallel or perpendicular to the foliation. These boundaries generally have a near rhombohedral or prism plane orientation (Fig. 4.4a & 4.12d).

Although in general, quartz contains bubbles and dislocations, defect free quartz grains have been observed (Fig. 4.6). Most of the plagioclase and K-feldspar grains have no dislocations and/or bubbles; some planar defects occur within K-feldspar (Fig. 4.6 and 4.9b). These planar defects might be interpreted as twin boundaries, as the diffraction contrast changes on opposite sides of the boundary (Fig. 4.9b) (Hirsch *et al.* 1976; Edington 1974; McLaren 1991); however no twin rotations have been observed in the diffraction patterns.

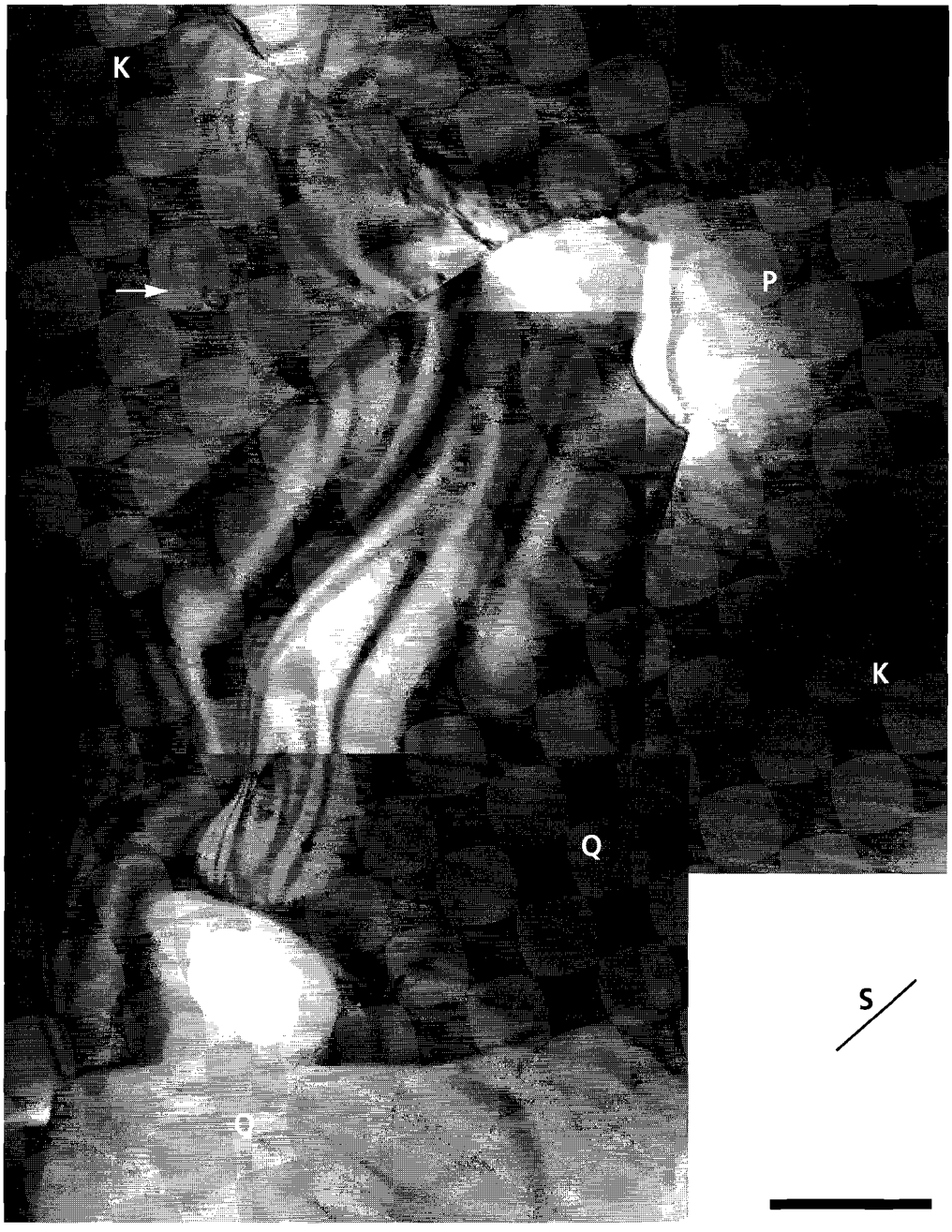

Fig. 4.6 Composite electron micrograph (BF) showing the microstructure of the type 1 ultramylonite. The quartz (Q) and plagioclase (P) are virtually defect free, while some planar defects (arrowed), interpreted to be twins, occur in the K-feldspar (K) on the top left. The orientation of the foliation is marked. Scale bar: 1 μm.

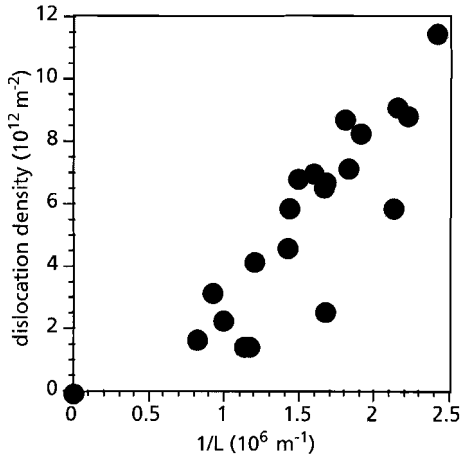

Fig. 4.7 Variation of inverse bubble spacing with dislocation density in quartz of the type 1 ultramylonite studied.

Intercrystalline defect structures

Most of the grain and interphase boundaries observed in TEM are marked by Moiré type of fringes 10 - 100 nm wide (Fig. 4.9) when rotated parallel to the electron beam. Some of the quartz-quartz grain boundaries parallel to the foliation are decorated with arrays of asymmetric, sigmodial shaped voids (Fig. 4.8). Such asymmetric, non-equilibrium shapes might be produced

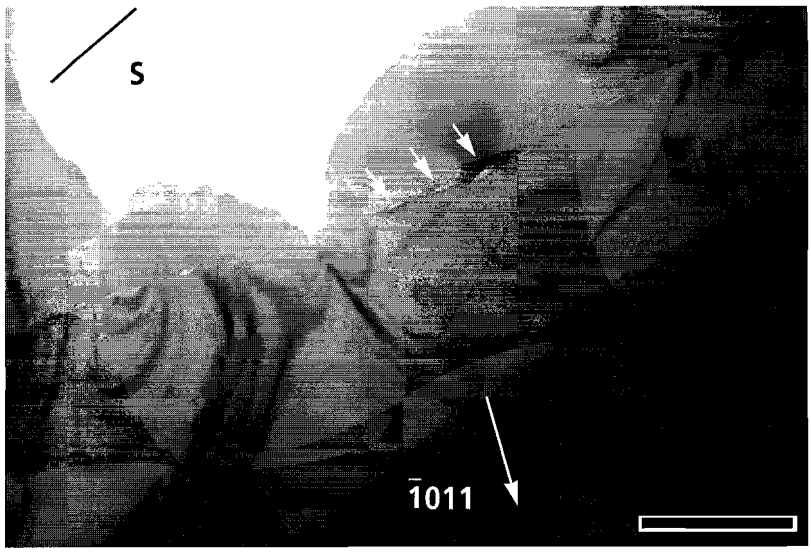

Fig. 4.8 Composite electron micrograph (BF) showing details of a quartz-quartz grain boundary decorated with asymmetric, sigmodial shaped voids. The orientation of the foliation is marked (S). Scale bar: 1 μm.

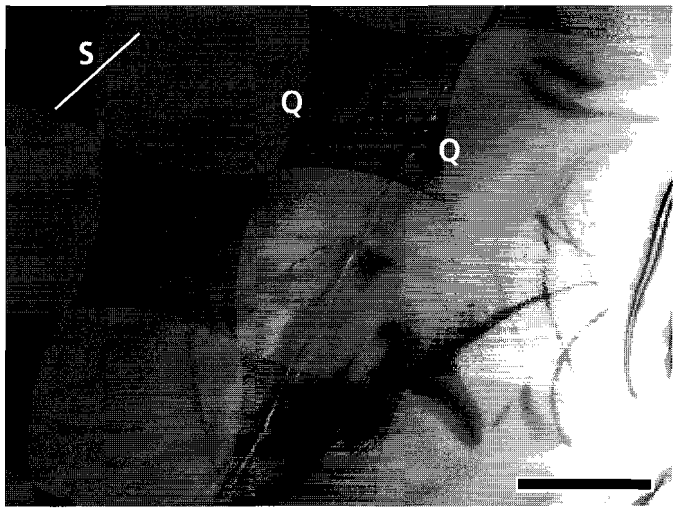

(a) Grain boundary between two quartz grains, tilted parallel to the electron beam, show a wide (≈ 50 nm) fringy contrast. Scale bar: 1 μm.

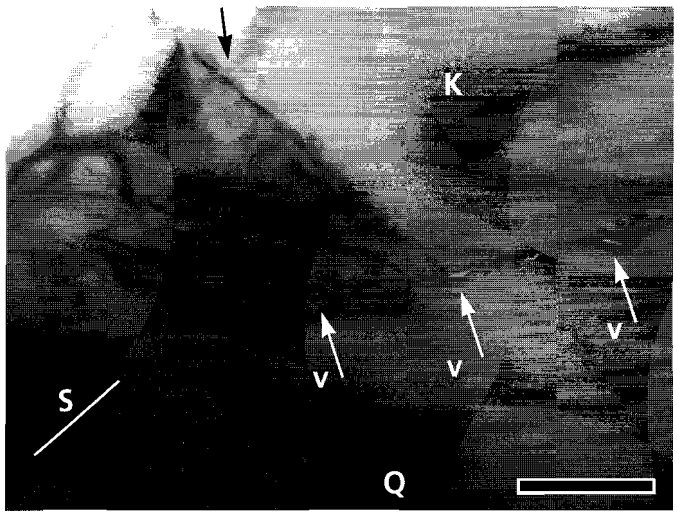

(b) Interphase boundary between a K-feldspar grain (K) and a quartz (Q) grain titled parallel to the electron beam. The interphase boundary contains voids (small arrows marked v). The contrast difference on opposite sides of the planar defect within the K-feldspar indicate a twin boundary. Scale bar: 1 μm.

Fig. 4.9 Details of grain and interphase boundaries encountered in the type 1 ultramylonite.

by sliding along a grain boundary with initial symmetrically shaped voids. Analysis of quartz-quartz grain boundary orientations show no preferred crystallographic planes (Fig. 4.12a); both the boundaries perpendicular and parallel to the foliation are scattered in the inverse pole figure.

Although the majority of interphase boundaries are straight and either parallel or perpendicular to the foliation (Fig. 4.6 and 4.9b), curved interphase boundaries have been observed, an example is given in Fig. 4.10. Here the interphase boundary between a K-feldspar and a quartz grain curves towards both the quartz and the K-feldspar. Such observations suggest that interphase boundary migration has occurred (Gordon & Vandermeer 1966).

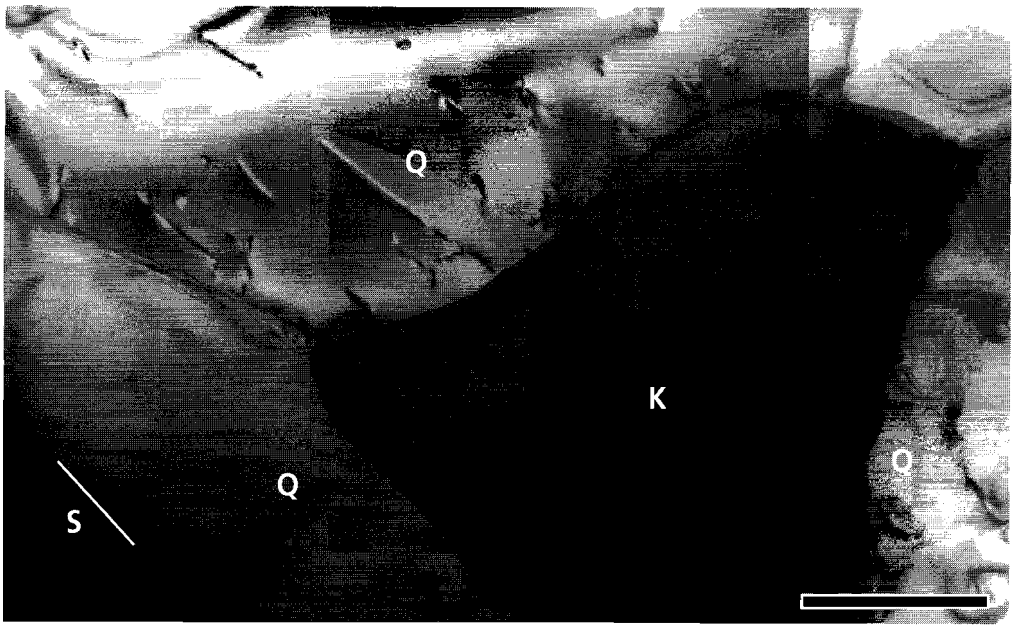

Fig. 4.10 Curved interphase boundary between quartz (Q) containing dislocations and a K-feldspar (K). The orientation of the foliation is marked (S).Scale bar: 1 μm.

Quartz microtexture analyses

The results of the texture analyses of quartz from the polyphase type 1 ultramylonite, using TEM are shown in Fig. 4.11. Only the *c*-axes show a very weak preferred orientation into a broad maximum near the centre of the polefigure (Fig. 4.11a). The *a*-axes (Fig. 4.11b), the normals to the m prisms (Fig. 4.11c) and to the rhombohedral planes (Fig. 4.11d) are randomly distributed. The *c*-axis texture is quite different from the one obtained optically, from the pure (60 μm) quartz bands (see Chapter 2; Fig 2.9c), the latter is a type 1 crossed girdle slightly asymmetric to the foliation.

The axes of misorientation measured between grains and the few subgrains encountered show a random distribution around the foliation (Fig. 4.12b & e). As can be seen in Figs. 4.12(c) & (f), the axes between grains with a grain boundary parallel to the foliation are as widely dispersed as axes between grains with grain boundaries perpendicular to the foliation. The few axes of misorientation between subgrains show a tendency to lie on great circles perpendicular to either [*c*], <*a*> and <*c*+*a*> (Fig. 4.12e). The axes between grains on the other hand (Fig. 4.12b), show no tendency to lie on such great circles. Using Frank's formula (see for details Chapter 3) this might be interpreted as that dislocation activity cannot solely account for the misorientation between adjacent grains. There are too few misorientation data points to infer the Burgers vectors of the dislocations that have been operative in accommodating the misorientation between subgrains.

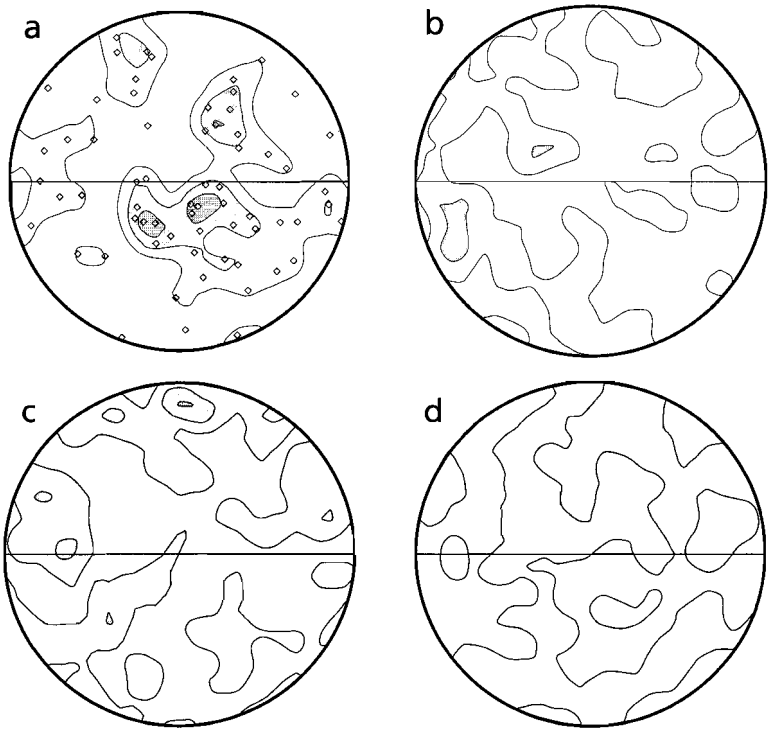

Fig. 4.11 Pole figure showing the weak texture of quartzes from the type 1 ultramylonite. (a) c-axes; (b) a-axes; (c) normals to m prisms; (d) normals to rhombohedral planes (both r and z). N = 65. Contours drawn at 1, 2 .. times a uniform distribution.

The misorientation relations between grains were tested against the coincidence site lattice (CSL) theory for hexagonal crystals (see for details Chapter 3). When the misorientation data presented in Fig. 4.12(b) are compared with the CSL relations for quartz (McLaren 1986, his Table 3) it is found that only 20% of the misorientation relations can be described as having a CSL with a Σ value lower than 49; 80% are random, or so-called general, grain boundaries.

4.5 TEM observations of type 2 ultramylonite

Due to the extremely fine grain size (< 5 μm) of the polyphase type 2 ultramylonite it is not possible to perform the same detailed SEM analyses as done for the type 1 ultramylonite. TEM has been used to study the microstructure; an example is shown in Fig. 4.13. The major drawback of using TEM is that mineral identification relies on qualitative EDS measurements and

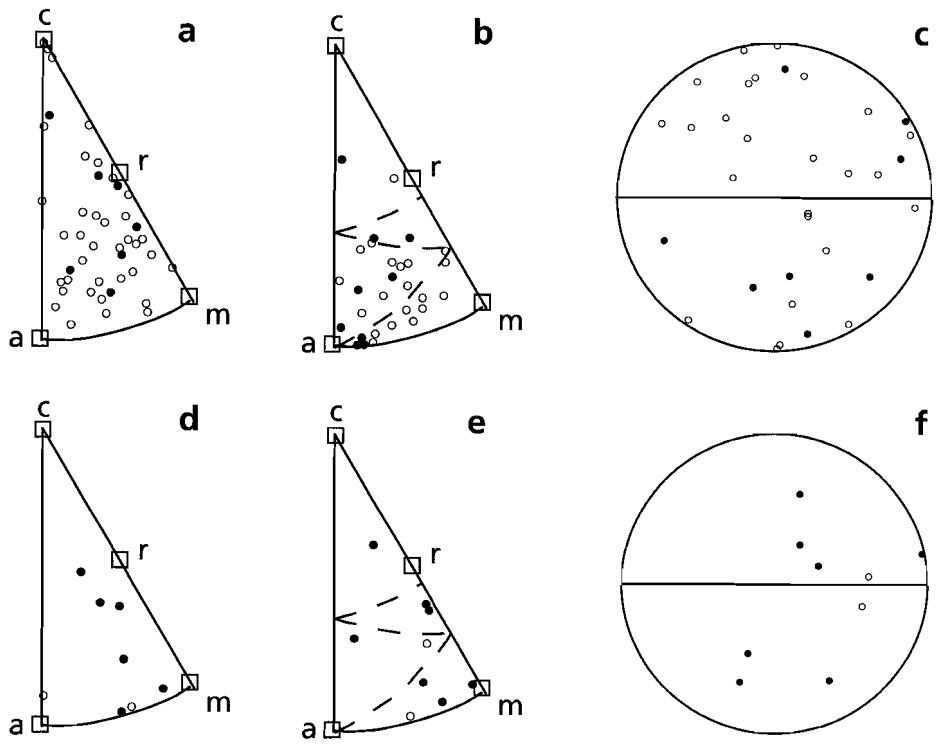

Fig. 4.12 (a & d) Grain and subgrain boundary orientation and (b, c & e, f) misorientation analyses of finite lattice misorientation across grain and subgrain boundaries of quartzes in the type 1 ultramylonite. (a) Inverse pole figure showing the orientation of quartz-quartz grain boundaries. (b & c) Axes of misorientation measured between grains presented in (b) an inverse pole figure and (c) a pole figure; the foliation is shown horizontal. (d) Inverse pole figure showing orientation of the (few) subgrain boundaries. (e & f) Axes of misorientation measured between subgrains presented in (e) an inverse pole figure and (f) a pole figure; the foliation is shown horizontal. Open symbols: boundaries parallel to the foliation; filled symbols: boundaries perpendicular to the foliation. The orientation of the foliation is marked (S). See text for discussion.

diffraction analyses of each grain. Fig. 4.13(b) shows a line drawing of Fig. 4.13(a) with mineral identification.

The ultramylonite consists of a mixture of 35% quartz, 20% K-feldspar (Or 94), 45% plagioclase (An 21) and various amounts of mica (up to 20%). The grain size is small, ranging from 0.1 - 4.0 μm (Md: 0.5 ± 0.2; Sk: 2.5; Km: 7.8). The grains have a rectangular to square grain shape (Fig. 4.13) and are slightly elongated (sub)parallel to the foliation. Some equiaxed grains have been observed (Fig. 4.14).

The dislocation and defect density in all phases is generally very low. Only within the larger (generally > 2 - 3 μm) quartz, plagioclase and K-feldspar grains some irregularly shaped low angle boundaries have been observed (Fig. 4.13); these occur mainly perpendicular to the foliation.

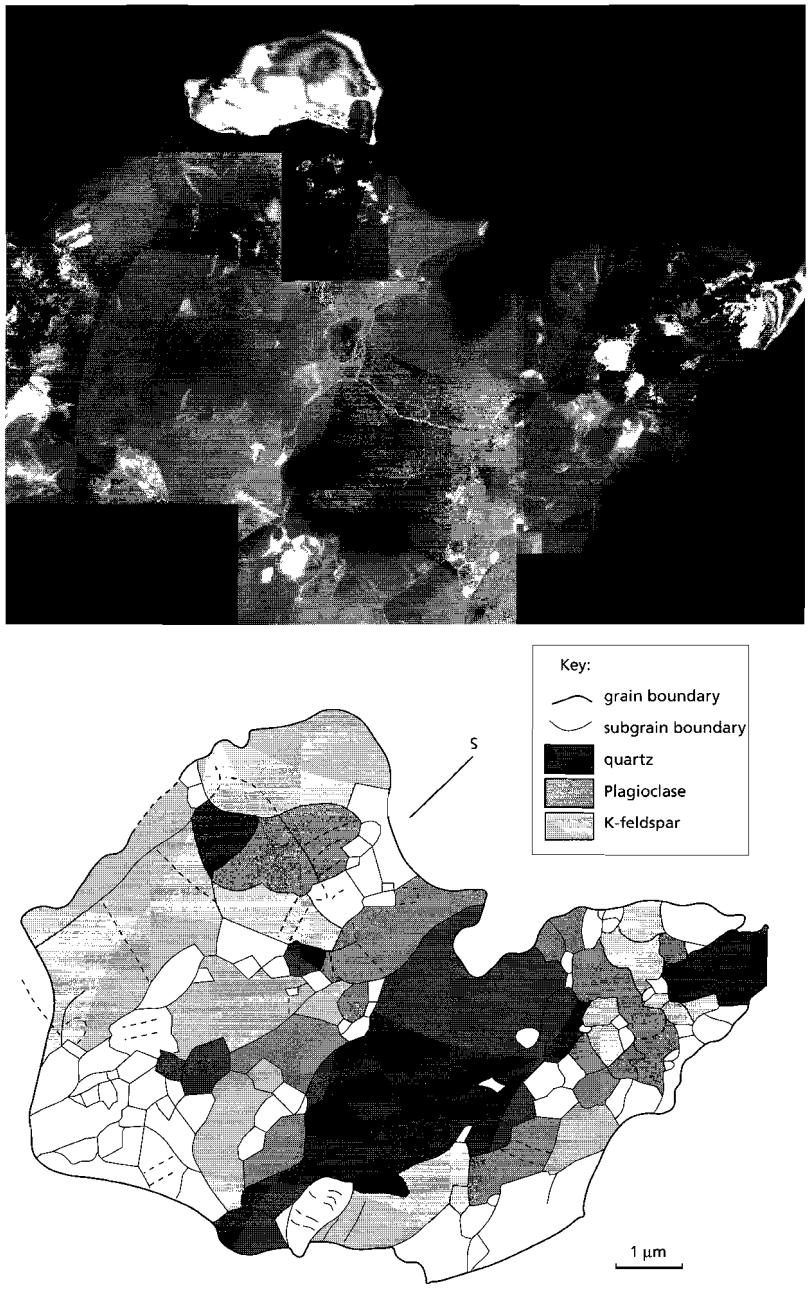

Fig 4.12 (a) Composite electron micrograph (ConDF), showing the microstructure of the type 2 ultramylonite. Note that the larger quartzes and K-feldspars contain irregular subgrain boundaries. The orientation of the foliation is marked (S). (b) Line drawing after (a) showing the continuous alignment of grain and interphase boundaries across several grain diameters.

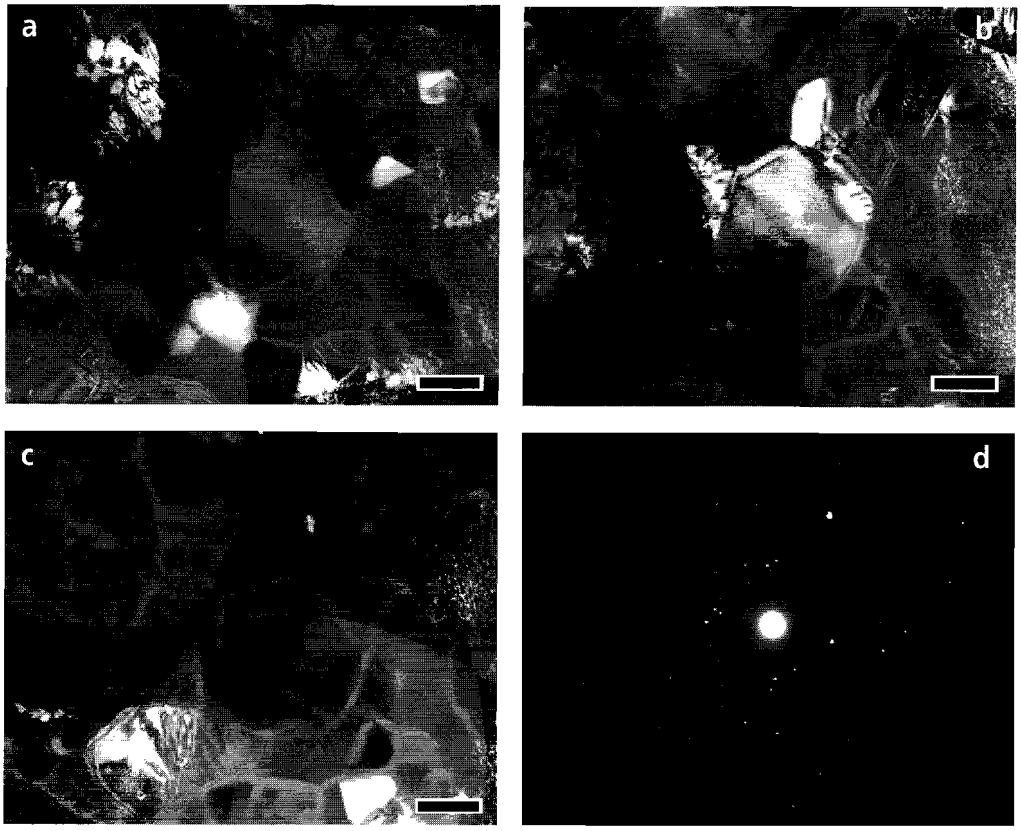

Fig. 4.14 (a-c) Preferential electron irradiation damage of interfacial boundaries (ConDF) of type 2 sample. With time the diffraction contrast of the boundary widens with time; the time difference between the first (a) and last image (c) was about 5 min. No voids and/or bubbles have been observed neither within the grains nor at the grain or interphase boundaries. The contrast differences between the images arises due to different rotations around the optic axis. Scale bars are 0.2 μm. (d) diffraction pattern of (a-c).

Occasionally planar defects occur within K-feldspar grains (Fig. 4.14), which are interpreted to be twinning microstructures.

Both grain and interphase boundaries are aligned parallel to the foliation (Fig. 4.13). Many of them are interlinked and are continuous across several grain diameters. The average spacing between these continuous grain boundaries is 1.7 ± 0.9 μm, which (as for the type 1 ultramylonite) equals 2 - 3 grain diameters. The average length of these continuous boundaries is 2.6 ± 0.9 μm; with an average grain size of 0.5 μm there are 4 - 5 grains adjacent to a continuous grain boundary.

No voids and/or bubbles have been observed neither within the grains nor at the grain or interphase boundaries (Figs. 4.13 & 4.14). Figure 4.14 shows 3 successive images during a ConDF experiment, the time difference between the first (Fig. 4.14a) and last image (Fig. 4.14c)

was about 5 min. The boundaries always show diffraction contrast, which widens with time. Such microstructures are interpreted to be the result of preferential beam damage of the grain and interphase boundaries. Attempts were made to resolve the structure of the grain boundaries using High Resolution Electron Microscopy (HREM). These were, however unsuccessful due to too rapid irradiation damage. This rapid damage and the diffraction contrast suggest an amorphous phase at the grain and interphase boundaries.

Microtextural analyses using TEM have been attempted as well. Again, these were not successful due to too rapid irradiation damage. This damage is thought to reflect high H_2O contents in the type 2 ultramylonite.

4.6 Discussion

Deformation mechanisms

The microstructural and microtextural observations indicate that flow in the fine grained polyphase ultramylonites studied (both type 1 and type 2) included a major component of grain boundary sliding. The pertinent observations are i) the rectangular to square grain shape, ii) the continuous alignment of grain and interphase boundaries across several grain diameters, and iii) that the grain size of the quartz within the polyphase ultramylonite (type 1: 10.8 ± 3.6 μm; type 2: 0.5 ± 0.2 μm) are smaller than the subgrain size within the pure, coarser grained quartz bands [type 1: 20 ± 5 μm (see Chapter 2); type 2: 2.1 ± 0.6 μm (see Chapter 3)].

In addition, texture analyses on the quartz of the type 1 ultramylonites, revealed a weak CPO and no crystallographic relation, in terms of the axis/angle of finite misorientation and Σ value, between adjacent grains. A crystallographic relation, in terms of grain boundaries with low Σ values, between adjacent crystals would develop if dislocation processes contributed significantly to the misorientation (see Chapter 3). This view is supported by Haruna *et al.* (1992) who measured, using SEM electron channeling patterns, the axis/angle of finite misorientation between lead grains in a fine grained, superplastically deformed, two-phase lead-tin alloy in which grain boundary sliding had played a prominent role (see also discussion in Chapter 3). They compared measured offsets across lead grain boundaries with the value of Σ. They observed that grain boundary sliding preferentially occurred along lead grain boundaries with Σ values > 49. Additional rotations between grains were also found in a fine grained, superplastically deformed, Mg-doped alumina in which grain boundary sliding had played a prominent role during deformation (Lartigue Korinek & Dupau 1994; see also discussion in Chapter 3).

Further evidence for grain boundary sliding processes comes from observations on the grain and interphase boundaries. Both the grain and interphase boundaries within the type 1 ultramylonites, are decorated with voids, some of which are asymmetric and sigmodial. They are thought to be the result of grain boundary sliding along boundaries with initial symmetrical shaped voids. Behrmann (1985) observed grain boundaries decorated with families of elliptical voids in very fine grained (5 - 10 μm) quartz mylonites. He inferred that grain-size-sensitive creep, with a major component of grain boundary sliding was the dominant deformation mechanism.

His observations were: (i) a weak CPO, (ii) a grain size smaller than the equilibrium subgrain size and (iii) a change in the relation between dislocation density and grain size from proportional to inverse. Grain boundary image contrasts in these quartzites were up to 100 nm wide.

The dark-field images of the interfacial boundaries of the type 2 samples (Fig. 4.14) look similar to those encountered in fine grained, superplastically deformed ceramics (0.1 - 10 μm) in which grain boundary sliding had played a prominent role (Clarke 1987; Carry 1990; Maehara & Langdon 1990; Wakai 1991). High resolution lattice fringe imaging on such ceramic boundaries (e.g. Rühle 1984; Clarke 1987) showed the presence of an amorphous intergranular film. Similar observations are made on olivine grain boundaries by Vaughan & Kohlstedt (1982) in samples hot-pressed at low pressures for short times.. They observed in dark-field TEM that almost every grain boundary appeared as a narrow < 10 nm wide, bright band. They interpreted such images to result from an amorphous phase at the grain boundaries.

Many minerals are unstable under the electron beam and transform to an amorphous phase. The rate at which this happens is a function of a number of variables such as beam intensity, beam current, accelerating voltage, temperature and impurity content. These variables have been discussed by McLaren (1991, pp 268 - 283). It is generally observed that for quartz, the beam damage rate increases with water content, although some exceptions are reported (see McLaren 1991). In this respect, the preferential irradiation damage of the interfacial boundaries of the type 2 samples is interpreted to be the result of water present in the grain boundary amorphous film. The increase in damage rate of the quartz grains in the type 2 sample compared to those in the high grade type 1 sample prevented microtextural analyses. It is suggested to reflect a higher H_2O content in the lower metamorphic grade type 2 ultramylonite. White & Knipe (1978) suggested that fluids can weaken grain boundaries, and therefore may facilitate grain boundary sliding.

Mechanisms accommodating grain boundary sliding

Grain boundary sliding deformation cannot occur without some accompanying deformation within the grains itself (Mukherjee 1971; Ashby & Verrall 1973; Gifkins 1976; 1977; Padmanabhan & Davies 1980). The grains change their shapes only as necessary to maintain continuity during creep if no fracturing occurs. In general grain boundary sliding is the faster process (Gifkins 1976), so the rates of accommodation control the overall strain rate.

If the accommodating mechanism is by either grain boundary diffusion or volume diffusion, the creep process is referred to as diffusion accommodated grain boundary sliding or Ashby-Verrall creep (Ashby & Verrall 1973; 1978). Other possible accommodating mechanisms are microfracturing, twinning and dislocation climb and/or dislocation glide processes. These dislocation motions can either occur within the grain interiors (Ball & Hutchinson 1969; Mukherjee 1971) or in the grain mantle (Friedel 1964; Gifkins 1976; 1977) or at triple point junctions (Gifkins 1976; 1977). Hybrid models are possible (the micro-multiplicity model of Gifkins 1982), in which some grains accommodate the grain boundary sliding by dislocation processes while other grains accommodate sliding by diffusion.

The observations of the intracrystalline defect structures within the type 1 mylonite suggest that different processes were operative within the different minerals during deformation. The

quartz defect structures indicate that dislocation motion occurred within the quartz during deformation. Whether the dislocations are related to an accommodation mechanism or that they are produced by parallel dislocation creep is difficult to assess. The rare occurrence of subgrain walls in the large grains and the inverse correlation between bubble spacing and dislocation density, i.e. the higher the dislocation density the smaller the average spacing between bubble, suggest that the dislocations are bound in their glide planes by these bubbles (White 1973; Knipe & White 1978). Drury (1993) observed the opposite correlation between bubble spacing and dislocation density as the one observed in this study. Higher dislocation densities were related to low bubble content, and hence, to a large bubble spacing. Drury (1993) inferred that such a relation is linked with the extend of recovery. It is therefore inferred that climb of the dislocations, i.e. recovery, is limited in the quartz of the polyphase type 1 mixtures and that the accommodating mechanism within the quartz involved dislocation glide.

While the accommodation within quartz involved dislocation processes, the accommodating mechanisms within plagioclase and K-feldspar are likely to be different. No defects have been observed within plagioclase grains, while some evidence for twinning within the K-feldspar has been observed. Microstructures indicative for microcracking have not been found. This suggests that diffusional processes were operative within the plagioclase and K-feldspar. Evidence for diffusional processes comes from the observations on interphase boundary migration, such as presented in Fig. 4.10 between K-feldspar and quartz. Migration of a boundary between two dissimilar phases, involves a flux of atoms (K, Al and Si in the case of Fig. 4.10) to and from the moving interphase boundary. Similar observations are reported by Gower & Simpson (1992) and Stünitz & Fitz Gerald (1993). From these observations it is inferred that the accommodating mechanism within the plagioclase and K-feldspar involved diffusive mass transport processes and minor twinning.

The accommodating mechanisms within the type 2 ultramylonite are difficult to assess. The observation that all phases were defect free except for the larger grains (>2 μm), and that only minor twinning has been observed, might suggest that accommodation involved diffusive mass transfer.

The similar grain shapes (in terms of circularity, elongation and grain shape factor) of the plagioclase, K-feldspar and the quartz in the type 1 ultramylonite, suggest that the fine grained phases were equally deformable at the ambient conditions (pressure, temperature, chemical environment). Similar observations are reported by Stünitz & Fitz Gerald (1993) who analysed grain size and grain shape distributions in several fine grained polyphase ultramylonites deformed at low greenschist facies conditions; the ultramylonites are composed of a mixture of albite, quartz and epidote. They observed no preferred curvature of quartz - albite interphase boundaries: bulging was directed towards both quartz and albite.

The grain size of the pure quartz bands within the ultramylonitic centre of the type 1 shear zone is much larger (60 μm) than the grain size of the quartz within the polyphase mixture (10.8 ± 3.6) suggesting that the latter grain size is in disequilibrium. Since numerous quartz - quartz grain boundaries occur within the polyphase mixture, the question arises what mechanism kept the grain size below the equilibrium grain size. Since no mica grains were found at the grain

boundaries, the usually invoked mechanism of small mica grains pinning the grain boundary is not appropriate in this instance. Voids and bubbles on grain boundaries are capable to inhibit grain boundaries from migrating (Rödel & Glaesen 1990). However, it is generally observed that in quartzites deformed by dislocation creep processes, major grain boundary migration had occurred and that these grain boundaries are commonly decorated with bubbles and voids (White & White 1981).

It has been observed in metals (e.g. Gordon & Vandermeer 1966) that the rate of grain boundary migration depends on the misorientation between the adjacent grains. Experiments on lead bicrystals (Gordon & Vandermeer 1966) show that grain boundary migration rates are lower at random boundaries compared to special, or CSL, boundaries. The misorientation relations between the quartz grains cannot be described as CSL relations. If the grain boundary migration relations of quartz are similar to those of lead bicrystals, this might be a cause for the small, disequilibrium quartz grain size.

The grain size of the plagioclase and K-feldspar grains in the polyphase ultramylonite is similar to that of small domains of only plagioclase or K-feldspar. These observations suggest that the plagioclase and K-feldspar grain sizes are stable. Similar observations have been reported by Stünitz & Fitz Gerald (1993) on fine grained albite-quartz-epidote mixtures. It is therefore concluded that the 3-D dispersion of the plagioclase, K-feldspar and biotite, together with slow grain boundary migration rates inhibit the grain growth of quartz to 10 μm compared to 60 μm, which is the stable grain size of the pure quartz bands.

From the above it is concluded that the main softening mechanism of the studied mylonites (both type 1 and type 2) was due to a process similar to recrystallization followed by mechanical mixing (see also Chapter 2) (*cf.* White & Knipe 1978; Rubie 1990; Stünitz & Fitz Gerald 1993), which produced an ultramylonite with a small grain size deforming by grain boundary sliding processes. The 3-D dispersion of the phases inhibited the grains in the polyphase mixture from growing, so that the ultramylonite could keep deforming by grain-size-sensitive processes with a major component of grain boundary sliding.

Finite strain.

It has been argued by Zelin and co-workers (Zelin & Mukherjee 1993a; 1993b; 1993d; Zelin *et al.* 1994) that grain boundary sliding deformation occurs in a non-homogeneous manner. They demonstrated that blocks of grains slide as an entity along grain boundary surfaces which consists of segments of sliding grain boundaries. Such co-operative grain boundary sliding results in the non homogeneity of deformation at the level of grain groups. The amount of sliding possible along such boundaries would be controlled by the accommodation of the blocking grain in front of such a continuous grain boundary (Fig. 4.15). Vastava & Langdon (1979) and Shariat *et al.* (1982) measured grain offsets across grain boundaries in superplastically deformed Zn - Al and Pb - Sn alloys. They observed displacements, at total sample elongations of 100%, in the order of 0.5 - 1.0 μm equivalent to 10 - 20% of the grain size. It is suggested that the maximum accommodation of such a blocking grain would be in the order of its grain size. If more accommodation is needed, the grain would split, or the continuous grain boundary has to diverge to a new boundary.

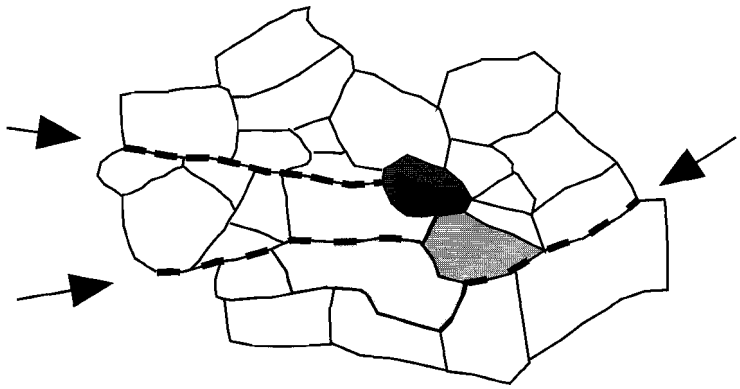

Fig. 4.15 Sketch showing three blocking grains (shaded) at the end of continuos boundaries (arrowed). The amount of sliding along such boundaries is controlled by these blocking grains.

In assuming that all strain in the polyphase ultramylonites described above occurred by grain boundary sliding along the continuous grain boundaries (cf. Gifkins 1982), a crude estimate of the total (finite) strain recorded in the microstructure can be obtained. The average spacing between the continuous grain and interphase boundaries within the type 1 ultramylonite is in the order of 15 μm. If this value doesn't change across the 50 meter wide ultramylonitic shear zone centre (see Chapter 2, Fig. 2.9) there would be 3×10^6 continuous grain boundaries in the entire ultramylonite. If each grain along such a boundary is displaced 1 - 2 μm, 4 - 6 grains per boundary produce 5 - 10 μm offset. This results in a total displacement across the ultramylonite in the order of 15 - 30 meters, equivalent to a shear strain of 0.3 to 0.7. The total displacement across the type 2 ultramylonite is estimated, in an analogous manner, to be in the order of 1 cm, equivalent to a shear strain of 0.1.

A very crude estimate of the uplift along the type 1 shear zones can be obtained from the field data presented in Fig. 2.3 and the P-T-t evolution given in Fig. 2.2, both taken from Shaw & Black (1991). As argued by Shaw and co-workers (Shaw & Black 1991; Black & Shaw 1992; Shaw *et al.* 1992), movement along the type 1 shear zones emplaced granulite facies rocks ($T \approx 700$ - 800 °C) next to amphibolite facies rocks ($T \approx 600$ °C). Assuming a constant geothermal gradient of 25 °C/km (Shaw & Black 1991; Shaw *et al.* 1992) this implies a relative displacement across the shear zone in the order of 4 - 8 km. Since there are 10 - 15 type 1 mylonites encountered in North - South cross-section through the Redbank Deformed Zone (Fig. 2.3), on average each shear zone takes up 400 - 800 meter of uplift. Furthermore, field evidence presented and discussed in Chapter 2, suggest shear strains in the ultramylonitic shear zone centres to be at least 5. Clearly, even considering the uncertainties of the above analyses, much less strain is recorded within the final microstructure of the ultramylonites. This implies that the microstructure is continuously reset during deformation, allowing for a quasi-steady state deformation. This is a process similar to continuous recrystallisation commonly observed in single phase metals deforming by dislocation creep processes (e.g. Gordon & Vandermeer 1966; Luton & Sellars 1969; Sellars 1978).

4.7 Conclusions

1) Both scanning and transmission electron microscopy investigations of the microstructure and microtexture of very fine grained polyphase quartzo-feldspathic ultramylonites (both type 1 and type 2) from the Redbank Deformed Zone of Central Australia, suggest that grain boundary sliding processes were the dominant deformation mechanisms operative.
2) Within the type 1 ultramylonite, different accommodating processes were operative within the different minerals. Dislocation processes were important within quartz, while diffusion and minor twinning accommodated grain boundary sliding within K-feldspar and plagioclase. The accommodating mechanisms within the type 2 ultramylonite are difficult to assess, it is suggested that diffusional processes accommodated the grain boundary sliding.
3) Analyses of axes and angles of finite misorientation between adjacent quartz grains within the type 1 ultramylonite indicate that dislocation activity cannot solely account for the misorientation between adjacent grains, and that it has resulted from grain rotations due to grain boundary sliding and neighbour switching events.
4) Softening of the studied mylonites (both type 1 and type 2) was due to mechanical breakdown assisted by some mineral chemical reactions, producing an ultramylonite with a small grain size (type 1: 5 - 11 μm; type 2: 0.5 ± 0.2 μm) deforming by grain boundary sliding processes. A 3-D dispersion of the phases inhibited the grains in the polyphase mixture from growing.
5) Uplift as estimated from field data are at least 1 order of magnitude higher than those recorded within the microstructure of the ultramylonites then. This implies that the microstructure is continuously reset during deformation, allowing for a quasi-steady state deformation.

Chapter 5

The effect of interfacial energies on microstructural evolution and mechanical properties in fine grained polyphase materials

5.1 Introduction

Grain-size-sensitive deformation processes in single phase materials are reasonably well understood. To allow large strains within polycrystals and to maintain continuity between grains during deformation, some grain boundary sliding must occur (Ashby & Verrall 1973). Grain boundary sliding is important within fine grained materials, but it cannot occur without some accompanying deformation within the grains itself (Mukherjee 1971; Gifkins 1976; 1977; Padmanabhan & Davies 1980; Perevezentsev *et al.* 1992b). The grains change their shapes only as necessary to maintain continuity during creep. In general grain boundary sliding[1] is the faster process (Gifkins 1982), so the rates of accommodation control the overall strain rate.

Grain size sensitive deformation has experimentally been identified in single phase geological materials like quartz (Rutter & Brodie 1993a; 1993b; 1994), calcite (Schmid *et al.* 1977; Walker *et al.* 1990; Rutter *et al.* 1994), feldspar (Tullis 1990; Tullis & Yund 1991), olivine (Chopra 1986; Karato *et al.* 1986) and spinel (Lappalainen *et al.* 1993) and in numerous engineering materials (e.g. Padmanabhan & Davies 1980; Langdon 1982; 1990; Venkatachari & Raj 1986; Nieh & Wadsworth 1990; Nieh *et al.* 1990; Sherby & Wadsworth 1990; Lartigue Korinek & Dupau 1994). Whether a material deforms by grain-size-sensitive processes or by dislocation creep processes largely depends on the grain size (Ashby & Verrall 1973; Gifkins 1976; 1982). Commonly, single phase materials exhibit deformation induced grain growth (Schmid *et al.* 1977; Karato *et al.* 1986; Walker *et al.* 1990; Sherwood & Hamilton 1994), which might result in a transition to grain-size-insensitive dislocation creep processes. Generally a low-volume fraction of stable second phase particle is added to stabilise the grain size of the single phase engineering material (Edington *et al.* 1976; Padmanabhan & Davies 1980).

Most geological and many engineering materials, however, contain more than one phase and are thus polyphase materials. It was noted in the previous chapters that within shear zones

[1] Terms as defined in Chapter 1

the highest strains are recorded within ultramylonites composed of a fine grained polyphase mixture deforming by grain boundary sliding processes. There are two end-member types of behaviour in the deformation of fine grained polyphase engineering materials (Chen 1982; 1985). In the first type each constituent phase deforms according to its own constitutive relation. One such case, is a soft (power-law creeping) material reinforced by rigid inclusions (Jordan 1988; Yoon & Chen 1990; Bons 1993), in which the resultant flow properties are made up of a combination of their end members (Jordan 1988; Yoon & Chen 1990; Tullis *et al.* 1991; Kulkarni & Kashyap 1992; Bons 1993; Fan & Moidownik 1993a; 1993b; Ravichandran & Seetharaman 1993).

In the second type, migration of interphase boundaries occurs, and diffusional flow is facilitated, lowering the deformation resistance to a value below those of both constituent phases (Chen 1982; 1985; Wheeler 1992). Deformation experiments on fine grained two-phase materials with various fractions of the constituent phases have shown that if the two-phase material deformed by grain size sensitive processes, the two phase material can be weaker than either constituent phase in the form of a single phase polycrystal (e.g. lead-tin: Cline & Alden 1968; Zehr & Backofen 1968; aluminium - zinc: Presnyakov & Chervyakova 1959; calcite-anhydrite: Bruhn *et al.* 1993; 1994).

Polyphase materials contain several types of interfaces, this in contrast to single phase materials where only grain boundaries exist. For example a 2-phase material has two different types of grain boundaries and one type of interphase boundary, whereas the 4-phase quartzo-feldspathic ultramylonites presented in Chapter 4 have 10 different types of interfaces of which 4 are grain boundaries and 6 are interphase boundaries. Studies on interfacial properties have shown that different types of interfaces have different interfacial energies (Smith 1948; Stanton 1964; Kretz 1966; 1969; Vernon 1968; 1970; Spry 1976), different boundary migration rates and boundary diffusion rates (Martin & Perraillon 1979; Kaur *et al.* 1989 and refs. therein) and grain boundary sliding resistances (Vastava & Langdon 1979; Shariat *et al.* 1982; Haruna *et al.* 1992). Therefore, not only will polyphase materials have different properties compared to their single phase end members, but also will variations in interface population produce variations in material behaviour.

Aims and approach

In this chapter, analyses of interface populations in a range of materials are presented aiming to access how these vary and evolve during grain growth and grain size sensitive deformation. The major aim is to determine the interface population in the ultramylonitic samples from the Redbank Deformed Zone (*cf.* Chapter 4) and to access its effect on the rheological behaviour. However, as will be shown in the next sections, the analyses of interface populations is currently limited to two phase materials. Consequently, 2-phase analogue materials have been studied. The results are subsequently used to infer the relation between microstructure and mechanical behaviour of the studied 2-phase materials in particular and to polyphase materials deforming by grain-size-sensitive processes in general.

5.2 Theoretical background

The quantitative characterisation of the microstructure of 2-phase materials involves analysis of both geometrical and topological quantities. The geometrical characterisation involves the analysis and measurement of grain size, volume fraction and particle spacing (*cf.* Underwood 1970; Fan *et al.* 1993). The topological characterisation involves the analysis and measurement of the number of sides per grain, kind of neighbouring grains, phase continuity, grain boundary curvature and grain junction type (Fan *et al.* 1993; Holm *et al.* 1993).

In general these analyses are performed on two-dimensional (2-D) cross-sections of the sample volume (*cf.* Underwood 1970). In 2-D, grain boundary curvature has a single component κ (Hillert 1965), and both grain topology and grain boundary migration rates depend on that curvature (see next section). In three-dimensions (3-D), curvature has two orthogonal components κ_1 and κ_2, and grain topology depends on the Gaussian curvature of a boundary ($\kappa_1\kappa_2$), while grain boundary migration rates depend on the geometric curvature ($\kappa_1 + \kappa_2$) (Von Neumann 1950; Hillert 1965; Holm *et al.* 1993). However, when the microstructure is spatially uniform, stereological relations require that a 2-D system resembles a cross-section of the corresponding 3-D system (i.e. grain corner angles in 2-D are the same as grain edge angles in 3-D) (Smith 1952; Underwood 1970; Holm *et al.* 1993). However, similar to that of a geometrical analyses, this sectioning effect will tend to produce a spread in the topological data around a mean value corresponding to the "true" topological quantity (Smith 1952; Underwood 1970). In this chapter it is assumed that the 2-D analyses resembles the corresponding 3-D system.

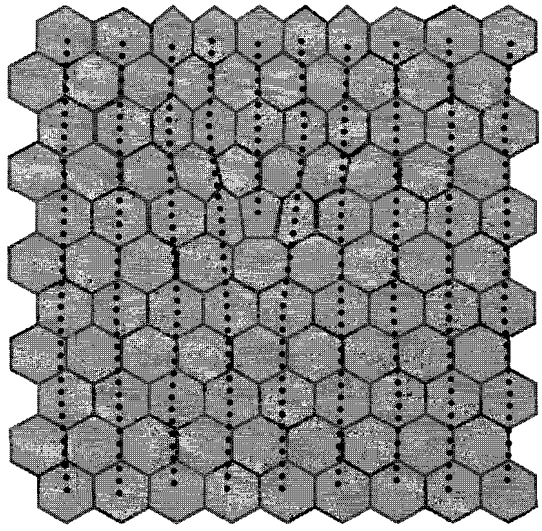

Fig. 5.1 Two dimensional grain structure of a single phase material with a "5-7" topological defect. This defect corresponds to an edge dislocation analogous to an edge dislocation in a crystal.

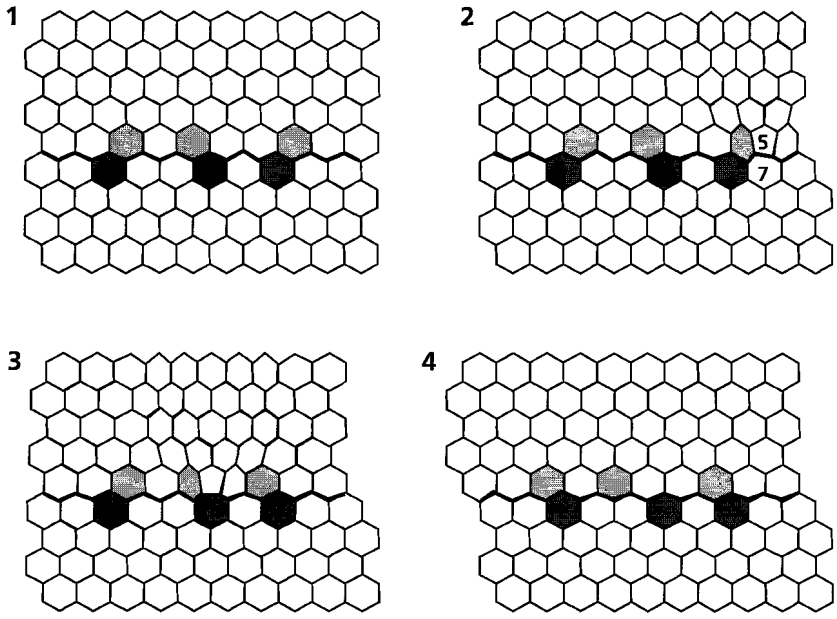

Fig. 5.2 Grain boundary sliding by the movement of a "5-7" topological defect through an array of grains in a single phase material. Some grains are shaded to serve as marker grains. (1) Initial microstructure before introduction of the topological defect. (2) Introduction of a "5-7" topological defect by giving one grain 5 neighbours and an adjacent grain 7. (3) Movement of topological defect perpendicular to extra half plane. Note that grains adjacent to the "glide plane" (thick line) change neighbours during sliding, that the process is conservative and that the defect persists during glide. (4) After glide of the defect, the top part has moved to the left relative to the bottom part (after Nix 1975).

Grain topology in single phase materials

In a 2-D polycrystalline, single phase material, conditions for equilibrium at a grain boundary tri-junction can be obtained by considering the total grain boundary energy associated with the configuration (Porter & Easterling 1992). Quadri-junctions, where 4 grains meet are never stable in a single phase polycrystalline material. If the boundary energy is independent of the (mis) orientation, the grain boundary behaves like a soap film and the angles at the tri-junction all equal 120°. This angular condition implies that only grains with 6 neighbours (i.e. a 6-sided grain) will have straight sides; the integrated grain boundary curvature (IGBC) of this grain will be zero, and the grain is stable. Those grains with less than 6 sides will bulge outwards between triple junctions resulting in a negative IGBC, while those grains with more than 6 sides will bulge inwards and thus have a positive IGBC. This topological "6 minus n" rule (where n is the number of sides) is often referred to as Von Neumann's rule (Von Neumann 1952; Hillert 1965; Holm *et al.* 1993) and can be expressed as:

$$\text{IGBC} = \int \kappa \, ds = \frac{\pi}{3}(6 - n) \tag{5.1}$$

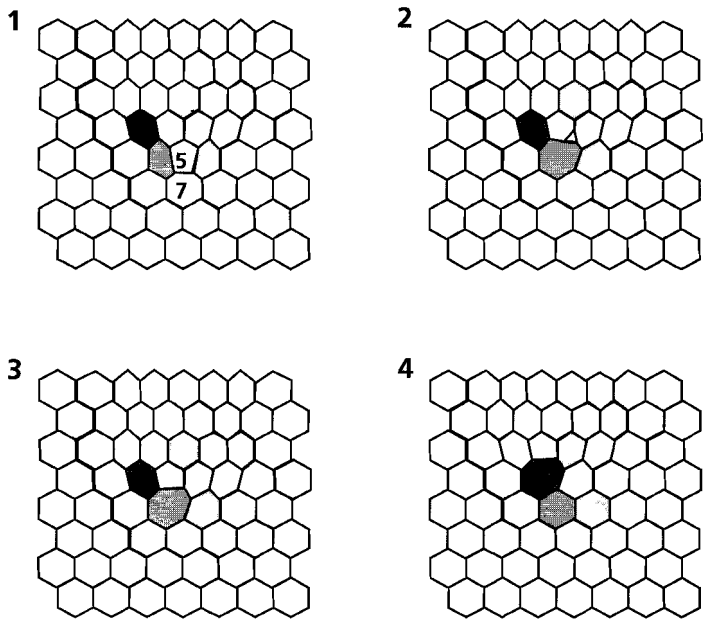

Fig. 5.3 Grain growth by the climb movement of a "5-7" topological defect in a single phase material. Some grains are shaded to serve as marker grains. (1) Initial microstructure after introduction of the topological defect. (2) The 5-sided grain reduces its number of sides to three and the 7-sided grain to 6, while an initial 6-sided grain increases its sides to 8. (3) The 5-sided grain in (1) has disappeared and the 8-sided grain in (2) has reduced its sides to 7. Note that during this grain growth neighbour switching events occur. (4) Repetition of stage (2) & (3) results again in the disappearance of a 5-sided grain. Note that within the microstructure the number of grains has reduced by two, resulting in a net grain growth. (after Hillert 1965).

where s is the grain boundary length, and the integral is over the arcs of the grain boundary between grain corners. The curvature due to bulging provides the driving force for the minimisation of the total grain boundary energy via boundary motion. A negative integrated curvature results in shrinking of the grain, while a positive IGBC results in growth. Hence, a 6-sided grain will neither grow nor shrink, a 7-sided grain always grows and a 5-sided grain always shrinks (Smith 1952; Hillert 1965). In a stable 2-D microstructure, all grains will have 6-sides.

The introduction of an imperfection in such a stable bee-hive or foam structure, by giving one grain 5 neighbours and an adjacent grain 7 neighbours, results in a "5-7" topological defect, which can be considered as an edge dislocation in the grain structure (Fig. 5.1) (Cahn & Padawar 1965; Morral & Ashby 1974; Nix 1975). It has been shown by Morall & Ashby (1974), that such topological defects or cellular dislocations resemble dislocations in crystals in that their glide motion (i.e. motion perpendicular to the extra "half plane" of cells) parallels exactly the glide motion of dislocations during deformation of crystals. The cellular dislocation glide motion is conservative (cells are neither created nor destroyed) and occurs by a neighbour-switching event (Fig. 5.2) and thus involves grain boundary sliding (Morral & Ashby 1974). Climb motion of the

cellular dislocation is non-conservative in the sense that cells are created or destroyed (Fig. 5.3), and thus can result in grain growth (Hillert 1965; Cahn & Padawar 1965; Morral & Ashby 1974). Unlike dislocation climb in crystals however, cellular dislocation climb requires no long range mass transport. As can be seen in Figs 5.2 and 5.3, neither glide nor climb can remove the cellular defect. As shown by Sherwood & Hamilton (1994) annihilation can occur between defects with opposite signs analogous to crystal dislocations, while mistakes in grain switching events will produce new topological defects. Extensions of the cellular dislocation concept to superplastic deformation (involving grain boundary sliding) and deformation enhanced grain growth have been made, among these are Morral & Ashby (1974), Nix (1975), Sato *et al.* (1990), Zelin & Mukherjee (1993a; 1995) and Sherwood & Hamilton (1992; 1994).

Grain topology in polyphase materials

The presence of two or more phases complicates the grain growth and grain boundary sliding analyses, because instead of one single grain boundary energy, two or more grain boundary energies ($\gamma_{\alpha\alpha}$ and $\gamma_{\beta\beta}$) and interphase boundary energies ($\gamma_{\alpha\beta}$) control grain junction angles. The relative boundary energy (R) and grain junction interior angle (ϕ) of a 2-phase (α - β) system can be defined by (*cf.* Holm *et al.* 1993):

$$R_\alpha = \frac{\gamma_{\alpha\alpha}}{\gamma_{\alpha\beta}} \quad \text{and} \quad R_\beta = \frac{\gamma_{\beta\beta}}{\gamma_{\alpha\beta}} \tag{5.2}$$

and

$$\phi_\alpha = 2\cos^{-1}\left(\frac{R_\beta}{2}\right) \quad \text{and} \quad \phi_\beta = 2\cos^{-1}\left(\frac{R_\alpha}{2}\right) \tag{5.3}$$

The stability of certain grain junctions depends on the relative interfacial energies; the stability regimes of the various grain junctions are shown in Fig. 5.4 (after Holm *et al.* 1993). The only stable quadri-junction in a 2-phase material, is an $\alpha\beta\alpha\beta$ junction at high relative boundary energies (Holm *et al.* 1993). It should be noted that Fig. 5.4 only catalogues the stability of grain junctions and that it does not predict the grain arrangements, phase distribution or preferred microstructural features of a given system due to grain growth and/or grain boundary sliding.

The grain topology of a tri-junction only system in a 2-phase material can be described, analogous to a single phase material, by its integrated grain boundary curvature (Holm *et al.* 1993):

$$\text{IGBC} = \int \kappa \, ds = \frac{\pi}{3}(6-n) + \left(\phi_\alpha - \frac{2\pi}{3}\right)(n_d - n_s) - \left(\phi_\beta - \frac{2\pi}{3}\right)n_s \tag{5.4}$$

where n is the number of sides, n_d is the number of unlike-phase neighbours, and n_s is half the

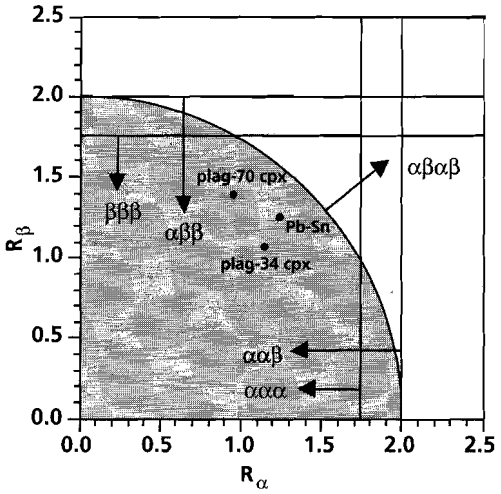

Fig. 5.4 Catalogue of stable grain junctions in a 2-phase system. The axes are the relative interfacial energies as given by Eq. 5.2 (after Holm *et al.* 1993). The relative energies of the clinopyroxene (cpx) - plagioclase (plag) systems (Section 5.4) and the lead (Pb) - tin (Sn) system (Section 5.5) are indicated. Note that in these systems only grain tri-junctions are stable.

number of switches from α to β as we examine the neighbour grains in a clockwise order (for a β grain one has to switch the α and β subscripts). Only grains with zero integrated curvature (ZIC) are stable and will not grow nor shrink. For instance for $\phi_\alpha = \phi_\beta$, Eq. 5.4 states that the only ZIC grains are 6-sided and occur for (n, n_d, n_s) of (6 ,4 ,2), (6 ,2 ,1) and (6, 0, 0), while for $2\phi_\alpha = \phi_\beta$, (4, 3, 1) is also a ZIC grain.

Phase distribution

A second aspect of a polyphase microstructure is the distribution of grains in the sample. The phases might be distributed randomly in the sample or, if the interfacial boundaries are free to move, a polyphase system might evolve to a lowest total interfacial energy configuration which minimises high energy boundaries and maximises low energy ones (Smith 1948). Holm *et al.* (1993) have presented a 2-D Monte-Carlo-Potts model computer simulation of 2-phase grain growth in which the only system variables were the interfacial energies (*cf.* Eq. 5.4.). They found that during grain growth, low energy boundaries were favoured above high energy ones. For instance, the system with $R_\alpha = R_\beta > 1$ favours maximising the amount of low energy, α - β interfaces present in the microstructure; the microstructure is characterised by α and β grains which alternate more than in case where $R_\alpha = R_\beta = 1$.

In Monte-Carlo simulations, grains may change their shape, i.e. grain and interphase boundaries are free to move. A different approach has been adopted in this chapter to model lowest total interfacial energy configurations, in that a fixed grain geometry has been chosen; the program is briefly outlined below. Two models with different grain shapes have been investigated: one is a bee-hive structure (Fig. 5.5) in which all grains are 6-sided and the other is a grid of square grains (Fig. 5.6). A 2-D continuous network of grains is only possible with 6-sided or 4-sided grains (Smith 1952; Underwood 1970). In the initial microstructure, the grid is filled randomly with the two phases (Figs. 5.5a and 5.6a). To establish a minimum energy configuration, grains

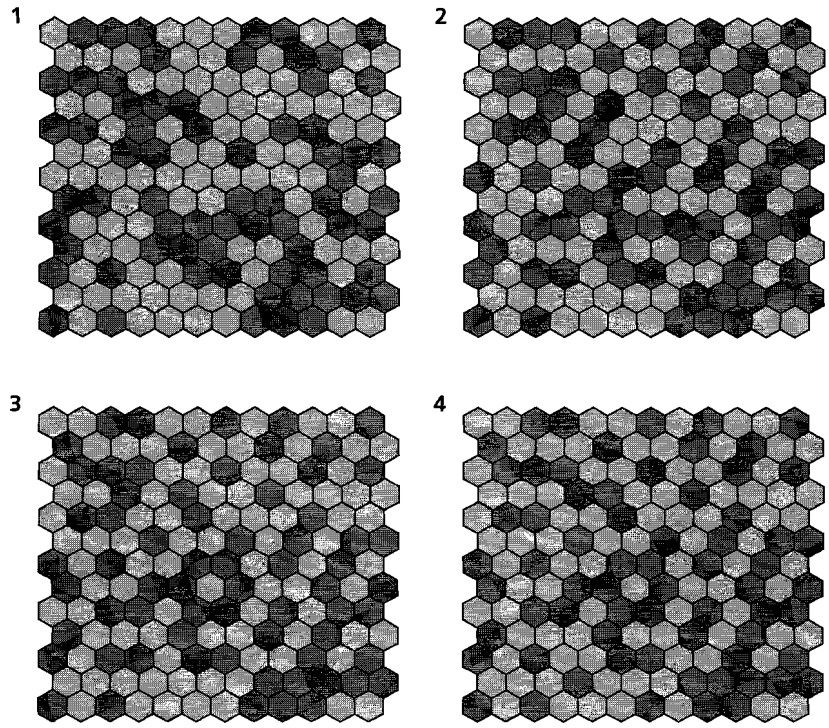

Fig. 5.5 Results of the grain swapping computer model in a bee-hive structure. $R_\alpha = R_\beta = 1.25$ as in the Pb-Sn system (see Section 5.5). Grains are allowed to change places with a neighbour only if the total interfacial energy is thereby reduced. (1) Initial random distribution. (2-4) Successive steps in the computer simulation; (4) resembles a minimum energy configuration where low energy interphase boundaries are favoured.

are allowed to swap (i.e. change places) with a neighbour only if the total interfacial energy is thereby reduced. In the examples given in Figs. 5.5 and 5.6, $R_\alpha = R_\beta = 1.25$ as in the Pb-Sn system (see later sections). After several iterative steps (Fig. 5.5b - d and 5.6b - d), the end microstructure will then have a "local" minimum energy (Figs. 5.5d and 5.6d). This "local" minimum energy configuration may deviate from an "absolute" minimum energy configuration, in that when α - β interfaces have the lowest energy in a square-grid structure a checker board configuration would have the lowest energy (*cf.* Wheeler 1992; Fan & Moidownik 1993a; 1993b). The calculations of minimum energy configuration used in the next sections, are based on a grid size of 100 x 100 grains.

To compare the observed grain distributions with either a random or a minimum energy configuration, Markov chain analyses have been performed (for details see Kretz 1969; Davis 1986). Markov chain analyses provide information on the tendency of one phase to follow another. For the analysis, a rectangular grid has been drawn over the microstructure and the number of transitions from one phase to another were counted, giving a transition

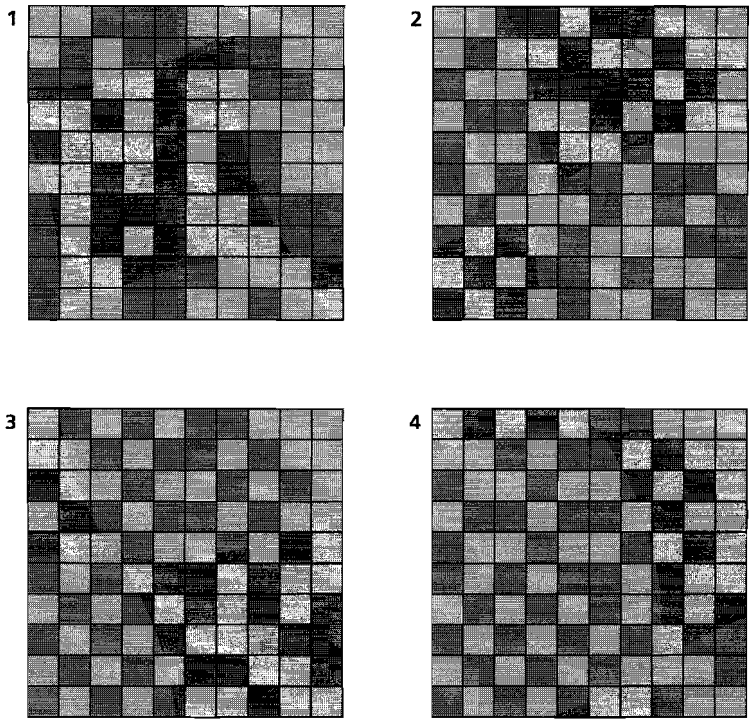

Fig. 5.6 Results of grain swapping computer model, as in Fig. 5.5 for square grid structure.

frequency matrix (TFM) (Davis 1986):

$$\text{TFM}: \begin{array}{c} \\ \text{A} \\ \text{B} \end{array} \begin{array}{c} \begin{array}{cc} \text{A} & \text{B} \end{array} \\ \begin{bmatrix} \alpha\alpha & \alpha\beta \\ \beta\alpha & \beta\beta \end{bmatrix} \end{array} \begin{array}{l} N_\alpha \\ N_\beta \\ N \end{array} \qquad \begin{array}{l} f_\alpha = N_\alpha / N \\ f_\beta = N_\beta / N \end{array} \tag{5.5}$$

where $\alpha\alpha$, $\alpha\beta$, $\beta\alpha$ and $\beta\beta$ are the transition frequencies, the row totals $N_\alpha = \alpha\alpha + \alpha\beta$ and $N_\beta = \beta\alpha + \beta\beta$ and N is the total number of transitions counted. This observed TFM can be compared to a TFM of either a random or a minimum energy configuration (as calculated by the computer model) using a χ^2 test (Davis 1986):

$$\chi^2 = \sum \frac{(O - E)^2}{E} \tag{5.6}$$

where O is the observed number of transitions from one phase to another, and E is the number of transitions expected in either a random or a minimum energy configuration; the summation (Σ) is over all possible transitions. The critical value of χ^2 at 5% level of significance for a 2-phase system is 3.84, for a 3-phase system 5.99 and for a 4-phase system 16.9 (Davis 1986). If the test value exceeds the critical value, it may be concluded that the observed TFM differs significantly from the one it is tested against (Davis 1986).

The TFM for the minimum energy configuration has been obtained in an analogous way to the observed TFM, while the TFM for a random distribution of phases is given by (see Davis 1986):

$$\text{Random TFM}: \begin{array}{c} \\ \text{A} \\ \text{B} \end{array} \begin{array}{c} \begin{array}{cc} \text{A} & \text{B} \end{array} \\ \begin{bmatrix} f_\alpha N_\alpha & f_\beta N_\alpha \\ f_\alpha N_\beta & f_\beta N_\beta \end{bmatrix} \end{array} \begin{array}{c} \\ N_\alpha \\ N_\beta \end{array} \tag{5.7}$$

Further information on the distribution of phases in a 2-phase system can be obtained by calculating the degree of phase continuity and the degree of phase separation (Fan *et al.* 1993). These are calculated from expressions for the contiguity and separation of phases (Fan *et al.* 1993). The contiguity (C) of a phase in a 2-phase mixture is defined by the fraction of the total grain boundary area of that phase, whereas the separation (S) of a phase is defined by the fraction of interphase boundary area. The contiguity and separation of an α-phase in an α - β mixture can mathematically be expressed as (Fan *et al.* 1993):

$$1 - S_\alpha = C_\alpha = \frac{2\,\alpha\alpha}{2\,\alpha\alpha + \alpha\beta + \beta\alpha} \tag{5.8}$$

(for a β-phase one has to switch the α and β's). The degree of continuity (F_C) and degree of separation (F_S) can now be expressed as follows (Fan *et al.* 1993):

$$F_C = f_\alpha C_\alpha + f_\beta C_\beta \quad \text{and} \quad F_S = f_\alpha S_\alpha + f_\beta S_\beta \tag{5.9}$$

5.3 Phase distributions in naturally deformed polyphase quartzo-feldspathic mylonites

As shown in Chapters 2 and 4, the matrix of the ultramylonitic centre of the type 1 shear zone of the Redbank Deformed Zone is composed of a fine grained (5 - 11 μm) mixture of quartz (Q), plagioclase (P), K-feldspar (K) and biotite (B) (Figs. 2.8c and 4.1). Grain boundary sliding processes have been inferred to be the dominant deformation mechanism operative. Figure 5.7(a)

shows the results of the Markov chain analyses (*cf.* Eq 5.5). Comparing the observed distribution with a distribution expected if the grains were randomly distributed through the sample (*cf.* Eq. 5.6), results in a χ^2 of 231.9. The critical value of χ^2 for a 4-phase system at 5% level of significance is 16.92; the test value comfortably exceeds this, so it can be concluded that the observed TFM differs significantly from randomness. There is a statistically significant tendency for certain phases to be preferentially followed by certain other phases: there are more plagioclase-plagioclase and biotite-biotite grain boundaries and less plagioclase-biotite interphase boundaries, as would be expected in a random distribution. A similar analysis could not be performed on the type 2 ultramylonite sample due to insufficient transitions encountered.

If the plagioclase-plagioclase and the biotite-biotite grain boundaries have lower energies compared to the plagioclase-biotite interphase boundaries, the distribution could resemble a minimum energy configuration. However, this cannot be tested due to the lack of interfacial energy data in wet, mica containing quartzo-feldspathic systems. Since, as shown above, the analyses of grain topology (Eq. 5.4) and phase separation (Eq. 5.9) are limited to two phase materials, these could not be calculated.

More examples of naturally deformed polyphase ultramylonites, preferentially 2-phase, have been searched for. The only study found with detailed enough images where both grain and interphase boundaries are resolved is reported by Stünitz & Fitz Gerald (1993) (their Fig. 6; Corvatsch mylonite zone, Switzerland). The ultramylonite contains however 3-phases; it consists of a fine grained (4 - 24 μm) quartz (Q), albite (P) and epidote (E); the mica content is very low (< 10%) and mica grains are absent in their figures. Figure 5.7b shows the results of the Markov chain analyses (*cf.* Eq 5.5). Comparing the observed distribution with a distribution expected if the grains were randomly distributed through the sample (*cf.* Eq. 5.6), results in a χ^2 of 17.3. The critical value of χ^2 for a 3-phase system at 5% level of significance is 5.99; the

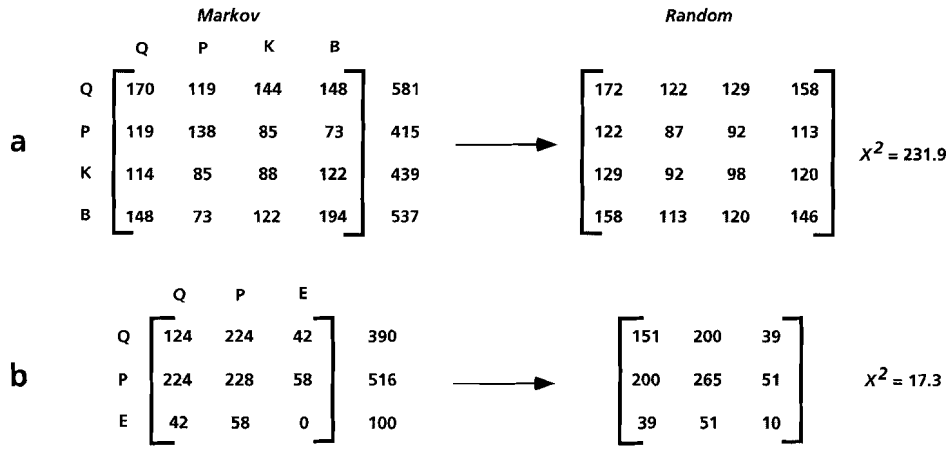

Fig. 5.7 (a) Transition Frequency Matrix (TFM) (Markov) and the TFM of a random distribution of the type 1 ultramylonite (Chapter 4). (b) TFM (Markov) and the TFM of a random distribution of Corvatsch ultramylonite (Stünitz & Fitz Gerald 1993). Q: quartz, P: plagioclase, K: K-feldspar, B: biotite and E: epidote.

test value comfortably exceeds this, so it can be concluded that the observed TFM differs significantly from randomness. As for the type 1 ultramylonites from the Redbank Deformed Zone, within the Corvatsch ultramylonite there is a statistically significant tendency for certain phases to be preferentially followed by certain other phases. In this case, there are more albite-quartz interphase boundaries and fewer quartz-quartz and albite-albite grain boundaries as would be expected if the grains were randomly distributed.

Vernon (1968) measured the interfacial angle and interfacial energies in a gneiss composed of plagioclase, quartz, pyroxene and hornblende; no mention of the mineral composition are reported by Vernon (1968). In that sample, he found that the energy of a plagioclase-quartz interphase boundaries is lower than those of plagioclase-plagioclase and quartz-quartz grain boundaries. If these results are applicable to the Corvatsch sample, the distribution could resemble a minimum energy configuration. However this hypothesis cannot be tested due to the lack of interfacial energy data in epidote containing quartzo-feldspathic systems.

Because of the lack of interfacial energy data and that the analyses of interface population and grain topology is limited to 2-phase materials, analogue materials have been studied to test these hypotheses. The first is a plagioclase - clinopyroxene rock annealed at granulite facies conditions (Section 5.4) and the second is a fine grained ($\approx$ 5 μm), lead - tin alloy which exhibits similar deformation mechanisms as the quartzo-feldspathic ultramylonites, *viz.* with a major contribution of grain boundary sliding (Section 5.5).

5.4 Phase distribution and grain topology in annealed 2-phase basic granulites

Vernon (1970) analysed the microstructure and interfacial angles within some granulites from the Lewisian Complex, Scourie, Sutherland. The granulites consist of relatively few phases (plagioclase (plag) + clinopyroxene (cpx) $\pm$ biotite $\pm$ opaque), which are relatively coarse grained ($\approx$ 1 mm); the grains are typically polygonal with straight or smoothly curved interfaces The rocks are thought to be igneous, which were subsequently statically metamorphosed at granulite facies conditions (Vernon 1968). The two granulites used in this study are taken from Vernon's study; one is a plagioclase rich sample (10020: 66% plag, 34% cpx) and the other is a clinopyroxene rich sample (10023: 30% plag, 70% cpx); the compositions of the phases in both samples are similar (Vernon 1970). Digitised line drawings have been made from Fig. 1 and 2 of Vernon (1970) and are presented in Figs. 5.8(a) and 5.9(a); a summary of the topological parameters is provided in Figs. 5.8(c - e) and 5.9(c - e), and in Table 5.1.

The interfacial angles and energies of these 2-phase granulites, as measured by Vernon (1970), yield different values for the plagioclase rich (R_{plag} = 1.16; R_{cpx} = 1.06; $\gamma_{pp} \approx \gamma_{cc} > \gamma_{pc}$) compared to those of the clinopyroxene rich sample (R_{plag} = 0.97; R_{cpx} = 1.39; $\gamma_{pp} \approx \gamma_{pc} < \gamma_{cc}$). This suggests an effect of phase content on the interfacial energies. Referring to Fig. 5.4, in both samples, the only stable grain junctions are between three grains; only these stable tri-junctions have been observed in the samples (Figs. 5.8e and 5.9e).

Table 5.1 Summary of topological parameters of basic granulites (section 5.4; Fig. 5.8 & 5.9).

		plag:	cpx:	total:
plag - 34% cpx Fig. 5.8	n	7.4 ± 2.5	3.9 ± 1.2	5.4 ± 2.5
	Sk	1.2	0.1	1.4
	Km	1.6	- 0.7	2.5
	range	4 / 14	2 / 6	2 / 14
	Md	6	4	5
	N	17	23	40
	IGBC	- 0.8 ± 2.4	1.3 ± 1.0	0.4 ± 2.0
	Sk	-1.1	- 0.2	-1.7
	Km	1.4		3.8
	range	- 7.0 / 2.4	- 0.4 / 3.0	-7.0 / 3.0
	Md	0.9	nd	1.7
	Fs			0.63
plag - 70% cpx Fig. 5.9	n	3.5 ± 0.9	8.5 ± 2.7	5.2 ± 2.9
	Sk	0.5	0.5	1.3
	Km	- 0.6	- 0.6	1.1
	range	2 / 6	5 / 14	2 / 14
	Md	4	nd	4
	N	34	18	52
	IGBC	1.5 ± 1.2	- 1.3 ± 2.8	0.6 ± 2.1
	Sk	- 0.4	- 0.5	- 1.1
	Km	0.2	0.4	1.3
	range	- 2.0 / 3.2	- 5.9 / 2.1	-5.9 / 3.2
	Md	1.1	nd	1.1
	Fs			0.55

Key: n: number of sides per grain (errors are 1 times the standard deviation); Sk: skewness; Km: kurtosis; Md: mode; IGBC: integratedgrain boundary curvature, N: sample size.

In both granulites the minor phase is mostly finer grained than the major phase and has 2 - 6 neighbours, with a mode (Md) of 4 (Table 5.1, Figs. 5.8c and 5.9c).The more abundant and larger phase has 4 - 14 neighbours, with a mode of 6 (Table 5.1, Figs. 5.8c and 5.9c). For both samples the number of sides, combining all phases in the sample, ranges from 2 - 14, with a mode of 5. Using Eq. 5.4, the integrated grain boundary curvature (IGBC) has been calculated (Figs. 5.8d and 5.9d) for the two samples. As shown in Figs. 5.8(d) and 5.9(d), generally the smaller phases have a positive IGBC, while the larger phases have a negative one. The average IGBC for the plagioclase rich and clinopyroxene rich samples are about equal (0.4 and 0.6 respectively).

Figure 5.8b shows the results of the Markov chain analyses (*cf.* Eq 5.5) of the plagioclase rich sample. Comparing the observed distribution with a distribution expected if the grains were randomly distributed through the sample (*cf.* Eq. 5.6), results in a χ^2 of 24.4. The critical value of χ^2 for a 2-phase system at 5% level of significance is 3.84; the test value comfortably exceeds this, so it can be concluded that the observed TFM differs significantly from randomness: there are fewer plag - plag and cpx - cpx grain boundaries and more plag - cpx interphase boundaries, as would be expected in a random distribution.

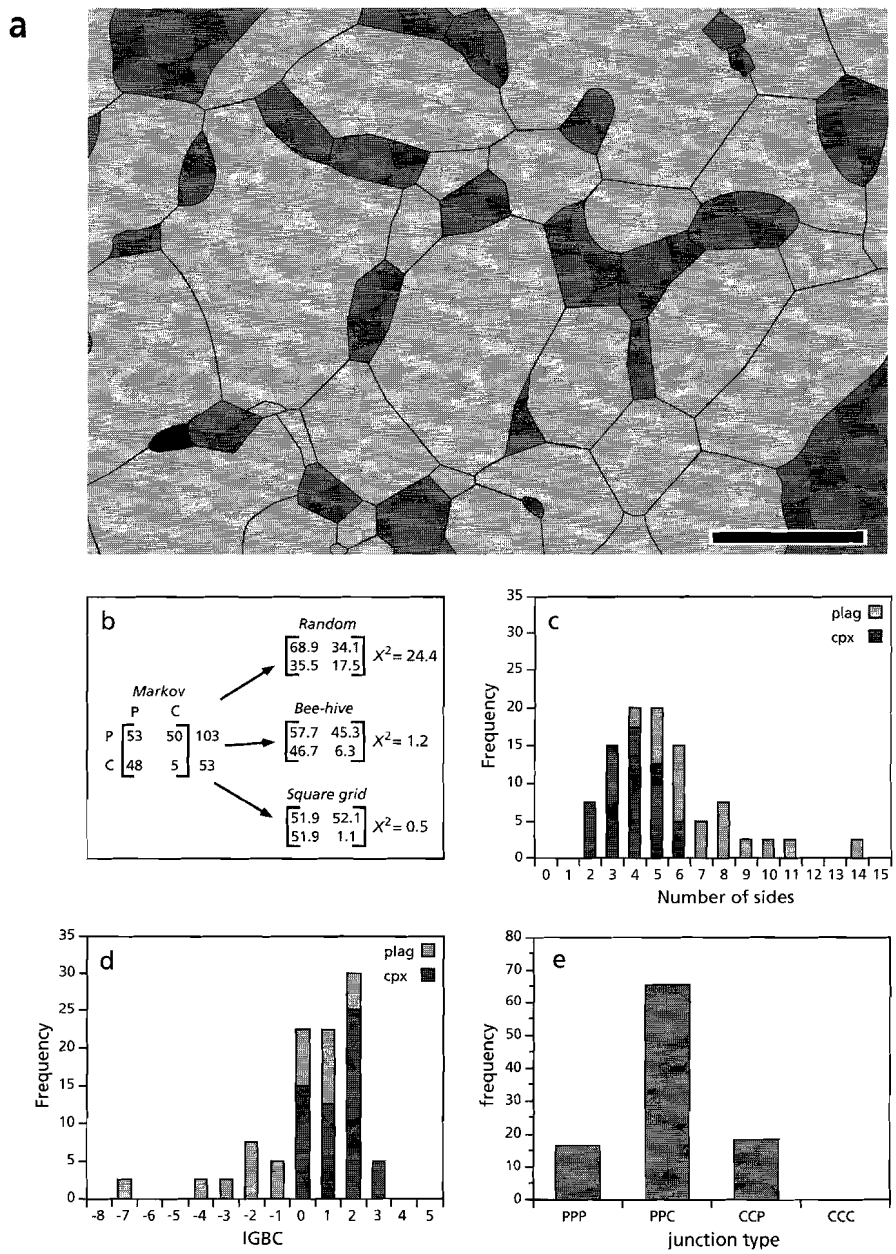

Fig. 5.8 Microstructure and topological parameters of a plagioclase rich basic granulite composed of 66 % plagioclase (P, light phase) and 34 % clinopyroxene (C, dark phase). (a) Line drawing after Fig. 1 (sample 10020) of Vernon (1970); black phases are opaques. Scale bar: 500 μm. (b) Observed TFM (Markov) compared with the TFM of a random distribution and with the TFM of a minimum energy configuration calculated for a bee-hive and square-grid structure. (c-e) Histograms showing the distribution of topological parameters. (c) number of sides per grain, (d) IGBC as calculated with Eq. 5.4 and (e) type of grain junction.

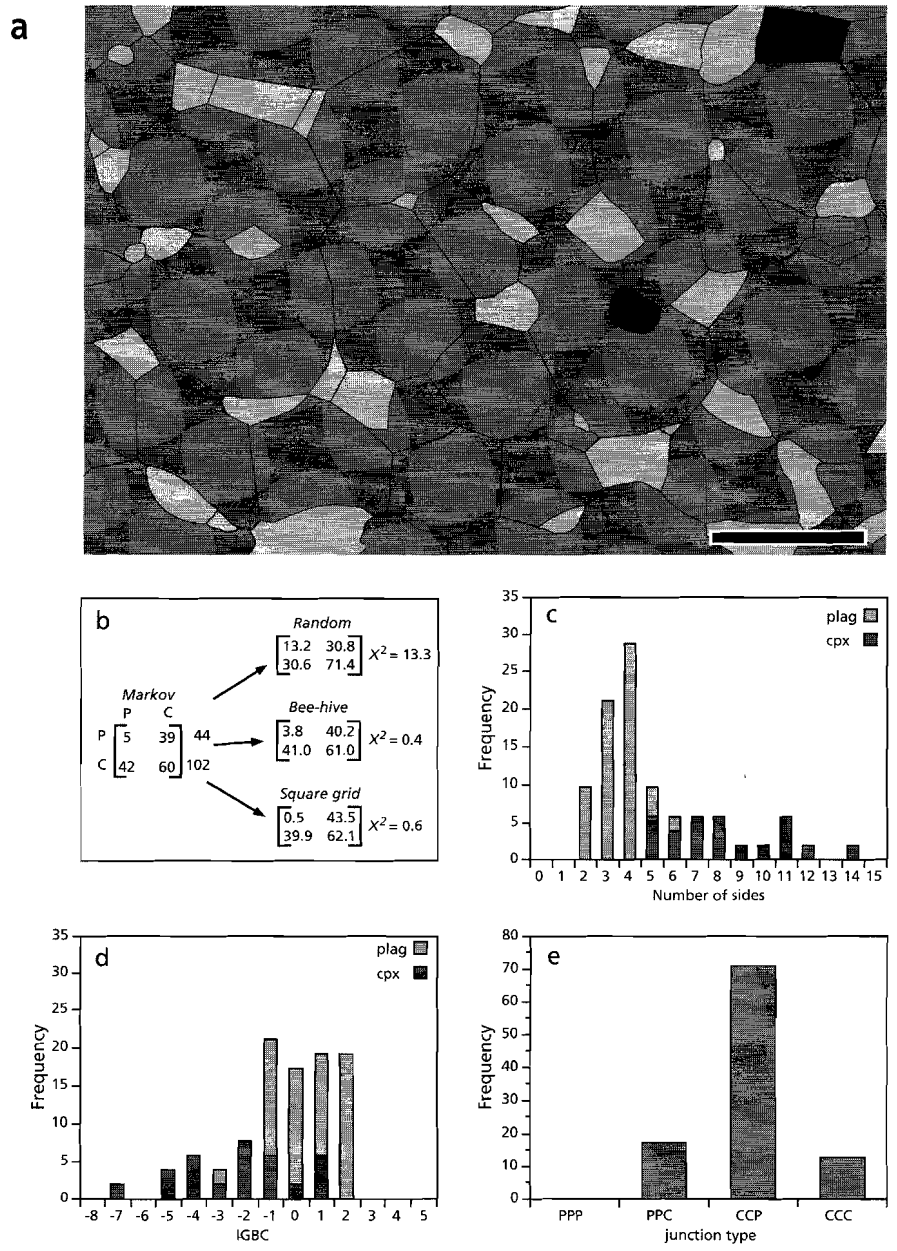

Fig. 5.9 Microstructure and topological parameters of a plagioclase rich basic granulite composed of 30 % plagioclase (P, light phase) and 70 % clinopyroxene (C, dark phase). (a) Line drawing after Fig. 2 (sample 10023) of Vernon (1970); black phases are opaques. Scale bar: 500 μm. (b-e) as in Fig. 5.5.

The interfacial angles measured by Vernon (1970) on the same sample indicate that within the plagioclase rich sample the plag-cpx interphase boundaries have lower interfacial energies compared the plag-plag and cpx-cpx grain boundaries. Comparing the observed distribution with a distribution expected with the grains in a minimum energy configuration (*cf.* Eq. 5.6), results in a χ^2 of 1.2 and 0.5, for respectively a bee-hive structure and a square grid structure. The critical value of χ^2 for a 2-phase system at 5% level of significance is 3.84; the test value doesn't exceed this, so it cannot be concluded that the observed TFM differs significantly from a minimum energy configuration, in which low energy boundaries are more common than high energy ones. The phase distribution in the clinopyroxene rich sample can, in an analogous manner, be described as a minimum energy configuration (Fig. 5.9b).

5.5 Effect of interfacial energies on grain boundary sliding deformation of 2-phase Pb-Sn alloys

As many ultramylonites contain more than one phase (Section 5.3; reviews in Chapters 2 and 4), one would like to study the deformation mechanisms and microstructural development in experimentally deformed fine grained rocks. Such experimental data is very limited, these include calcite - anhydrite (Bruhn *et al.* 1993; 1994) and some experiments on quartzo - feldspathic rocks by Tullis (1990). However, in both studies no detailed microstructures and/or stress strain relations are reported.

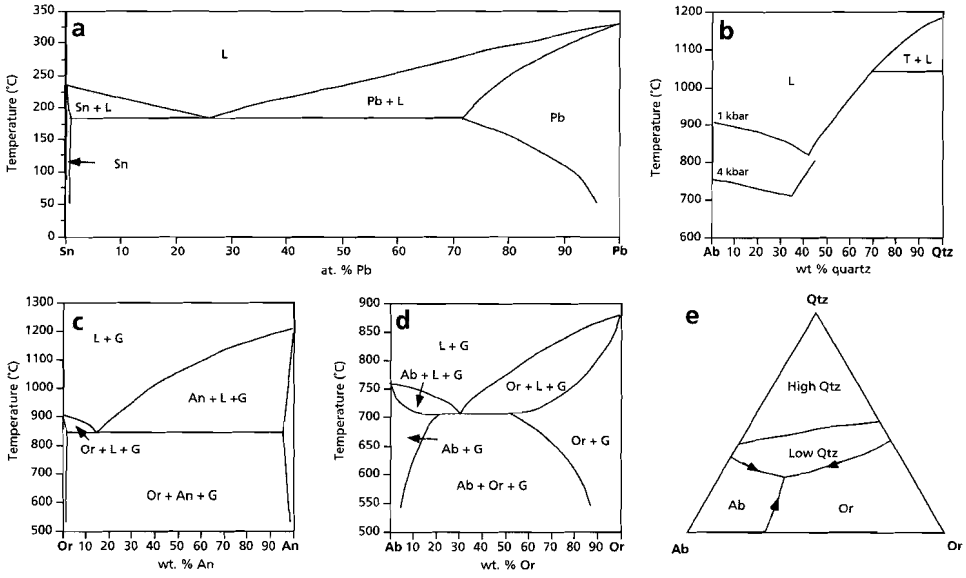

Fig. 5.10 Phase diagrams of (a) Pb-Sn alloy, (b) albite-quartz (Ab-Qtz) at 1 Kbar P_{H2O} and 4 Kbar P_{H2O}, (c) orthoclase-anorthite (Or-An) at 5 Kbar P_{H2O}, (d) albite-orthoclase (Ab-Or) at 5 Kbar P_{H2O} and (e) albite-orthoclase-quartz (Ab-Or-Qtz) at 6 Kbar P_{H2O}. [(a) after Karakaya & Thompson (1988); (b-e) after Ehlers (1972)]

Like the ultramylonites, many engineering materials deforming by grain boundary sliding deformation processes contain more than one phase. It is frequently observed that those that exhibit increased stability and optimum (highest) extensibility (showing so-called superplastic behaviour) are composed of phases with approximately the same ductilities and which are present in nearly equal proportions. Many of these (superplastic) alloys are therefore based on eutectic or eutectoid systems (for review see Johnson 1970; Padmanabhan & Davies 1980; Sherby & Wadsworth 1990).

In this section analyses on interface population and grain topology in a 2-phase lead-tin (Pb - Sn) alloy are presented as an analogue for the polyphase quartzo-feldspathic ultramylonites. The reason for the choice of the Pb - Sn system is two fold. Firstly it has a relatively simple binary phase diagram (Fig. 5.10a) (Karakaya & Thompson 1988), similar to those of the common granitoid forming minerals (Ehlers 1972), e.g. that of the albite - quartz (Fig. 10b), orthoclase - anorthite (Fig. 5.10c) and albite - orthoclase (Fig. 5.10d) systems in the presence of water. Secondly, the Pb - Sn system is a well studied superplastic alloy with similar deformation mechanisms as inferred for the fine grained quartzo-feldspathic ultramylonites, *viz.* involving a major component of grain boundary sliding processes with accommodating diffusional processes (Cline & Alden 1967; Zehr & Backofen 1968; Rawal & Murty 1972; Gecklini & Barrett 1974; 1976; Ma & Langdon 1994; Yan *et al.* 1994; Zelin & Mukherjee 1993b; 1993c; 1995; Zelin *et al.* 1994). The other superplastic system studied extensively is the Al-Zn system (Presnyakov & Chervyakova 1959; Backofen *et al.* 1964; Melton & Edington 1975; Langdon 1982; Hirohashi & Asanuma 1989) but it has a more complicated phase diagram, with several intermediate phases (Murray 1983). Furthermore, the experimental and microstructural data of the Al-Zn system has been found to be less complete than of the Pb-Sn system.

Experimental results

Details on the deformation experiments can be found in Cline & Alden (1967) and Zehr & Backofen (1968), the most important of them are outlined below. Seven different compositions, 5 from within the 2-phase region of the Pb-Sn system and pure Pb and pure Sn, have been tested in elongation at various strain rates (10^{-5} to 10^{-2} s^{-1}), various temperatures (25 to 170 °C) and various grain sizes (3 - 20 μm)[2]. All stress-strain rate curves show the similar sigmodial shape, characteristic for superplastic materials. Stress values reported were taken at 5% strain. Diffusion accommodated grain boundary sliding deformation has been inferred to be the dominant deformation process in all samples (Cline & Alden 1967; Zehr & Backofen 1968; Gecklini & Barrett 1974; 1976). The experimental runs reported in this study include the two most complete data sets: one at 26 °C and a second at 120 °C at a strain rate within the dominant diffusion accommodated grain boundary sliding regime (5×10^{-5} s^{-1}) and one within the dominant dislocation creep regime (5×10^{-2} s^{-1}) (*cf.* Zehr & Backofen 1968; Gecklini & Barrett 1974). During deformation grain growth occurred, with the amount of growth dependent on the strain rate (the lower the strain rate the more pronounced the grain growth); only limited grain elongations occurred.

[2] Both Cline & Alden (1967) and Zehr & Backofen (1968) report grain sizes in terms of their mean lineal intercept. In this study, their values have been corrected for sectioning effects using a factor of 1.75 (*cf.* Underwood 1970)

The variation of the strength of the two-phase alloy with composition is shown in Fig. 5.11(a). The original data of Zehr & Backofen (1968; their Fig. 15) at 25 °C are shown as dashed lines in Fig. 5.11(a) (curve 1 and 2). Curve 1 is for a grain size of 4.5 μm at a strain rate (5×10^{-2} s^{-1}) within the dominant dislocation creep regime (Zehr & Backofen 1968), whereas curve 2 is for a grain size of 4.5 μm at a strain rates (5×10^{-5} s^{-1}) within the dominant diffusion accommodated grain boundary sliding creep regime. The different alloys of the two reports (Cline & Alden 1967; Zehr & Backofen 1968) were tested with different grain sizes, which hinders a direct comparison. Therefore, some of these have been recalculated to a constant grain size of 3.5 μm by linear interpolation and is shown as curve 3 (strain rate: 5×10^{-5} s^{-1}). This grain size of 3.5 μm lies closest to the experimental data of the finest grained samples, which ranges from 3 to 10 μm.

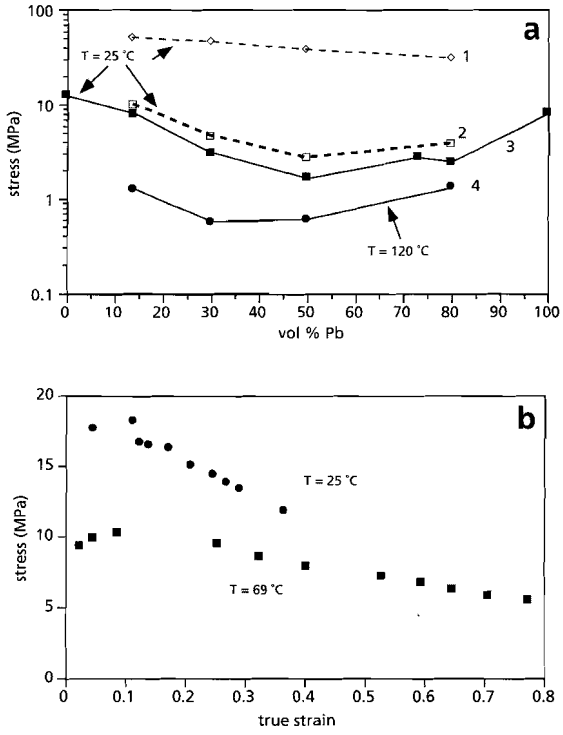

Fig. 5.11 Experimental deformation results on Pb-Sn system. (a) variation of flow stress with vol.% Pb; curve (1): grain size 4.5 μm, strain rate 5×10^{-2} s^{-1}, T = 25 °C, dislocation creep (after Zehr & Backofen 1968). Curve (2): grain size 4.5 μm, strain rate 5×10^{-5} s^{-1}, T = 25 °C, diffusion accommodated grain boundary sliding (after Zehr & Backofen 1968). Curve (3): Combined data of Cline & Alden (1967) and Zehr & Backofen (1968) recalculated to a grain size of 3.5 μm, strain rate 5×10^{-5} s^{-1}, T = 25 °C, diffusion accommodated grain boundary sliding. Curve (4): As for (3) data recalculated to T = 120 °C. Note that the strength passes through a minimum at Pb - 50 vol.% Sn if the material is deforming by diffusion accommodated grain boundary sliding and that such an effect is absent in curve (1).
(b) Relation between true stress and true strain for a Pb - 70 vol. % Sn alloy showing a weakening of the material with increasing strain at T = 25 °C and T = 69 °C. Grain size 5.3 μm, and strain rate 5×10^{-5} s^{-1} (after Gecklini & Barrett 1974).

Curve 4 is for a grain size of 3.5 μm at a strain rate within the dominant grain boundary sliding regime (5×10^{-5} s^{-1}) at a higher temperature (T = 120 °C).

From Fig. 5.11(a) it can clearly be seen that at 25 °C the flow stress passes through a minimum when both phases are at 50% by volume: the flow stress of the Pb - 50 vol.% Sn mixture is a factor of 8 - 10 less than either of the pure tin or the pure lead. At higher temperatures, this effect is less pronounced. Such a weakening effect is not observed when the material deformed by dominant dislocation creep processes at high strain rates. There the addition of Sn, generally observed to be the harder phase, tends to strengthen the material. Similar observations on other metal systems have been reviewed by Chen (1985).

The variation of stress with strain (elongation) in a eutectic Pb - 70 vol.% Sn has been studied by Rawal & Murty (1972); Gecklini & Barrett (1974) and Haruna *et al.* (1992). Fig. 5.11(b) shows an example of such a true stress versus true strain curve (taken after Gecklini & Barrett 1974) at a grain size of 5.3 μm and strain rates of 4.6×10^{-4} s^{-1}; no microstructural data were presented by the authors. With strain, the material shows a progressive softening, i.e. the higher the strain the weaker the materials becomes; the flow stress of the alloy at a strain of 50 - 80% is a factor of 2 less than the flow stress at 5% strain. Therefore, since the stress values reported by Zehr & Backofen (1969) were taken at 5% strain, the effect observed in Fig. 5.11(a) underestimates the softening at high strains.

Although the data on grain boundary diffusion is extensive (see Kaur *et al.* 1989; Mehrer 1990), the data on interphase boundary diffusion is very limited; no such data has been found for the Pb-Sn system. Data is available for the Ag-Fe and Ag-Cu systems and these have been used to provide insight into what can be expected for interphase boundary and grain boundary diffusion in the Pb - Sn system. The data are taken from Martin & Perraillon (1979) and Kaur *et al.* (1989) and are presented in Fig. 5.12. For these two systems, at elevated temperatures, interphase boundary diffusion has been found to be faster than grain boundary diffusion; the absolute diffusivity depending on the temperature. At lower temperatures grain boundary diffusion is faster than interphase boundary diffusion.

Although only grain boundary diffusivities are known for the Pb-Sn system, some indication on interphase boundary diffusivities can be obtained as follows (data from Mehrer 1990). At 250 °C, the addition of Sn in solid solution to Pb (still a single phase alloy) results in an increase in the Pb-Sn interdiffusion (Fig. 5.12d). This might suggest that, as for the Ag-Fe and Ag-Cu systems, at elevated temperatures in the Pb-Sn system, interphase boundary diffusion is faster than grain boundary diffusion. The grain boundary diffusivities for Pb and Sn are similar within a factor of 5 (Fig. 5.12a).

The above presented mechanical data showed that a Pb - 50 vol.% Sn alloy deforming by diffusion accommodated grain boundary sliding processes has a lower flow stress than either of the pure phases. The data further shows a weakening with strain of a Pb - 70 vol.% Sn alloy with similar deformation mechanisms. It is suggested that these might be the result of variations in microstructure, grain topology and interfacial distribution. To test this hypothesis, interfacial populations and phase distributions have been analysed in two 2-phase Pb - 70 vol.% Sn alloys: one before deformation and one after 50% elongation. The results are presented in the next section.

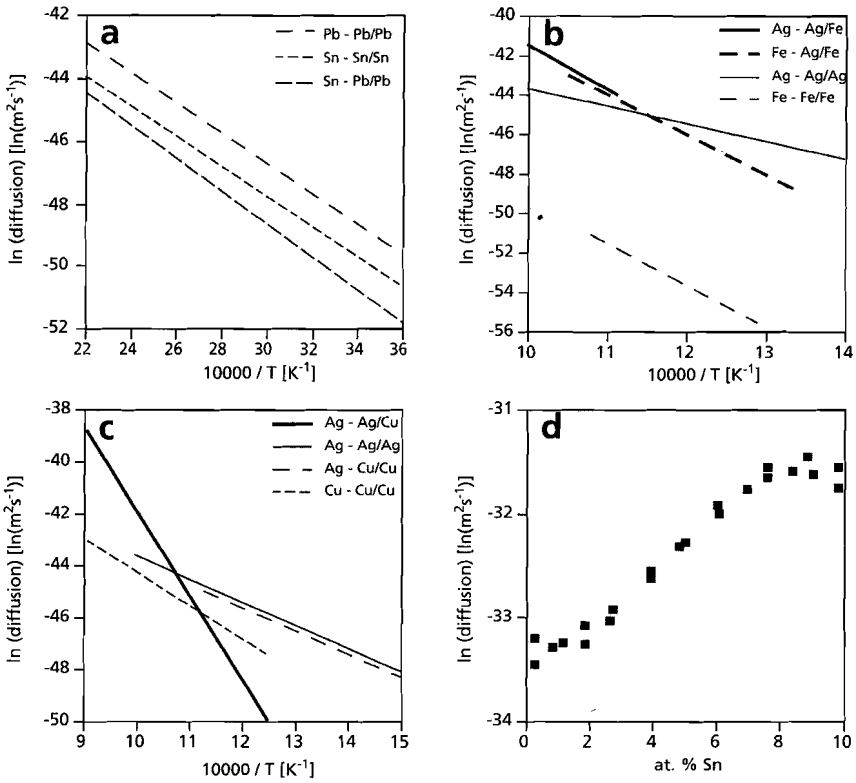

Fig. 5.12 Grain and interphase boundary diffusion data. Ahhrenius graphs of (a) Pb-Sn grain boundary diffusion (Kaur *et al.* 1989), (b) Ag-Fe grain and interphase boundary diffusion (Kaur *et al.* 1989) and (c) Ag - Cu grain and interphase boundary diffusion (Martin & Perraillon 1979; Kaur *et al.* 1989). The graphs are constructed for a 1 nm grain and interphase boundary width. A - A/B denotes diffusion of species A through an A-B boundary. (d) Variation of Pb-Sn interdiffusion with at % Sn (in solid solution) in single phase Pb at 250 °C (after Mehrer 1990). Note the increase in diffusivity with increasing at % Sn.

Microstructural observations

Edington *et al.* (1976, p. 90) report the microstructure at various strains (elongations) of a eutectic, Pb - 70 vol.% Sn alloy in tensile deformation at 160 °C; neither strain rates nor the pre-treatment of the starting material were reported. For both the undeformed sample and at 50% elongation the individual grains could be resolved from their micrographs (their Fig 15); digitised line drawings have been made from these and are presented in Figs. 5.13(a) and 5.14(a), respectively. Interfacial angles have been measured (*cf.* Spry 1976) from a sample annealed at 160 °C (Fig. 15e of Edington *et al.* 1976) and result in $R_{Pb} = R_{Sn} = 1.25$ ($\gamma_{Pb} \approx \gamma_{Sn} > \gamma_{Pb\text{-}Sn}$). The individual grains could not be resolved in the samples at higher elongations. A summary of the topological parameters is provided in Figs. 5.13(c - e) and 5.14(c - e), and in Table 5.2.

In the undeformed material the average overall grain size of the phases is around 5 μm (Fig. 5.13a), with generally the Pb phase finer grained (≈ 4 μm) than the Sn phase (≈ 5.5 μm). The Pb

Table 5.2 Summary of topological parameters of lead - tin alloy (section 5.5; Fig. 5.10 & 5.11).

		Sn:	Pb:	total:
	n	6.0 ± 1.8	4.6 ± 1.3	5.4 ± 1.7
	Sk	0.2	0.6	0.5
	Km	- 0.6	- 0.2	- 0.3
	range	2 / 10	2 / 8	2 / 10
	Md	6	4	4
Pb - Sn	N	100	72	172
0% strain				
Fig. 5.10	IGBC	0.2 ± 1.8	0.7 ± 1.5	0.4 ± 1.7
	Sk	- 0.3	- 0.7	- 0.5
	Km	- 0.3	0.0	0.2
	range	- 4.5 / 4.5	- 3.5 / 3.5	- 4.5 / 4.5
	Md	1.4	1.8	1.8
	Fs			0.32
	n	6.9 ± 1.9	4.3 ± 1.2	5.8 ± 2.1
	Sk	0.5	0.2	0.6
	Km	- 0.5	- 0.5	- 0.1
	range	3 / 12	2 / 7	2 / 12
	Md	6	5	5
Pb - Sn	N	100	79	179
50% strain				
Fig. 5.11	IGBC	- 0.3 ± 1.9	1.0 ± 1.5	0.2 ± 1.8
	Sk	- 0.6	- 0.3	- 0.6
	Km	0.0	0.1	0.5
	range	- 5.3 / 3.5	-3.5 / 4.5	- 5.3 / 4.5
	Md	1.7	2.1	2.1
	Fs			0.28

Key: n: number of sides per grain (errors are 1 times the standard deviation); Sk: skewness; Km: kurtosis; Md: mode; IGBC: integratedgrain boundary curvature, N: sample size.

phase has 2 - 8 neighbours, with a mode (Md) of 4 (Table 5.2 and Fig. 5.13c), whereas the Sn phase has 2 - 10 neighbours with a mode of 6; combining both phases in the sample, the number of sides ranges from 2 - 10 with a mode of 4 (Fig. 5.13c). Using Eq. 5.4, the integrated grain boundary curvature (IGBC) has been calculated (Fig. 5.13d). As shown in Fig. 5.13(d), generally the smaller Pb grains have a positive IGBC, while the larger Sn grains have a negative IGBC. The difference between all negative and all positive IGBC values (Fig. 5.13d) is around 3. Besides stable tri-junctions (*cf.* Fig. 5.4), up to 20% of unstable quadri-junctions are present in the sample (Fig. 5.13e).

At 50% elongation (Fig. 5.14a), the overall grain size has only slightly increased (≈ 5.5 μm), with, as for the undeformed material, generally the Sn phase coarser grained (≈ 6.5 μm) than the Pb grains (≈ 4 μm). All topological parameters of the alloy at 50% elongation are similar to those of the starting material (compare Fig. 5.14c - d with 5.13c - d). The main difference is that the number of unstable quadri-junctions is reduced to below 5% (Fig. 5.14e) and only stable tri-junctions exist in the sample elongated to 50%.

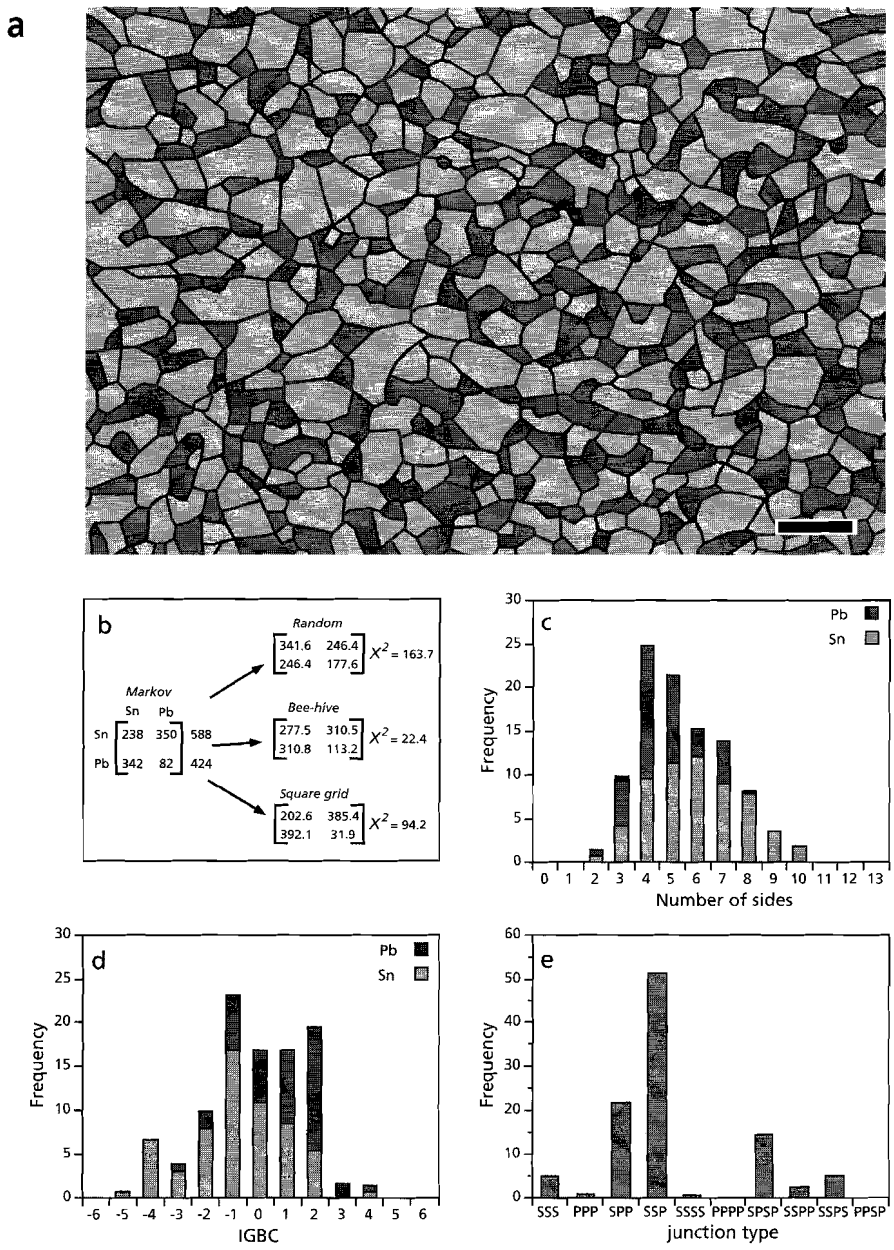

Fig. 5.13 Microstructure and topological parameters of an undeformed Pb - 70 vol.% Sn alloy. (a) Line drawing after Fig. 15a of Edington *et al.* (1976); Pb: dark phase, Sn: light phase. Scale bar: 10 μm. (b) Observed TFM (Markov) compared with the TFM of a random distribution and with the TFM of a minimum energy configuration calculated for a bee-hive and square-grid structure. (c-e) Histograms showing the distribution of topological parameters. (c) number of sides per grain, (d) IGBC as calculated with Eq. 5.4 and (e) type of grain junction. Note that there are up to 20 % of unstable quadri-junctions.

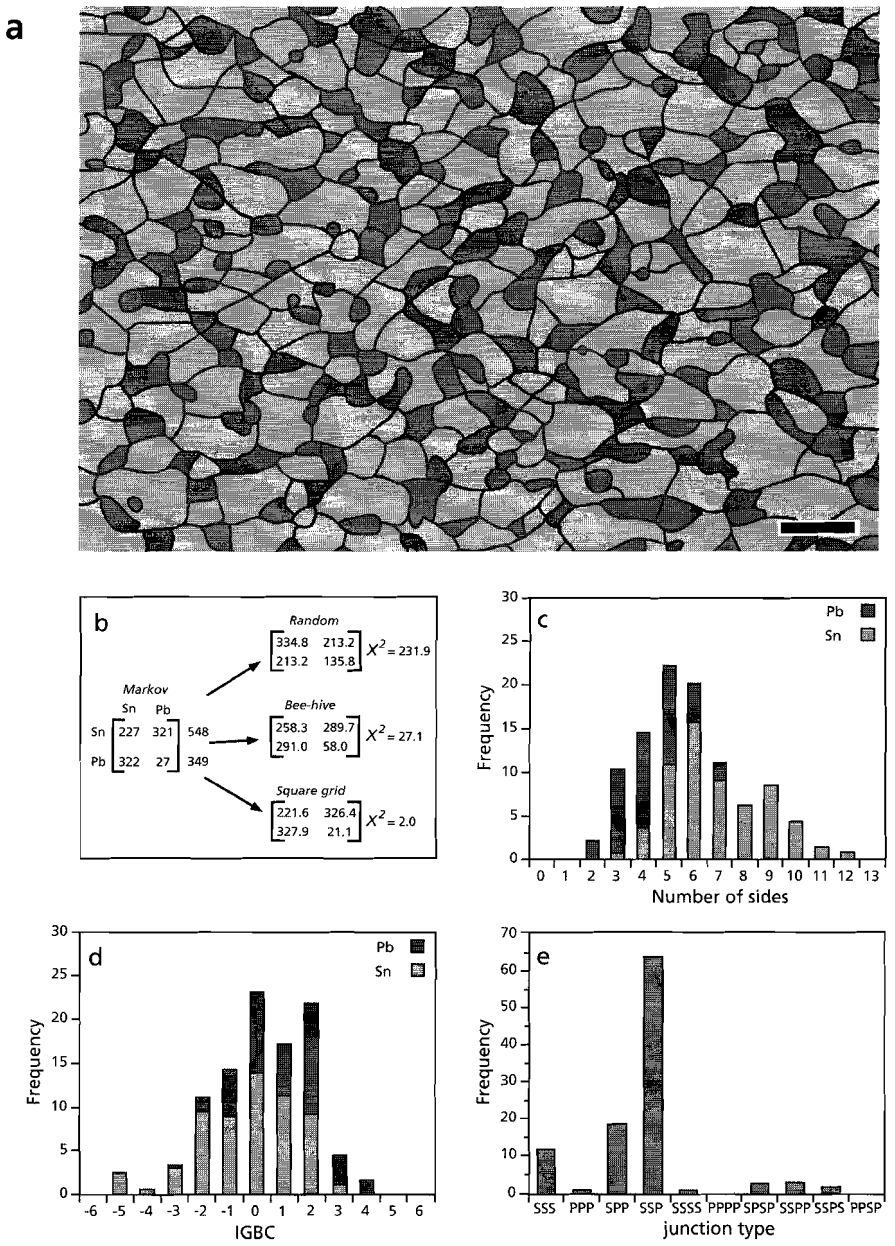

Fig. 5.14 Microstructure and topological parameters of a Pb - 70 vol.% Sn alloy at 50 % elongation. (a) Line drawing after Fig. 15b of Edington *et al.* (1976); Pb: dark phase, Sn: light phase. Scale bar: 10 μm. (b-e) as in Fig. 5.14. Note the reduction of unstable quadri-junctions with respect to the starting material (Fig. 5.13e).

Figure 5.13(b) shows the results of the Markov chain analyses (*cf.* Eq 5.5) of the undeformed sample. Comparing the observed distribution with a distribution expected if the grains were randomly distributed through the sample (*cf.* Eq. 5.6), results in a χ^2 of 163.7. The critical value of χ^2 for a 2-phase system at 5% level of significance is 3.84; the test value comfortably exceeds this, so it can be concluded that the observed TFM differs significantly from randomness: there are fewer Pb - Pb grain boundaries and Sn - Sn grain boundaries and more Pb - Sn interphase boundaries, as would be expected in a random distribution.

Since the interphase boundaries have lower interfacial energies than the grain boundaries, the microstructure might resemble one of lowest interfacial energy. Comparing the observed distribution with a distribution expected with the grains in a minimum energy configuration (*cf.* Eq. 5.6), results in a χ^2 of 22.4 and 94.2, for respectively a bee-hive structure and a square grid structure. The critical value of χ^2 for a 2-phase system at 5% level of significance is 3.84; the test value comfortably exceed this, so it can be concluded that the observed TFM differs significantly from a minimum energy configuration, either based on square or hexagonal grain shapes.

When comparing the results of the Markov chain analyses of the sample at 50% elongation with that of the undeformed sample, some marked differences occur (compare Fig. 5.13b with 5.14b). The percentage of (low energy) Pb-Sn interphase boundaries has increased from 68% in the undeformed sample to 72% in the sample elongated to 50%. This is also reflected in the degree of phase separation, which reduced from 0.32 in the starting material to 0.28 in the sample at 50% elongation.

Testing the TFM of the sample at 50% elongation with a distribution expected with the grains in a minimum energy configuration, results in a χ^2 of 27.1 and 2.0, for respectively a bee-hive structure and a square grid structure. Although one cannot reject the hypothesis that the microstructure resembles a minimum energy configuration, grain topology indicates that the number of neighbours ranges from 2 - 12, with a mode of 5. Whether or not the microstructure resembles a minimum energy configuration is difficult to establish using the "fixed" grain geometry computer model, and remains to be tested by Monte Carlo Potts computer simulations where grain and interphase boundaries are free to move resulting in a wider variety of grain shapes. However, from the above it can be concluded that the deformation of the Pb-Sn alloy resulted in an increase of low energy Pb-Sn interphase boundaries and an associated reduction in total interfacial energy.

Modelling of interphase boundary population and total interfacial energy

The relative interfacial energies and the distribution of the phases in both the bee-hive and square-grid microstructures have been used to calculate the percentage of Pb - Sn interphase boundaries and the associated total interfacial energy as a function of Pb content of grains in a random and a minimum energy configuration. The results are presented in Fig. 5.15. The curve marked R is for a random distribution of phases, the curves marked B and S are for minimum energy configurations calculated respectively for a bee-hive and square grid structure.

For all three models (Fig. 5.15a), the percentage of interphase boundaries increases with increasing Pb content and reaches a maximum at 50% Pb, after which it decreases again. This

rate of increase however, differs for the three models. The percentage of interphase boundaries for the square grid minimum energy microstructure at 50 vol.% Pb has a maximum value of 83%, whereas for the bee-hive minimum energy structure a maximum value of 65% has been calculated. The percentage of Pb - Sn interphase boundaries encountered in a random distribution is even lower (50%). The total interfacial energy variation with Pb content is clearly associated with the changes in interfacial distribution and is shown in Fig. 5.15(c): the more interphase boundaries the lower the total interfacial energy.

The calculation of a minimum energy configuration involved grain swapping, i.e. two grains change places only if the interfacial energy is thereby reduced. After several iterative steps, the end microstructure will then have a minimum energy (Figs. 5.5 and 5.6). The evolution of total interphase boundary content for both the bee-hive and square grid structures are shown in Fig.

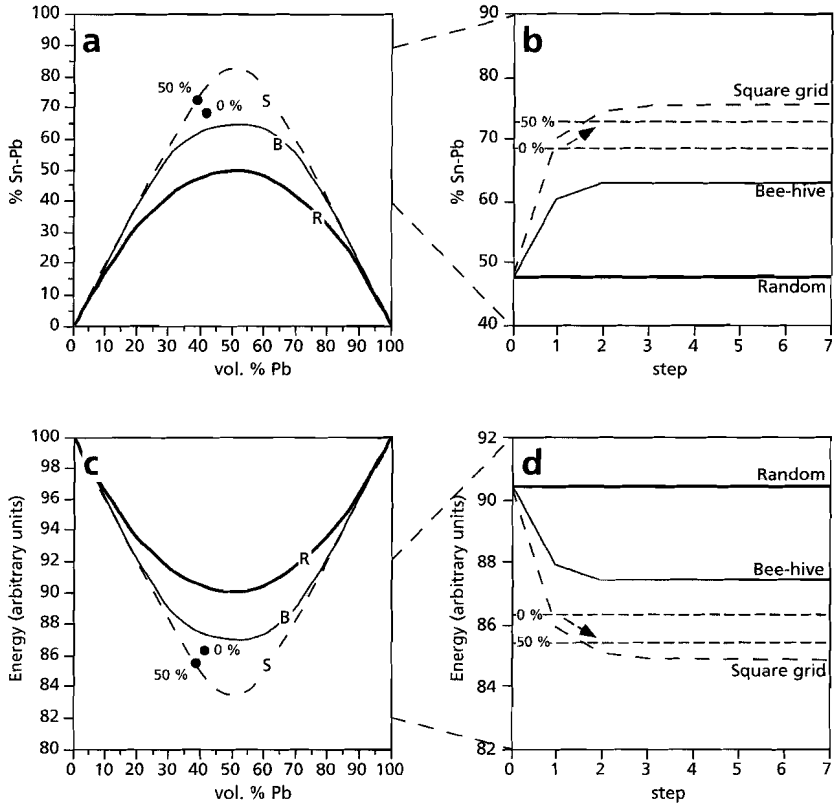

Fig. 5.15 Interphase boundary population and associated interfacial energy variations in the Pb-Sn system. (a) variation of Pb-Sn interphase boundary population with vol.% Pb; R: random microstructure, B: minimum energy configuration based on bee-hive grid, and S: and minimum energy configuration based on a square-grid. Note that the Pb-50 vol. % Sn has the highest amount of interphase boundaries. (b) Evolution of Pb-Sn interphase boundary population as a result of the grain swapping computer model. Note the increase of interphase boundaries with successive steps towards a stable configuration. (c) & (d) Interfacial energies associated with respectively (a) and (b). 0% & 50%: denote respectively the interface population of starting material (Fig. 5.13) and at 50% elongation. See text for discussion.

5.15(b); the associated energy variation is shown in Fig. 5.15(d). Starting with an initial random distribution of the phases, the microstructure evolves to one having more (low energy) interphase boundaries and thus fewer Pb - Pb and Sn - Sn grain boundaries.

Also shown in Fig. 5.15 are the interfacial distribution data of the undeformed alloy (marked 0% in Fig. 15) and the sample at 50% elongation (marked 50% in Fig. 15). As shown in these figures, neither the random distribution nor the minimum energy configuration in a bee-hive microstructure is capable in explaining the interfacial distribution of both the starting material or the sample at 50% elongation; the percentage of Pb - Sn interphase boundaries observed in the materials in higher than the one calculated. The interfacial evolution in a square grid microstructure (Fig. 5.15b) first increases to the level of the starting material, followed by the level of the sample at 50% elongation, before it reaches a constant level just above the latter. Accompanying this increase in interphase boundary population is a decrease in total interfacial energy.

5.6 Discussion

Relation between microstructure and physical properties

From the experimental data and the microstructural observations on the 2-phase Pb - Sn alloy system it is inferred that interfacial distributions have a significant effect on the mechanical properties of the 2-phase alloy. The Pb - 50 vol.% Sn alloy exhibited lower flow stresses, compared to the pure phases, when deforming by diffusion accommodated grain boundary sliding. Within the Pb - Sn alloy system, the highest number of interphase boundaries occur within the Pb - 50 vol.% Sn alloy. The actual amount of interphase boundaries is found to depend on the configuration of the phases (random or minimum energy) and on the grain shape of the phases (bee-hive or square). No such weakening effect has been observed when the material deformed by dominant dislocation creep processes. The deformation of the Pb - 70 vol.% Sn alloy resulted in an increase in Pb - Sn interphase boundaries with strain, while grain topologies remained similar. Deformation experiments on similar Pb - 70 vol.% Sn alloys (Fig. 5.11b; Rawal & Murty 1972; Gecklini & Barrett 1974; Haruna *et al.* 1992) show that with strain the alloy weakened. It is therefore concluded that the mechanical behaviour of a Pb - Sn alloy is closely linked to the content of Pb - Sn interphase boundaries in the material.

Studies on interfacial properties within the Pb - Sn system have shown that different types of interfaces have different grain boundary sliding resistances (Vastava & Langdon 1979; Haruna *et al.* 1992). At room temperature, Haruna *et al.* (1992) observed that sliding occurred mainly along the Sn - Sn and Pb - Pb boundaries, whereas sliding along Pb - Sn boundaries was limited. At higher temperatures (T = 150 °C), Vastava & Langdon (1979) observed that no sliding along Pb - Pb boundaries occurred, limited sliding took place along Pb - Sn interphase boundaries; most sliding occurred along Sn - Sn grain boundaries. If the experimentally observed weakening was dominated by these different grain boundary sliding resistances, one would expect that a material with the highest amount of 'weak' boundaries would be the weakest alloy, i.e. pure Pb or Sn at room temperature, and pure Sn at 150 °C. Since the Pb - 50 vol.% Sn alloy is the weakest alloy

in the Pb - Sn system, different grain boundary sliding resistances cannot be the main cause for the observed weakening.

The analyses on grain and interphase boundary diffusion in 2-phase Ag - Fe and Ag - Cu alloys indicate that at elevated temperatures interphase boundary diffusion is faster than grain boundary diffusion. The increase in Pb-Sn interdiffusion with the addition of Sn in solid solution to Pb (Fig. 5.12d) suggest that similar relations apply to the Pb-Sn system. Since diffusion is generally found to be the rate limiting step (e.g. Zehr & Backofen 1968; Padmanabhan & Davies 1980; Gifkins 1982), it is expected that the more interphase boundaries a Pb - Sn alloy has, the faster the overall diffusion. If the deformation mechanism involved a major component of diffusion, this will result in a weaker alloy. Three pieces of evidence support this view. Firstly, the highest amount of interphase boundaries occur within the Pb - 50 vol.% Sn (Fig. 5.15a) which is observed to be the weakest alloy in the Pb - Sn system (Fig. 5.11a). Secondly, the deformation of the Pb - 70 vol.% Sn alloy resulted in an increase in such interphase boundaries with strain; the deformation experiments on similar Pb - Sn alloys (Fig. 5.11b) show that with strain the alloy weakened. Thirdly, the experiments on the alloy within the dislocation creep regime, do not show the weakening with composition (Fig. 5.11a, curve 1).

It is therefore concluded that interfacial distributions have a significant effect on the mechanical behaviour of the 2-phase Pb - Sn alloy. An increase in low energy, high diffusivity paths, will reduce flow stresses in the 2-phase alloy deforming by diffusion accommodated grain boundary sliding processes, by at least 1 order of magnitude.

Formation of minimum interfacial energy configuration

It is widely known that if a single phase material is annealed, grain boundaries tend to be straight (reduction of IGBC) and that grain angles at triple junctions are at 120° (e.g. Porter & Easterling 1992); the microstructure resembles one of minimum interfacial energy. The microstructural observations on the annealed 2-phase plagioclase - clinopyroxene granulites show that such an annealed 2-phase material can be described as a stable (no unstable grain junctions) minimum total interfacial energy microstructure. Similar observations have been made by Smith (1948) on annealed 2-phase α - β copper. The diffusion accommodated grain boundary sliding deformation of a 2-phase Pb - Sn alloy, resulted in the reduction of unstable quadri-junctions and an increase in low energy interphase boundaries.

The computer algorithm for the minimum energy configuration calculation involved grain swapping, i.e. 2 grains only change places if the interfacial energy is thereby reduced. Such a process is physically not very realistic and therefore Morral & Ashby's model of climb and glide of topological defects (Figs. 5.2 and 5.3; Morral & Ashby 1974) has been extended and applied to the 2-phase Pb-Sn system (Figs. 5.16 and 5.17). A bee-hive microstructure has been filled randomly with Pb (dark) and Sn (light) grains (Figs. 5.16a and 5.17a). Before the introduction of a "5-7" topological defect in Fig. 5.16(a) only 3 out of 16 grains are stable (IGBC = 0). The glide of such a defect, as shown in successive steps in Fig. 5.16, can result in an increase of stable grains (5 out of 16) and in a reduction of total interfacial energy. Climb of such a topological defect (Fig. 5.17) can result in a decrease in the amount of (high energy) grain boundaries and can also produce

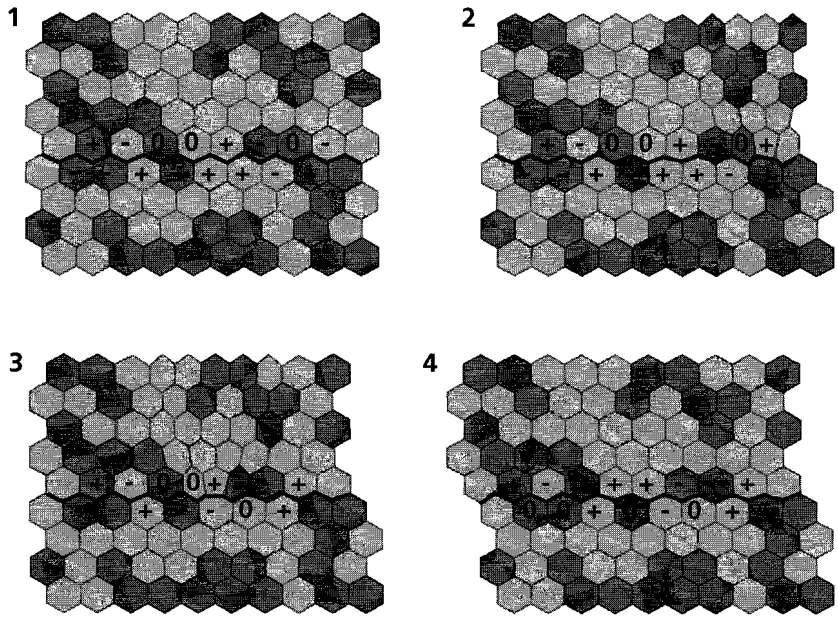

Fig. 5.16 Grain boundary sliding by the movement of a "5-7" topological defect through an array of grains in a 2-phase material with $R_\alpha = R_\beta = 1.25$ as in the Pb - Sn system. (1) Initial microstructure with a random distribution of grains before introduction of the topological defect. Note that adjacent to the "glide plane" only 3 out of 16 grains are stable (IGBC = 0); +, 0, - denotes respectively a positive, zero and negative IGBC. (2) Introduction of a "5-7" topological. (3) Movement of topological defect results. Note that grains adjacent to the "glide plane" (thick line) change neighbours during sliding, producing stable grains. (4) After glide of the defect, the top part has moved to the left relative to the bottom part, both the number of stable grains and the number of interphase boundaries has increased.

stable grains (IGBC = 0). As noted in section 5.2, glide of the defects produces grain boundary sliding, while climb produces grain growth or grain shrinking. It is therefore suggested that the climb and glide of the defects can be the mechanism by which a deforming polyphase material evolves towards a stable minimum energy microstructure.

Driving forces for the microstructural change

The stability of a microstructure depends on the driving force for change within the material. Which of the possible mechanisms for change dominate under certain conditions, however, is determined by the kinetics of each process (Martin & Doherty 1976). Thus comparing driving forces associated with microstructural changes alone, is not sufficient in determining the dominant process of microstructural change. The rate of microstructural change (v) can be described as (Martin & Doherty 1976):

$$v = M \Delta F \tag{5.10}$$

where ΔF is the driving force and M is a mobility term. The mobility term is the rate of

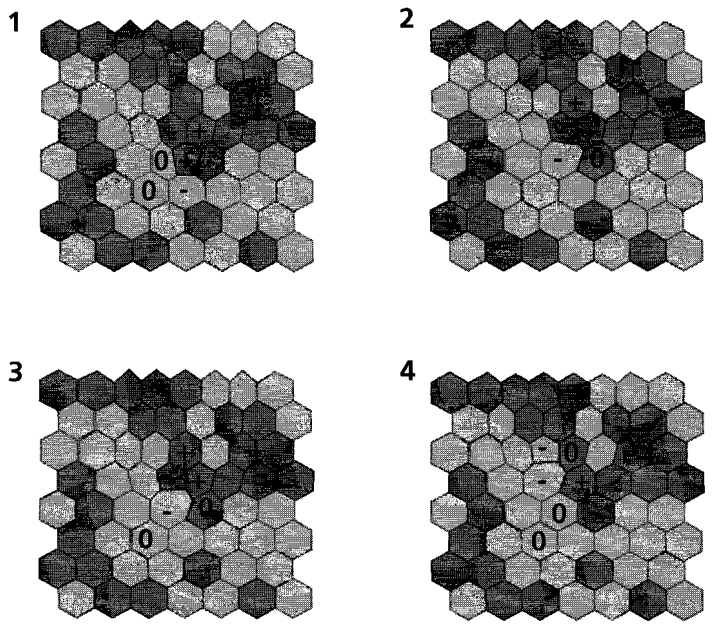

Fig. 5.17 Grain growth by the climb movement of a "5-7" topological defect in a 2-phase material with $R_\alpha = R_\beta = 1.25$ as in the Pb - Sn system. (1) Initial microstructure with a random distribution of grains after introduction of the topological defect. (2 - 4) Disappearance of grains results in a reduction of high energy grain boundaries.

microstructural change for unit driving force, it is a kinetic term and includes the scale over which the driving force acts (Martin & Doherty 1976; Poirier 1985). Decreases in several types of energy are available as driving forces for the microstructural change, these include (*cf.* Martin & Doherty 1976; Urai *et al.* 1986; Wheeler, 1987; 1991): intragranular lattice defect energy (plastic strain energy), chemical free energy, energies due to non-hydrostatic stresses, and grain and interphase boundary energies.

The existence of a distortion around an intragranular defect implies that a body containing that defect has an extra strain energy (Friedel 1964; Hull & Bacon 1984). In the case of a dislocation, this energy is proportional to the length of the Burgers vector squared . A boundary between a defect free crystal and one containing a high defect density is acted on by a force due to the difference in stored strain energy. The mobility of the boundary is related to the ease of atomic transfer across the grain boundary (Gordon & Vandermeer 1966; Martin & Doherty 1976; Porter & Easterling 1982). If a polycrystal is deforming by dislocation creep processes, the density of free dislocations is related to the stress (Kohlstedt & Weathers 1980). The stored strain energy is the product of the energy per dislocation and the free dislocation density. Other defect types causing stored strain energy are dislocation networks, stacking faults, twin boundaries and deformation bands (Friedel 1964; Martin & Doherty 1976).

Chemical free energy may be important as a driving force for microstructural change if there is a difference in composition between crystals of the same phase on either side of a migrating

boundary (Etheridge & Hobbs 1974; Vernon 1975) or between porphyroclast and recrystallized grains (Allison *et al.* 1979; Behrmann & Mainprice 1987). However, if all phases in the material are stable (given the pressure, temperature, chemical conditions etc.), driving forces resulting from the chemical free energy differences in the system can be neglected (Martin & Doherty 1976). The kinetics of the microstructural change are similar to those of grain boundary or lattice diffusion.

As proposed by Nabarro (1948), a non-hydrostatic stress field can give rise to different vacancy concentrations on boundaries of a crystal with different orientations with respect to the stress field; these vacancy concentration differences can cause a flux of vacancies and atoms between the surfaces. The driving force for the diffusion is a result of a change in equilibrium concentration and thus of free energy changes (Nabarro 1948; Coble 1963; Poirier 1985). This driving force is proportional to the applied stress (σ), and can be expressed as (Nabarro 1948; Coble 1963; Poirier 1985):

$$\Delta F \propto \sigma\Omega \tag{5.11}$$

where Ω is the atomic volume. If lattice diffusion is dominant the kinetics are similar to those of Nabarro - Herring creep (Nabarro 1948; Herring 1950; 1951), while if grain boundary diffusion is dominant, kinetics are similar to those of Coble creep (Coble 1963). In the case of the latter they will also depend on the grain boundary structure and grain boundary chemistry.

Grain boundary energies can provide a strong driving force if the grain boundary is curved. This driving force can be expressed as (Hillert 1965; Holm *et al.* 1993):

$$\Delta F = \frac{\gamma}{d}\Delta(\text{IGBC}) \tag{5.12}$$

where d is the grain size, γ is the grain boundary energy ($\approx 1\ J\ m^{-2}$) and Δ(IGBC) is the difference in integrated grain boundary curvature (Eq. 5.4) between two grains. Since the migration of a boundary due to this driving force involves diffusion either along the grain (or interphase) boundaries or through the crystal lattice, the kinetics of IGBC driven grain boundary migration are likely to be similar to those of diffusional creep (see above).

In order to evaluate the relative contribution of the above mechanisms for microstructural change in the microstructural evolution of the 2-phase Pb - Sn alloy presented in Section 5.5, both the kinetics and driving forces should be known. Since the material is deforming by diffusion accommodated grain boundary sliding and because both the Pb phase and Sn phase are stable, differences in chemical free energies and stored strain energy can be neglected. As mentioned above, the kinetics of processes for microstructural change driven by either a non-hydrostatic stress field and driven by grain boundary energies are likely to be similar. Therefore a graph has been constructing delimiting fields of dominant driving force, thus assuming similar kinetics (see above); the graph is presented in Fig. 5.18(a). A value of 3 was taken for Δ(IGBC), which is the difference between all negative and all positive IGBC values for both the starting and deformed material (*cf.* Figs. 5.13d and 5.14d). The boundary between the fields are indicated with a thick

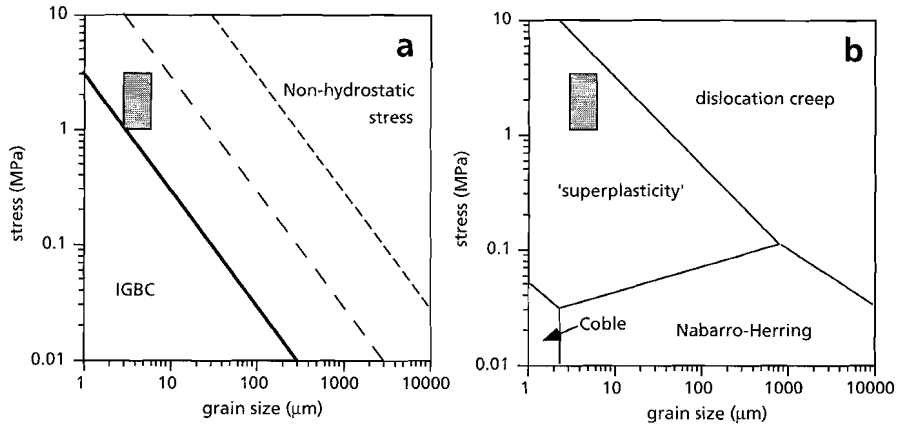

Fig. 5.18 (a) Graph showing fields of dominant driving force. The thick line marks the position where the IGBC driving force equals the driving force due to non-hydrostatic stress. Thin dashed lines mark differences of respectively, 1 and 2 orders of magnitude. Shaded area denotes the experimental conditions used for the experiments described in Section 5.5. (b) Deformation mechanism map for a Pb-70 vol.% Sn alloy at 150 °C reproduced from Mohamed & Langdon (1976). See text for discussion.

line and marks the positions where the two driving forces are equal. The dashed lines within the 'non-hydrostatic stress' field mark driving force differences of 1 and 2 orders of magnitude, respectively. Also indicated in this graph are the experimental conditions used for the experiments described in Section 5.5. Figure 5.18(b) shows a deformation mechanism map for a Pb - 70 vol.% Sn alloy at 150 °C reproduced from Mohamed & Langdon (1976).

The graph shows that the IGBC driven processes for microstructural change, will predominate at small grain sizes and low stresses, while at higher stresses and larger grain sizes non-hydrostatic stress driven processes will be dominant. However, IGBC driven processes are expected to occur (but not dominate) well within the non-hydrostatic stress field. This view is supported by diffusion accommodated grain boundary sliding creep experiments on fine grained (0.55 - 0.7 μm) Al_2O_3/ZrO_2 (Baddi *et al.* 1993). Deformation at low stresses (< 80 MPa) of the 2-phase composites with an initial random phase distribution, resulted in an increase of low energy interphase boundaries. At higher stresses (> 80 MPa) however, the distribution was more random.

The experimental conditions (shaded in Fig. 5.18) used for the experiments described in Section 5.5 fall near the transition between IGBC driven processes and driven by a non-hydrostatic stress. The production of interphase boundaries and the associated reduction of interfacial energy during deformation has been inferred to be the result of integrated grain boundary curvature (IGBC) driven processes. Comparing Fig. 5.18(a) and 5.18(b) shows a marked overlap in stress and grain size between IGBC driven processes and the deformation field for dominant 'superplastic' flow, i.e. deformation involving diffusion accommodated grain boundary sliding. It is therefore concluded that IGBC driven processes for microstructural change will occur during diffusion accommodated grain boundary sliding processes. These interfacial processes can cause the formation of low energy, high diffusivity paths, which in turn will weaken the 2-phase alloy.

Other models dealing with 2-phase flow

A number of different attempts have been made to describe and model processes and mechanisms in polyphase materials (Weertman 1970; 1978; Chen 1982; 1985 & Wheeler 1987; 1991; 1992). These are briefly discussed below.

According to Weertman (1970; 1978), the viscosity (or strength) of a material is inversely proportional to the diffusion coefficient. In single phase materials, this diffusion coefficient depends upon the melting temperature (T_m) of the material by the empirical relation as (Weertman 1970):

$$D = D_o \exp\left(\frac{-gT_m}{T}\right) \tag{5.13}$$

where g and D_o are material constants. This relation implies that the lower the melting point the higher the diffusivity and the lower the viscosity of the material. Borch & Green (1987; 1989) showed that this expression does fit data for experimentally deformed synthetic peridotites, deforming by dominant dislocation creep processes. However, the experiments on the Pb - Sn alloys do not show this relation. No strength reduction is observed in the material deforming by dislocation creep processes and the alloy with the lowest melting point, *viz.* the Pb - 70 vol.% Sn, is stronger than the Pb - 50 vol.% Sn alloy. Furthermore, the relation between viscosity and melting temperature cannot explain the observed interfacial variations and related weakening in the Pb - 70 vol.% Sn alloy (Fig. 5.12b).

Chen (1982; 1985) developed a model for diffusional flow in 2-phase alloys in which not the slowest, but the fastest diffusing species through the highest diffusion path controls the diffusion process in a fine grained 2-phase material. This in contrast to the single phase end-members, where diffusion is controlled by the slowest diffusion species along its fastest path. The reason for this difference is that due to phase equilibrium requirements at interphase boundaries, no segregation of chemical components can build up. This solute segregation will slow down the diffusion kinetics (Martin & Doherty 1976; Chen 1982; 1985). The excessive flow of fast diffusant arriving at the sink will be taken up into one of the two phases simply by the movement of the interphase boundary; similar processes will take place at the source-site.

In the Wheeler (1987; 1991; 1992) model, diffusion is enhanced if the two phases share chemical components and/or if the chemical components affect each others diffusion. In the former process, growth or dissolution of one phase will affect the other through the shared component. If one of the shared components is immobile, the Wheeler (1992) model predicts that the other component can still diffuse and hence deformation may continue. This in contrast to the single phase end-members, where diffusion will cease. In the latter process, fluxes of one component will be linked to the other, this may for instance arise to maintain charge neutrality of the diffusing species. The effective diffusivity is thereby enhanced, and the Wheeler (1992) model becomes similar to the Chen (1982; 1985) model.

Both the Chen (1982; 1985) and Wheeler (1987; 1991; 1992) models explain why interphase boundaries can have higher diffusivities when compared to grain boundaries, and consequently

predict that the 2-phase material, deforming by diffusional creep processes, will be weaker than the single phase end members. In principle, these models are also capable in explaining the weakening with strain observed in the Pb - 70 vol.% Sn alloy (Fig. 5.12b). However, they fail to explain the observed interfacial population variations within the deforming Pb - Sn alloy, as explained by the formation of a minimum interfacial energy microstructure (see above).

Natural deformation of quartzo-feldspathic ultramylonites

Both examples of naturally deformed polyphase quartzo-feldspathic ultramylonites presented in section 5.3, the type 1 ultramylonite of the Redbank Deformed Zone and the Corvatsch ultramylonite from Stünitz & Fitz Gerald (1993), show a phase distribution which deviates from randomness. If the interfacial energies of these systems were known, it would in principle be possible to calculate whether these microstructures resembles a minimum energy configuration. However, interfacial energy data in wet granitic systems are currently unknown. Furthermore, to assess whether these polyphase mixtures are weaker than all of its constituent phases awaits grain and interphase boundary diffusion data as well as mechanical testing.

Several parameters influence the interfacial energies. These include chemical environment (Parks 1984; Watson & Brenan 1987; Holness 1995), phase content (Smith 1948; Vernon 1970; Holness 1995) and grain boundary characteristics (Goodhew 1979; Cooper & Kohlstedt 1982). These are briefly discussed below.

It has been shown by Parks (1984), Watson & Brenan (1987) and Holness (1995) that interfacial energies of quartz-quartz grain boundaries depend on the chemical environment of the specimen. Trace amount of CO_2, H_2O and NaCl can reduce the interfacial energy (Parks 1984; Watson & Brenan 1987) as can temperature (Holness 1995). Holness (1995) also reports differences in interfacial energies between quartz specimens with either added perthitic microcline or amelia albite. Further, it has been shown by Vernon (1970) that the relative amounts of phases present in a sample can affect the relative interfacial energies (section 5.4). A third effect can be extracted from Smith (1948), who analysed interfacial angles and energies in a 3-phase annealed Pb - α Cu - β Cu alloy. A third phase introduced into a 2-phase alloy will distribute itself in such a manner to achieve the lowest total interfacial energy. The energies of 2-phase triple junctions are found to be the same as they would be in 2-phase alloys. However, 3-phase corners show relative interfacial energies different from the ones calculated from a 2-phase alloy. A fourth effect would be that interfacial energy depends on the crystallography of the grain boundary (Cooper & Kohlstedt 1982) or on the misorientation between the crystals (Goodhew 1979).

Despite the difficulties addressed above, it is suggested that in an analogous way to the Pb-Sn system, the rheology of fine grained quartzo-feldspathic ultramylonites, such as the type 1 ultramylonite of the Redbank Deformed Zone or the Corvatsch ultramylonite from Stünitz & Fitz Gerald (1993), will differ from the rheology of its constituent phases. The flow law will not be some combination of the flow laws of single phase quartz, K-feldspar, plagioclase or mica, like the models proposed by Handy (1990) and Tullis *et al.* (1991) or Fan & Moidownik (1993a; 1993b). It will depend on the mineralogy of the rock, the relative amount of phases present, their distribution through the rock, their grain and interphase boundary diffusivities, grain boundary

sliding resistances, fluid content, temperature. Using grain-size-sensitive flow laws of the constituent phases will tend to overestimate the strength of the polyphase ultramylonite by at least 1 order of magnitude.

As mentioned in Chapter 2, the formation of the fine grained quartzo-feldspathic ultramylonites of the Redbank Deformed Zone from a (proto)mylonitic precursor was a two step process. First a process equivalent to recrystallisation of the feldspar clasts and pure quartz bands resulted in a grain size reduction. This is subsequently followed by mechanical mixing by grain boundary sliding processes, resulting in a fine grained homogeneous quartz-feldspar mixture. The movement of topological defects, driven by IGBC's might provide an insight in how this mechanical mixing might occur. Generally, during recrystallisation the grain size distribution is positively skewed (Ranalli 1984), implying that besides large grains also numerous small grains occur. At the contacts between a fine grained recrystallized rim around a porphyroclast and a pure quartz band these finely sized grains might change neighbours due to grain boundary sliding processes. This results in a fine grained polyphase mixture. Some preliminary computer modelling has been performed analogous to those presented in Fig. 5.5 and 5.6, but instead of an initial random distribution of grains, the starting microstructure consisted of alternating layers of phases. After several iterative steps, the resulting microstructure was similar to Fig. 5.5d and 5.6d, if the layers were only a few grains wide. Some remnant layering was still present if the layers were more than 5 - 7 grains wide. Such a process of grain switching might provide the formation of the quartzo-feldspathic ultramylonites.

5.7 Conclusion

1) Interfacial distributions have a significant effect on the mechanical behaviour of the 2-phase Pb-Sn alloy. An increase in low energy, high diffusivity paths, will reduce flow stresses in the 2-phase alloy deforming by diffusion accommodated grain boundary sliding processes, below those of the single phase end members
2) Annealed 2-phase granulites have stable minimum interfacial energy microstructures. The interfacial distribution favours low energy boundaries, and stable grain junctions.
3) Minimum energy microstructures can develop during grain growth and grain-size-sensitive deformation by the movement of topological defects. The reduction of interfacial energy provides the driving force, while the kinetics are similar to those of diffusion creep processes. This driving force is strongest at small grain sizes and low stresses.
4) The phase distribution in naturally deformed fine grained quartzo-feldspathic mylonites deviates from randomness. It is suggested that, analogous to the Pb-Sn system, flow of such polyphase rocks will differ significantly from that of its single phase end members. The flow law will not be some combination of the flow laws of single end members as previously proposed, but will depend on the mineralogy of the rock, the relative amount of phases present, their distribution through the rock, their grain and interphase boundary diffusivities, grain boundary sliding resistances, fluid content, temperature.

Chapter 6

Grain-size-sensitive deformation of quartzitic and quartzo-feldspathic rocks.

6.1 Introduction

Rocks, like other crystalline solids, may deform plastically by a number of, often competing, mechanisms. Omitting brittle behaviour, transient creep and cold-working, these flow mechanisms under creep or hot-working conditions, can be divided into two groups: those that depend on grain size (e.g. lattice or grain boundary diffusion creep, grain boundary sliding creep) and those that are independent of grain size (e.g. dislocation creep). The first group of mechanisms is favoured at the expense of the second with decreasing grain size, decreasing stress and/or decreasing temperature (White 1976; Etheridge & Wilkie 1979; Frost & Ashby 1982). Although grain-size-sensitive (GSS) creep has been inferred in quartzose and quartz framework rocks, intracrystalline plasticity by dislocation processes has been inferred to be the dominant deformation mechanism (White 1973; 1976; 1977; Bossière & Vauchez 1978; Watts & Williams 1979; Simpson 1985; Lloyd & Knipe 1992; Lloyd *et al.* 1992) and are considered to be the main factors controlling the deformation of quartzo-feldspathic rocks. Therefore, it is generally assumed that the rheology of the crust under middle- to upper-crustal conditions can be described by that of wet quartzite deforming by dislocation creep processes (White & Bretan 1985; White *et al.* 1986; Carter & Tsenn 1987; Ord & Hobbs 1989; Rutter & Brodie 1993b).

However, the progressive mylonitization of quartzo-feldspathic rocks involves the reduction in both size and number, of K-feldspar and plagioclase porphyroclasts and the decrease in pure quartz band volume at the expense of very fine polyphase mixtures. (e.g. Wakefield 1977; Berthé *et al.* 1979; White *et al.* 1982; Chapter 2; Chapter 4). A number of studies have inferred that the deformation mechanism within these polyphase mixtures involved a major component grain boundary sliding processes, i.e. the mixtures deformed by grain-size-sensitive processes (e.g. Kerrich *et al.* 1980; Stünitz & Fitz Gerald 1993; Chapter 4). At low temperatures in hydrous environments, this transition in deformation mechanism is generally accompanied by chemical breakdown reactions of K-feldspar and plagioclase to micaeous and epidote minerals (Kerrich *et al.* 1980; Williams & Dixon 1982; Dixon & Williams 1983; Knipe & Wintsch 1985; Stünitz 1993).

Observations similar to those within quartzo-feldspathic rocks have been made on other crustal rock types like gabbros (Stünitz 1993) in which the rock transforms to a fine grained mixture of albite and epidote, and in upper mantle peridotites, where the highest strained parts of the shear zones consist of a mixture of fine grained olivine ± pyroxene ± amphibole ± spinel

± plagioclase (Drury *et al.* 1990; 1991; Hoogerduijn Strating *et al.* 1990; Vissers *et al.* 1991), or abundant phyllosilicates (Brodie & Rutter 1986; Rutter & Brodie 1988; Drury *et al.* 1990; Hoogerduijn Strating *et al.* 1990). The deformation mechanisms inferred for these fine grained polyphase mixtures included a major component of grain boundary sliding creep processes (Stünitz 1993; Drury *et al.* 1991).

Aims and approach

The aim of this chapter is to compare the results of a literature survey on the grain-size-sensitive deformation of pure and near pure quartzites and quartzo-feldspathic rocks to the observations of the Redbank Deformed Zone shear zones presented in Chapters 2, 3 and 4 of this thesis. This chapter starts with a short summary of available quartz flow laws and paleopiezometric equations. In a third section, the results of a literature survey on the grain-size-sensitive deformation of pure and near pure quartzites will be presented. The quartz deformation microstructures of the mylonites from the Redbank Deformed Zone, described in Chapters 2 & 3, will be compared with these results and with flow laws for pure quartzites. In the fourth part of this chapter a literature survey is presented on deformation microstructures in quartzo-feldspathic mylonites. The microstructures of the polyphase quartzo-feldspathic ultramylonites from the Redbank Deformed Zone, presented in Chapters 2 & 4, will be compared with these results. Furthermore, the results of the literature survey will be compared with flow laws for pure quartzites. This, bearing in mind the conclusions of Chapter 5, namely that describing the flow of polyphase materials with the use of single phase flow laws might underestimate the strength of the polyphase rocks by at least 1 order of magnitude.

6.2 Construction of deformation mechanism maps

Deformation mechanism maps (Donath *et al.* 1972; Ashby 1972; Mohamed & Langdon 1976; Rutter 1976; White 1976; Ashby & Verrall 1978; Frost & Ashby 1982; Handy 1989) are convenient means of showing how various deformation mechanisms are related to the environmental conditions, such as stress, strain rate, temperature and grain size. Generally, such deformation mechanism maps are constructed using experimentally derived flow laws and show under which conditions a deformation mechanism is predominant. Boundaries between two fields on a mechanism map mark the conditions where two mechanisms produce equal strain rates (Ashby 1972; Rutter 1976; White 1976; Frost & Ashby 1982; Handy 1989).

The constitutive equation describing intracrystalline plasticity by dislocation creep processes (i.e. grain-size-insensitive (GSI) creep) is generally expressed as (Ashby 1972; Mohamed & Langdon 1976; Frost & Ashby 1982; Poirier 1985):

$$\dot{\varepsilon} = A \exp\left(\frac{-H}{RT}\right) \sigma^n \, d^{-m} \qquad (6.1)$$

where A is a pre-exponential constant, H is the activation enthalpy, R is the universal gas constant (8.3144 J $mol^{-1}K^{-1}$), T is the absolute temperature, σ is the differential stress, n is the power law exponent, and d is the grain size in meters. Since the flow is grain-size-insensitive, the grain size exponent m is zero.

Numerous flow laws for quartzite deforming by dislocation creep processes have been reported in the literature (see Table 6.1). However, a number of problems surround the existing flow laws for dislocation creep in quartzites. A first problem stems from the fact that most of the deformation experiments (see Table 6.1) have been performed in a solid medium deformation apparatus for which large errors in stress measurements and large temperature gradients have been suspected (Tullis & Horowitz 1980; Green & Borch 1990; Den Brok 1992; Gleason & Tullis 1993). Gleason & Tullis (1993; 1994) performed deformation experiments on quartz aggregates in a modified version of the molten salt cell designed by Green & Borch (1989), in which stresses can be more accurately measured, and illustrated the errors associated with strengths measurements in various solid confining media. However, only in such solid medium apparatus high enough confining pressures enable to deform quartz in the α stability field.

A second problem is the role of water on the mechanical behaviour of quartz. It is widely agreed that the presence of water is essential to make quartz flow under natural conditions (e.g. Jaoul *et al.* 1984; Paterson 1989). Dislocation mobility is assumed to be promoted by water-related point defects in the quartz lattice. However, the exact mechanisms for this water-weakening effect and its influences on the creep parameters are poorly understood (see reviews by e.g. Blacic & Christie 1984; Paterson 1989; Tullis 1990; Den Brok 1992).

A third problem is the wide disagreement when the different flow laws are compared (Table 6.1 and Fig. 6.1). Figure 6.1(a) compares the flow stresses according to the equations listed in Table 6.1, needed to deform quartz aggregates with strain rates of 10^{-7} s^{-1} and 10^{-6} s^{-1}, respectively at a temperature of 1175 K, ; most experiments on quartz aggregate deformation are performed at this temperature. The calculated stresses span more than one order of magnitude.

Furthermore, the apparent activation enthalpy for deformation ranges between 134 KJ mol^{-1} (Koch 1983) and 223 KJ mol^{-1} (Gleason & Tullis 1994), thus making the extrapolation of these flow laws to natural conditions (low temperatures, low strain rates) problematic. Figure 6.1(b) compares the flow stresses according to the equations listed in Table 6.1 needed to deform quartz aggregates at geologically realistic strain rates of 10^{-14} s^{-1} and 10^{-12} s^{-1} respectively, at lower greenschist temperatures of 600 K (White 1975; Paterson 1989). Stresses calculated at a strain rate of 10^{-14} s^{-1} range between 50 MPa (Koch 1983) and 900 MPa (Hansen & Carter 1982), whereas extremely high stresses are calculated for a strain rate of 10^{-12} s^{-1}, ranging from 300 MPa (Koch 1983) to 10,000 MPa (Hansen & Carter 1982).

Even the experiments performed in a gas medium apparatus are in disagreement. At 600 K, the experimental data on wet quartzite of Paterson & Luan (1990), predict stresses of 100 MPa and 475 MPa at strain rate of respectively 10^{-14} s^{-1} and 10^{-12} s^{-1}, while the experimental data of Rutter & Brodie (1993a; 1993b; 1994) at these conditions, predict stresses twice as high, respectively 260 MPa and 1000 MPa. The experimental data of Gleason & Tullis (1994) from a molten salt cell predict at these conditions respectively 230 MPa and 730 MPa.

Table 6.1. Steady state flow law parameters for quartzites deforming by dislocation creep processes (Eq. 6.1)

ref. ¥	Symbol Fig. 6.1	log A ($Pa^{-n}s^{-1}$)	Q (KJ mol^{-1})	n	m	comments	stability field	apparatus	diffusional creep rate
[a]	■	-25.80	150	3.1	0	average wet	β	gas medium	8×10^{-6}
[a]	●	-33.40	150	4	0	silicic acid	β	gas medium	8×10^{-6}
[b]	▲	-25.18	200	3.4	0	wet Brazilian aggregate	β	gas medium	4×10^{-7}
[b]	✖	-18.28	200	1	2	wet Brazilian aggregate	β	gas medium	1×10^{-7} *
[b]	✙	-18.28	200	1	3	wet Brazilian aggregate	β	gas medium	1×10^{-7} *
[c]	◆	-14.96	167	2	0	dried Heavitree quartzite	α	solid medium	3×10^{-6}
[d]	□	-23.52	134	2.72	0	dry	α	solid medium	2×10^{-5}
[e]	○	-15.86	173	1.9	0	dry Quadrant orthoquartzite	α	solid medium	2×10^{-6}
[f]	△	-22.26	184	2.8	0	as recieved Heavitree quartzite	α	solid medium	1×10^{-6}
[g]	◇	-27.96	223	4	0	as recieved	α	molten salt	1×10^{-7}

¥ References: [a] Paterson & Luan (1990); [b] Rutter & Brodie (1993a; 1993b; 1994); [c] Shelton & Tullis (1981); [d] Koch (1983); [e] Hansen & Carter (1982); [f] Jaoul *et al.* (1984); [g] Gleason & Tullis (1994). Strain rates calculated using Eq. 6.2 at 10 MPa, 1200 °C, 1 μm *: experimental result of Rutter & Brodie (1993a; 1993b)

Another problem in the extrapolation of experimentally derived flow laws to naturally deformed rocks lies in the fact that experiments are generally performed over strain increments of only about 20 %. It is generally not well established to what extent the experimentally derived flow laws hold for the very large strains usually inferred for natural deformation (White 1976; 1979d; Rutter & Brodie 1991).

Although many constitutive equations have been proposed for grain-size-sensitive creep (GSS) mechanisms (i.e. lattice or grain boundary diffusion creep, grain boundary sliding creep (e.g. Gifkins 1976; 1977; 1982; Padmanabhan & Davies 1980; Frost & Ashby 1982) they are commonly expressed in the form of the combined flow laws for Coble creep (Coble 1963) and Nabarro-Herring creep (Nabarro 1948; Herring 1950; 1951):

$$\dot{\varepsilon} = \frac{A_d D_{eff} \Omega}{kTd^2} \sigma^n \tag{6.2}$$

with

$$D_{eff} = D_v + \left(\frac{\pi\delta}{d}\right) D_{gb} \tag{6.3}$$

and

$$D_i = D_{oi} \exp\left(\frac{-H_i}{RT}\right) \tag{6.4}$$

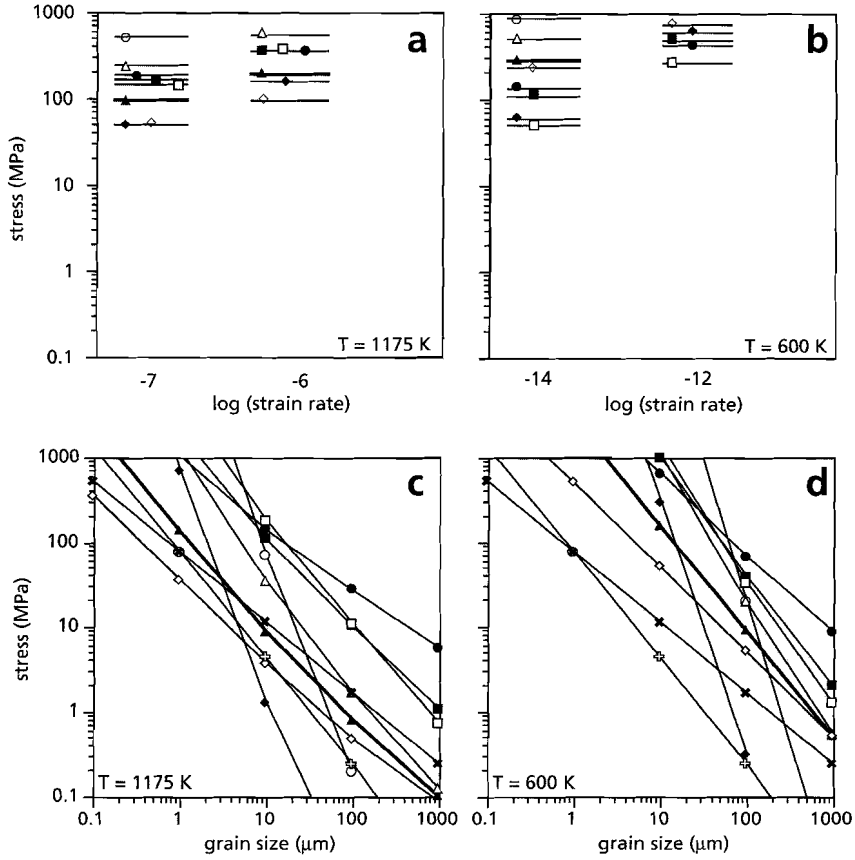

Fig. 6.1 Experimental flow laws for pure quartzite. Flow stresses needed at (a) 900 °C and (b) 325 °C in order to achieve a certain strain rate according to experimental flow laws. Transition from intracrystalline plasticity by dislocation creep processes to grain-size-sensitive creep processes at (c) 900 °C and (d) 325 °C for different flow laws. Flow laws and symbols are indicated in Table 6.1 (see text for discussion).

where D_i is either D_v for volume diffusion or D_{gb} for grain boundary diffusion, D_{oi} is the absolute diffusivity, A_d is a pre-exponential constant for diffusional creep, Ω is the atomic volume, k is Boltzmann's constant (1.381×10^{-23} J K^{-1}), d is the grain size and δ is the grain boundary width; the power law exponent n is generally 1.

Besides Coble creep and Nabarro-Herring creep, a third type of diffusion creep can occur in rocks, namely diffusive mass transport assisted by the presence of water at the grain boundaries, i.e. pressure solution creep (Rutter 1976; 1983; McClay 1977; Spiers & Schutjens 1990). Pressure solution creep is thought to be important under low metamorphic environments and wet conditions, generally below lower greenschist facies conditions (Rutter 1976; McClay 1977). The flow law for pressure solution creep has the same form as that for Coble creep (Eq. 6.2), with appropriate diffusivities (*cf.* Rutter 1976; 1983; McClay 1977; Spiers & Schutjens 1990).

Although the experimental data is large for quartz deforming by dislocation creep processes, experimental data for quartz deforming by grain-size-sensitive processes are sparse. Rutter & Brodie (1993a; 1993b; 1994) have deformed fine grained Brazilian quartz aggregates (0.4, 1.0 and 4.0 μm) at 1000 to 1200 °C and 300 MPa confining pressure in a gas medium apparatus. The lowest flow stress attained was 10 MPa at 1200 °C in a 1 μm quartzite at a strain rate of 10^{-7} s^{-1}, deforming by grain-size-sensitive processes; strains were in the order of 5 to 15 %. An activation enthalpy of 200 KJ mol^{-1} was estimated from temperature stepping tests. Rutter & Brodie (1993b) report an approximate flow law for this grain-size-sensitive flow in the form of Eq. 6.1, with A = 5.2 x 10^{-19}, however m, the grain size exponent is not reported. Extrapolation of this flow law to lower temperatures and strain rates is problematic since, besides the above addressed problems, the grain size exponent m is not known. In the experiments, the quartzites are probably deforming by a Nabarro-Herring type of diffusional creep (m = 2) (Rutter personal comm. 1995), which is generally thought only to occur at high temperatures; at lower temperatures Coble creep (m = 3) is thought to predominate (Ashby 1972; Rutter 1976; White 1976; Frost & Ashby 1982).

In order to obtain a grain-size-sensitive flow law for quartz, a similar procedure as outlined in Rutter (1976) who followed Raj & Ashby (1971) and Ashby (1972) has been used, i.e. using Eq. 6.2 with appropriate values for the activation enthalpy and diffusion constants. The parameters adopted for the combined Coble creep and Nabarro-Herring creep equations (Eq. 6.2) are: A_d = 21, Ω = 0.7 b^3, with b the Burgers vector for quartz which is 5 x 10^{-10} m, D_{ov} = 1 x 10^{-12} m^2s^{-1}, D_{ogb} = 1 x 10^{-11} m^2s^{-1} (Joesten 1991; both for hydrous conditions), H_{gb} = 2/3 H_v (Shewmon 1963). A grain boundary width δ of 2b has been assumed in the construction of the maps, which can be an under estimate in wet conditions (White & White 1981); wider grain boundaries will expand the diffusion creep field in the deformation mechanism maps.

For each dislocation creep experimental flow law, listed in Table 6.1, a grain-size-sensitive creep law has been calculated. To compare these constructed diffusion creep flow laws with the experiments of Rutter & Brodie (1993a; 1993b), strain rates are calculated for a grain size of 1 μm deforming at 1200 °C with a flow stress of 10 MPa. The differences between the various diffusion creep flow laws arise due to the different activation enthalpies observed in the experimentally determined dislocation creep flow laws. Although there is quite some scatter between the constructed flow laws, they all scatter around 1 x 10^{-6} s^{-1} which is one order of magnitude faster than the experimental data of Rutter & Brodie (1993a; 1993b; 1994), which is 1 x 10^{-7} s^{-1}.

The boundaries between dislocation creep (Eq. 6.1) and grain-size-sensitive creep (Eq. 6.2) for all the constructed flow laws (i.e. Table 6.1) have been calculated and are shown in Fig. 6.1(c) (T = 900 °C) and Fig. 6.1(d) (T = 325 °C). In such a deformation mechanism map of stress versus grain-size, the slope of each boundary line is given by:

$$\text{slope} = \frac{\Delta m}{\Delta n} \tag{6.5}$$

where $\Delta m = m_{gsi} - m_{gss}$, $\Delta n = n_{gsi} - n_{gss}$, with n and m respectively, the stress exponent and

grain size exponent of grain-size-insensitive creep (GSI Eq. 6.1) and grain-size-sensitive creep (GSS Eq. 6.2). Comparison of these two graphs reveals that the scatter, both in slope and location, at high temperatures, becomes more pronounced at low temperatures.

For the construction of the deformation mechanism maps and strain rate estimates, presented in this chapter, the dislocation creep equation of Rutter & Brodie (1993a; 1993b; 1994) and the constructed (Eq. 6.2) grain-size-sensitive equation based on the same experiments have been used. The latter is hereafter referred to as Re-calculated Rutter & Brodie equation, as opposed to their experimental flow law. The reasons that these flow laws have been chosen are the following. First, Rutter & Brodie (1993a; 1993b; 1994) have performed experiments using a gas confined deformation apparatus. Second, experiments on the same material, but with different conditions, resulted in both grain-size-sensitive and grain-size-insensitive deformation mechanism, giving an internally consistent data set. Third, the Re-calculated grain-size-sensitive flow law predict the observed grain-size-sensitive experiments best. And four, because these equations approximate to an average for all available quartz flow data (Fig. 6.1).

6.3 Paleopiezometry

There are a number of methods available to determine the paleostress in materials deforming by dislocation creep (*cf.* Kohlstedt & Weathers 1980). It has long been known that the size of subgrains and recrystallized grains, and the free dislocation density are related to the magnitude of the differential stress responsible for the deformation of the polycrystal (Bird *et al.* 1969; Luton & Sellars 1969; Twiss 1977; Mercier *et al.* 1977; White 1979a; 1979b; Kohlstedt & Weathers 1980; Derby & Ashby 1987; Derby 1990).

Dislocation density is highly susceptible to changes in temperature and stress and commonly reflects a later stage stress-free anneal or late stress pulse (White 1979a). It has been found that subgrain size decreases with increasing stress, but not vice versa, so subgrains commonly record maximum stress levels, unless a later episode at lower stress has produced a large enough strain allowing the structure to evolve (Nicolas 1978; Toriumi 1979; Matsui *et al.* 1980; Van der Wal 1993; Van der Wal *et al.* 1993). For grain size, we must also consider the recrystallisation mechanism (Twiss 1977; Drury *et al.* 1985), i.e. rotation recrystallisation or migration recrystallisation. It is generally accepted that subgrain size and recrystallized grain size are better indicators of the paleostress (White 1979a). The paleopiezometric equations relating stress to quartz subgrain size include those of Koch (1983) and White (1979b) (using the experiments of Ardell *et al.* 1973), McCormick (1977) for dislocation density, and Mercier *et al.* (1977), Twiss (1977) and White (1979b) (using the experiments of Ardell *et al.* 1973) for recrystallized grain size with a recrystallisation mechanism involving both subgrain rotation and grain boundary migration.

The major aim of this chapter is to compare the results of a literature survey on the grain-size-sensitive deformation of pure and near pure quartzites and quartzo-feldspathic mylonites to the data presented in this thesis. The comparison has been made using three different paleopiezometric relations for recrystallized grain size, namely those of Mercier *et al.* (1977), Koch (1983) and of

Table 6.2 Paleopiezometric equations for quartz aggregates.

		$\sigma = A\ d^{-m}$		
		A	m	σ at d = 7 μm
Mercier *et al.* (1977)	grain size	381	0.71	100
Koch (1983)	grain size	23036	1.72	800
Twiss (1977)	grain size	603	0.68	170
White (1979b)	subgrain size	525	1	

Note: grain size d in μm and stress s in MPa.

Twiss (1977), and one for subgrain size (White 1979b). These are listed in Table 6.2.

Most paleopiezometric relations for quartz have been determined using experiments in solid media confined deformation apparatus. Twiss (1977) however, used a non-dimensional plot of experimentally determined relations between stress and recrystallized grain size for a variety of metals, alloys and minerals and found a uniform relation. As noted in Section 6.2, large errors in stress measurements are suspected with solid medium deformation apparatus. Recently, Gleason & Tullis (1993) have performed deformation experiments on quartz aggregates in a molten salt cell to verify previously published paleopiezometric relations. Their sample, deformed at 170 MPa, 1000 °C and $10^{-5}s^{-1}$, has a recrystallized grain size of 5.3 to 8.5 μm. They compared this experimental result with the paleopiezometric relations of Koch (1983) and Twiss (1977), and obtained stresses of respectively, 800 MPa and 170 MPa (see also Table 6.2), and concluded that their result was more consistent with the theoretical relation of Twiss (1977). The relation of Mercier *et al.* (1977) predict slightly lower stresses (100 MPa).

6.4 Grain-size-sensitive deformation in pure and near pure quartzites

When a material deforms, the microstructure that develops will depend on the deformation mechanisms operative. Within quartz, undulatory extinction, subgrain development, recrystallized grains, deformation lamellae, high dislocation densities and a strong texture or crystallographic preferred orientation (CPO) are commonly regarded as being indicative of dislocation creep processes (see White 1973b; Hobbs *et al.* 1976; Knipe 1989; Den Brok 1992).

Microstructural criteria used to infer grain-size-sensitive creep processes within quartzites, with a major contribution of grain boundary sliding processes, have been presented in Chapter 3. These include (see also Table 6.3): i) a grain size comparable to or smaller than the equilibrium subgrain size (STC in Table 6.3), ii) a diamond or rectangular grain shape (SHC), iii) a continuous alignment of grain boundaries over several grain diameters (CGA), iv) open grain boundaries and grain boundary voids or grain boundary inclusions (GBV), v) high dislocation densities at triple junctions, vi) an inverse relation between finite strain and grain size (SIG), vii) a switch in the relation between dislocation density and grain size from proportional to inverse,

and viii) overgrowth structures. In addition any CPO generated should be weak (Padmanabhan & Davies 1980, pp 111 - 117; Rutter *et al.* 1994) and there should be no crystallographic relation between adjacent grains due to grain rotations and neighbour switching events which accompany grain boundary sliding (Beeré 1978). As the transition between dislocation creep and grain-size-sensitive creep processes depends on the grain size, temperature and stress (see Fig. 6.2), the often used (e.g. Boullier & Gueguen 1975; White 1977; Bossière & Vauchez 1978; Lloyd *et al.* 1992) criteria of a small, generally smaller than 10 μm, grain size is not appropriate.

There are numerous reports on (near) pure quartzites deforming by dislocation creep processes (e.g. McLaren & Phakey 1965a; 1965b; White 1973a; 1973b; 1976; 1977; 1979b; Wilson 1973; White & Treagus 1975a; 1975b; Hobbs *et al.* 1976; Kerrich 1976; Nicolas & Poirier 1976; Ball & White 1978; Cahn 1978; Knipe & White 1978; White *et al.* 1978; 1982; Ord & Christie 1984; Behrmann 1985; Knipe 1989; Knipe 1990; Law *et al.* 1990; Feldmann *et al.* 1991; Lloyd & Freeman 1991; Lloyd & Knipe 1992; Drury 1993; Mainprice *et al.* 1993; Mawer & Fitz Gerald 1993; Chapter 3).

The data on quartzites deforming by grain-size-sensitive processes, on the other hand is very limited and these are compiled in Table 6.3 and Figs. 6.2 and 6.3. Only those data are given where the phyllosilicate content of the rock is low (< 15 %). It should be noted that in most of the naturally deformed samples phyllosilicates were present as small flakelets at the grain boundaries. For comparison, the data of the very fine grained (2.3 ± 0.8 μm) type 2 mylonite has been included ([8]). In Chapter 3 of this study it has been inferred that dislocation creep processes were the dominant deformation mechanism operative within these fine grained quartzes.

Table 6.3 lists further the criteria used to infer that the deformation mechanism was grain-size-sensitive; temperature and grain sizes are as listed in the original articles. The data fall into two groups, namely those in which only grain-size-sensitive deformation has been identified ([4a-c], [5], [7], [10a & b] and [11]) and those for which a transition from dislocation creep to a grain-size-sensitive creep mechanism has been inferred ([1], [2], [3], [6] and [9]). For the latter stresses are estimated using the recrystallized grain size paleopiezometric equations (*cf.* Table 6.2) on (nearby) quartzes deforming by dislocation creep processes. Stresses in the former group are estimated by using the subgrain size paleopiezometric equations of White (1979b), taking the equilibrium subgrain size as being equal to the grain size (STC criteria). The last two columns in Table 6.3 list strain rate estimates for both dislocation creep and grain-size-sensitive creep by using the flow laws as given at the end of Section 6.2, assuming a constant stress between the rocks deforming by dislocation creep and grain-size-sensitive creep; stresses are calculated using the relation of Mercier *et al.* (1977). In doing so, strain rates in the rocks deforming by grain-size-sensitive creep have been calculated, which are at 1 to 3 orders of magnitude higher than those calculated for rocks deforming by intracrystalline plasticity by dislocation creep processes.

Figure 6.2 shows a compilation of the data in Table 6.3 in grain size versus stress at three different temperature intervals; stresses have been calculated using the paleopiezometric equations of Mercier *et al.* (1977) and White (1979b). Figure 6.3 has been drawn, using the paleopiezometric relations of Twiss (1977) and Koch (1983), in order to compare the different relations for stress estimates. Figure 6.2(a) is at low greenschist facies (T ≈ 325 °C), Fig. 6.2(b) at

Table 6.3 Observations on grain-size-sensitive deformation in pure or near pure quartzites.

ref.[¥]	No.	T(°C)	gss(μm)	gsi(μm)	σ(MPa) Mercier	σ(MPa) Koch	σ(MPa) Twiss	σ(MPa) White	STC	CPO	SHC	CGA	GBV	SIG	DIG	MIG	log(ε̇) gss	log(ε̇) gsi
[a]	[1]	250-400	5-10	10-50	24-74	28-439	42-126		+	weak			+		+	+	-14.9	-16.5
[b]	[2]	300-400	≈5	80-100	14-17	8-12	26-31		+	+	+		+			+	-14.4	-17.5
[c]	[3]	≈300	≈6	15-25	39-56	91-219	68-96		+		+	+	+			+	-15.2	-17.4
[d]*	[4a]	≈300	1000					0.5										
	[4b]	≈450	100					5										
	[4c]	≈500	10					50										
[e]*	[5]	≈325	≈700					0.8										
[f]	[6]	≈350	≈50	50-200	9-24	3-28	16-42				+		+			+	-17.4	-17.4
[g]	[7]	370–420	140-260					2-4	+	weak				+			-19.4	(-19.4)
[h]**	[8]	≈425		1.5-3.1	171-287	3291-∞	279-458			strong								-11.7
[i]	[9]	≈450	0.5-2	2-8	87-233	644-∞	147-376				+		+		+		-10.4	-11.7
[j]	[10a]	540-630	10-30					15-50	+					+		+	-13.4	(-13.1)
[j]	[10b]	540-630	80-150					2-4	+					+		+	-16.4	(-15.9)
[k]	[11]	≈650	70-300					2-4						+			-16.3	(-15.1)

¥ References: [a] Behrmann (1984; 1985); [b] Gapais & White (1982); [c] White (1979b); White *et al.* (1982); [d] Kerrich *et al.* (1977); [e] Mitra, S. (1976); [f] Norton (1982); [g] Evans *et al.* (1980); [h] Chapter 3; [i] Obee (1985); Obee & White (1985); [j] J. White (1982); [k] Lisle & Savage (1983).

Key: gss: grain size at which grain size senstive deformation has been inferred; gsi: grain size at which dislocation creep processes were inferred to be dominant; stresses according to Mercier *et al.* (1977), Koch (1983), Twiss (1977) for recrystallised grain size, and White (1979b) for subgrain size. STC: grain size stability criteria, a + denotes that the grain size is smaller or equal to the equilibrium subgrain size; CPO: crystallographic preffered orientation, a + denotes present; SHC: grain shape criteria, a + denotes a rectangular to blocky grain shape; CGA: continuous grain boundary alignment across several grain diameters; GBV: grain boundary voids and open grain boundary structures; SIG: an inverse relation between finite strain and grain size; DIG: a change in the relation between dislocation density and grain size from proportional to inverse. MIC: phyllosilicates present at grain boundaries; log(ε̇) gss: log of grain size sensitive strain rate using Eq. 6.2; log(ε̇) gsi: log of dislocation creep strain rate using Eq. 6.1. Rates between brackets denotes that no grain size of gsi was given. *: overgrowth structures; **: dislocation creep, *cf.* Chapter 3.

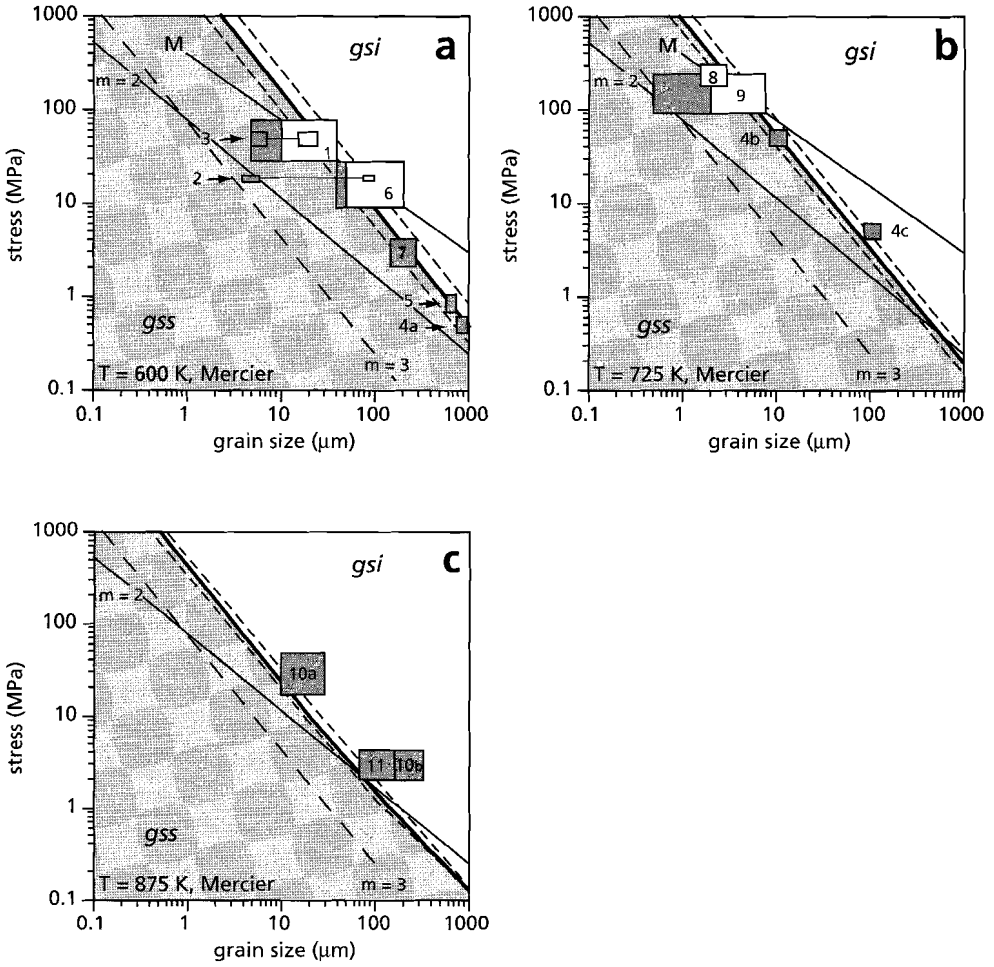

Fig. 6.2 Deformation mechanism maps for pure quartzites based on the dislocation creep flow law of Rutter & Brodie (1993a; 1993b) and the Re-calculated grain-size-sensitive creep Rutter & Brodie flow law. Stresses are calculated using the paleopiezometric relation for recrystallized grain size of Mercier *et al.* (1977) and subgrain size of White (1979b). Stress and grain size conditions for which grain-size-sensitive creep has been identified are shaded, where as conditions for dislocation creep are white; numbers are as in Table 6.3. Also indicated are the extrapolations of the experimental grain-size-sensitive flow law of Rutter & Brodie (1993a; 1993b) for two different grain size exponents (m = 2; m = 3). (a) T = 325 ± 50 °C; (b) T = 450 ± 50 °C; (c) T = 600 ± 50 °C. GSI: grain-size-insensitive creep field; GSS: grain-size-sensitive creep field. See text for discussion.

middle to upper greenschist facies (T ≈ 425 °C) and Fig. 6.2(c) is at amphibolite facies conditions (T ≈ 600 °C). Conditions for which the flow was grain-size-sensitive are shaded whereas dislocation creep conditions are white. The boundaries between fields mark the positions where the two processes produce equal strain rates, the thin dashed lines on either side of such a boundary mark a temperature difference of 50 °C; also shown are the boundary between the experimental

dislocation creep flow law and the experimental grain-size-sensitive flow laws (for m = 2 and m = 3) of Rutter & Brodie (1993b). The recrystallized grain size paleopiezometers used to calculate stresses from the data set are indicated (Mercier *et al.* (1977): Fig. 6.2; Twiss (1977): Figs. 6.3a and b; Koch (1983): Fig. 6.3c). As noted above, the relation between subgrain size and stress of White (1979b) has been used for those data where only the grain-size-sensitive creep mechanism has been inferred.

As shown in Figs. 6.2 and 6.3, there is a reasonable agreement between the natural data and the experimental data, in that the transition from grain-size-sensitive to grain-size-insensitive creep occurs at higher stresses when the grain size is small. High stresses (>200 MPa) are calculated for the very fine grained (2.3 ± 0.8 μm) pure quartz bands of the type 2 mylonites of the Redbank Deformed Zone, described in Chapter 3 (no. [8] in Table 6.3 and Figs. 6.2 and 6.3). The microstructural and microtextural observations by TEM on these rocks suggest that dislocation creep processes were the dominant deformation mechanism operative. The observation that the subgrain size (2.1 ± 0.6 μm) is only slightly smaller than the grain size (2.3 ± 0.8 μm), suggest that the rock deformed near the transition to a grain-size-sensitive creep mechanism. As shown in Figs. 6.2 and 6.3, the transition from grain-size-sensitive to grain-size-insensitive creep lies very near this mylonite, validating the general observation that high stresses favours dislocation creep at small grain sizes.

Very high stresses are calculated for the fine grained rocks using the paleopiezometric relation of Koch (1983) (see Table 6.3). For the very fine grained pure quartz bands of the type 2 mylonites, stresses exceeding 3000 MPa have been calculated. Although there is evidence for high differential stresses in the literature (Zobac *et al.* 1993), these don't exceed 300 - 400 MPa. This observation validates the results of Gleason & Tullis (1993) discussed in Section 6.3, in that Koch's relation predicts too high stresses at small grain sizes.

Based on the presence or absence of overgrowth structures, Kerrich *et al.* (1977) ([4a-c]) inferred the transition between the fields of diffusion creep and dislocation creep to occur at grain sizes of 10 μm at temperatures of 500 °C. For grain sizes of 100 μm and 1000 μm the dominant deformation mechanism changes from diffusion to dislocation creep at temperatures of 450°C and 300 °C, respectively. As shown in Fig. 6.2, these are in good agreement with the experimental data.

In general, the natural data match the experimental predictions. In detail, however (omitting the results using the Koch (1977) relation to estimate stresses), the slope of the transition line (Eq. 6.5) given by the experimental results is too large (-1.25); a 'best fit' results in a slope of -0.75. The slope of the transition line using the Mercier *et al.* (1977) relations to calculate stresses parallels that using the paleopiezometric relations of Twiss (1977); in the latter slightly higher (1.6 times) stresses are calculated. Since the slope of the curve is given by Eq. 6.5, either Δm should be smaller or the Δn should be larger to fit with the data, several possibilities are given below.

(i) It is generally thought that Coble Creep (with an m = 3) prevails over Nabarro-Herring Creep (with m = 2) at low temperatures. In order to have a slope of -0.75 this would mean that Δn = 4, so that with n_{gss} = 1, n_{gsi} should be 5; all experimental data (see Table 6.1) however suggest that n_{gsi} ranges between 1.9 and 4. (ii) As pointed out by Joesten (1991), volume dif-

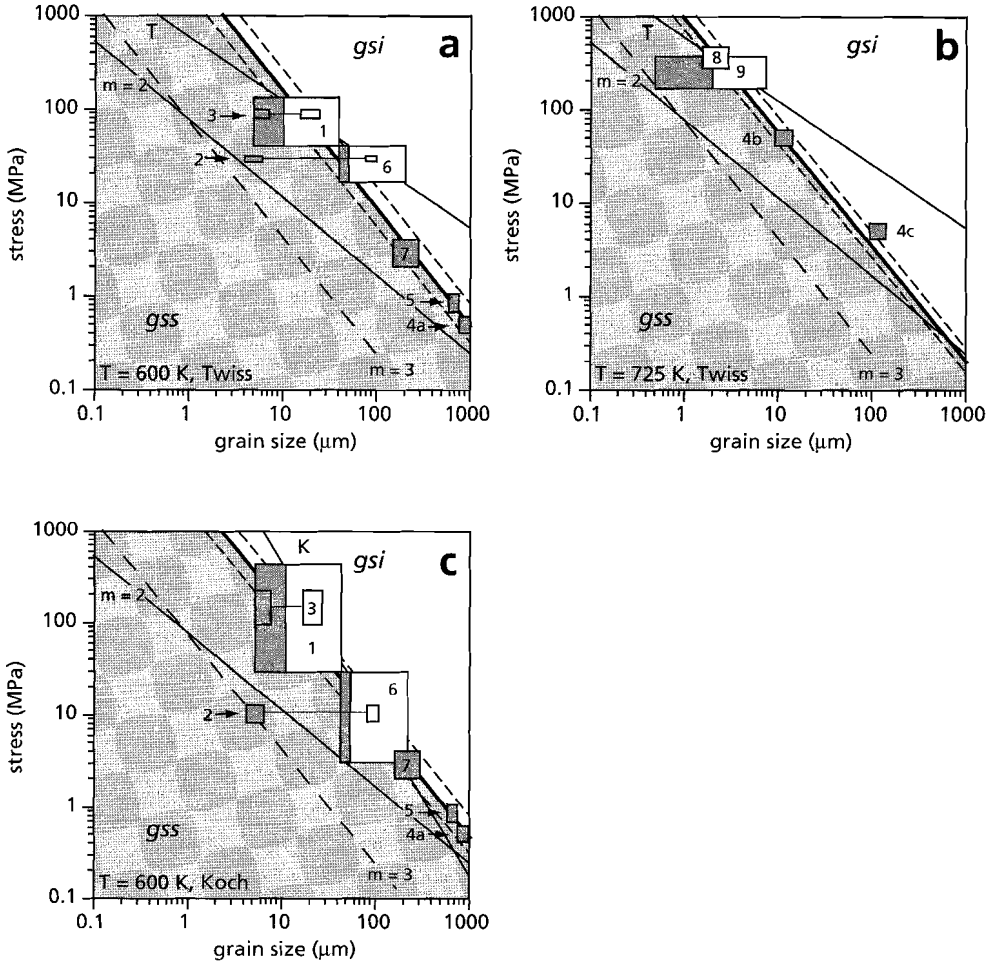

Fig. 6.3 Deformation mechanism maps for pure quartzites (as Fig. 6.2) (a & b) Stresses are calculated using the paleopiezometric relation for recrystallized grain size of Twiss (1977) and subgrain size of White (1979b) (a) T = 325 ± 50 °C; (b) T = 450 ± 50 °C . (c) Stresses are calculated using the paleopiezometric relation for recrystallized grain size of Koch (1983) at T = 325 ± 50 °C. Note, no graph at 600 °C has been shown, since data at these conditions only list grain-size-sensitive flow. No graph of Koch (1983) at T = 450 °C has been given, since stresses exceed 1000 MPa. See text for discussion.

fusion in hydrous quartzes might be faster than grain boundary diffusion and thus Nabarro-Herring creep might be important at low temperatures in wet conditions. Rutter (personal comm. 1995) reports that Nabarro-Herring type of creep processes might be important in the experimental deformation of very fine grained quartzes up to 800 °C. Since the grain size exponent in Nabarro-Herring Creep $m_{gss} = 2$, this would result in a n_{gsi} of 3.7 which is in reasonable agreement with the experimental data (Table 6.1). (iii) If there is a major component of grain boundary sliding to the deformation, the stress exponent of the grain-size-sensitive flow

law may range between 1 and 2, with a grain size exponent of 2 (Nix 1975; Gifkins 1976; 1977). In assuming a stress exponent $n_{gss} = 4$, this results in transition slope ranging between 0.67 and 1.

Whether a material, at a certain stress, deforms by grain-size-sensitive processes is largely dependent on its grain size. It is commonly observed that single phase materials, deforming by grain-size-sensitive creep, exhibit deformation induced grain growth (Schmid *et al.* 1977; Karato *et al.* 1986; Sherwood & Hamilton 1992; 1994), which might lead to a switch in deformation mechanism to intracrystalline dislocation creep processes. There are several possibilities to keep the grain size small. If, after a small grain size is set at high stresses, the stress is reduced to conditions where grain-size-sensitive processes predominate, the grain size should tend to equilibrate to this new stress. As pointed out by Tullis & Yund (1982) and Joesten (1983), the rate at which this can be attained is very sensitive to the temperature. For instance, if a quartzite deforms at 75 MPa, the dynamically recrystallized grain size is about 10 μm (using the paleopiezometric equations of Mercier *et al.* 1977; Table 6.2). If the stress drops to 45 MPa, the material is brought into the grain-size-sensitive creep field; the equilibrium grain size is however 20 μm. The grain growth relation of Joesten (1983) has been used to calculated the time needed for the grains to grow from 10 μm to 20 μm. The relation is (Joesten 1983):

$$\frac{d^2 - d_o^2}{2} = \frac{K^\star}{T} e^{\frac{-Q}{RT}} \Delta t \qquad (6.6)$$

where d and d_o are the final and initial grain size, respectively; the grain growth factor $K^\star = 5.329 \times 10^{-6}$ $m^2K\ s^{-1}$, the activation energy $Q = 210$ KJ mol^{-1}, T is the temperature and Δt is the time difference for the grains to grow from d_o to d.

Using this relation (Eq. 6.6), it can be calculated that at 325 °C, it will take about 1×10^9 years for grains to grow from 10 μm to 20 μm; at 425 °C it will take about 1×10^6 years, whereas at 600 °C it will take 27×10^3 years. So at low temperatures, a decrease in stress can result in grain-size-sensitive deformation which can persist over relatively large time scales.

A second cause of maintaining a small grain size, is by grain boundary pinning. The presence of small second phase particles at the grain boundaries, might prevent the boundaries to move. Behrmann (1985) has observed a distinct relation between fine grained mica content and grain size. So after an initial grain size is set at high stresses, a stress drop might bring the material into the grain-size-sensitive creep field, while the grain size is kept small by the mica flakelets pinning the grain boundaries. As shown in Table 6.1, most of the quartzites for which grain-size-sensitive deformation has been inferred, have phyllosilicates at the grain boundaries.

To summarise this section, it can be concluded that grain-size-sensitive creep in pure or near pure quartzes has been identified and that these results are in reasonable agreement with the experimental flow laws. TEM investigations of the microstructures and microtextures of very fine grained (2.3 ± 0.8 μm) quartz bands in mylonites from the Redbank Deformed Zone, as described in Chapter 3, suggested that dislocation creep processes were the dominant deformation mechanism operative. These observations are in accordance with the experimental data. Transition from

intracrystalline plasticity by dislocation creep processes to grain-size-sensitive creep not only depends on the grain size, but also depends on stress and temperature. Low stresses, small grain sizes and low temperatures favour grain-size-sensitive creep. The transition enhances the strain rate with 1 to 3 orders of magnitude. Grain sizes remained small due to very slow grain growth kinetics and due to grain boundaries being pinned by small mica grains.

6.5 Grain-size-sensitive deformation in quartzo-feldspathic mylonites

As noted and reviewed in Chapters 2 & 4, it is commonly observed that the mylonitization of many quartzo-feldspathic rocks deforming under middle- to upper-crustal conditions, leads to a mesoscopic augen-gneiss structure formed by elongate quartz bands alternating with finer grained polyphase bands both anastomosing around less deformed feldspar augen. The polyphase ultramylonitic centre of the shear zone commonly records the highest strains. These rocks are composed of a fairly homogeneous fine grained matrix in which the micas define the foliation. The matrix is generally composed of quartz + feldspar + mica ± epidote ± garnet; the actual mineralogy depending on the pressure and temperature conditions. While the pure quartz bands deform mainly by dislocation creep processes, there is growing evidence (Allison *et al.* 1979; Kerrich *et al.* 1980; Behrmann & Mainprice 1987; Stünitz & Fitz Gerald 1993; Chapter 4) that these polyphase bands deform by some grain-size-sensitive process with a major component of grain boundary sliding. The criteria used to identify the dominance of grain-size-sensitive creep are those used in single phase materials and have been presented in Section 6.3 and Chapters 3

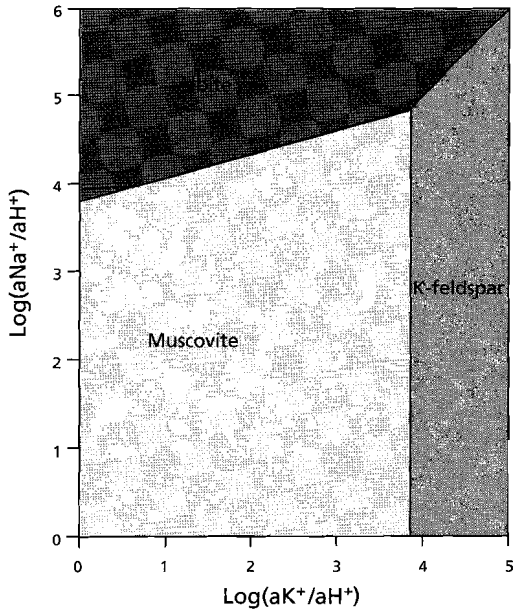

Fig. 6.4 Plot of the stability fields of albite, K-feldspar and muscovite at T = 300 °C, in terms of Na^+, K^+ and H^+ ions in coexisting fluid (after Philpotts 1990).

Table 6.4 Observations on grain-size-sensitive deformation in polyphase quartzo-feldspathic mylonites

a

ref.¥	No.	T(°C)	gsR(μm)	gsP(μm)	σ(MPa) Mercier	σ(MPa) Koch	σ(MPa) Twiss	STC	CPO	SHC	CGA	GBV	DIQ	IPBM	log(ε̇) gsR	log(ε̇) gsP
[a]	[1]	200-300	70-300	10-20	7 - 19	1-15	12-34			+					-21.0	-18.0
[b]	[2]	≈250	20-60	2-12	21-45	20-133	37-79			+	+	+	+	+	-19.6	-16.6
	[3]!	300-400	40-80	4-24	14-28	12-40	31-49			+	+	+	+	+	-16.9	-15.6
	[4]	300-400	40-100	6-20	171-287	8-40	26-49			+	+	+	+	+	-17.0	-15.6
[c]	[5]	≈425	1.5-1.3	0.3-0.7	7-11	3291-∞	279-458	+		+	+		no		-11.7	-9.1
[d]	[6]	400-450	150-300	≈10	26-34	1-4	12-20		weak						-16.5	-14.4
[e]	[7]	450-550	30-45	10-20	16-31	33-66	46-60			+					-13.3	-13.5
[f]	[8]!*	≈550	35-85	6-11	11-28	11-51	29-54	+	weak	+	+	+	+	+	-12.8	-12.3
[g]	[9]	≈600	40-140	8-15	11-14	5-40	21-49		weak			+	+	+	-12.3	-12.3
[h]	[10]	≈620	100-150	6-10	171-287	4-8	20-26			+				+	-12.7	-11.9
[i]	[11]	650-750	200-2000	40-200	2-9	0.1-3	3-16		+					+	-13.1	-15.0

b

ref. ¥	No.	T(°C)	gsR (μm)	gsP (μm)	quartz	plagioclase	K-feldspar	epidote	phyllosil.
[a]	[1]	200 - 300	70 - 300	10 - 20	+	Ab	±	+	Mu
[b]	[2]	≈ 250	20 - 60	2 - 12	+	Ab	±	+	Mu
	[3]	300 - 400	40 - 80	4 - 24	+	Ab		+	Mu
	[4]	300 - 400	40 - 100	6 - 20	+	Ab		+	Mu +Chl
[c]	[5]	≈ 425	1.5 - 3.1	0.3 - 0.7	+	An 21	+	±	Bt
[d]	[6]	400 - 450	150 - 300	≈ 10	+	An 10	+		Mu + Bt
[e]	[7]	450 - 550	30 - 45	10 - 20	+	Ab	+	±	Mu + Bt
[f]*	[8]	≈ 550	35 - 85	6 -11	+	An 38	+	±	Bt
[g]	[9]	≈ 600	40 - 140	8 - 15	+	+	+		
[h]	[10]	≈ 620	100 - 150	6 -10	+	+	+		Bt
[i]	[11]	650 - 750	200 - 2000	40- 200	+	An 28	+		Bt

¥ References: [a] Allison et al. (1979); Kerich et al. (1980); [b] FitzGerald & Stünitz (1993); Stünitz & FitzGerald (1993); [c] Section 4.5; [d] Berthé et al. (1979); [e] Gillotti (1992); [f] Chapter 4; [g] Behrmann & Mainprice (1987); [h] Vauchez (1987); [i] Gower & Simpson (1992).Key: gsR: grain size of pure quartz ribbons/; gsP: grain size of polyphase matrix; STC: grain size stability criteria, + : grain size is smaller or equal to the equilibrium subgrain size; CPO: crystallographic preffered orientation; SHC: grain shape criteria, + : rectangular to blocky grain shape; CGA: continuous grain boundary alignment across several grain diameters; GBV: grain boundary voids and open grain boundary structures; DIQ: dislocation creep microstructures in quartz of polyphase matrix; IPBM: interphase boundary migration as suggested by interphase boundary bulges. log(ε̇) gsP: log of grain size sensitive strain rate using Eq. 6.2; log(ε̇) gsR: log of dislocation creep strain rate using Eq. 6.1. *: no CSL relation between quartzes, ! phase distribution non-random (cf. Chapter 5). Ab: albite, An: anorthite content of plagioclase, phyllosil.: phyllosilicates, Mu: muscovite, Chl: chlorite, Bt: biotite. + : phase is present, ± denotes limited amount present

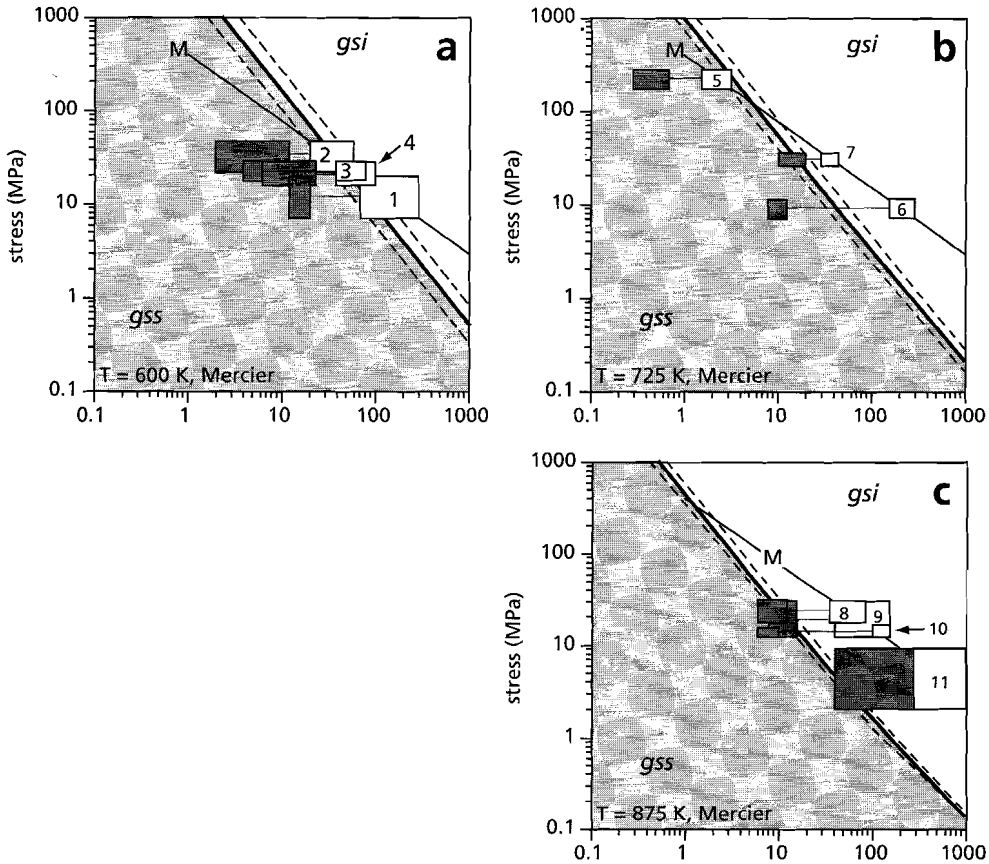

Fig. 6.5 Deformation mechanism maps for polyphase quartzo-feldspathic mylonites based on the dislocation creep flow law of Rutter & Brodie (1993a; 1993b) and the Re-calculated grain-size-sensitive creep Rutter & Brodie flow law. Stresses are calculated using the paleopiezometric relation for recrystallized grain size of Mercier *et al.* (1977). Stress and grain size conditions for polyphase bands are shaded, where as conditions for the pure quartz bands are white; numbers are as in Table 6.4. (a) T = 325 ± 50 °C; (b) T = 450 ± 50 °C; (c) T = 600 ± 50 °C. GSI: grain-size-insensitive creep field; GSS: grain-size-sensitive creep field. See text for discussion.

& 4. One additional criterion is the indication of interphase boundary migration, i.e. the curving of interphase boundaries (*cf.* Chapter 4; Gower & Simpson 1992; Stünitz & Fitz Gerald 1993). For interphase boundary migration to occur, diffusion along grain boundaries and/or through the crystal lattice is essential (Chen 1982; 1985; Wheeler 1987).

Table 6.4a gives a compilation of the microstructural observations on the deformation of quartzo-feldspathic rocks. In Table 6.4b the mineralogy of the polyphase mixtures are presented. Omitted are those data where a considerable reaction of K-feldspar and plagioclase to micaeous and epidote minerals had taken place (e.g. Williams & Dixon 1982; Dixon & Williams 1983; Knipe & Wintsch 1985; Stünitz 1993). The K-feldspar and/or plagioclase typically break down

to muscovite at lower to middle greenschist facies conditions. However, the breakdown not only depends on temperature but also depends on the H^+ activity (Philpotts 1990), i.e. it depends also on the fluid present (Fig. 6.4). At high H^+ activities muscovite is stable, whereas at low H^+ activities either albite or K-feldspar is stable (Fig. 6.4). The presence of feldspar in the polyphase mixtures at low temperatures, therefore suggest a relatively dry environment during deformation.

The stresses are estimated using the recrystallized grain size paleopiezometric equations (*cf.* Table 6.2) on the pure quartz bands which alternate with the polyphase quartz-feldspar bands. Also listed in Table 6.4a is whether or not quartz within the polyphase bands showed microstructures indicative for dislocation processes (strong CPO, dislocations present, subgrain formation). The last two columns of Table 6.4a list strain rate estimates for both the pure quartz bands (gsR) and polyphase quartzo-feldspathic mixtures (gsP). The strain rates are calculated using the flow laws as given at the end of Section 6.2, assuming a constant stress (calculated using the Mercier *et al.* 1977) between the pure quartz bands and the polyphase mixtures. The Re-calculated Rutter & Brodie grain-size-sensitive flow law has been used to estimate strain rates in these polyphase mixtures. In doing so, the strain rates calculated for these polyphase mixtures are 1 to 3 orders of magnitude higher than those calculated for the pure quartz bands.

As pointed out in Chapter 5, using the grain-size-sensitive flow law for a single phase material to obtain a strain rate estimate might underestimate the 'real' strain rate of the polyphase material by at least one order of magnitude. It has been suggested in Chapter 5, that, in an analogous way to the Pb-Sn system, flow of such polyphase rocks will differ significantly from that of its single phase end members. The flow behaviour will depend on factors such as the mineralogy of the rock, the relative amount of phases present, their distribution through the rock, the grain and interphase boundary diffusivities and grain boundary sliding resistances. Although it has been observed in Chapter 5 (Section 5.3) that the phase distribution in some of these polyphase mixtures may deviate from the distribution expected if the phases were randomly distributed in the rock, the effect of this on the rheology remains to be established. However, it is suggested in Chapter 5, that such a polyphase mixture deforming by grain-size-sensitive processes might be at least 1 order of magnitude weaker than both its constituent phases. Therefore, using a single phase flow law for strain rate calculations of the polyphase mixtures, will be expected to give minimum strain rate estimates.

Figure 6.5 shows a compilation of the data in Table 6.3 in grain size versus stress, analogous to the compilation of the data on pure or near pure quartzites (*cf.* Fig. 6.2), for three different temperature intervals; stresses have been calculated using the paleopiezometric equation of Mercier *et al.* (1977). Figure 6.6 has been drawn, using the paleopiezometric relations of Twiss (1977) and Koch (1983), to compare the different relations for stress estimates. Figure 6.5(a) is at low greenschist facies ($T \approx 325$ °C), Fig. 6.5(b) at middle to upper greenschist facies ($T \approx 425$ °C) and Fig. 6.5(c) is at amphibolite facies conditions ($T \approx 600$ °C). The boundaries between fields mark the positions where dislocation creep processes (GSS) in the pure quartz bands produce a strain rate equal to grain-size-sensitive creep processes (based on pure quartzite flow laws) of the polyphase bands; the thin dashed lines on either side of such a boundary mark a temperature

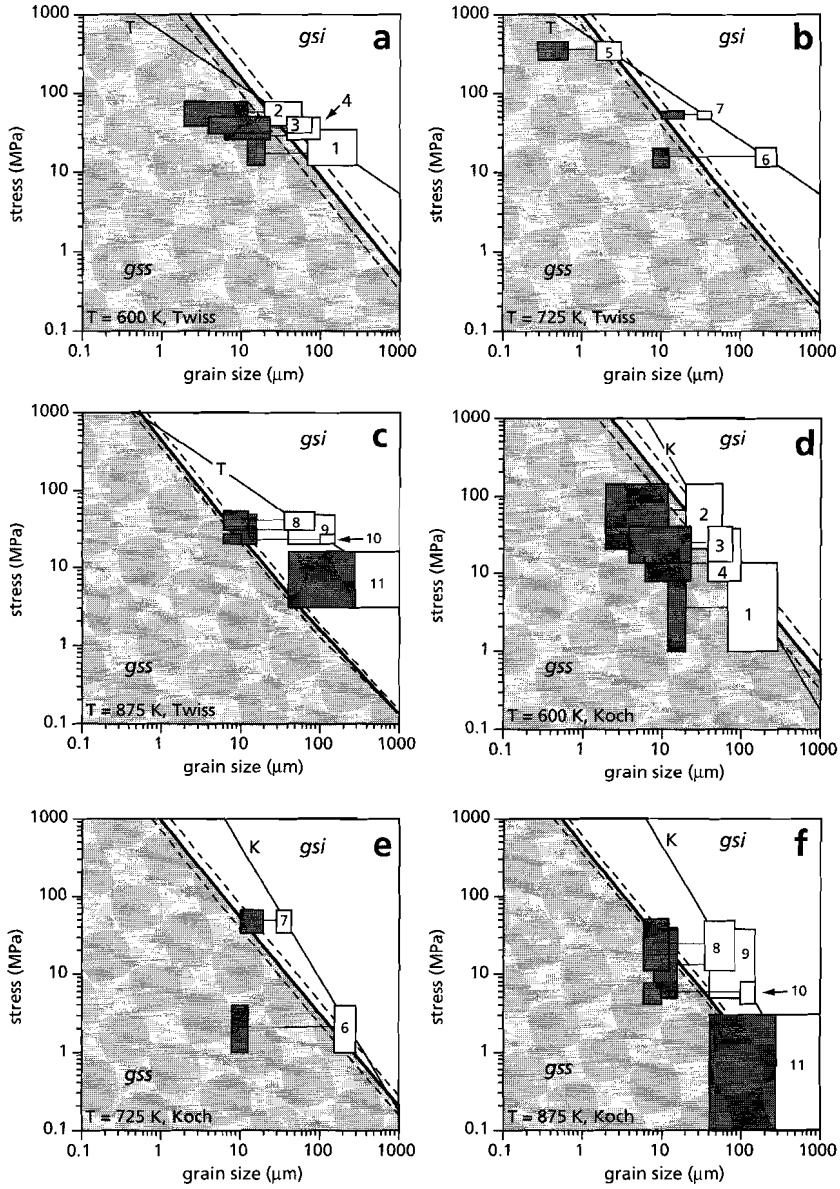

Fig. 6.6 Deformation mechanism maps for polyphase quartzo-feldspathic mylonites (as Fig. 6.5). (a - c) Stresses are calculated using the paleopiezometric relation for recrystallized grain size of Twiss (1977). (d - f) Stresses are calculated using the paleopiezometric relation for recrystallized grain size of Koch (1983). See text for discussion.

difference of 50 °C. Conditions, in terms of stress and grain size of the polyphase mixtures are shaded, whereas the pure quartz band conditions are white. Applying the paleopiezometric equations of Twiss (1977) to the pure quartz bands, results in only slightly higher stresses compared to the relation of Mercier *et al.* (1977), whereas the Koch (1983) relation predicts too high stresses at small grain sizes (> 3000 MPa at 2.3 μm; see Section 6.3).

In general, the natural data match the experimental outcomes in a similar way as for the pure or near pure quartzites. The transition from grain-size-sensitive to grain-size-insensitive creep occurs at high stresses when the grain size is small. In general, the pure quartz bands plot inside the dislocation creep field (GSS), whereas most of the polyphase bands plot in the grain-size-sensitive (GSI) field, but near the transition to dislocation creep. The microstructural and microtextural observations by TEM on very fine grained (5 - 11 μm) quartzo-feldspathic, type 1, ultramylonites of the Redbank Deformed Zone, described in Chapter 4 (no. [8] in Table 6.4 and Fig. 6.5) indicated that grain boundary sliding processes were accommodated in the different minerals by different mechanisms. It has been inferred that dislocation processes as well as diffusion were important within quartz, while diffusion and minor twinning accommodated grain boundary sliding within feldspar. Some microstructural and microtextural studies presented in Table 6.4a, also show evidence for dislocation creep microstructures within the quartzes of the polyphase mixture, these include [2], [3], [4], [9] and [11]. It is therefore suggested that the quartzes within these polyphase mixtures accommodated grain boundary sliding by dislocation processes. Further support for this suggestion comes from microstructural observations the very fine grained (0.5 ± 0.2 μm) polyphase quartzo-feldspathic type 2 mylonites of the Redbank Deformed Zone (Chapter 4) using TEM (no. [5] in Table 6.4 and Fig. 6.5). The study showed very low dislocation densities within quartz, except for the larger (> 3 μm) grains. These larger grains plot in the dislocation creep field.

To summarise this section, it can be concluded that grain-size-sensitive creep has been inferred to be operative in fine grained, polyphase quartzo-feldspathic mylonites. The transition from intracrystalline plasticity by dislocation creep processes in pure quartz bands to grain-size-sensitive creep in the polyphase mixtures of the shear zone centres enhances the strain rate with 1 to 3 orders of magnitude, if a constant stress is maintained. Bearing in mind, however, that, in an analogous way to the Pb-Sn system (*cf.* Chapter 5), the strength of such polyphase rocks might be one order of magnitude less than that of its single phase end-members. However, most models describing the rheology of quartzo-feldspathic rocks are based on flow laws for quartz deforming by dislocation creep processes. Grain-size-sensitive deformation mechanisms of such polyphase mixtures must be added into these rheological models.

6.6 Conclusions

1) The conditions, in terms of stress, temperature and grain size, for the transition from intracrystalline plasticity by dislocation creep to grain-size-sensitive deformation in naturally deformed pure and near pure quartzites are in reasonable agreement with extrapolated experimental flow laws. It is found that the transition not only depends on the grain size, but also on stress and temperature. Low stresses, small grain sizes and low temperatures favour grain-size-sensitive creep; the transition enhances, if a constant stress is maintained, the strain rate with 1 to 3 orders of magnitude. Grain sizes, during grain-size-sensitive flow, remained small due to very slow grain growth kinetics and due to grain boundaries being pinned by small phyllosilicate grains. The inferred dominance of dislocation creep mechanisms within very fine grained (2.3 $\pm$ 0.8 μm) quartz bands in type 2 mylonites from the Redbank Deformed Zone, as described in Chapter 3, using TEM are in accordance with the natural and experimental data.
2) Grain-size-sensitive creep in fine grained, polyphase, quartzo-feldspathic mylonites has been identified. The inferred dominance of grain boundary sliding processes within fine grained polyphase mixtures in both the type 1 and type 2 mylonites of the Redbank Deformed Zone, as described in Chapters 2 & 4, are in accordance with other natural observations and the experimental data. The transition from intracrystalline plasticity by dislocation creep processes in pure quartz bands to grain-size-sensitive creep in the polyphase mixtures of the shear zone centres enhances, if a constant stress is maintained, the strain rate with at least 1 to 3 orders of magnitude.
3) Models describing the rheology of quartzo-feldspathic rocks based on flow laws for quartz deforming by dislocation creep processes should be reconsidered. Grain-size-sensitive deformation mechanisms both of pure quartz and of the polyphase mixtures must be added into these rheological models.

Chapter 7

Summary and conclusions

In the light of the major aim of this thesis, namely to determine the intra and intercrystalline deformation mechanisms that lead to the observed strain partitioning in fine grained quartzo-feldspathic mylonites of the Redbank deformed Zone, Central Australia, the purpose of this chapter is to summarise the information presented in the previous chapters in order to draw general conclusions and to assess the implications of the results in terms of rheological models of shear zones. In addition, several problems are outlined to provoke further studies on the deformation mechanisms operative within fine grained polyphase rocks.

7.1 Deformation mechanisms in quartzo-feldspathic mylonites

Two types of mylonites have been recognised in the Redbank Deformed Zone (*cf.* Shaw & Black 1991; Chapter 2): type 1 and type 2, the former contain amphibolite facies mineral assemblages (550 - 650 °C) whereas the latter contain greenschist facies mineral assemblages (350 - 450 °C). The country rock in which both mylonites have developed includes migmatite, banded gneiss and weakly foliated granitic gneiss with large feldspar augen. Samples of both types of mylonites have been studied. As a result of advanced Transmission Electron Microscopy (TEM) techniques together with light microscopy (LM) and Scanning Electron Microscopy (SEM) the following results have been obtained.

Type 1 mylonites

The type 1 mylonites are characterised by porphyroclasts of K-feldspar, plagioclase and a few garnets embedded in a fine grained foliated matrix. The matrix is composed of discrete, relatively coarse grained (60 μm) pure quartz bands that alternate with continuous polyphase bands made up of a mixture of finer grained (5 - 11 μm) K-feldspar, plagioclase, quartz and biotite. The pure quartz bands are thought to form a stress supporting framework. Field, LM and SEM observations presented in Chapter 2 show that, towards the centre of a type 1 shear zone, the size and number of the porphyroclasts, as well as the amount of pure quartz bands are reduced in favour of polyphase quartz-feldspar bands. In the finest grained parts of the shear zones the feldspar clasts and pure quartz bands are eventually assimilated into the polyphase mixture, leaving only a few smaller augen in the fine grained (5 - 11 μm) polyphase mixture, *viz.* the rock type changed to an ultramylonite. Microstructural observations, such as curvatures of mylonitic foliations, boudinaged and folded quartz bands and asymmetric *c*-axis preferred orientations, were taken as evidence, in Chapter 2, that both strain and strain rate within these ultramylonites were orders of magnitude greater than the encapsulating mylonites. The coarser sized (60 μm) pure quartz bands exhibited a strong texture (CPO) of *c*-axis, the quartz grains showed undulatory

extinction, subgrain formation (with a size of 20 ± 5 μm) and serrated grain boundaries. These observations imply that flow in these pure quartz bands was due to dislocation creep processes.

On the other hand, the microstructural and microtextural studies described in Chapter 4, indicate that flow in the polyphase quartzo-feldspathic mixtures was due to grain-size-sensitive processes with a major contribution of grain boundary sliding. The pertinent observations are a rectangular to square grain shape, a continuous alignment of grain and interphase boundaries across several (≈ 10) grain diameters, a grain size (5 - 11 μm) smaller than the equilibrium subgrain size (20 μm), open and commonly void-containing grain and interphase boundaries and a weak quartz texture. A new key criterion for the identification of grain boundary sliding deformation is the analysis of crystal rotations between adjacent grains using TEM. Applying such an analysis to the quartzes within the quartz-feldspar mixtures, revealed apparent rotations between grains which cannot be explained by dislocation creep processes. The rotations are of the type expected if grain boundary sliding processes had contributed significantly to the deformation. Grain shape similarities between the K-feldspar, plagioclase and quartz grains indicate that all these fine grained phases were equally deformable at the ambient conditions.

Type 2 mylonites

The microstructures and microstructural changes of the type 2 mylonites, as described in Chapters 2, 3 and 4, are similar to those of the type 1 mylonite in that, with progressive shear deformation, the rock type changes to an ultramylonite composed of a very fine grained (0.5 ± 0.2 μm) mixture of K-feldspar, plagioclase, quartz, biotite and epidote. The main difference with the type 1 mylonite studied is, however, that with deformation the grain size of the pure quartz bands reduces from 30 μm to below 10 μm; the grain size of the quartz-feldspar mixture is below 1 μm.

Microstructural and microtextural studies using TEM on fine grained (2.3 ± 0.8 μm) pure quartz bands of the type 2 mylonite are presented in Chapter 3. These indicate that dislocation creep processes were the dominant deformation mechanism operative in these fine grained quartzes. The pertinent observations are the presence of dislocations, subgrains (with a size of 2.1 ± 0.6 μm) and sharp *c*- and *a*-axes CPO's. In addition, microtextural analyses of the axis/angle of finite misorientation between grains are consistent with dominant <*c*+*a*> and <*a*> slip. There were no apparent additional rotations of the type expected to result from grain boundary sliding processes. The stresses operative during the flow of the fine grained mylonite have been estimated to be in the range 220 - 250 MPa; such high stresses are of the magnitude that may be required for the operation of <*c*+*a*> slip. The usually invoked deformation mechanism for fine grained materials (< 10 μm), *viz.* grain-size-sensitive creep with a major component of grain boundary sliding, is not appropriate for the quartz bands in this mylonite. It was shown in Chapter 6, that fine grained materials deformed at high stresses favour dislocation creep processes above grain-size-sensitive processes.

Microstructural observations using TEM on the very fine grained (0.5 ± 0.2 μm) quartz-feldspar mixtures within the same mylonite showed rectangular grains with a low defect density, a grain size smaller than the subgrain size encountered in the pure quartz bands and a continuous alignment of grain and interphase boundaries across several grain diameters. Rapid irradiation

damage prevented a TEM based microtextural analyses on these polyphase mixtures. From these observations it was inferred that flow in these fine grained mixtures involved a major component of grain boundary sliding.

Deformation mechanisms

It is therefore concluded that the dominant deformation mechanism in the ultramylonitic shear zone centre of the two shear zones studied, differs from that of the surrounding mylonites. In the latter, where the pure quartz bands form the stress supporting framework, dislocation creep processes are the dominant deformation mechanism, whereas grain boundary sliding creep processes are dominant in the fine grained ultramylonites.

7.2 Flow of polyphase materials

Ideally, one would like to study the deformation processes in experimentally deformed fine grained polyphase rocks. Such experimental data is, however, very limited. It has been argued in Chapter 5 that a fine grained 2-phase Pb-Sn alloy which has similar deformation mechanisms as the polyphase quartzo-feldspathic ultramylonites, is a good analogue material.

As described in Chapter 5, previously published studies (Zehr & Backofen 1968) on experimentally deformed fine grained Pb-Sn alloys showed that the 2-phase Pb - 50 vol.% Sn alloy was at least one order of magnitude weaker than its constituent phases, when undergoing deformation by diffusion accommodated grain boundary sliding creep processes. These studies also showed a progressive weakening of such 2-phase alloys with strain (Gecklini & Barrett 1974). The opposite effect occurred when the material deformed by dislocation creep processes; in this regime the resultant flow law was some combination of the flow laws of the constituent phases.

Polyphase materials contain several different types of interfaces, each with its own mechanical and chemical properties. In Chapter 5 interface population variations with strain have been analysed in a 2-phase Pb-Sn alloy deforming by grain boundary sliding processes. The analyses show that the interface population evolved with strain, resulting in a microstructure in which low energy, high diffusivity interphase boundaries are more common than high energy grain boundaries; the resultant distribution deviates from randomness.

Based on the observations of the Pb-Sn alloy, a model has been developed in Chapter 5 relating variations in interface population to the mechanical properties of the 2-phase material. Low energy interfacial distributions can develop during grain-size-sensitive deformation by the movement of topological defects in the grain boundary network. The reduction of interfacial energy provides the driving force, while kinetics are similar to those of diffusional creep processes. An increase in such low energy high diffusivity paths will reduce flow stresses in polyphase materials deforming by diffusion accommodated grain boundary sliding processes to values below those of the single phase end members.

Phase distribution analyses in fine grained quartzo-feldspathic ultramylonites, like those of the Redbank Deformed Zone are presented in Chapter 5. The analyses showed that the

distribution deviates from randomness. Flow of such polyphase rocks will, analogous to the Pb-Sn system, differ significantly from that of its single phase end members. The rheology will depend on factors such as the mineralogy of the rock, the relative amounts of phases present, their distribution through the rock, the grain and interphase boundary diffusivities and grain boundary sliding resistances.

7.3 Implications for rheological modelling of shear zones

Most models describing the rheology of shear zones are based on flow laws for single phase materials deforming by dislocation creep (Kirby 1985; White & Bretan 1985; Carter & Tsenn 1987; Ord & Hobbs 1989), i.e. quartz for upper- to middle- crustal levels, feldspar for lower crustal levels and olivine for the upper mantle. However, most of these rocks contain more than one phase, i.e. quartzo-feldspathic rocks exist in the middle- and upper-crust, and peridotites occur in the upper-mantle.

Within polyphase rocks, metamorphic reactions and/or mechanical breakdown processes similar to recrystallization are the main processes that account for the inferred strain softening in shear zones. Metamorphic reactions ("reaction softening") induce softening by producing new, weak, mostly micaeous phases and/or produce small grains, which subsequently deform by grain boundary sliding processes. These processes have been identified in quartzo-feldspathic rocks deformed at various conditions of stress, strain rate, grain size and temperature and are outlined in Chapter 6. The production of phyllosilicate phases is thought to be important under hydrous retrograde metamorphic conditions (generally lower to middle-greenschist) and commonly leads to phyllonite formation (*cf.* Kerrich *et al.* 1980; Wilson 1980; Williams & Dixon 1982; Dixon & Williams 1983; Knipe & Wintsch 1985).

The two shear zones studied in this thesis deformed at temperatures higher than upper greenschist facies (Chapter 2), and showed no retrograde reactions of feldspar to phyllosilicates. At such metamorphic conditions, of temperature and fluid pressure, the production of phyllosilicates is limited, and the deformation results in a fairly homogeneous polyphase mixture of quartz ± plagioclase ± K-feldspar ± epidote ± mica that deforms by grain size sensitive creep processes (Chapter 2, 4 & 6).

For phyllonitic rocks, flow laws based on phyllosilicates would be an appropriate choice for the rheological modelling of shear zones, e.g. the flow laws for biotite of Kronenberg *et al.* (1990). Discussions in Chapters 5 and 6 suggest that estimates on the flow properties of the polyphase quartzo-feldspathic ultramylonites can be obtained by using grain-size-sensitive flow laws of one of the constituent minerals. Bearing in mind, however, that such polyphase rocks might be even weaker. Similar processes are inferred to operate within other crustal rocks like gabbros (Stünitz 1993) as well as in upper mantle peridotites (Brodie & Rutter 1986; Drury *et al.* 1991).

Therefore the models describing shear zone rheologies on the basis of flow laws for single phase materials deforming by dislocation creep processes should be reconsidered. At low temperatures (generally lower to middle-greenschist facies conditions), the flow behaviour of

phyllosilicates must be considered. Whereas, at high temperatures (generally upper greenschist facies conditions and higher) and/or dry conditions, grain-size-sensitive deformation mechanisms of polyphase mixtures should be added into rheological models.

7.4 Conclusions

The aim of the present research was to identify the intra and intercrystalline deformation mechanisms that lead to the observed strain partitioning in fine grained quartzo-feldspathic mylonites. From this thesis the following conclusions can be drawn.

1) Field, LM and SEM observations show that towards the centre of both types of quartzo-feldspathic shear zones from the Redbank Deformed Zone, the size and number of the porphyroclasts, as well as the amount of pure quartz bands, is reduced in favour of polyphase quartz-feldspar bands. In the ultramylonites, the feldspar clasts and pure quartz bands are eventually assimilated into the polyphase mixture, leaving only a few smaller augen in the fine grained (5 - 11 μm) polyphase quartzo-feldspathic mixture.

2) Microstructural and microtextural studies using TEM indicate that in fine grained (2.3 ± 0.8 μm) pure quartz bands of the type 2 mylonite, dislocation creep processes were the dominant deformation mechanism operative with <*c+a*> and <*a*> slip being important. Microstructural and microtextural studies using LM indicate that the deformation mechanism of coarser sized pure quartz bands of the type 1 mylonites involved major dislocation creep processes.

3) The transition from intracrystalline plasticity by dislocation creep processes to grain-size-sensitive creep depends not only on grain size, but also on stress and temperature. Low stresses, small grain sizes and low temperatures favour grain-size sensitive creep. Fine grained materials deformed at high stresses favour dislocation creep processes above grain size sensitive processes. The usually invoked criterion that materials with a grain size smaller than 10 μm deform by a grain-size sensitive deformation mechanism is not appropriate.

4) Microstructural and microtextural studies using TEM indicate that flow in the polyphase quartzo-feldspathic ultramylonites of both types of mylonites was caused by grain-size-sensitive processes, with a major contribution of grain boundary sliding.

5) The dominant deformation mechanism in both types of ultramylonitic shear zone centres differs from that inferred for the encapsulating mylonites. In the latter, where the pure quartz bands form the stress supporting framework, dislocation creep processes are the dominant deformation mechanism, whereas grain boundary sliding creep processes are dominant in the fine grained polyphase ultramylonites.

6) Interfacial distributions have a significant effect on the mechanical behaviour of 2-phase Pb-Sn alloys deforming by diffusion accommodated grain boundary sliding. An increase in low energy, high diffusivity paths will reduce flow stresses in the alloy below those of the single phase end members.

7) Interfacial populations in fine grained quartzo-feldspathic ultramylonites, like those of the Redbank Deformed Zone, were found to deviate from randomness. Flow of such polyphase rocks will differ significantly from that of its single phase end members, analogous to the Pb-Sn system. The flow of such fine grained polyphase mixtures will depend on factors such as the mineralogy of the rock, the relative amounts of phases present, their distribution through the rock, the grain and interphase boundary diffusivities and grain boundary sliding resistances.

8) Models describing shear zone rheologies on the basis of flow laws for single phase materials deforming by dislocation creep processes should be reconsidered. At low temperatures (generally lower to middle-greenschist facies conditions) the flow behaviour of phyllosilicates must be considered. At high temperatures (generally upper greenschist facies conditions and higher) and/or dry conditions, grain-size-sensitive deformation mechanisms of polyphase mixtures should be added into rheological models.

7.5 Suggestions for further research

While the present study has addressed some of the questions concerning the deformation mechanisms in major shear zones, it will be apparent that many have remained unanswered or partly answered, and that many new questions have been raised. These require further experimental, theoretical, microstructural studies and field work.

This thesis has concentrated on one particular rock type, namely those with a quartzo-feldspathic bulk composition at particular conditions where K-feldspar was stable. In Chapter 6 it was noted that the break down of K-feldspar to muscovite is not only a function of temperature but also depends on the type of fluid present. Some form of rheological stratification within quartzo-feldspathic rocks can take place, depending on both temperature and fluid. However, data is not well known under what conditions the stratification takes place and this remains to be established.

In this thesis the deformation mechanisms have been studied in two fine grained quartzo-feldspathic mylonites. Although similarities with previously published studies on similar and different rock types have been drawn in Chapter 6, further work is needed to prove how general these conclusions are. Furthermore, do the processes presented in this thesis and observations on quartzo-feldspathic rocks occur within different rock types, such as lower crustal dolerites or diorites, upper mantle peridotites and lherzolites, and even lower mantlepericlase - perovskites?

Analyses similar to those employed in this study could provide insight in the deformational behaviour of the polyphase earth.

Theoretical considerations and analogies with the deformational behaviour of a 2-phase Pb-Sn alloy presented in Chapter 5, suggest that interfacial energy driven re-distribution of the phases during deformation might have a profound weakening effect on a polyphase material deforming by grain-size-sensitive processes. In order to assess the significance of these interfacial energy driven processes to the mechanical behaviour of polyphase rocks further experimental, theoretical and microstructural studies are required.

Experimental data on the flow properties of polyphase rocks are needed to determine the conditions, in terms of stress, strain, strain rate, metamorphic conditions and grain size, under which interfacial energy driven processes occur and will have an effect on the rheological behaviour of the material. Since each process for microstructural change and deformation will leave its own imprint on the materials microstructure, such experimental studies should include a thorough characterisation of the material. Such a analyses should include the phase distribution, interfacial population, intracrystalline deformation microstructures and grain boundary characters of the material.

The experimental and microstructural studies should be used to develop models that describe the processes on a micromechanical scale, such that the experimental flow properties can be extrapolated towards natural conditions. These models than can serve as a guide to the recognition of interfacial energy driven processes in naturally deformed rocks, and subsequently provide an input for the rheological modelling of high strain shear zones.

References

Allison, I., Barnett, R.L. & Kerrich, R. 1979. Superplastic flow and changes in crystal chemistry of feldspars. *Tectonophysics.* **53**, T41 - T46.

Amelinckx, S. & Dekeyser, W. 1959. The structure and properties of grain boundaries. *Solid State Phys.* **8**, 325 - 499.

Ardell, A.J., Christie, J.M. & McCormick, J.W. 1974. Dislocation images in quartz and the determination of Burgers vectors. *Phil. Mag.* **29**, 1399 - 1411.

Ardell, A.J., Christie, J.M. & Tullis, J. 1973. Dislocation substructures in deformed quartz rocks. *Crystal Lattice Defects.* **4**, 275 - 285.

Ashby, M.F. 1972. A first report on deformation-mechanism maps. *Acta Metall.* **20**, 887 - 897.

Ashby, M.F. & Verrall, R.A. 1973. Diffusion accommodated flow and superplasticity. *Acta Metall.* **21**, 149 - 163.

Ashby, M.F. & Verrall, R.A. 1978. Micromechanisms of flow and fracture, and their relevance to the rheology of the upper mantle. *Phil. Trans. R. Soc. Lond.* **A288**, 59 - 95.

Backofen, W.A., Turner, I.R. & Avery, D.H. 1964. Superplasticity in an Al-Zn alloy. *Trans. ASM.* **57**, 980 - 990.

Baddi, R., Duclos, R. & Crampon, J. 1993. Neighbour switching by grain boundary penetration during diffusional deformation of an aluminia/zirconia composite. *Mater. Sci. Eng.* **A165**, L1 - L3.

Baëta, R.D. & Ashbee, K.H.G. 1969a. Slip systems in quartz: I. Experiments. *Am. Mineral.* **54**, 1551 - 1573.

Baëta, R.D. & Ashbee, K.H.G. 1969b. Slip systems in quartz: II. Interpretation. *Am. Mineral.* **54**, 1574 - 1582.

Ball, A. & Hutchinson, M.M. 1969. Superplasticity in the aluminium-zinc eutectoid. *Met. Sci. J.* **3**, 1 - 7.

Ball, A. & White, S.H. 1978. On the deformation of quartzite. *Phys. Chem. Mineral.* **3**, 163 - 172.

Beck, P.A. & Sperry, P.R. 1950. Strain induced grain boundary migration in high purity aluminium. *J. Appl. Phys.* **21**, 150.

Beeré, W. 1978. Stresses and deformation at grain boundaries. *Phil. Trans. R. Soc. Lond.* **A288**, 177 - 196.

Behrmann, J.H. 1984. Patterns of palaeostress and strain beneath the Aguilon Nappe, Betic Cordilleras (Spain). *Z. dt. geol. Ges.* **135**, 293 - 305.

Behrmann, J.H. 1985. Crystal plasticity and superplasticity in quartzite: a natural example. *Tectonophysics.* **115**, 101 - 129.

Behrmann, J.H. & Mainprice, D. 1987. Deformation mechanisms in a high-temperature quartz-feldspar mylonite: evidence for superplastic flow in the lower continental crust. *Tectonophysics.* **140**, 297 - 305.

Berman, R.G. 1990. Mixing properties of Ca-Mg-Fe-Mn garnets. *Am. Mineral.* **75**, 328 - 344.

Berthé, D., Choukroune, P. & Jegouzo, P. 1979. Orthogneiss, mylonite and non-coaxial deformation of granites: the example of the South Armorican Shear zone. *J. Struct. Geol.* **1**, 31 - 42.

Bird, J.E., Mukherjee, A.K. & Dorn, J.F. 1969. Correlations between high temperature creep behaviour and structure. In: *Quantitative Relation between Properties and Microstructure* (edited by Brandon, D.G. & Rosen, R.), Haifa, Israel, 255 - 342.

Bishop, G.H., Harrison, R.J., Kwok, T. & Yip, S. 1979. Comments on sliding and migration based on computer molecular dynamics simulations of grain boundaries. In: *Grain Boundary Structure and Kinetics* (edited by Balluffi, R.W.), Milwaukee, Wisconsin, ASM, 373 - 377.

Blacic, J.D. & Christie, J.M. 1984. Plasticity and hydrolic weakening of quartz single crystals. *J. Geophys. Res.* **89, (B6),** 4223 - 4239.

Black, L.P. & Shaw, R.D. 1992. U-Pb zircon chronology of prograde Proterozoic events in the Central and Southern Provinces of the Arunta Block, central Australia. *Aust. J. Earth Sci.* **39**, 153 - 171.

Bleris, G.L., Nouet, G., Hagège & Delavignette, P. 1982. Characterization of grain boundaries in the hexagonal system based on tables of coincidence site lattices (CSL's). *Acta Cryst.* **A38**, 550 - 557.

Bollmann, W. 1970. *Crystal Defects and Crystalline Interfaces.* Springer Verlag, Berlin.

Bons, P.D. 1993. *Experimental Deformation of Polyphase Rock Analogues*, PhD. Thesis Utrecht University, *Geologica Ultraiectina,* **110.**

Borch, R.S. & Green II, H.W. 1987. Dependence of creep in olivine on homologous temperature and its implications for flow in the mantle. *Nature.* **330**, 345 - 348.

Borch, R.S. & Green II, H.W. 1989. Deformation of peridotite at high pressure in a new molten salt cell: comparison of traditional and homologous temperature treatments. *Phys. Earth Planet. Inter.* **55**, 269 - 276.

Bossière, G. & Vauchez, A. 1978. Déformation naturelle par cisaillement ductile d'un granite de Grande Kabylie occidentale (Algérie). *Tectonophysics.* **51**, 57 - 81.

Bouchez, J.L. 1978. Preferred orientations of quartz <a> axes in some tectonites: kinematic inferences. *Tectonophysics.* **49**, T25 - T30.

Boullier, A.M. & Gueguen, Y. 1975. Origin of some mylonites by superplastic flow. *Contrib. Mineral. Petrol.* **50**, 93 - 104.

Brodie, K.H. 1980. Variations in mineral chemistry across a shear zone in phlogopite peridotite. *J. Struct. Geol.* **2**, 265 - 272.

Brodie, K.H. & Rutter, E.H. 1985. On the relationship between deformation and metamorphism, with special reference to the behavior of basic rocks. In: *Metamorphic Reactions: Kinetics, Textures, and Deformation* (edited by Thompson, A.B. & Rubie, D.C.). *Adv. Phys. Geochem.* **4,** Springer Verlag, New York, 138 - 179.

Brodie, K.H. & Rutter, E.H. 1986. The role of transiently fine-grained reaction products in syntectonic

metamorphism: natural and experimental examples. *Can. J. Earth Sci.* **24**, 556 - 564.

Bruhn, D., Olgaard, D.L. & Dell'Angelo, L.N. 1994. Experiments on plastic flow of fine-grained two-phase rocks. *EOS, Transactions AGU.* **75**, 636.

Bruhn, D., Olgaard, D.L., Dell'Angelo, L.N. & Siddiqi, G. 1993. Rheology of fine-grained rocks containing two phases of similar strengths: preliminary results. *Terra Nova, Terra Abstracts.* **5**, 287.

Buttler, R.W.H. & Coward, M.P. 1984. Geological constraints, structural evolution and deep geology in NW Scottish Caledonides. *Tectonics.* **3**, 347 - 365.

Cahn, J.W. & Padawar, G.E. 1965. On Hillert's grain growth catalyst. *Acta Metall.* **13**, 1091 - 1092.

Cahn, R.W. 1978. Deformation and recystallization textures in metals and quartz. *Phil. Trans. R. Soc. London.* **A288**, 159 - 176.

Carry, C. 1990. Microstructures, grain boundaries and superplasticity in fine grained ceramics. In: *Mat. Res. Soc. Symp. Proc.* (edited by Christen, D., Narayan, J. & Schneemeyer, L.), **196**, MRS, 313 - 323.

Carter, N.L. & Tsenn, M.C. 1987. Flow properties of continental lithosphere. *Tectonophysics.* **136**, 27 - 63.

Chatterjee, N.D., Johannes, W. & Leistner, H. 1984. The system CaO-Al2O3-SiO2-H2O: new phase equilibria, some calculated phase relations, and their petrological applications. *Contrib. Mineral. Petrol.* **88**, 1 - 13.

Chen, I.-W. 1982. Diffusional creep of two phase materials. *Acta Metall.* **30**, 1655 - 1664.

Chen, I.-W. 1985. Superplastic flow of two-phase alloys. In: *Superplasticity* (edited by Baudelet, B. & Suéry, M.). CNRS, Paris, 5.1 - 5.20.

Chopra, P.N. 1986. The plasticity of some fine-grained aggregates of olivine at high pressure and temperature. In: *Mineral and Rock Deformation: Laboratory Studies, The Paterson Volume* (edited by Hobbs, B.E. & Heard, H.C.). *Geophys. Monogr. Ser.* **36**, AGU, Washington D.C., 25 - 33.

Choukroune, P. & ECORS-team 1989. The ECORS Pyrenean deep seismic profile: reflection data and the overall structure of an orogenic belt. *Tectonics.* **8**, 23 - 39.

Clark, W.A.V. & Hosking, P.L. 1986. *Statistical Methods for Geographers.* John Wiley and Sons, New York.

Clarke, D.R. 1987. Grain boundaries in polycrystalline ceramics. *Ann. Rev. Mater. Sci.* **17**, 57 - 74.

Cline, H.E. & Alden, T.H. 1967. Rate-sensitive deformation in tin-lead alloys. *Trans. AIME.* **239**, 710 - 714.

Coble, R.L. 1963. A model for boundary diffusion controlled creep in polycrystalline materials. *J. Appl. Physics.* **34**, 1679 - 1682.

Cooper, R.F. & Kohlstedt, D.L. 1982. Interfacial energies in the olivine-basalt system. In: *High Pressure Research in Geophysics* (edited by Akimoto, S. & Manghani, M.H.). *Adv. Earth Planet. Sci.* **12**, Center for Academic Publications, Tokyo, 217 - 228.

Coward, M.P., Windley, B.F., Broughton, R.D., Luff, I.W., Petterson, M.G., Pudsey, C.J., Rex, D.C. & Asif Kahn, M. 1986. Collision tectonics in the NW Himalayas. In: *Collision Tectonics* (edited by Coward, M.P. & Ries, A.C.). *Geological Society Special Publication.* **19**, London, 203 - 219.

Davis, J.C. 1986. *Statistics and Data Analysis in Geology.* John Wiley & Sons, New York.

De Bresser, J.H.P. 1991. *Intracrystalline Deformation of Calcite*, PhD. Thesis Utrecht University, *Geologica Ultraiectina*, **79.**

Den Brok, S.W.J. 1992. *An Experimental Investigation into the Effect of Water on the Flow of Quartzite*, PhD. Thesis Utrecht University, *Geologica Ultraiectina*, **95.**

Derby, B. 1990. Dynamic recrystallization and grain size. In: *Deformation Processes in Minerals, Ceramics and Rocks* (edited by Barber, D.J. & Meredith, P.G.). Unwin Hyman Ltd, London, 354 - 364.

Derby, B. & Ashby, M.F. 1987. On dynamic recrystallization. *Scripta Metall.* **21**, 832 - 837.

Dixon, J. & Williams, G. 1983. Reaction softening in mylonites from the Arnaboll thrust, Sutherland. *Scott. J. Geol.* **19**, 157 - 168.

Donath, F.A., Faill, R.T. & Tobin, D.G. 1971. Deformation mode fields in experimenatlly deformed rocks. *Geol. Soc. Am. Bull.* **82**, 1441 - 1462.

Drury, M.R. 1993. Deformation lamellae in metals and minerals. In: *Defects and Processes in the Solid state: Geoscience Applications. The McLaren Volume* (edited by Boland, J.N. & Fitz Gerald, J.D.). *Developments in Petrology.* Elsevier, Amsterdam, 195 - 212.

Drury, M.R., Hoogerduijn Strating, E.H. & Vissers, R.L.M. 1990. Shear zone structures and microstructures in mantle peridotites from the Voltri massif, Ligurian Alps, N.W. Alps. *Geol. Mijnbouw.* **69**, 3 - 17.

Drury, M.R. & Humpreys, F.J. 1988. Microstructural shear criteria associated with grain-boundary sliding during ductile deformation. *J. Struct. Geol.* **10**, 83 - 89.

Drury, M.R., Humpreys, F.J. & White, S.H. 1985. Large strain deformation studies using polycrystalline magnesium as a rock analogue. Part II: dynamic recrystallisation mechanisms at high temperatures. *Phys. Earth Planet. Sci.* **40**, 208 - 222.

Drury, M.R. & Urai, J.L. 1990. Deformation-related recrystallization processes. *Tectonophysics.* **172**, 235 - 253.

Drury, M.R., Vissers, R.L.M., Van der Wal, D. & Hoogerduijn Strating, E.H. 1991. Shear localization in upper mantle peridotites. *Pageoph.* **137**, 439 - 460.

Edington, J.W. 1974. *Monographs in practical electron microscopy in materials science.* Philips Technical Library, The Macmillan Press Ltd., London.

Edington, J.W., Melton, K.N. & Cutler, C.P. 1976. Superplasticity. *Progress in Mat. Sci.* **21**, 61 - 170.

Ehlers, E.G. 1972. *The Interpretation of Geological Phase Diagrams.* Dover Publications, Inc., New York.

Etheridge, M.A. & Hobbs, B.E. 1974. Chemical and deformational controls on recrystallization of mica.

Contrib. Mineral. Petrol. **43**, 111 - 124.

Etheridge, M.A. & Wilkie, J.C. 1979. Grainsize reduction, grain boundary sliding and the flow strength of mylonites. *Tectonophysics.* **58**, 159 - 178.

Evans, B., Rowen, M. & Brace, W.F. 1980. Grain-size sensitive deformation of stretched conglomerate from Plymouth, Vermont. *J. Struct. Geol.* **2**, 411 - 424.

Fan, Z., Miodownik, A.P. & Tsakiropoulos, P. 1993. Microstructural characterisation of two phase materials. *Mater. Sci. Technol.* **9**, 1094 - 1100.

Fan, Z. & Moidownik, A.P. 1993a. The deformation behaviour of alloys comprising two ductile phases - I. Deformation theory. *Acta Metall. Mater.* **42**, 2403 - 2414.

Fan, Z. & Moidownik, A.P. 1993b. The deformation behaviour of alloys comprising two ductile phases - II. Application of the theory. *Acta Metall. Mater.* **42**, 2415 - 2424.

Feldmann, K., Bankwitz, E., Bankwitz, P., Kleinsteuber, W., Voitus, W. & Walther, K. 1991. Quartz fabric and microstructural analysis of mylonites from the Elbe zone. *Textures and Microstructures.* **14 - 18**, 397 - 402.

Ferry, J.M. & Spear, F.S. 1978. Experimental calibration of the partitioning of Fe and Mg between biotite and garnet. *Contrib. Mineral. Petrol.* **66**, 113-117.

Fitz Gerald, J.D. & Stünitz, H. 1993. Deformation of granitoids at low metamorphic grade. I: Reactions and grain size reduction. *Tectonophysics.* **221**, 269-297.

Fliervoet, T.F. & White, S.H. 1995. Quartz deformation in a very fine grained quartzo-feldspathic mylonite: A lack of evidence for dominant grain boundary sliding deformation. *J. Struct. Geol.* **17**, 1095-1109.

Forwood, C.T. & Clarebrough, L.M. 1991. *Electron Microscopy of Interfaces in Metals and Alloys. Electron Microscopy in Materials Science Series.* Adam Hilger, Bristol.

Friedel, J. 1964. *Dislocations.* Pergamon, Oxford.

Frost, H.J. & Ashby, M.F. 1982. *Deformation Mechanism Maps. The Plasticity and Creep of Metals and Ceramics.* Pergamon, Oxford.

Gapais, D. & White, S.H. 1982. Ductile shear bands in a naturally deformed quartzite. *Textures and Microstructures.* **5**, 1 - 17.

Geckinli, A.E. & Barrett, C.R. 1974. Internal stresses and superplastic flow in the Pb-Sn eutectic. *Scripta Metall.* **8**, 115 - 120.

Gecklini, A.E. & Barrett, C.R. 1976. Superplastic deformation of the Pb-Sn eutectic. *J. Mater. Sci.* **11**, 510 - 521.

Gifkins, R.C. 1976. Grain boundary sliding and its accomodation during creep and superplasticity. *Met. Trans.* **7A**, 1225 - 1232.

Gifkins, R.C. 1977. The effect of grain size upon grain boundary sliding. *Met. Trans.* **8A**, 1507 - 1516.

Gifkins, R.C. 1982. Mechanisms of superplasticity. In: *Superplastic Forming of Structural Alloys* (edited by Baton, N.E. & Hamilton, C.H.). The metallurgical Society of AIME, Warrendale, 3 - 26.

Gilotti, J.A. 1992. The rheologically critical matrix in arkosic mylonites along the Särv thrust, Swedish Caledonides. In: *Structural geology of fold and thrust belts* (edited by Mittra, S. & Fisher, G.W.). Hopkins University Press, Baltimore, 145 - 160.

Gleason, G.C. & Tullis, J. 1993. Improving flow laws and piezometers for quartz and feldspar aggregates. *Geophys. Res. Lett.* **20**, 2111 - 2114.

Gleason, G.C. & Tullis, J. 1994. A flow law for dislocation creep in quartzite and its implications for the strength of the crust. *EOS, Transactions AGU.* **75 no. 16**, 329.

Gleiter, H. 1982. On the structure of grain boundaries in metals. *Mat. Sci. Eng.* **52**, 91 - 131.

Glikson, A.Y. 1986. An upthrusted early proterozoic basic granulite-anorthosite suite and anatectic gneisses, South-West Arunta block, central Australia: evidence on the nature of the lower crust. *Trans. geol. Soc. Afr.* **89**, 263 - 283.

Glikson, A.Y. 1987. Regional structure and evolution of the Redbank-Mount Zeil thrust zone: a major lineament in the Arunta Inlier, central Australia. *BMR J. Aus. Geol. Geoph.* **10**, 89 - 107.

Goldsmith, J.R. 1982a. Review of the behavior of plagioclase under metamorphic conditions. *Am. Mineral.* **67**, 643 - 652.

Goldsmith, J.R. 1982b. Plagioclase stability at elevated temperatures and water pressures. *Am. Mineral.* **67**, 653 - 675.

Goleby, B.R., Shaw, R.D., Wright, C., Kennet, B.L.N. & Lambeck, K. 1989. Geophysical evidence for 'thick-skinned' crustal deformation in central Australia. *Nature.* **337**, 325 - 330.

Goodhew, P.J. 1979. The relationship between grain boundary structure and energy. In: *Grain Boundary Structure and Kinetics* (edited by Baluffi, R.W.), Milwaukee, Wisconsin, ASM, 155 - 179.

Gordon, P. & Vandermeer, R.A. 1966. Grain boundary migration. In: *Recrystallization, Grain Growth and Textures* (edited by Margolin, H.). ASM, Metals Park, Ohio,

Gower, R.J.W. & Simpson, C. 1992. Phase boundary mobility in naturally deformed, high-grade quartzo-feldspathic rocks: evidence for diffusional creep. *J. Struct. Geol.* **14**, 301 - 314.

Green, H.W. & Borch, R.S. 1989. A new molton salt cell for precision stress measurement at high stress. *Eur. J. Mineral.* **1**, 213 - 219.

Green, H.W. & Borch, R.S. 1990. High pressure and temperature deformation experiments in a liquid confining medium. In: *The Brittle-Ductile Transition in Rocks* (edited by Duba, A.G., Durham, W.B., Handin, J.W. & Wang, H.F.). *Geoph. Monograph Ser.* **56,** Am. Geoph. Union., Washington,

Grimmer, H. 1980. A unique description of the relative orientation of neighbouring grains. *Acta Cryst.* **A36**, 382 - 389.

Grimmer, H. 1989a. Systematic determination of coincidence orientations for all hexagonal lattices with axial ration c/a in a given interval. *Acta Cryst.* **A45**, 320 - 325.

Grimmer, H. 1989b. *Koinzidenzorientierungen von Körnern in rhomboedrischen und hexagonalen Materialien. PSI Bericht.* Wurlingen.

Hall, M.G. & Lloyd, G.E. 1981. The SEM examination of geological samples with a semiconducter back-scattered electron detector. *Am. Mineral.* **66**, 362 - 386.

Handy, M.R. 1989. Deformation regimes and the rheological evolution of fault zones in the lithosphere: the effects of pressure, temperature, grainsize and time. *Tectonophysics.* **163**, 119 - 152.

Handy, M.R. 1990. The solid-state flow of polymineralic rocks. *J. Geophys. Res.* **95, (B6),** 8647 - 8661.

Handy, M.R. & Zingg, A. 1991. The tectonic and rheological evolution of an attenuated cross section of the continental crust: Ivrea crustal section, southern Alps, northwestern Italy and southern Switzerland. *GSA Bull.* **103**, 236 - 253.

Hansen, F.D. & Carter, N.L. 1982. Creep of selected crustal rocks at 1000 MPa. *EOS, Transactions AGU.* **63**, 437.

Harris, K.E. & King, A.H. 1994. Localized texture formation and its detection in polycrystalline thin films of gold. In: *Mechanisms of Thin film Evolution* (edited by Yalisove, S., Thompson, C.V. & Eaglesham, D.J.), *MRS Conf. Proc.* **317**, Boston, MA, USA, M.R.S., Pittsburg, USA, 425 - 430.

Haruna, T., Shibayanagi, T., Hori, S. & Furushiro, N. 1992. Effect of grain boundary characters on grain boundary sliding during superplastic deformation. *Materials Transactions JIM.* **33**, 374 - 379.

Herring, C. 1950. Diffusional viscocity of a polycrystalline solid. *J. Appl. Phys.* **21**, 437 - 445.

Herring, C. 1951. Surface tension as a motivation for sintering. In: *The Physics of Powder Metallurgy* (edited by Kingston, W.E.). McGraw-Hill, New York, Ch. 8.

Hillert, M. 1965. On the theory of normal and abnormal grain growth. *Acta Metall.* **13**, 227 - 238.

Hirohashi, M. & Asanuma, H. 1989. Superplasticity of hypo-eutectoid Al-Zn alloy sheets. In: *MRS Int'l Mtg on Adv. Mat* **7**, 125 - 132.

Hirsch, P., Howie, A., Nicholson, R.B., Pashley, D.W. & Whelan, M.J. 1967. *Electron Microscopy of Thin Crystals.* R.E. Krieger Publ. Comp,

Hirth, G. & Tullis, J. 1992. Dislocation creep regimes in quartz aggregates. *J. Struct. Geol.* **14**, 145 - 159.

Hitchings, R.S., Paterson, M.S. & Bitmead, J. 1989. Effects of iron and magnetite additions in olivine-pyroxene rheology. *Phys. Earth. Planet. Inter.* **55**, 277 - 291.

Hobbs, B.E., Means, W.D. & Williams, P.F. 1976. *An Outline of Structural Geology.* John Wiley & Sons, New York.

Hobbs, B.E., Ord, A. & Teyssier, C. 1986. Earthquakes in the ductile regime. *Pageoph.* **124**, 309 - 336.

Holm, E.A., Srolovitz, D.J. & Cahn, J.W. 1993. Microstructural evolution in two-dimensional two-phase polycrystals. *Acta Metall. Mater.* **41**, 1119 - 1136.

Holness, M.B. 1995. The effect of feldspar on quartz-H2O-CO2 dihedral angles at 4kbar, with consequences for the behaviour of aqueous fluids in migmatites. *Contrib. Mineral. Petrol.* **118**, 356 - 364.

Hoogerduijn Strating, E.H., Piccardo, G.B., Rampone, E., Scambelluri, M., Vissers, R.L.M., Drury, M.R. & Van der Wal, D. 1990. The structure and petrology of the Erro-Tobbio peridotite, Voltri massif, Ligurian Alps. Guidebook for a two-day-excursion with emphasis on processes in the upper mantle (Voltri Massif, June 26-28, 1989). *Ofioloiti.* **15**, 119 - 184.

Hull, D. & Bacon, D.J. 1984. *Introduction to Dislocations. Int. series on Mat. Sci. Tech.* Pergamon, Oxford.

Janecke, S.U. & Evans, J.P. 1988. Feldspar-influenced rock rheologies. *Geology.* **16**, 1064 - 1067.

Jaoul, O., Tullis, J. & Kronenberg, A. 1984. The effect of varying water contents on the creep behavior of Heavitree quartzite. *J. Geophys. Res.* **89, (B6),** 4298 - 4312.

Joesten, R. 1983. Grain growth and grain-boundary diffusion in quartz from the Christmas Mountains (Texas) contact aureole. *Am. J. Sci.* **283A**, 233 - 254.

Joesten, R. 1991. Grain-boundary diffusion kinetics in silicate and oxide minerals. In: *Diffusion, Atomic Ordering, and Mass Transport* (edited by Ganguly, J.). *Adv. in Phys. Chem.* **8**, Springer-Verlag, Berlin, 345 - 395.

Johnson, R.H. 1970. Superplasticity. *Metallurgical reviews.* **15**, 115 - 134.

Jordan, P. 1988. The rheology of polymineralic rocks - an approach. *Geol. Rundschau.* **77**, 285 - 294.

Karakaya, I. & Thompson, W.T. 1988. The Pb-Sn system. *Bull. Alloy Phase Diagrams.* **9, (2),** 201.

Karato, S.I., Paterson, M.S. & FitzGerald, J.D. 1986. Rheology of synthetic olivine aggregates: influence of grain size and water. *J. Geophys. Res.* **91, (B8),** 8151 - 8176.

Kaur, I., Gust, W. & Kozma, L. 1989. *Handbook of Grain and Interphase Boundary Diffusion Data.* Ziegler Press, Stuttgart.

Kerrich, R. 1976. Some effects of tectonic recrystallization on fluid inclusions in vein quartz. *Contrib. Mineral. Petrol.* **59**, 195 - 202.

Kerrich, R., Allison, I., Barnett, R.L., Moss, S. & Starkey, J. 1980. Microstructural and chemical transformations accompanying deformation of granite in a shear zone at Miéville, Switzerland; with implications for stress corrosion cracking and superplastic flow. *Contrib. Mineral. Petrol.* **73**, 221-242.

Kerrich, R., Beckinsale, R.D. & Durham, J.J. 1977. The transition between deformation regimes dominated by intercrystalline diffusion and intracrystalline creep evaluated by oxygen isotope thermometry. *Tectonophysics.* **38**, 241 - 257.

Kirby, S.H. 1985. Rock mechanics observations pertinent to the rheology of the continental lithosphere and the

localization of strain along shear zones. *Tectonophysics*. **119**, 1 - 27.

Knipe, R.J. 1989. Deformation mechanisms - recognition from natural tectonites. *J. Struct. Geol.* **11**, 127 - 146.

Knipe, R.J. 1990. Microstructural analysis and tectonic evolution in thrust systems: examples from the Assynt region of the Moine Thrust Zone, Scotland. In: *Deformation Processes in Minerals, Ceramics and Rocks* (edited by Barber, D.J. & Meredith, P.G.). Unwin, London, 228 - 261.

Knipe, R.J. & Law, R.D. 1987. The influence of crystallographic orientation and grain boundary migration on microstructural and textural evolution in an S-C mylonite. *Tectonophysics*. **135**, 155 - 169.

Knipe, R.J. & White, S.H. 1978. On the deformation of quartz containing bubbles. *Jl. geol. Soc. Lond.* **135**, 313 - 316.

Knipe, R.J. & Wintsch, R.P. 1985. Heterogeneous deformation, foliation development, and metamorphic processes in a polyphase mylonite. In: *Metamorphic Reactions - Kinetics, Textures, and Deformation* (edited by Thompson, A.B. & Rubie, D.C.). *Adv. in Phys. Chem.* **4,** Springer-Verlag, New York, 180 - 210.

Koch, P.S. 1983. *Rheology and Microstructures of Experimentally Deformed Quartz Aggregates*, PhD. Thesis University of California,

Kohlstedt, D.L. & Weathers, M.S. 1980. Deformation-induced microstructures, paleopiezometers, and differential stresses in deeply eroded fault zones. *J. Geophys. Res.* **85, (B11),** 6269 - 6285.

Kretz, R. 1966. Interpretation of the shape of mineral grains in metamorphic rocks. *J. Petrology*. **7**, 68 - 94.

Kretz, R. 1969. On the spatial distribution of crystals in rocks. *Lithos*. **2**, 39 - 66.

Kronenberg, A.K., Kirby, S.H. & Pinkston, J. 1990. Basal slip and mechanical anisotropy of biotite. *J. Geoph. Res.* **95, (B12),** 19257 - 19278.

Kulkarni, M.S. & Kashyap, B.P. 1992. Microstructural evolution and hardness variation in the two phase Al - Cu alloys. *Z. Metallkd.* **83**, 123 - 126.

Langdon, T.G. 1982. Experimental observations in superplasticity. In: *Superplastic Forming of Structural Alloys* (edited by Paton, N.E. & Hamilton, C.H.). The Metallurgical Society of AIME, Warendale, 27 - 40.

Langdon, T.G. 1990a. Superplastic ceramics - an overview. In: *Superplasticity in Aerospace II* (edited by McNelly, T.R. & Heikkenen, H.C.), Warendale, Met. Soc. AIME, 3 - 18.

Langdon, T.G. 1990b. Superplastic ceramics. They're not a stretch of the imagination anymore. *JOM*. 8 - 13.

Lappalainen, R., Pannikkat, A. & Raj, R. 1993. Superplastic flow in a non-stoichiometric ceramic: magnesium aluminate spinel. *Acta Metall. Mater.* **41**, 1229 - 1236.

Lartigue Korinek, S. & Dupau, F. 1994. Grain boundary behavior in superplastic Mg-doped alumina with Yttria codoping. *Acta Metall. Mater.* **42**, 293 - 302.

Law, R.D., Knipe, R.J. & Dayan, H. 1984. Strain path partitioning within thrust sheets: microstructural and petrofabric evidence from the Moine Thrust zone at Loch Eriboll, northwest Scotland. *J. Struct. Geol.* **6**, 477 - 497.

Law, R.D., Schmid, S.M. & Wheeler, J. 1990. Simple shear deformation and quartz crystallographic fabrics: a possible natural example from the Torridon area of NW Scotland. *J. Struct. Geol.* **12**, 29 - 45.

Lisle, R. & Savage, J. 1983. Factors influencing rock competence: data from a Swedish deformed conglomerate. *Geolog. Foren. Stockholm Forh.* **104**, 219 - 224.

Lister, G.L. 1977. Crossed-girdle c-axis fabrics in quartzites plastically deformed by plane strain and progressive simple shear. *Tectonophysics*. **35**, 51 - 54.

Lloyd, G.E. & Freeman, B. 1991a. Dynamic recrystallization of a quartz porphyroclast. *Textures and Microstructures*. **14 - 18**, 751 - 756.

Lloyd, G.E. & Freeman, B. 1991b. SEM electron channeling analysis of dynamic recrystallization in a quartz grain. *J. Struct. Geol.* **13**, 945 - 953.

Lloyd, G.E. & Freeman, B. 1994. Dynamic recrystallization under greenschist facies conditions. *J. Struct. Geol.* **16**, 867 - 881.

Lloyd, G.E. & Hall, M.G. 1981. Application of scanning electron microscopy to the study of deformed rocks. *Tectonophysics*. **78**, 687 - 698.

Lloyd, G.E. & Knipe, R.J. 1992. Deformation mechanisms accommodating faulting of quartzite under upper crystal conditions. *J. Struct. Geol.* **14**, 127 - 144.

Lloyd, G.E., Law, R.D., Mainprice, D. & Wheeler, J. 1992. Microstructural and crystal fabric evolution during shear zone formation. *J. Struct. Geol.* **14**, 1079 - 1100.

Lloyd, G.E., Mainprice, D., Law, R.D. & Wheeler, J. 1991. Micromechanics of formation of a quartzo-feldspathic shear zone. *Textures and Microstruc.* **14 - 18**, 333 - 338.

Luton, M.J. & Sellars, C.M. 1969. Dynamic recrystallisation in nickel and nickel-iron alloys during high temperature deformation. *Acta Metall.* **17**, 1033 - 1043.

Ma, Y. & Langdon, T.G. 1994. Factors influencing the exceptional ductility of a superplastic Pb - 62 pct Sn alloy. *Metall. Mater. Trans. A.* **25 A**, 2309 - 2311.

Maehara, Y. & Langdon, T.G. 1990. Review. Superplasticity in ceramics. *J. Mat. Sci.* **25**, 2275 - 2286.

Mainprice, D., Lloyd, G.E. & Casey, M. 1993. Individual orientation measurements in quartz polycrystals: advantages and limitations for texture and petrophysical property determinations. *J. Struct. Geol.* **15**, 1169 - 1187.

Marjoribanks, R.W. & Black, L.P. 1974. Geology and geochronology of the Arunta Complex north of Ormiston Gorge, Central Australia. *J. Geol. Soc. Austr.* **21**, 291 - 299.

Martin, G. & Perraillon, B. 1979. Measurements of grain

boundary diffusion. In: *Grain Boundary Structure and Kinetics* (edited by Balluffi, R.W.), Milwaukee, Wisconsin, ASM, 239 - 295.

Martin, J.W. & Doherty, R.D. 1976. *Stability of Microstructure in Metallic Systems. Cambridge Solid State Science Series.* Cambridge University Press, Cambridge.

Matsui, T., Karato, S. & Yokokura, T. 1980. Dislocation structures from pallasite meteorites. *Geoph. Res. Lett.* **7**, 1007 - 1010.

Mawer, C.K. & FitzGerald, J.D. 1993. Microstructure of kink band boundaries in naturally deformed chewings range quartzite. In: *Defects and Processes in the Solid State: Geoscience Applications. The McLaren Volume* (edited by Boland, J.N. & FitzGerald, J.D.). *Developments in Petrology.* **14,** Elsevier, Amsterdam, 49 - 67.

McClay, K.R. 1977. Pressure solution and Coble creep in rocks and minerals: a review. *Jl. geol. Soc. Lond.* **134**, 57 - 70.

McGeary, S. & Warner, M.R. 1985. Seismic profiling the continental lithosphere. *Nature.* **317**, 795 - 797.

McLaren, A.C. 1986. Some speculations on the nature of high-angle grain boundaries in quartz rocks. In: *Mineral and Rock Deformation: Laboratory Studies, The Paterson Volume* (edited by Hobbs, B.E. & Heard, H.C.). *Geophys. Monogr. Ser.* **36,** AGU, Washington D.C., 233 - 245.

McLaren, A.C. 1991. *Transmission Electron Microscopy of Minerals and Rrocks. Cambridge Topics in Mineral Physics and Chemistry.* Cambridge University Press, Cambridge.

McLaren, A.C. & Phakey, P.P. 1965a. A transmission electron microscope study of amethyst and citrine. *Aust. J. Phys.* **18**, 135 - 141.

McLaren, A.C. & Phakey, P.P. 1965b. Dislocations in quartz observed by Transmission Electron Microscopy. *J. appl. Physics.* **36**, 3244 - 3246.

Mehrer, H. 1990. *Group III: Crystal and Solid State Physics, Diffusion in Solid Metals and Alloys.* Springer-Verlag, Berlin,

Melton, K.N. & Edington, J.W. 1975. Superplasticity in Zn-40 wt% Al and Zn-50 wt% Al alloys at 300 °C. *Scripta Metall.* **9**, 559 - 562.

Mercier, J.C., Anderson, D.A. & Carter, N.L. 1977. Stress in the lithosphere: inferences from steady state flow of rocks. *Pageoph.* **115**, 199 - 226.

Mitra, G. 1992. Deformation of granitic basement rocks along fault zones at shallow to intermediate crustal levels. In: *Structural Geology of Fold and Thrust Belts* (edited by Mitra, S. & Fisher, G.W.). Johns Hopkins University Press, Baltimore, 123 - 144.

Mitra, S. 1976. A quantitavive study of deformation mechanisms and finite strain in quartzites. *Contrib. Mineral. Petrol.* **59**, 203 - 226.

Mohamed, F.A. & Langdon, T.G. 1976. Deformation mechanism maps for superplastic materials. *Scripta Metall.* **10**, 759 - 762.

Morral, J.E. & Ashby, M.F. 1974. Dislocated cellular structures. *Acta Metall.* **22**, 567 - 575.

Morrison-Smith, D.J., Patterson, M.S. & Hobbs, B.E. 1976. An electron microscope study of plastic deformation in single crystals of synthetic quartz. *Tectonophysics.* **33**, 43 - 79.

Mukherjee, A.K. 1971. The rate controlling mechanism in superplasticity. *Mater. Sci. Eng.* **8**, 83 - 89.

Murray, J.L. 1983. The Al-Zn (Aluminium-Zinc) system. *Bull. Alloy Phase Diagrams.* **4, (1),** 55.

Nabarro, F.R.N. 1948. Deformation of crystals by the motion of single ions. In: *Report of a Conference on Strength of Solids (Bristol) The Physical Soc.* London, 75 - 90.

Nicolas, A. 1978. Stress estimates from structural studies in some mantle peridotites. *Phil. Trans. R. Soc. London.* **A288**, 49 - 57.

Nicolas, A. & Poirier, J.P. 1976. *Crystalline Plasticity and Solid State Flow in Metamorphic Rrocks.* Wiley-Interscience, London.

Nieh, T.G. & Wadsworth, J. 1990. Superplastic ceramics. *Ann. Rev. Mater. Sci.* **20**, 117 - 140.

Nieh, T.G., Wadsworth, J. & Sherby, O.D. 1990. Superplastic behavior in ceramics, ceramic composites, metal matrix composites, and intermetallics. In: *Superplasticity in Aerospace II* (edited by McNelly, T.R. & Heikkenen, H.C.), Met. Soc. AIME, 19 - 32.

Nix, W.D. 1975. On the possible relation between grain boundary migration and the kinetics of grain boundary sliding in polycrystals. In: *Rate Processes and Plastic Deformation of Materials* (edited by Li, J.C.M. & Mukherjee, A.K.). **4**, ASM, Metals Park, USA, 384 - 409.

Norton, M.G. 1982. *The Kinematic and Microstructural Development of Some Shear Zones*, PhD. Thesis Imperial College, London,

Obee, H.K. 1985. *Fault Rock and Deformation Studies of a Major Continental Fault System*, PhD. Thesis Imperial College, London,

Obee, H.K. & White, S.H. 1985. Faults and associated fault rocks of the Southern Arunta block, Alice Springs, Central Australia. *J. Struct. Geol.* **7**, 701 - 712.

Obee, H.K. & White, S.H. 1986. Microstructural and fabric heterogeneities in fault rocks associated with a fundamental fault. *Proc. R. Soc. London.* **A317**, 99 - 109.

Offe, L.A. & Shaw, R.D. 1983. *Alice Springs Region, Northern Teritory, 1 : 100 000 Geological map commentary.* Bureau of Mineral Resources, Geology and Geophysics, Canberra

Ord, A. & Christie, J.M. 1984. Flow stresses from microstructures in mylonitic quartzites of the Moine Thrust zone, Assynt area, Scotland. *J. Struct. Geol.* **6**, 639 - 654.

Ord, A. & Hobbs, B.E. 1989. The strength of the continental crust, detachment zones and the

development of plastic instabilities. *Tectonophysics.* **158**, 269 - 289.

Padmanabhan, K.A. & Davies, G.J. 1980. *Superplasticity. Materials Research and Engineering.* Springer-Verlag, Berlin.

Parks, G.A. 1984. Surface and interfacial free energy of quartz. *J. Geophys. Res.* **89, (B6),** 3997 - 4008.

Passchier, C.W. 1982. *Mylonitic Deformation in the Saint-Barthélemy Massif, French Ppyrenees, with the Emphasis on the Genetic Relationship between Ultramylonite and Pseudotachylite*, PhD. Thesis Amsterdam University, *GUA papers of Geology,* **16.**

Paterson, M.S. 1989. The interaction of water with quartz and its influence in dislocation flow - an overview. In: *Rheology of Solids and of the Earth* (edited by Karato, S.-I. & Toriumi, M.). Oxford University Press, Oxford, 107 - 142.

Paterson, M.S. & Luan, F.C. 1990. Quartzite rheology under geological conditions. In: *Deformation Mechanisms, Rheology and Tectonics* (edited by Knipe, R.J. & Rutter, E.H.). *Geological Society Special Publications.* **54**, 299 - 307.

Perevezentsev, V.N., Rybin, V.V. & Chuvil'deev, V.N. 1992. The theory of structural superplasticity - II. Accumulation of defects on the interphase boundaries. accommodation of the grain-boundary sliding. the upper bound of the superplastic strain rate. *Acta Metall. Mater.* **40**, 895 - 905.

Peterson, N.L. 1979. Grain-boundary diffusion - structural effects, models, and mechanisms. In: *Grain Boundary Structure and Kinetics* (edited by Balluffi, R.W.), Milwaukee, Wisconsin, ASM, 209 - 238.

Philpotts, A.R. 1990. *Principles of Igneous and Metamorphic Petrology.* Prentice Hall, Englewood Cliffs, New Jersey.

Poirier, J.P. 1985. *Creep of crystals.* Cambridge university press, Cambridge.

Porter, D.A. & Easterling, K.E. 1992. *Phase Transformations in Metals and Alloys.* Chapman & Hall, London.

Presnyakov, A.A. & Chervyakova, V.V. 1959. On the subject of "super-ductility" of alloys. *Phys. Met. Metall.* **8, (1),** 96 - 102.

Raj, R. & Ashby, M.F. 1971. On grain boundary sliding and diffusion creep. *Metall. Trans.* **2**, 1113 - 1126.

Ramsay, J.G. 1982. Rock ductility and its influence on the development of tectonic structures in mountain belts. In: *Mountain Building Processes* (edited by Hsü, K.J.). Academic press, London, 111 - 127.

Ramsay, J.G. & Allison, I. 1979. Structural analysis of shear zones in an alpinised Hercynian granite. *Schweiz. Mineral. Petrogr. Mitt.* **59**, 251 - 279.

Ramsay, J.G. & Graham, R.H. 1970. Strain variation in shear belts. *Can. J. earth Sci.* **7**, 786 - 813.

Ranalli, G. 1984. Grain size distribution and flow stress in tectonites. *J. Struct. Geol.* **6**, 443 - 447.

Randle, V. 1992. *Microtexture Determination and its Applications.* Institue of Materials, London.

Randle, V. 1993. *The Measurement of Grain Boundary Geometry. Electron Microscopy in Materials Science.* IOP, Bristol.

Randle, V. & Ralph, B. 1986. A practical approach to the determination of the crystallography of grain boundaries. *J. Mat. Sci.* **21**, 3823 - 3828.

Ravichandran, K.S. & Seetharaman, V. 1993. Prediction of steady state creep behaviour of two phase composites. *Acta Metall. Mater.* **41**, 3351 - 3361.

Rawal, S.P. & Murty, G.S. 1972. Some observations on superplasticity in the Pb-Sn eutectic alloy. *Trans. JIM.* **13**, 57 - 58.

Rödel, J. & Glaeser, A. 1990. Pore drag and pore-boundary separation in alumina. *J. Am. Ceram. Soc.* **73**, 3302 - 3312.

Rubie, D.C. 1990. Mechanisms of reaction-enhanced deformability in minerals and rocks. In: *Deformation Processes in Minerals, Ceramics and Rocks* (edited by Barber, D.J. & Meredith, P.G.). Unwin Hyman Ltd, London, 262 - 295.

Rühle, M. 1984. TEM observations of grain boundaries in ceramics. In: *MRS Symposia Proceedings. Electron Microsopcy of Materials* (edited by Krakow, W., Smith, D.A. & Hobbs, L.W.), **31**, North-Holland, New York, 317 - 323.

Rutter, E.H. 1976. The kinetics of rock deformation by pressure solution. *Phil. Trans. R. Soc. Lond.* **A283**, 203 - 219.

Rutter, E.H. 1983. Pressure solution in nature, theory and experiment. *Jl. geol. Soc. London.* **140**, 725 - 740.

Rutter, E.H. & Brodie, K.H. 1988. The role of tectonic grain size reduction in the rheological stratification of the lithosphere. *Geol. Rundschau.* **77**, 295 - 308.

Rutter, E.H. & Brodie, K.H. 1991. Lithosphere rheology - a note of caution. *J. Struct. Geol.* **13**, 363 - 367.

Rutter, E.H. & Brodie, K.H. 1993a. Experimental deformation of synthetic, hot-pressed, fine-grained aggregates of Brazilian quartz. *Terra Nova, Terra Abstracts.* **5**, 297.

Rutter, E.H. & Brodie, K.H. 1993b. *Experimental Study of the Role of Grain Size Reduction in the Mechanical Properties and Microstructures of Rocks.* (NERC Report **GR3/6174**), Dept. Geology, Manchester University, 30 October 1993.

Rutter, E.H. & Brodie, K.H. 1994. Experimental intracrystalline plastic and grain-size sensitive flow of hot-pressed brazilian quartz aggregates. *EOS, Transactions AGU.* **75**, 636.

Rutter, E.H., Casey, M. & Burlini, L. 1994. Preferred crystallographic orientation development during the plastic and superplastic flow of calcite rocks. *J. Struct. Geol.* **16**, 1431 - 1446.

Sato, E., Kuribayashi, K. & Horiuchi, R. 1990. A mechanism of superplastic deformation and deformation induced grain growth based on grain switching. *Mat. Res. Soc. Symp. Proc.* **196**, 27 - 32.

Schmid, S.M., Boland, J.N. & Paterson, M.S. 1977. Superplastic flow in finegrained limestone. *Tectonophysics.* **43**, 257 - 291.

Schmid, S.M. & Casey, M. 1986. Complete fabric analysis of some commonly observed quartz c-axis patterns. In: *Mineral and Rock Deformation: Laboratory studies, The Patterson Volume* (edited by Hobbs, B.E. & Heard, H.C.). *Geophys. Monogr. Ser.* **36**, AGU, Washington D.C., 263 - 286.

Schmid, S.M. & Handy, M.R. 1991. Towards a genetic classification of fault rocks: geological usage and tectonophysical implications. In: *Controversies in Modern Geology* (edited by Müller, D.W., McKenzie, J.A. & Weissert, H.). Academic Press, London, 339 - 361.

Scholz, C.H. 1990. *The Mechanics of Earthquakes and Faulting.* Cambridge University Press, Cambridge.

Schwarzer, R.A. 1990. Measurement of local textures with transmission electron and scanning electron microsocpes. *Textures and Microstructures.* **13**, 15 - 30.

Schwarzer, R.A. & Weiland, H. 1988. Texture analysis by the measurement of individual grain orientations - Electron microscopical methods and application on dual phase steel. *Textures and Microstructures.* **8 -9**, 551 - 577.

Sellars, C.M. 1978. Recrystallization of metals during hot deformation. *Phil. Trans. R. Soc. London.* **A288**, 147 - 158.

Shariat, P., Vastava, R.B. & langdon, T.G. 1982. An evaluation of the roles of intercrystalline and interphase boundary sliding in two-phase superplastic alloys. *Acta Metall.* **30**, 285 - 296.

Shaw, R.D. & Black, L.P. 1991. The history and tectonic implications of the Redbank Thrust Zone, central Australia, based on structural, metamorphic and Rb-Sr isotopic evidence. *Aust. J. Earth Sci.* **38**, 307 - 332.

Shaw, R.D., Stewart, A.J. & Black, L.P. 1984. The Arunta Inlier: a complex ensialic mobile belt in central Australia. Part 2: tectonic history. *Aust. J. Earth Sci.* **31**, 457 - 484.

Shaw, R.D. & Wells, A.T. 1983. *Alice Springs, Northern Territory 1 : 250 000 Geological Map Commentary.* Bureau of Mineral Resources, Geology and Geophysics, Canberra

Shaw, R.D., Zeitler, P.K., McDougall, I. & Tingate, P.R. 1992. The palaeozoic history of an unusual intracatonic thrust belt in central Australia based on 40Ar-39Ar, K-Ar and fission track dating. *Jl. geol. Soc. Lond.* **149**, 937 - 954.

Shelton, G. & Tullis, J. 1981. Experimental flow laws for crustal rocks. *EOS, Transactions AGU.* **62**, 396.

Sherby, O.D. & Wadsworth, J. 1990. Observations on historical and contemporary developments in superplasticity. In: *Mat. Res. Soc. Symp. Proc.* (edited by Christen, D., Narayan, J. & Schneemeyer, L.), **196**, MRS, 3 - 14.

Sherwood, D.J. & Hamilton, C.H. 1992. Production of cellular defects contributing to deformation-enhanced grain growth. *Scripta Metall. Mater.* **27**, 1771 - 1776.

Sherwood, D.J. & Hamilton, C.H. 1994. The neighbour-switching mechanism of superplastic deformation: the constitutive relationship and deformation-enhanced grain growth. *Phil. Mag.* **70**, 109 - 143.

Shewmon 1963. *Diffusion in Solids.* McGraw-Hill Book Co., New York.

Sibson, R.H. 1977. Fault rocks and fault mechanisms. *Jl. geol. Soc. London.* **133**, 191 - 213.

Sibson, R.H., White, S.H. & Atkinson, B.K. 1979. Fault rock distribution and structure in the Alpine Fault Zone: A preliminary account. *Royal Soc. of New Zealand Bull.* **18**, 55 - 65.

Simpson, C. 1985. Deformation of granitic rocks across the brittle-ductile transition. *J. Struct. Geol.* **7**, 503 - 511.

Smith, C.S. 1948. Grains, phases, and interfaces: an interpretation of microstructure. *Trans. Metall. Soc. AIME.* **175**, 15 - 51.

Smith, C.S. 1952. Grain shapes and other metallurgical applications of topology. In: *Metal Interfaces* (edited by Brick, R.M.). ASM, Cleveland, Ohio, 63 - 108.

Smith, D.A., Rae, C.M.F. & Grovenor, C.R.M. 1979. Grain boundary migration. In: *Grain Boundary Structure and Kinetics* (edited by Balluffi, R.W.), Milwaukee, Wisconsin, ASM, 337 - 371.

Spiers, C.J. & Schutjens, P.M.T.M. 1990. Densification of crystalline aggregates by fluid phase diffusional creep. In: *Deformation Processes in Minerals, Ceramics and Rocks* (edited by Barber, D. & Meredith, P.). Unwin Hyman Ltd., London, 0.

Spry, A. 1976. *Metamorphic Textures.* Pergamon Press, Oxford.

Stanton, R.L. 1964. Mineral interfaces in stratiform ores. *Inst. Mining and Metall.* 45 - 79.

Stünitz, H. 1993. Transition from fracturing to viscous flow in a naturally deformed metagabbro. In: *Defects and Processes in the Solid State: Geoscience Applications The McLaren Volume* (edited by Boland, J.N. & Fitz Gerald, J.D.). *Developments in Petrology.* **16**, Elsevier, Amsterdam, 121 - 150.

Stünitz, H. & Fitz Gerald, J.D. 1993. Deformation of granitoids at low metamorphic grade. II: Granular flow in albite-rich mylonites. *Tectonophysics.* **221**, 299-324.

Toriumi, M. 1979. Relation between dislocation density and subgrain size of naturally deformed olivine in peridotites. *Contrib. Mineral. Petrol.* **68**, 181 - 186.

Treagus, S.H. 1988. Strain refraction in layered systems. *J. Struct. geol.* **10**, 517 - 527.

Trepied, L. & Doukhan, J.C. 1982. Evidence of <a+c> dislocations in synthetic quartz single crystals compressed along the c axis. *Bull. Minèral.* **105**, 176 - 180.

Trepied, L., Doukhan, J.C. & Paquet, J. 1980. Subgrain boundaries in quartz. Theoretical analysis and microscopic observations. *Phys. Chem. Minerals.* **5**, 201

- 218.
Tullis, J. 1990. Experimental studies of deformation mechanisms and microstructures in quartzo-feldspathic rocks. In: *Deformation Processes in Minerals, Ceramics and Rocks* (edited by Barber, D.J. & Meredith, P.G.). Unwin Hyman Ltd, London, 190 - 226.
Tullis, J., Christie, J.M. & Griggs, D.T. 1973. Microstructures and preferred orientations of experimentally deformed quartzites. *Bull. Geol. Soc. Am.* **84**, 297 - 314.
Tullis, J. & Yund, A. 1991. Diffusion creep in feldspar aggregates: experimental evidence. *J. Struct. Geol.* **13**, 987 - 1000.
Tullis, J. & Yund, R.A. 1982. Grain growth kinetics of quartz and calcite aggregates. *J. Geology.* **90**, 301 - 318.
Tullis, T.E. & Horowitz, F. 1980. The strength of dry olivine. *EOS, Transactions AGU.* **61**, 375 - 376.
Tullis, T.E., Horowitz, F.G. & Tullis, J. 1991. Flow laws of polyphase aggregates from end-member flow laws. *J. Geophys. Res.* **96, (B5),** 8081 - 8096.
Turner, F.J. & Weiss, V. 1963. *Structural Analysis of Metamorphic Tectonites.* McGraw-Hill, New York.
Twiss, R.J. 1977. Theory and applicability of a recrystallized grain size paleopiezometer. *Pageoph.* **115**, 227 - 244.
Underwood, E.E. 1970. *Quantitative Stereology.* Addison-Wesley Publishing Company, Reading, Massachusetts.
Urai, J.L., Means, W.D. & Lister, G.S. 1986. Dynamic recrystallization of minerals. In: *Mineral and Rock Deformation: Laboratory Studies, The Paterson Volume* (edited by Hobbs, B.E. & Heard, H.C.). *Geophys. Monogr. Ser.* **36,** AGU, Washington D.C., 161 - 199.
Van der Wal, D. 1993. *Deformation Processes in Mantle Peridotites*, PhD. Thesis Utrecht University, *Geologica Ultraiectina*, **102.**
Van der Wal, D., Chopra, P., Drury, M.R. & Fitz Gerald, J. 1993. Relationships between dynamically recrystallized grain size and deformation conditions in experimentally deformed olivine rocks. *Geoph. Res. Lett.* **20**, 1479 - 1482.
Vastava, R.B. & Langdon, T.G. 1979. An investigation of intercrystalline and interphase boundary sliding in the superplastic Pb-62% Sn eutectic. *Acta Metall.* **27**, 251 - 257.
Vauchez, A. 1987. The development of discrete shear-zones in a granite: stress, strain and changes in deformation mechanisms. *Tectonophysics.* **133**, 137 - 156.
Vaughan, P.J. & Kohlstedt, D.L. 1982. Distribution of glass phase in hot-pressed, olivine-basalt aggregates: an electron microscopy study. *Contrib. Mineral. Petrol.* **81**, 253 - 261.
Venkatachari, K.R. & Raj, R. 1986. Superplastic flow in fine-grained alumina. *J. Am. Ceram. Soc.* **69**, 135 - 138.
Vernon, R.H. 1968. Microstructures of high-grade metamorphic rocks at Broken Hill, Australia. *J. Petrology.* **9**, 1 - 22.
Vernon, R.H. 1970. Comparative grain-boundary studies of some basic and ultrabasic granulites, nodules and cumulates. *Scott. J. Geol.* **6**, 337 - 351.
Vernon, R.H. 1975. Deformation and recrystallization of a plagioclase grain. *Am. Mineral.* **60**, 884 - 888.
Vernon, R.H. & Flood, R.H. 1988. Conrasting deformation and metamorphism of S- and I-type granitoids in the Lachlan Fold Belt, eastern Australia. *Tectonophysics.* **147**, 127 - 143.
Vernon, R.H., Williams, V.A. & D'Arcy, W.F. 1983. Grain-size reduction and foliation development in a deformed granitoid batholith. *Tectonophysics.* **92**, 123 - 145.
Vissers, R.L.M., Drury, M.R., Hoogerduijn Starting, E.H. & Van der Wal, D. 1991. Shear zones in the upper mantle: a case study in an alpine lherzolite massif. *Geology.* **19**, 990 - 993.
Von Neumann, J. 1952. Discussion to 'Grain shapes and other metallurgical applications of topology' by C.S. Smith. In: *Metal Interfaces* (edited by Brick, R.M.). ASM, Cleveland, Ohio, 108 - 110.
Wakai, F. 1991. Superplasticity of ceramics. *Ceram. Int.* **17**, 153 - 163.
Wakefield, J. 1977. Mylonitization in the Lethakane shear zone, eastern Botswana. *Jl. geol. Soc. Lond.* **133**, 263 - 275.
Walker, A.N., Rutter, E.H. & Brodie, K.H. 1990. Experimental study of grain-size sensitive flow of synthetic, hot-pressed calcite rocks. In: *Deformation Mechanisms, Rheology and Tectonics* (edited by Knipe, R.J. & Rutter, E.H.). *Geological Society Special Publication.* **54,** 259 - 284.
Watson, E.B. & Brenan, J.M. 1987. Fluids in the lithosphere, 1. Experimenatlly-determined wetting characteristics of CO2-H2O fluids and their implications for fluid transport, host-rock properties, and fluid inclusion formation. *Earth. Planet. Sci. Lett.* **85**, 497 - 515.
Watterson, J. 1975. Mechanisms for the persistence of tectonic lineaments. *Nature Phys. Sci.* **253**, 520 - 521.
Watts, M.J. & Williams, G.D. 1979. Fault rocks as indicators of progressive shear deformation in the Guingamp region of Brittany. *J. Struct. Geol.* **1**, 323 - 332.
Watts, M.J. & Williams, G.D. 1983. Strain geometry, microstructure and mineral chemistry in metagabbro shear zones: a study of softening mechanisms during progressive mylonitization. *J. Struct. Geol.* **5**, 507 - 517.
Weertman, J. 1970. The creep strength of the Earth's mantle. *Rev. Geophys. Space. Phys.* **8**, 145 - 168.
Weertman, J. 1978. Creep laws for the mantle of the earth. *Phil. Trans. R. Soc. London.* **A288**, 9 - 26.
Wenk, H.R. & Christie, J.M. 1991. Comments on the interpretation of deformation textures in rocks. **13**, 1091 - 1110.
Wheeler, J. 1987. The significance of grain-scale stresses in the kinetics of metamorphism. *Contrib. Mineral. Petrol.* **97**, 397 - 404.
Wheeler, J. 1991. A view of texture dynamics. *Terra Nova.*

3, 123 - 136.

Wheeler, J. 1992. Importance of pressure solution and Coble creep in the deformation of polymineralic rocks. *J. Geophys. Res.* **97, (B4),** 4579 - 4586.

White, J.C. 1982. Quartz deformation and the recognition of recrystallization regimes in the Flinton Group canglomerates, Ontaria. *Can. J. Earth. Sci.* **19**, 81 - 93.

White, J.C. & White, S.H. 1981. On the structure of grain boundaries in tectonites. *Tectonophysics.* **78**, 613 - 628.

White, S. 1979d. Large strain deformation: report on a Tectonic Studies Group discussion meeting held at Imperial College, London on 14 November 1979. *J. Struct. Geol.* **1**, 333 - 339.

White, S.H. 1973a. Dislocations and bubbles in vein quartz. *Nature Phys. Sci.* **243**, 11 - 14.

White, S.H. 1973b. Syntectonic recrystallization and texture development in quartz. *Nature.* **244**, 267 - 268.

White, S.H. 1975. Estimation of strain rates from microstructures. *Jl. geol. Soc. Lon.* **131**, 577 - 583.

White, S.H. 1976. The effects of strain on the microstructures, fabrics, and deformation mechanisms in quartzites. *Phil. Trans. R. Soc. London.* **A283**, 69 - 86.

White, S.H. 1977. Geological significance of recovery and recrystallization processes in quartz. *Tectonophysics.* **39**, 143 - 170.

White, S.H. 1979a. Difficulties associated with paleostress estimates. *Bull. Mineral.* **102**, 210 - 215.

White, S.H. 1979b. Grain and sub-grain size variations across a mylonite zone. *Contrib. Mineral. Petrol.* **70**, 193 - 202.

White, S.H. 1979c. Paleostress estimates in the Moine thrust, Eriboll, Scotland. *J. Struc. Geol.* **280**, 222 - 223.

White, S.H. & Bretan, P.G. 1985. Rheological controls on the geometry of deep faults and the tectonic delamination of the continental crust. *Tectonics.* **4**, 303 - 309.

White, S.H., Bretan, P.G. & Rutter, E.H. 1986. Fault-zone reactivation: kinematics and mechanisms. *Phil. Trans. R. Soc. Lond.* **A317**, 81 - 97.

White, S.H., Burrows, S.E. & Carreras, J. 1978. Textural and microstructural development in a naturally deformed quartzite: a metallurgical approach. In: *5th Int. Conf. on Textures of Materials* (edited by Gottstein, G. & Luecke, K.), **2**, Aachen, Germany, Springer-Verlag, 211 - 220.

White, S.H., Burrows, S.E., Carreras, J., Shaw, N.D. & Humphreys, F.J. 1980. On mylonites in ductile shear zones. *J. Struct. Geol.* **2**, 175 - 187.

White, S.H., Evans, D.J. & Zhong, D.-L. 1982. Fault rocks of the Moine thrust zone: microstructures and textures of selected mylonites. *Textures and Microstructures.* **5**, 33 - 61.

White, S.H. & Knipe, R.J. 1978. Transformation- and reaction-enhanced ductility in rocks. *J. geol. Soc. Lond.* **135**, 513 - 516.

White, S.H., Shaw, H.F. & Huggett, J.M. 1984. The use of back-scattered electron imaging for the petrographic study of sandstones and shales. *J. Sed. Petrol.* **54**, 487 - 494.

White, S.H. & Treagus, J.E. 1975a. The effects of polyphase deformation on the intracrystalline defect structures of quartz. I The defect structures. *N. Jb. Mineral. Abh.* **123**, 219 - 236.

White, S.H. & Treagus, J.E. 1975b. The effects of polyphase deformation on the intracrystalline defect structures of quartz. II Origin of the defect structures. *N. Jb. Mineral. Abh.* **123**, 237 - 252.

Williams, G. & Dixon, J. 1982. Reaction and geometrical softening in granitoid mylonites. *Textures and Microstructures.* **4**, 223 - 239.

Wilson, C.J.L. 1973. The prograde microfabric in a deformed quartzite sequence, Mount Isa, Australia. *Tectonophysics.* **19**, 39 - 81.

Wilson, C.J.L. 1980. Shear zones in a pegmatite: a study of albite-mica-quartz deformation. *J. Struct. Geol.* **2**, 203 - 209.

Yan, S., Earthman, J.C. & Mohamed, F.A. 1994. Effect of Cd on superplastic flow in the Pb - 62 wt% Sn eutectic. *Phil. Mag.* **69**, 1017 - 1038.

Yardley, B.W.D. 1989. *An Introduction to Metamorphic Petrology. Longman Earth Science Series.* Longman Group UK, Harlow, Essex.

Yoon, C.K. & Chen, I.-W. 1990. Superplastic low of two-phase ceramics containing rigid inclusions-Zirconia/Mullite composites. *J. Am. Ceram. Soc.* **73**, 1555 - 1565.

Zehr, S.W. & Backofen, W.A. 1968. Superplasticity in lead-tin alloys. *Trans. ASM.* **61**, 300 - 313.

Zelin, M.G., Krasilnikov, N.A., Valiev, R.Z., Grabski, M.W., Yang, H.S. & Mukherjee, A.K. 1994. On the microstructural aspects of the nonhomogeneity of superplastic deformation at the level of grain groups. *Acta Metall. Mater.* **42**, 119 - 126.

Zelin, M.G. & Mukherjee, A.K. 1993a. Analysis of the cooperative grain boundary sliding in terms of cellular dislocations. *Phil. Mag.* **68**, 1183 - 1194.

Zelin, M.G. & Mukherjee, A.K. 1993b. Common features of intragranular dislocation slip and intergranular sliding. *Phil. Mag. Lett.* **68**, 207 - 214.

Zelin, M.G. & Mukherjee, A.K. 1993c. Deformation strengthening of grain-boundary sliding in a Pb - 62 wt% Sn alloy. *Phil. Mag. Lett.* **68**, 201 - 206.

Zelin, M.G. & Mukherjee, A.K. 1993d. Microstructural aspects of non-homogeneity of grain boundary sliding. *J. Mat. Sci.* **28**, 6767 - 6773.

Zelin, M.G. & Mukherjee, A.K. 1995. Cooperative phenomena at grain boundaries during superplastic flow. *Acta Metall. Mater.* **43**, 2359 - 2372.

Zobac, M.D., Apel, R., Baumgärtner, J., Brudy, M., Emmermann, R., Engeser, B., Fuchs, K., Kessels, W., Rischmüller, H., Rummel, F. & Vernik, L. 1993. Upper-crustal strength inferred from stress measurements to 6 km depth in the KTB borehole. *Nature.* **365**, 633 - 635.

Curriculum Vitae

Timon Fliervoet werd geboren op 18 april 1967 in Nijmegen. In 1985 behaalde hij het VWO-diploma aan de R.K. Scholengemeenschap Canisiuscollege - Mater Dei te Nijmegen. In 1986 begon hij met de studie geologie aan de Universiteit Utrecht. Het doctoraal examen met als hoofdvak structurele geologie van kristallijne gesteenten en als bijvakken electronenmicroscopie en magmatische petrologie werd in juni 1991 cum laude behaald.

Van juli 1991 tot juli 1995 was hij werkzaam als onderzoeker-in-opleiding (OIO) bij de vakgroep geologie van de Universiteit Utrecht. Tijdens deze periode is het in dit proefschrift beschreven onderzoek verricht.